

# Chapter 1

## Introduction

### Symbols

$E$	modulus of elasticity, Pa	$\eta_o$	absolute viscosity at $p = 0$ and constant temperature, Pa·s
$E'$	effective elastic modulus, $2 \left( \frac{1 - \nu_a^2}{E_a} + \frac{1 - \nu_b^2}{E_b} \right)^{-1}$ , Pa	$\mu$	coefficient of sliding friction
$H_s$	Hersey number, $\eta\omega/p$	$\nu$	Poisson's ratio
$h$	film thickness, m	$\xi$	pressure-viscosity coefficient, $\text{m}^2/\text{N}$
$p$	pressure, Pa	$\omega$	rotational speed, rad/s
$p_a$	ambient pressure, Pa		
$p_s$	supply pressure, Pa		
$R$	curvature sum, m		
$u$	velocity, m/s		
$w_a$	squeeze velocity, m/s	$a$	solid $a$
$w_z$	normal load component, N	$b$	solid $b$
$x, y, z$	Cartesian coordinate system, m	max	maximum
$z$	coordinate in film direction, m	min	minimum
$\eta$	viscosity, Pa·s	$x, y, z$	Cartesian coordinate system, m

### Subscripts

### 1.1 Introduction

In 1966 with the publication in England of the “Department of Education and Science Report,” sometimes known as the “Jost Report,” the word “tribology” was introduced and defined as the science and technology of interacting surfaces in relative motion and of the practices related thereto. A better definition might be the lubrication, friction, and wear of moving or stationary parts. The “Department of Education and Science Report” (1966) also claimed that industry could save considerable money by improving their lubrication, friction, and wear practices.

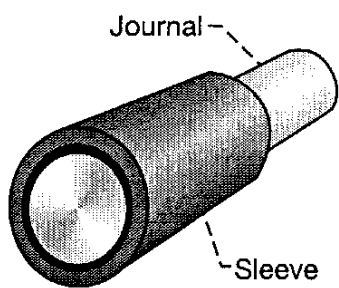


Figure 1.1: Conformal Surfaces. [From Hamrock and Anderson (1983).]

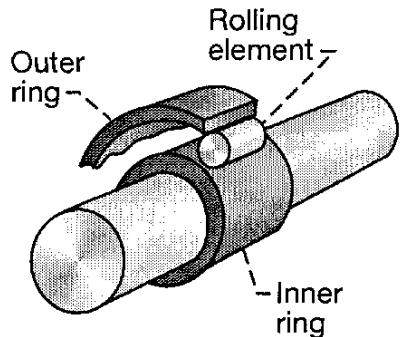


Figure 1.2: Nonconformal Surfaces. [From Hamrock and Anderson (1983).]

This book focuses on the fundamentals of fluid film lubrication. Fluid film lubrication occurs when opposing bearing surfaces are completely separated by a lubricant film. The applied load is carried by pressure generated within the fluid, and frictional resistance to motion arises entirely from the shearing of the viscous fluid. The performance of fluid film bearings can be determined by applying well-established principles of fluid mechanics, usually in terms of slow viscous flow.

Boundary lubrication, where considerable contact between the surfaces occurs, uses less established principles but is still commonly encountered.

## 1.2 Conformal and Nonconformal Surfaces

Conformal surfaces fit snugly into each other with a high degree of geometrical conformity so that the load is carried over a relatively large area. For example, the lubrication area of a journal bearing would be  $2\pi$  times the radius times the length. The load-carrying surface area remains essentially constant while the load is increased. Fluid film journal bearings (Fig. 1.1) and slider bearings have conformal surfaces. In journal bearings the radial clearance between the journal and the sleeve is typically one-thousandth of the journal diameter; in slider bearings the inclination of the bearing surface to the runner is typically one part in a thousand.

Many machine elements that are fluid film lubricated have surfaces that do not conform to each other well. The full burden of the load must then be carried by a small lubrication area. The lubrication area of a nonconformal conjunction is typically three orders of magnitude less than that of a conformal conjunction. In general, the lubrication area between nonconformal surfaces enlarges considerably with increasing load, but it is still smaller than the lubrication area between conformal surfaces. Some examples of nonconformal surfaces are mating gear teeth, cams and followers, and rolling-element bearings (Fig. 1.2).

## 1.3 Lubrication Regimes

A lubricant is any substance that reduces friction and wear and provides smooth running and a satisfactory life for machine elements. Most lubricants are liquids (such as mineral oils, synthetic esters, silicone fluids, and water), but they may be solids (such as polytetrafluoroethylene, or PTFE) for use in dry bearings, greases for use in rolling-element bearings, or gases (such as air) for use in gas bearings. The physical and chemical interactions between the lubricant and the lubricating surfaces must be understood in order to provide the machine elements with satisfactory life. As an aid in understanding the features that distinguish the four lubrication regimes from one another, a short historical perspective is given, followed by a description of each regime.

### 1.3.1 Historical Perspective

By the middle of the 20th century two distinct lubrication regimes were generally recognized: hydrodynamic lubrication and boundary lubrication. The understanding of hydrodynamic lubrication began with the classic experiments of Tower (1885), in which the existence of a film was detected from measurements of pressure within the lubricant, and of Petrov (1883), who reached the same conclusion from friction measurements. This work was closely followed by Reynolds' (1886) celebrated analytical paper in which he used a reduced form of the Navier-Stokes equations in association with the continuity equation to generate a second-order differential equation for the pressure in the narrow, converging gap between bearing surfaces. This pressure enables a load to be transmitted between the surfaces with extremely low friction, since the surfaces are completely separated by a fluid film. In such a situation the physical properties of the lubricant, notably the dynamic viscosity, dictate the behavior in the conjunction.

The understanding of boundary lubrication is normally attributed to Hardy and Doubleday (1922a,b), who found that extremely thin films adhering to surfaces were often sufficient to assist relative sliding. They concluded that under such circumstances the chemical composition of the fluid is important, and they introduced the term "boundary lubrication." Boundary lubrication is at the opposite end of the lubrication spectrum from hydrodynamic lubrication. In boundary lubrication the physical and chemical properties of thin films of molecular proportions and the surfaces to which they are attached determine contact behavior. The lubricant viscosity is not an influential parameter.

In the last 50 years, research has been devoted to a better understanding and more precise definition of other lubrication regimes between these extremes. One such lubrication regime occurs between nonconformal surfaces, where the pressures are high and the surfaces deform elastically, in this situation the viscosity of the lubricant may rise considerably, and this further assists the formation of an effective fluid film. A lubricated conjunction in which such effects are found is said to be operating "elastohydrodynamically." Significant

progress has been made in understanding the mechanism of elastohydrodynamic lubrication, generally viewed as reaching maturity.

Since 1970 it has been recognized that between fluid film and boundary lubrication some combined mode of action can occur. This mode is generally termed “partial lubrication” or is sometimes referred to as “mixed lubrication.” To date, most of the scientific unknowns lie in this lubrication regime. An interdisciplinary approach will be needed to gain an understanding of this important lubrication mechanism. Between conformal surfaces, the mode of lubrication goes directly from hydrodynamic to partial as the lubricant film thins. For nonconformal surfaces, the mode of lubrication goes from elastohydrodynamic to partial as the lubricant thins. A more in-depth historical development of lubrication, or tribology in general, can be obtained from Dowson (1998).

### 1.3.2 Hydrodynamic Lubrication

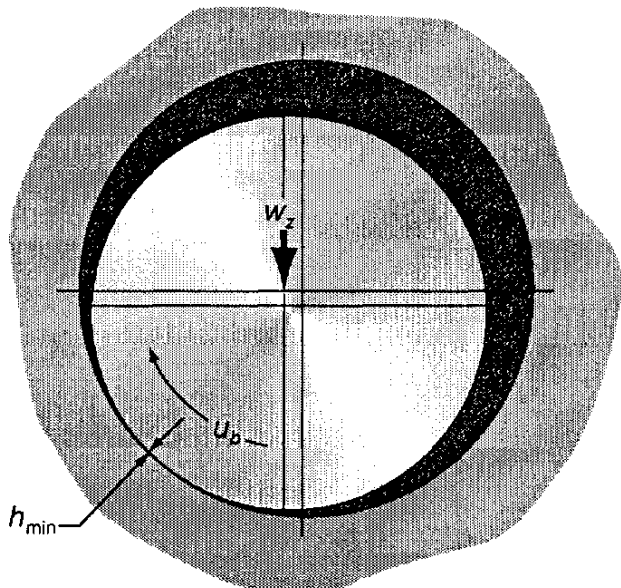
Hydrodynamic lubrication (HL) is generally characterized by conformal surfaces. A positive pressure develops in a hydrodynamically lubricated journal or thrust bearing because the bearing surfaces converge and the relative motion and the viscosity of the fluid separate the surfaces. The existence of this positive pressure implies that a normal applied load may be supported. The magnitude of the pressure developed (usually less than 5 MPa) is not generally large enough to cause significant elastic deformation of the surfaces. It is shown later that the minimum film thickness in a hydrodynamically lubricated bearing is a function of normal applied load  $w_z$ , velocity  $u_b$  of the lower surface, lubricant viscosity  $\eta_0$ , and geometry ( $R_x$  and  $R_y$ ). Figure 1.3 shows some of these characteristics of hydrodynamic lubrication. Minimum film thickness  $h_{\min}$  as a function of  $u_b$ , and  $w_z$  for sliding motion is given as

$$(h_{\min})_{HL} \propto \left( \frac{u_b}{w_z} \right)^{1/2} \quad (1.1)$$

The minimum film thickness normally exceeds 1  $\mu\text{m}$ .

In hydrodynamic lubrication the films are generally thick so that opposing solid surfaces are prevented from coming into contact. This condition is often referred to as “the ideal form of lubrication,” since it provides low friction and high resistance to wear. The lubrication of the solid surfaces is governed by the bulk physical properties of the lubricant, notably the viscosity, and the frictional characteristics arise purely from the shearing of the viscous lubricant.

For a normal load to be supported by a bearing, positive-pressure profiles must be developed over the bearing length. Figure 1.4 illustrates three ways of developing positive pressure in hydrodynamically lubricated bearings. For a positive pressure to be developed in a slider bearing (Fig. 1.4a) the lubricant film thickness must be decreasing in the sliding direction. In a squeeze film bearing (Fig. 1.4b) the squeeze action with squeeze velocity  $w_a$  has the bearing surfaces approach each other. The squeeze mechanism of pressure generation provides a valuable cushioning effect when the bearing surfaces approach each



Conformal surfaces

$$p_{\max} \sim 5 \text{ MPa}$$

$$h_{\min} = f(w_z, u_b, \eta_0, R_x, R_y) > 1 \mu\text{m}$$

No elastic effect

Figure 1.3: Characteristics of hydrodynamic lubrication.

other. Positive pressures will be generated only when the film thickness is diminishing. In an externally pressurized bearing, sometimes referred to as “a hydrostatic bearing” (Fig. 1.4c), the pressure drop across the bearing supports the load. The load-carrying capacity is independent of bearing motion and lubricant viscosity. There is no surface contact wear at starting and stopping as there is with the slider bearing.

### 1.3.3 Elastohydrodynamic Lubrication

Elastohydrodynamic lubrication (EHL) is a form of hydrodynamic lubrication where elastic deformation of the lubricated surfaces becomes significant. The

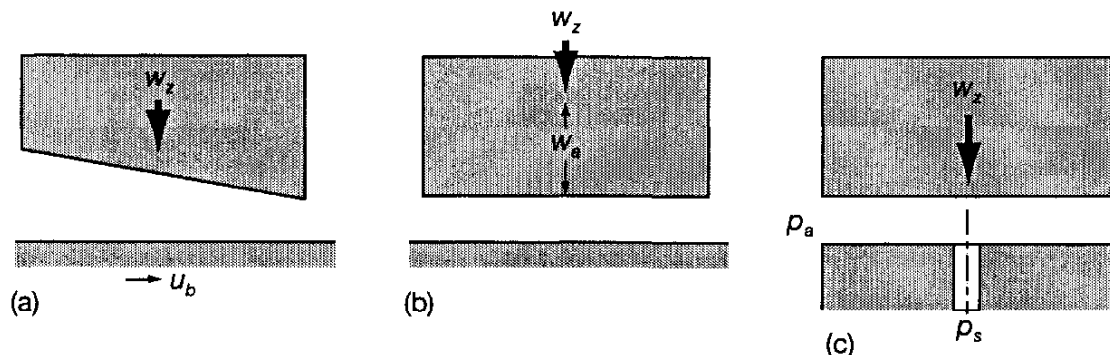
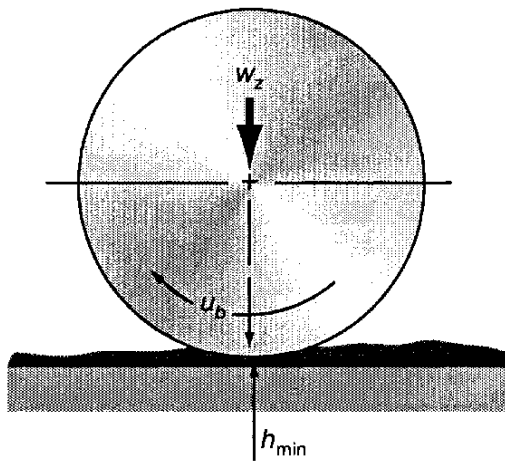
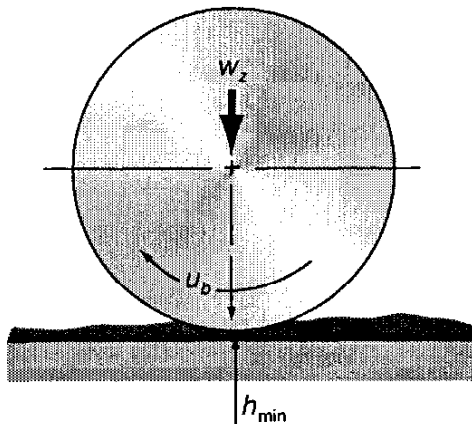


Figure 1.4: Mechanisms of pressure development for hydrodynamic lubrication. (a) Slider bearing; (b) squeeze film bearing; (c) externally pressurized bearing.



Nonconformal surfaces  
High-elastic-modulus material (e.g., steel)  
 $p_{\max} \sim 1 \text{ GPa}$   
 $h_{\min} = f(w_z, u_b, \eta_0, R_x, R_y, E') > 0.1 \mu\text{m}$   
Elastic and viscous effects both important

Figure 1.5: Characteristics of hard elastohydrodynamic lubrication



Nonconformal surfaces (e.g., nitrile rubber)  
 $p_{\max} \sim 1 \text{ MPa}$   
 $h_{\min} = f(w_z, u_b, \eta_0, R_x, R_y, E') \sim 1 \mu\text{m}$   
Elastic effects predominate

Figure 1.6: Characteristics of soft elastohydrodynamic lubrication

features important in a hydrodynamically lubricated slider bearing (Fig. 1.4a) - converging film thickness, sliding motion, and a viscous fluid between the surfaces - are also important here. Elastohydrodynamic lubrication is normally associated with nonconformal surfaces. There are two distinct forms of EHL.

### Hard EHL

Hard EHL relates to materials of high elastic modulus such as metals. In this form of lubrication the elastic deformation and the pressure-viscosity effects are equally important. Figure 1.5 gives the characteristics of hard elastohydrodynamically lubricated conjunctions. The maximum pressure is typically between 0.5 and 3 GPa; the minimum film thickness normally exceeds 0.1  $\mu\text{m}$ . These conditions are dramatically different from those found in a hydrodynamically lubricated conjunction (Fig. 1.3). At loads normally experienced in nonconformal machine elements the elastic deformations are several orders of magnitude larger than the minimum film thickness. Furthermore, the lubricant viscosity can vary by as much as 10 orders of magnitude within the lubricating conjunction. The minimum film thickness is a function of the same parameters as for hydrodynamic lubrication (Fig. 1.3) but with the additions of the effective elastic modulus  $E'$  and the pressure-viscosity coefficient  $\xi$  of the lubricant.

$$E' = \frac{2}{\frac{1 - \nu_a^2}{E_a} + \frac{1 - \nu_b^2}{E_b}} \quad (1.2)$$

The relationships between the minimum film thickness and the normal applied load and speed for hard EHL, as obtained from Hamrock and Dowson

(1977) are

$$(h_{\min})_{HEHL} \alpha w_z^{-0.073} \quad (1.3)$$

$$(h_{\min})_{HEHL} \alpha u_b^{0.68} \quad (1.4)$$

Comparing the results for hard EHL [Eqs. (1.3) and (1.4)] with those for hydrodynamic lubrication [Eq. (1.1)] yields the following conclusions:

1. The exponent on the normal applied load is nearly seven times larger for hydrodynamic lubrication than for hard EHL. This implies that the film thickness is only slightly affected by load for hard EHL but significantly affected for hydrodynamic lubrication.
2. The exponent on mean velocity is slightly higher for hard EHL than for hydrodynamic lubrication.

Some of the important results are presented in this chapter and substantiated in subsequent chapters. Engineering applications in which elastohydrodynamic lubrication is important for high-elastic-modulus materials include gears, rolling-element bearings, and cams.

## Soft EHL

Soft EHL relates to materials of low elastic modulus such as rubber. Figure 1.6 shows the characteristics of soft-EHL materials. In soft EHL the elastic distortions are large, even with light loads. The maximum pressure for soft EHL is typically 1 MPa, in contrast to 1 GPa for hard EHL (Fig. 1.5). This low pressure has a negligible effect on the viscosity variation throughout the conjunction. The minimum film thickness is a function of the same parameters as in hydrodynamic lubrication with the addition of the effective elastic modulus. The minimum film thickness for soft EHL is typically 1  $\mu\text{m}$ . Engineering applications in which elastohydrodynamic lubrication is important for low elastic-modulus materials include seals, human joints, tires, and a number of lubricated machine elements that use rubber as a material. The common features of hard and soft EHL are that the local elastic deformation of the solids provides coherent fluid films and that asperity interaction is largely prevented. This implies that the frictional resistance to motion is due to lubricant shearing.

### 1.3.4 Boundary Lubrication

Because in boundary lubrication the solids are not separated by the lubricant, fluid film effects are negligible and there is considerable asperity contact. The contact lubrication mechanism is governed by the physical and chemical properties of thin surface films of molecular proportions. The properties of the bulk lubricant are of minor importance, and the friction coefficient is essentially independent of fluid viscosity. The frictional characteristics are determined by the properties of the solids and the lubricant film at the common interfaces. The

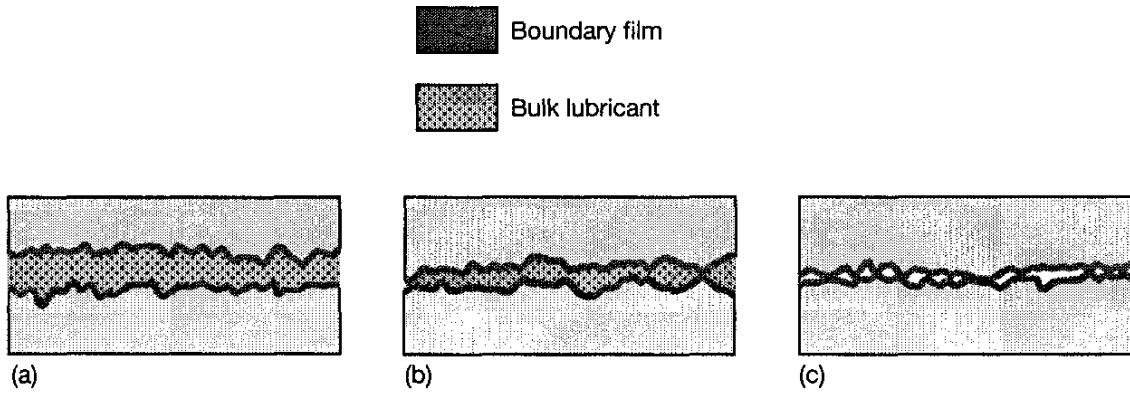


Figure 1.7: Film conditions of lubrication regimes. (a) Fluid film lubrication - surfaces separated by a bulk lubricant film; (b) partial lubrication - both bulk lubricant and boundary film play a role; (c) boundary lubrication - performance depends entirely on boundary film.

surface films vary in thickness from 1 to 10 nm, depending on the molecular size.

Figure 1.7 illustrates the film conditions existing in fluid film and boundary lubrication. The surface slopes in this figure are greatly distorted for purposes of illustration. To scale, real surfaces would appear as gently rolling hills rather than sharp peaks. The surface asperities are not in contact for fluid film lubrication but are in contact for boundary lubrication.

Figure 1.8 shows the behavior of the friction coefficient in the different lubrication regimes. In boundary lubrication, although the friction is much higher than in the hydrodynamic regime, it is still much lower than for unlubricated surfaces. The mean friction coefficient increases a total of three orders of magnitude in going from the hydrodynamic to the elastohydrodynamic to the boundary to the unlubricated regime.

Figure 1.9 shows the wear rate in the various lubrication regimes as determined by the operating load. In the hydrodynamic and elastohydrodynamic regimes there is little or no wear, since there is no asperity contact. In the boundary lubrication regime the degree of asperity interaction and the wear rate increase as the load increases. The transition from boundary lubrication to an unlubricated condition is marked by a drastic change in wear rate. As the relative load is increased in the unlubricated regime, the wear rate increases until scoring or seizure occurs and the machine element can no longer operate successfully. Most machine elements cannot operate long with unlubricated surfaces. Together Figs. 1.8 and 1.9 show that the friction and wear of unlubricated surfaces can be greatly decreased by providing boundary lubrication.

Boundary lubrication occurs when the film thickness is very small, typically less than the composite surface roughness. However, it should be noted that this corresponds to the mean separation of the surface; the minimum film thickness

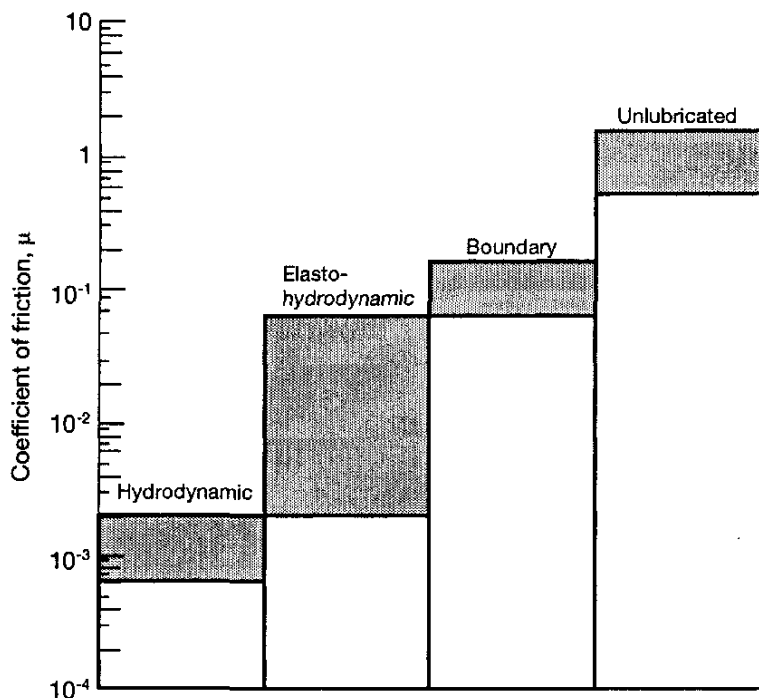


Figure 1.8: Bar diagram showing friction coefficient for various lubrication conditions.

in the boundary regime is on the order of molecular dimensions. Hence, effective boundary lubrication requires the presence of materials that satisfy the many functions of a lubricant with only one or two molecular layers.

Boundary lubricants are present to some extent in most natural oils and petroleum lubricants, but are often purposefully added to a formulation to improve performance. The effect of the additive on the viscous properties of the oil is fairly minimal, since the typical boundary additive content in an industrial lubricant is 0.1-0.5%. While this may seem to be an insignificant amount, it should be recognized that this is sufficient for the formation of

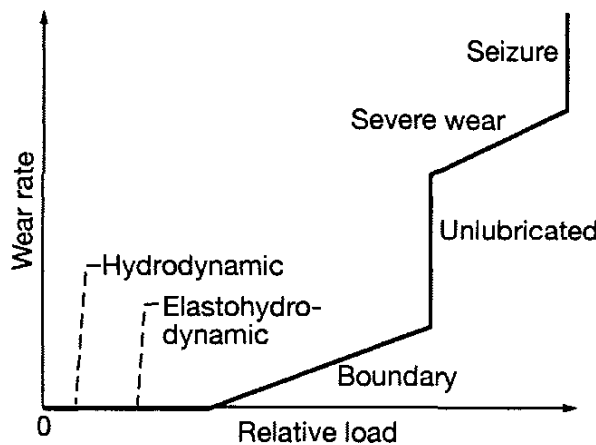


Figure 1.9: Wear rates for various lubrication regimes. [From Beerbower (1972)].

continuous protective layers on surfaces.

Boundary lubrication as discussed in this chapter is focused upon traditional machine design and manufacturing applications of fluid film lubrication. Applications in the MEMS area are still applicable to many of the issues discussed in this chapter, but the surfaces are so smooth in these applications that the devices can still be considered to operate in the partial or full film regimes.

Boundary lubrication is a very multi-disciplinary field, drawing heavily on chemistry, materials science and engineering. Of the lubrication regimes, it is the most empirical, with the few existing models merely serving as qualitative guides to designers. Many theories are fairly controversial, and only a broad outline of the art and science of boundary lubrication is contained here. Further information can be found in Bhushan (2002), Ku (1970), Lockwood and Bridger (1987) or Williams (1994).

There are a large number of mechanisms through which boundary films act, and a wide variety of chemicals are known to be advantageous with respect to boundary lubrication. However, it is a common practice among lubricant formulators to classify additives as either organic or inorganic additives. This is somewhat misleading, since generally they are all organic molecules in the true sense of the word to ensure solubility in lubricants. The distinction arises in the particular chemical groups that are used to provide boundary lubrication.

### Organic Boundary Lubricants

Organic boundary lubricants, also referred to simply as boundary lubricants, are typically fatty acids and esters. As discussed further in Chapter 4, an ester is a compound of an organic acid and an alcohol. Thus, these two classes of lubricant behave similarly, since the esters break down and release the acid under elevated temperature. The effectiveness of fatty acid content in a lubricant is shown in Table 1.1. Both acids and esters are long chain molecules with a polar end that bonds to metal surfaces, and therefore provides some protection against direct contact between asperities.

There is evidence that the effectiveness of a boundary lubricant depends on its chain length. Figure 1.10a shows some results from Bowden and Tabor

Table 1.1: Fatty acids in oil as lubricants. [*From Dorinson and Ludema (1985).*]

Speed, cm/s	Coefficient of friction				
	Stearic acid, mol/1000 g		Lauric acid, mol/1000 g		
0.017	0.126	0.078	—	—	—
0.034	0.131	0.085	0.141	0.116	0.109
0.051	0.132	0.088	0.145	0.123	0.115
0.085	0.133	0.091	—	0.126	0.120
0.169	0.135	0.094	—	0.130	0.126
0.254	—	0.095	—	—	—

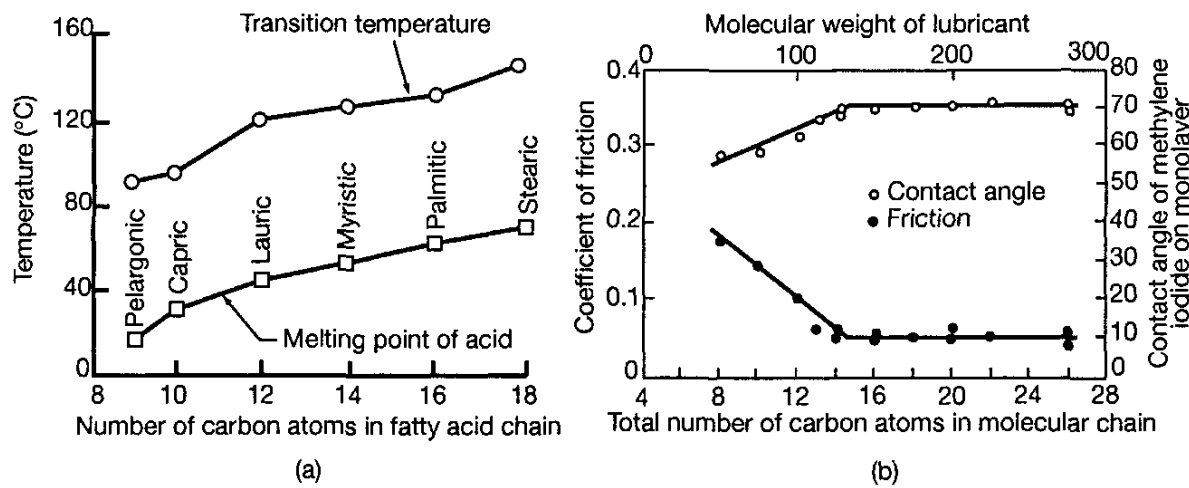


Figure 1.10: Effect of chain length on the effectiveness of a boundary lubricant. (a) Critical temperature as a function of chain length [From Bowden and Tabor (1950)]; (b) friction coefficient as a function of chain length. [From Zisman (1959).]

(1950), showing a decrease in friction coefficient with an increase in the molecular weight of a paraffinic hydrocarbon or a fatty acid. Figure 1.10b shows results from Zisman (1959), where friction decreases to a threshold value when there are approximately fifteen carbon atoms in the molecular chain. This suggests that the effectiveness of a boundary lubricant can be improved by increasing its molecular weight, but that there is a limit to this trend.

There is some evidence that organic boundary lubricants will stack up in multilayers, but the mechanisms are still not well understood. For example, it is possible to study the effect of multilayers through the Langmuir-Blodgett (L-B) technique, wherein an insoluble monolayer on the surface of water is transferred to a solid through successive dippings. Bowden and Tabor (1950) examined the effects of stearic acid on a stainless steel surface slid against an unlubricated surface at 10 mm/s. Their results are shown in Figure 1.11 and demonstrate that the lubricating effectiveness increases with an increasing number of boundary films. As discussed by Bhushan (2002), such multilayers are not entirely equivalent to self-forming films, but did result in stearic acid films that were closely packed and regularly oriented with the polar group initially in the water surface and then transferred to the metal surface. The main drawback to boundary lubricants such as fatty acids and esters is that they tend to decompose at temperatures above 200°C and lose their effectiveness. Fatty acids and esters are sometimes called “oiliness additives” because of their effectiveness at low temperature.

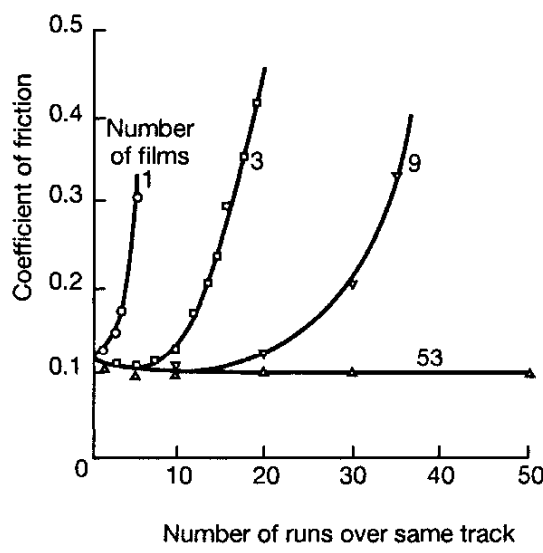


Figure 1.11: Effect of boundary lubricant thickness on friction for Langmuir-Blodgett films. [From Bowden and Tabor (1950).]

## Inorganic Boundary Lubricants

Inorganic boundary lubricants, also referred to as extreme pressure (EP) lubricants, are inorganic molecules that provide good lubrication at elevated temperatures and pressures. As discussed below, the dominant mechanisms for inorganic additives are temperature driven, so “extreme pressure” is a misnomer. The label is an artifact from the early experiments that demonstrated the value of inorganic additives for highly loaded bearings.

Inorganic additives traditionally involve compounds of chlorine, phosphorus, sulfur and iodine, although there has been a significant effort to eliminate these additives for environmental reasons and also because these materials are often carcinogenic. This has been difficult because of performance reasons, but also for practical reasons. For example, sulfur compounds are present in small amounts in petroleum-based lubricants and would require elaborate and expensive refining techniques for their removal.

Chlorine-containing materials react with metals. For example, copper alloys will form  $\text{CuCl}$  or  $\text{CuCl}_2$  on their surfaces, providing some protection against adhesive wear and low friction up to  $800^\circ\text{C}$ . Chromium and chromium-containing stainless steels will form chromium chloride,  $\text{CrCl}_3$ , which provides effective boundary lubrication up to around  $700^\circ\text{C}$ .

Sulfur and phosphorus are common additives for iron and steel. They form complex compounds, as will be discussed later, and provide good lubrication up to around  $400^\circ\text{C}$ . A common example is zinc dialkyl dithiophosphate (ZDDP), a very common additive for automotive engine oils. Iodine is of interest for titanium (forming  $\text{TiI}_2$ ), which works well up to around  $400^\circ\text{C}$ . Given the widespread use of titanium alloys in aerospace applications, it is not surprising that it has specialized use in this area.

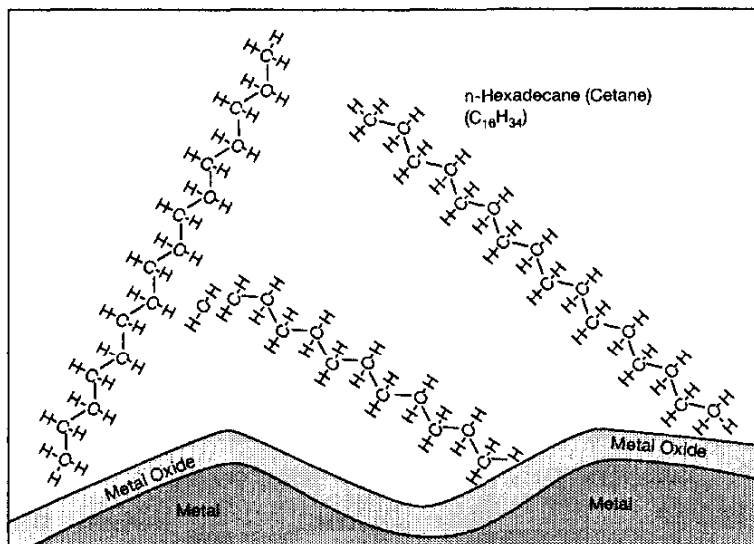


Figure 1.12: Physisorption of *n*-hexadecane molecules to a metal surface. [From Ku (1970).]

### Mechanisms of Boundary Lubrication

A number of surface film formation mechanisms have been described, a general review of which is given by Ku (1970). The most important of these are the following:

1. *Physical adsorption, or physisorption.* This occurs most under very mild sliding conditions, and is defined from a chemical standpoint as a bonding interaction that is less than 40 kJ/mol (Buckley 1981). Figure 1.12 shows a typical example of physisorption, where *n*-hexadecane molecules are attracted to a metal surface. Note that no special additives are needed for physisorption, and that all of the lubricants (petroleum or synthetic) have some potential for forming boundary films by this mechanism. Under light loads and low temperatures, this is sufficient to provide some protection, but these materials are easily displaced under more demanding applications.
2. *Chemical adsorption, or chemisorption.* In chemisorption, the bonding energies are much greater than in physisorption, and are in excess of 40 kJ/mol (Buckley 1981). Fatty acids can react with metals to form metal soaps which may or may not be attached to a surface. Figure 1.13 shows stearic acid molecules adhering to an iron or iron oxide surface (through physisorption) and then bonding to the iron to form iron stearate. Notice that the iron remains in its lattice position on the surface, and the iron stearate is strongly attached to the surface. With polar and paraffinic (that is, linear) molecules, chemisorbed lubricants can be very closely packed on a surface.

The straight chain molecules such as stearic acid depicted in Fig. 1.13

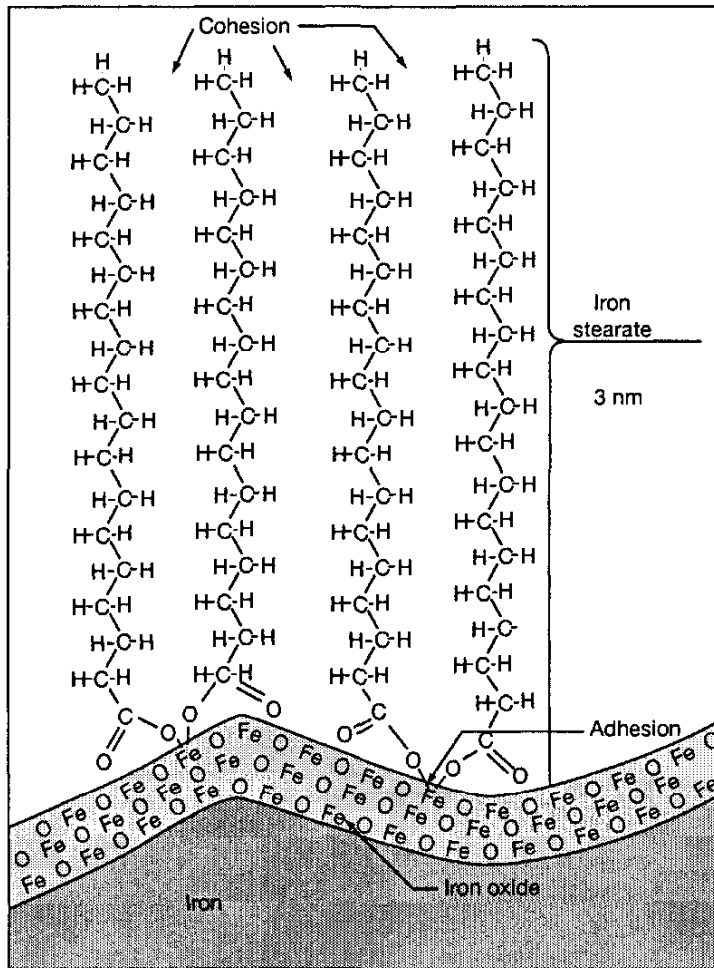


Figure 1.13: Chemisorption of stearic acid to an iron-containing surface to form iron stearate. [From Ku (1970).]

are common as boundary lubricants and are widely applied, as they are much more effective than ring or cross-linked molecules. There are a number of explanations for this trend, as discussed above. Clearly, these paraffinic molecules can pack efficiently on a surface, which is one feature desired in a boundary lubricant. Beltzer and Jahanmir (1988) noted that the most effective boundary lubricants combine a chemical reaction with the surface and a cohesive interaction between the lubricant species, a circumstance that is achieved by paraffinic acids.

3. *Chemical reactions not involving the substrate.* Especially with phosphorus-containing compounds, the solubility in lubricants is very low. The solution is to provide the phosphorus in a soluble carrier molecule, which degrades at elevated temperatures. The phosphorus then separates from the lubricant and plates a film onto the metal surface, usually in the form of phosphorus soaps.
4. *Chemical reactions involving the substrate.* Figure 1.14 depicts the forma-

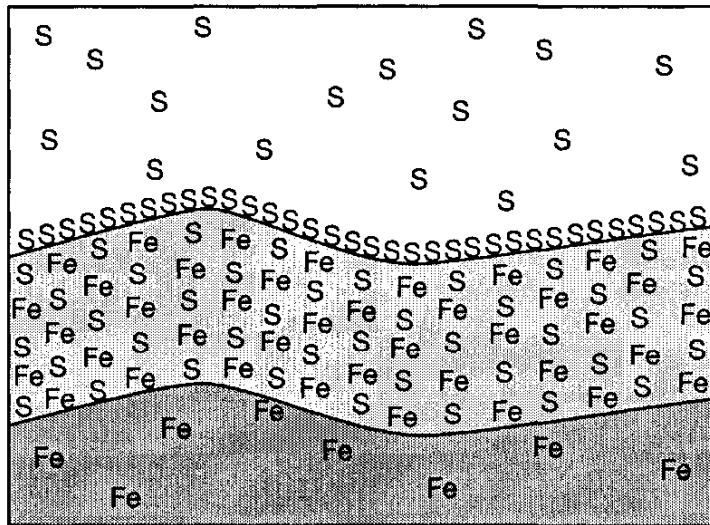


Figure 1.14: Formation of sulfide layers on steel, an example of boundary lubrication through chemical reactions involving the substrate.

tion of sulfide layers on steel. The lubricious sulfide compounds provide low friction and good adhesive wear resistance.

It should be noted that this mechanism can be considered to be active on almost all metal surfaces exposed to oxygen. For example, with iron or steel surfaces, a persistent oxide layer can exist to depths of up to 100  $\mu\text{m}$ ; this layer consists of the oxides  $\text{FeO}$ ,  $\text{Fe}_3\text{O}_4$ , and  $\text{Fe}_2\text{O}_3$  in varying concentrations through the thickness. Since the oxide layer prevents direct metal-to-metal contact in steel-on-steel contacts, it reduces wear and provides boundary lubrication through this mechanism.

Chemisorbed films are restricted to one molecular layer in thickness, whereas the films resulting from other mechanisms can be multiple layers. The mechanisms listed here are in order of increasing film stability and durability, that is, physisorbed layers are less durable than chemisorbed layers, which are less durable than chemical reaction films, etc.

## Chemical-Mechanical Effects

The methods through which a protective surface layer can be developed have been described above. An additional mechanism thought to occur in some circumstances are chemical-mechanical effects [Opalka, et al. (1999); Westwood and Lockwood (1982); Lockwood et al. (1989)]. There is some evidence that a reduction in surface energy is accompanied with a reduction in hardness (and hence surface flow strength) for many materials, including oxidized metals, and will also result in a reduction in wear [see, for example, Moore (1975)]. A reduction in surface hardness would result in reduced adhesive and abrasive friction, but could potentially have detrimental effects on wear.

Often it is difficult to separate the effects of chemical-mechanical effects,

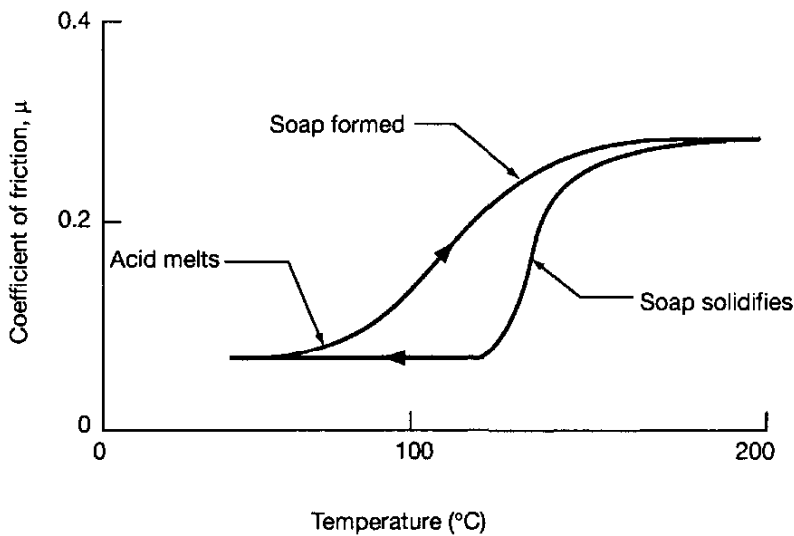


Figure 1.15: Thermal activation of a boundary lubricant during the initial thermal cycle.

which change the material properties just below the surface, to surface films, which leave the substrate unchanged. It should be noted that a film such as shown in Fig. 1.14 will display a chemical-mechanical effect and is not strictly a surface phenomenon.

### Thermal Activation

Many organic and inorganic boundary lubricants are ineffective until one or both surfaces in the tribopair have been elevated in temperature. For example, the observations shown in Fig. 1.15 have been noted for a ball bearing lubricated by a naphthenic mineral oil with an inorganic additive that is subjected to one thermal cycle. At initial low temperature, the friction is initially very high, but as the temperature increases, the inorganic additive forms a protective layer, eventually leading to lower friction and wear coefficients. Upon cooling, and indeed during the next thermal cycle, the protective film that has been formed is still present and good lubrication persists. Thus, an inorganic additive becomes effective only after exposed to elevated temperatures, a phenomenon referred to as “thermal activation”.

Similar effects can be seen with organic additives. This is usually attributed to the formation of a soap at elevated temperatures, which solidifies and adheres to the metal surface as temperature is reduced. The soap persists for subsequent thermal cycles, and therefore an effective boundary lubricant can be maintained at higher temperatures.

### 1.3.5 Partial Lubrication

If the pressures in elastohydrodynamically lubricated machine elements are too high or the running speeds are too low, the lubricant film will be penetrated. Some contact will take place between the asperities, and partial lubrication (sometimes referred to as “mixed lubrication”) will occur. The behavior of the conjunction in a partial lubrication regime is governed by a combination of boundary and fluid film effects. Interaction takes place between one or more molecular layers of boundary-lubricating films. A partial fluid film lubrication action develops in the bulk of the space between the solids. The average film thickness in a partial lubrication conjunction is less than 1 and greater than 0.01  $\mu\text{m}$ .

It is important to recognize that the transition from elastohydrodynamic to partial lubrication does not take place instantaneously as the severity of loading is increased, but rather a decreasing proportion of the load is carried by pressures within the fluid that fills the space between the opposing solids. As the load increases, a larger part of the load is supported by the contact pressure between the asperities of the solids. Furthermore, for conformal surfaces the regime of lubrication goes directly from hydrodynamic to partial lubrication.

### 1.3.6 Stribeck Curve

A useful concept for the understanding of the role of different regimes of lubrication is the Stribeck curve as shown in Fig. 1.16 (Stribeck, 1902). Historically, the Stribeck curve was first widely disseminated because of Stribeck’s systematic and definitive experiments that explained friction in journal bearings, a topic that had been the source of considerable confusion. The ordinate in Fig. 1.16 is the coefficient of friction under steady state conditions. The abscissa in Fig. 1.16 is a dimensionless number, sometimes referred to as the Hersey number, and is given as

$$H_s = \frac{\eta\omega}{p} \quad (1.5)$$

where

$\eta$  = absolute viscosity, Pa·s

$\omega$  = rotational speed, rps

$p$  = pressure, Pa

A high Hersey number usually means a relatively thick lubricant film, whereas a small number results in a very thin film. The regimes of lubrication have been indicated on Fig. 1.16 and can be inferred from the friction behavior of the bearing system. At an extremely low Hersey number, no real lubricant film can develop and there is significant asperity contact, resulting in high friction. This high friction value is persistent with increasing Hersey number until a first threshold value is reached. This represents the dominance of boundary lubrication in determining load transfer and friction between surfaces. As the

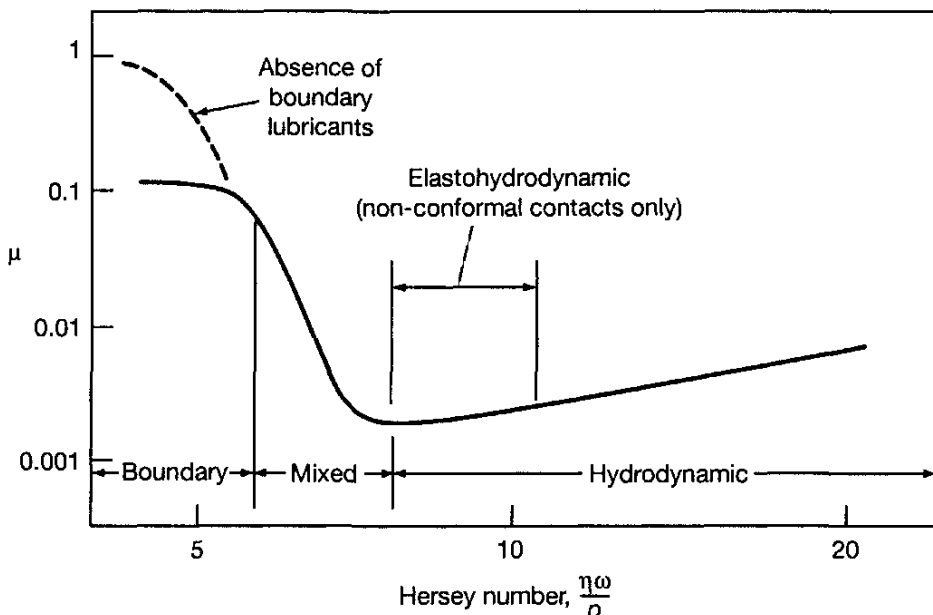


Figure 1.16: A Stribeck curve, showing the effects of Hersey number ( $\eta\omega/p$ ) on friction coefficient.

Hersey number increases, a noticeable and rapid decrease in friction values is observed. This is explained by an increasing lubricant film thickness and shared load support between the surface asperities and the pressurized liquid lubricant present in the conjunction. In this regime, widely varying friction values can be measured and are strongly dependent on operating conditions. With a further increase in Hersey number, friction reaches a lower plateau value, corresponding to the onset of hydrodynamic lubrication. At this point, the surfaces are effectively separated by the liquid lubricant, and asperity contact has negligible effect on load support and friction.

Figure 1.16 shows a slight increase in friction with respect to Hersey number in the hydrodynamic regime. This is a common occurrence for certain bearing geometries, such as journal bearings, where film thickness is limited by geometric influences and not operating conditions. Increased friction can be attributed to increased redundant work in the lubricant or to increases in shear strength, but these are seen to be relatively minor effects. Similarly, the plateau value of friction in the boundary regime may not be present if the lubricant does not contain the proper chemistry, and the friction may continue increasing with decreasing film thickness.

A further distinction is often made between elastohydrodynamic and full film lubrication in a Stribeck curve. This is useful for some bearing types, gears or cams, but it should be recognized that conformal contacts do not encounter elastohydrodynamic lubrication. Therefore, this regime may or may not be identified in the Stribeck curve, depending on the source.

## 1.4 Closure

In this chapter conformal and nonconformal surfaces were defined. Conformal surfaces fit snugly into each other with a high degree of geometric conformity so that the load is carried over a relatively large area and the load-carrying surface area remains essentially constant as the load is increased. Nonconformal surfaces do not geometrically conform to each other well and have small lubrication areas. The lubrication area enlarges with increasing load but is still small in comparison with the lubrication area of conformal surfaces.

The development of understanding of a lubricant's physical and chemical action within a lubricated conjunction was briefly traced, and four lubrication regimes were described: hydrodynamic, elastohydrodynamic, partial, and boundary. These are most clearly demonstrated through a Stribeck curve. Hydrodynamic lubrication is characterized by conformal surfaces. The lubricating film is thick enough to prevent the opposing solids from coming into contact. Friction arises only from the shearing of the viscous lubricant. The pressures developed in hydrodynamic lubrication are low (usually less than 5 MPa) so that the surfaces may generally be considered rigid and the pressure-viscosity effects are small. Three modes of pressure development within hydrodynamic lubrication were presented: slider, squeeze, and external pressurization. For hydrodynamic lubrication with sliding motion the minimum film thickness is quite sensitive to load, being inversely proportional to the square root of the normal applied load.

Elastohydrodynamic lubrication is characterized by nonconformal surfaces, and again there is no asperity contact of the solid surfaces. Two modes of elastohydrodynamic lubrication exist: hard and soft. Hard EHL is characterized by metallic surfaces, and soft EHL by surfaces made of elastomeric materials. The pressures developed in hard EHL, are high (typically between 0.5 and 3 GPa) so that elastic deformation of the solid surfaces becomes important as do the pressure-viscosity effects of the lubricant. As with hydrodynamic lubrication, friction is due to the shearing of the viscous lubricant. The minimum film thickness for hard EHL is relatively insensitive to load because the contact area increases with increasing load, thereby providing a larger lubrication area to support the load. For soft EHL the elastic distortions are large, even for light loads, and the viscosity within the conjunction varies little with pressure because the pressures are relatively low and the elastic effect predominates. Both hydrodynamic and elastohydrodynamic lubrication are fluid film lubrication phenomena in that the film is thick enough to prevent opposing solid surfaces from coming into contact.

In boundary lubrication considerable asperity contact occurs, and the lubrication mechanism is governed by the physical and chemical properties of thin surface films that are of molecular proportion (from 1 to 10 nm). The frictional characteristics are determined by the properties of the solids and the lubricant film at the common interfaces. Partial lubrication (sometimes referred to as "mixed lubrication") is governed by a mixture of boundary and fluid film

effects. Most of the scientific unknowns lie in this lubrication regime.

## 1.5 Problems

- 1.1 Describe at least three applications for each of the four lubrication regimes.
- 1.2 Describe the differences between conformal and nonconformal surfaces.
- 1.3 Determine which of the following contact geometries is conformal and which is non-conformal:
  - (a) Meshing gear teeth
  - (b) Ball and inner race of a ball bearing
  - (c) Journal bearing
  - (d) Railway wheel and rail contact
  - (e) Car tire in contact with the road
  - (f) Egg and egg cup
  - (g) Eye and socket
  - (h) Golf ball and club
  - (i) Human hip joint
- 1.4 A hydrodynamic journal bearing is loaded with a normal load  $w_z$  and rotating with a surface velocity  $u_b$ . According to Eq. (1.1) find how much higher rotational speed the bearing needs to maintain the same minimum film thickness if the load  $w_z$  is doubled.
- 1.5 A ball bearing lubricated with a mineral oil runs at 3000 rpm. The bearing is made of AISI 52100 steel and is loaded to a medium-high level. Find how much thinner the oil film will be if the load is increased 10 times. How much must the speed be increased to compensate for the higher load while keeping the oil film constant?

## References

- Beerbower, A. (1972): *Boundary Lubrication*. GRU.IGBEN.72, Report on Scientific and Technical Application Forecasts (Avail. NTIS, AD-747336).
- Beltzer, M., and Jahanmir, S. (1988): Effect of Additive Molecular Structure on Friction, *Lubrication Science*, v. 1, pp. 3-26.
- Bhushan, B., (2002) *Introduction to Tribology*. New York, John Wiley & Sons.
- Bowden, F.P., and Tabor, D.,(1950) *Friction and Lubrication of Solids*, Part I. Oxford (UK), Clarendon Press.
- Buckley, D.H., (1981) *Surface Effects in Adhesion, Friction, Wear, and Lubrication*. *Tribology Series* 5. New York, Elsevier.

- Department of Education and Science, Great Britain (1966): Lubrication (Tribology), Education and Research; A Report on the Present Position and Industry's Needs. HMSO, London.
- Dorinson, A., and Ludema, K.C., (1985) *Mechanics and Chemistry in Lubrication*. *Tribology Series 9*, New York, Elsevier.
- Dowson, D. (1998): *History of Tribology*, 2nd ed. Professional Engineering Publishing. London and Bury St. Edmunds, UK.
- Hamrock, B. J., and Anderson, W. J. (1983): *Rolling-Element Bearings*. NASA Ref. Publ. 1105.
- Hamrock, B. J., and Dowson, D. (1977): Isothermal Elastohydrodynamic Lubrication of Point Contacts. Part III-Fully Flooded Results, *J. Lubr. Technol.*, vol. 99, no. 2. pp. 264-276.
- Hardy, W.B., and Doubleday, I. (1922a): Boundary Lubrication-The Paraffin Series. *Proc. R. Soc. London Ser. A*, vol 100, Mar. 1, pp. 25-39.
- Hardy, W.B., and Doubleday, I., (1922b): Boundary Lubrication-The Temperature Coefficient. *Proc. R. Soc. London Ser. A*, vol 101, Sept. 1, pp. 487-492.
- Ku, P.M., (1970) *Interdisciplinary Approach to the Lubrication of Concentrated Contacts*, SP-237. Washington, D.C., NASA.
- Lockwood, F.E., and Bridger, K, (1987) Liquid Wetting on Metal Surfaces and the Heat of Immersion/Adsorption in Lubrication, *ASLE Trans*, v. 30, pp. 339-354.
- Lockwood, F.E., Bridger, K., and Hsu, S.M., (1989) Heats of Immersion, Friction and Wear of Base Oil Fractions, *Trib. Trans.*, v. 32, 1989, pp. 506-516.
- Moore, D.F. (1975): *Principles and Applications of Tribology*. Pergamon Press, New York.
- Opalka, S.M., Hector, L.G., Schmid, S.R., Reich, R.A., and Epp, J.A., (1999) Boundary Additive Effect on Abrasive Wear During Single Asperity Plowing of a 3004 Aluminum Alloy, *J. Tribology*, v. 121, pp. 384-393.
- Petrov, N.P. (1883): Friction in Machines and the Effect of the Lubricant. *Inzh. Zh. St. Petersburg*, vol 1, pp. 71-140; vol.2, pp. 227-279; vol. 3., pp. 377-436; vol. 4, pp. 535-564.
- Reynolds, O. (1886): On the Theory of Lubrication and Its Application to Mr. Beauchamp Tower's Experiments, Including an Experimental Determination of Viscosity of Olive Oil. *Philos. Trans. R. Soc. London Ser. A*, vol. 177, pp. 157-234.
- Stribeck, R., Characteristics of Plain and Roller Bearings. *Zeit. Ver. Deut. Ing.* v. 46, 1902, pp. 1341-1348, 1432-1438, 1463-1470.
- Tower, B. (1885): Second Report on Friction Experiments (Experiments on the Oil Pressure in a Bearing). *Proc. Inst. Mech. Eng.*, pp. 58-70.
- Westwood, A.R.C., and Lockwood, F.E., (1982) "Chemomechanical Effects in Lubrication," in Georges, J.M., ed., *Microscopic Aspects of Adhesion and Lubrication*, *Tribology Series 7*. New York, Elsevier.
- Williams, J.A., (1994) *Engineering Tribology*. Oxford, Oxford Science Publications, 1994

Zisman, W.A.,(1959) "Durability and Wettability Properties of Monomolecular Films on Solids," in Davies, R., (ed.), *Friction and Wear*, Amsterdam, Elsevier, pp. 110-148.

# Chapter 2

# Bearing Classification and Selection

## 2.1 Introduction

Design is a creative process aimed at finding a solution to a particular problem. In all forms of design a particular problem may have many different solutions, mainly because design requirements can be interpreted in many ways. For example, it may be desirable to produce:

- The cheapest design
- The easiest to build with available materials
- The most reliable
- The one that takes up the smallest space
- The one that is lightest in weight
- The best from any of a whole variety of possible standpoints

The task of the designer is therefore not clearcut, because he or she has to choose a reasonable compromise between these various requirements and then has to decide to adopt one of the possible designs that could meet this compromise. The process of bearing selection and design usually involves these steps:

1. Selecting a suitable type of bearing
2. Estimating a bearing size that is likely to be satisfactory
3. Analyzing bearing performance to see if it meets the requirements
4. Modifying the design and the dimensions until the performance is near to whichever optimum is considered the most important

The last two steps in the process can be handled fairly easily by someone who is trained in analytical methods and understands the fundamental principles of the subject. The first two steps, however, require some creative decisions to be made and for many people represent the most difficult part of the design process.

## 2.2 Bearing Classification

A bearing is a support or guide that locates one machine component with respect to others in such a way that prescribed relative motion can occur while the forces associated with machine operation are transmitted smoothly and efficiently. Bearings can be classified in several ways: according to the basic mode of operation (rubbing, hydrodynamic, hydrostatic, or rolling element), according to the direction and nature of the applied load (thrust or journal), or according to geometric form (tapered land, stepped parallel surface, or tilting pad). There is much to be said for classification according to the basic mode of operation, with subdivisions to account for different geometric forms and loading conditions. That classification is used in this book.

### 2.2.1 Dry Rubbing Bearings

In dry rubbing bearings the two bearing surfaces rub together in rolling or sliding motion, or both, and are lubricated by boundary lubrication. Examples of dry rubbing bearings are unlubricated journals made from materials such as nylon, polytetrafluoroethylene, and carbon and diamond pivots used in instruments. The load-carrying and frictional characteristics of this class of bearings can be related directly to the basic contact properties of the bearing materials.

### 2.2.2 Impregnated bearings

In this type of bearing a porous material (usually metal) is impregnated with a lubricant, thus giving a self-lubricating effect. The porous metal is usually made by sintering (heating to create a coherent mass without melting) a compressed metal powder (e.g., sintered iron or bronze). The pores serve as reservoirs for the lubricant. The load-carrying and frictional characteristics of the bearing depend on the properties of the solid matrix and the lubricant in conjunction with the opposing solid. The lubricant may be a liquid or a grease.

In general, the application of impregnated bearings is restricted to low sliding speeds (usually less than 1 or 1.5 m/s), but they can carry high mean pressures (often up to 7 to 15 MPa). A great advantage of these bearings is that they are simple and cheap, just like rubbing bearings, and they are frequently used in low-speed or intermittent-motion situations such as automobile chassis, cams, and oscillating mechanisms.

Impregnated separators for small ball bearings such as those used in precision instruments are sometimes used as lubricant reservoirs for the rolling

elements when a minimum amount of lubricant is required. In this case the porous material is generally a plastic (e.g., nylon).

It is usually doubtful that the impregnated bearing operates in true hydrodynamic fashion owing to the small amount of lubricant that is present. The behavior can be described as partial hydrodynamic lubrication, therefore implying partial lubrication. The bearing's hydrodynamic performance can be analyzed by assuming that a full film exists in the clearance space and that the lubricant flow within the porous material is covered by Darcy's law as pointed out, for example, in Cameron (1976). Darcy's simple formula for porous bearings relates the pressure gradient to the flow within a porous material while neglecting inertial effects and assuming that there is no relative surface velocity. A simultaneous solution of the Reynolds equation and the flow equation for a porous matrix yields flow patterns, pressure distributions, and load-carrying capacities that can be used to construct design charts. Satisfactory design procedures, however, usually embody a considerable amount of experimental information and operating experience to supplement the hydrodynamic analysis. Difficulty in qualifying the separate actions that govern bearing behavior reflects the partial hydrodynamic operation of many bearings in this class.

### 2.2.3 Conformal Fluid Film Bearings

The opposing surfaces of hydrodynamic fluid film bearings are completely separated by a lubricant film. The lubricant may be a liquid or a gas, and the load-carrying capacity derived from the pressure within the lubricating film may be generated by the motion of the machine elements (self-acting or hydrodynamic bearings) or by external pressurization (hydrostatic) or hydrodynamic squeeze motion, or by a combination of these actions. In all cases the frictional characteristics of the bearings are governed by the laws of viscous flow. The load-carrying capacities are similarly dictated by hydrodynamic action, but the properties of the bearing materials have to be considered (e.g., the fatigue life or low friction properties) at extremely low speeds.

The methods of feeding lubricant to a conformal fluid film bearing vary considerably. At low speeds and modest loads a simple ring-oiler that draws oil up to the bearing from a reservoir by means of viscous lifting might suffice, but in many modern machines the oil is supplied to the bearing under pressure to ensure adequate filling of the clearance space. Externally pressurized, or hydrostatic, bearings require elaborate lubricant supply systems, and the lubricant enters the bearing under a pressure of the order of a megapascal. This type of bearing is particularly useful at high loads and low speeds or when film stiffness perpendicular to surface motion is important.

A simple subdivision of conformal fluid film bearings that accounts for the nature of the lubricant, the mode of operation, the direction of motion, the nature of the load, and the geometric form of the bearing is shown in Fig. 2.1.

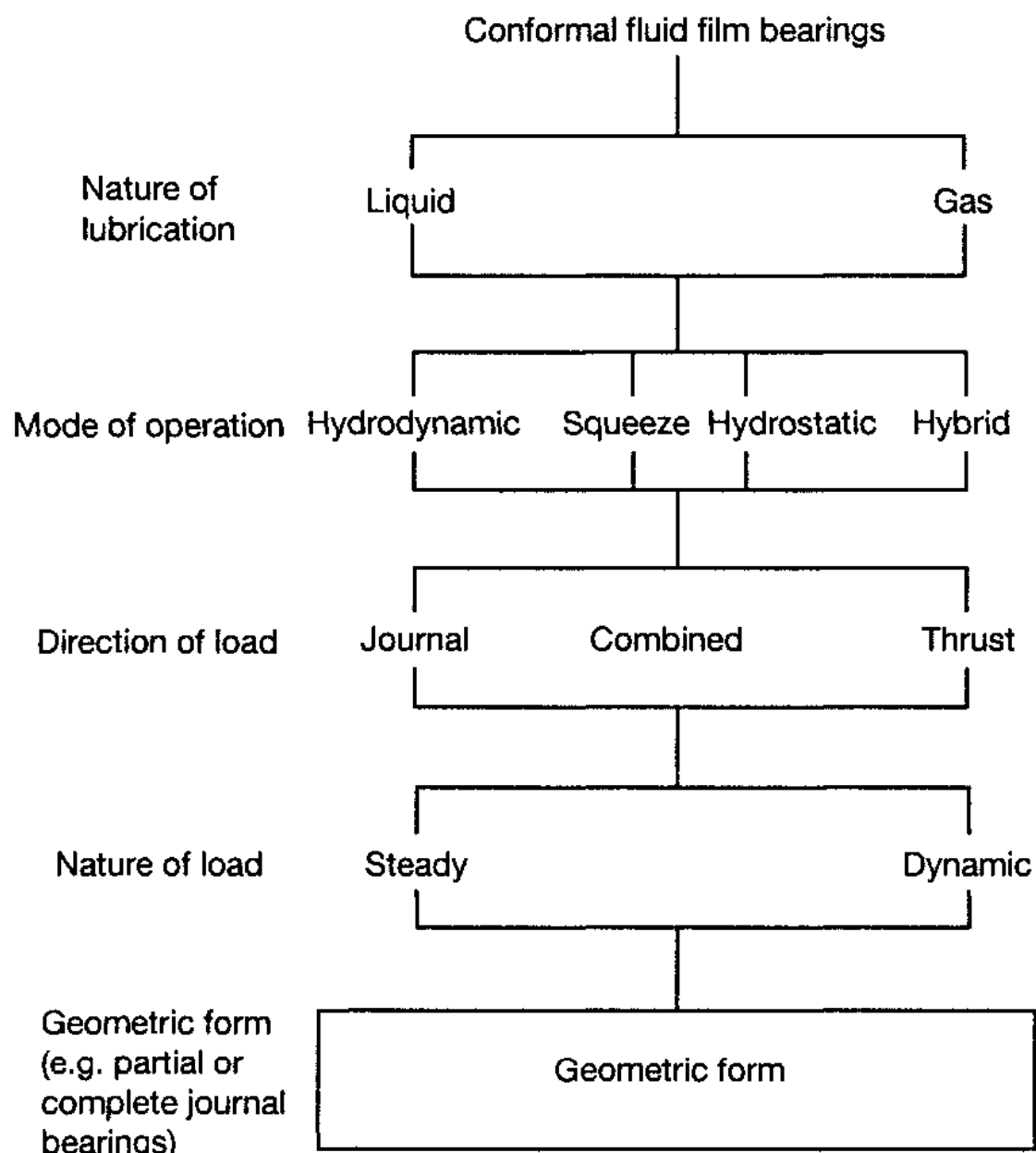


Figure 2.1: Divisions of conformal fluid film bearings.

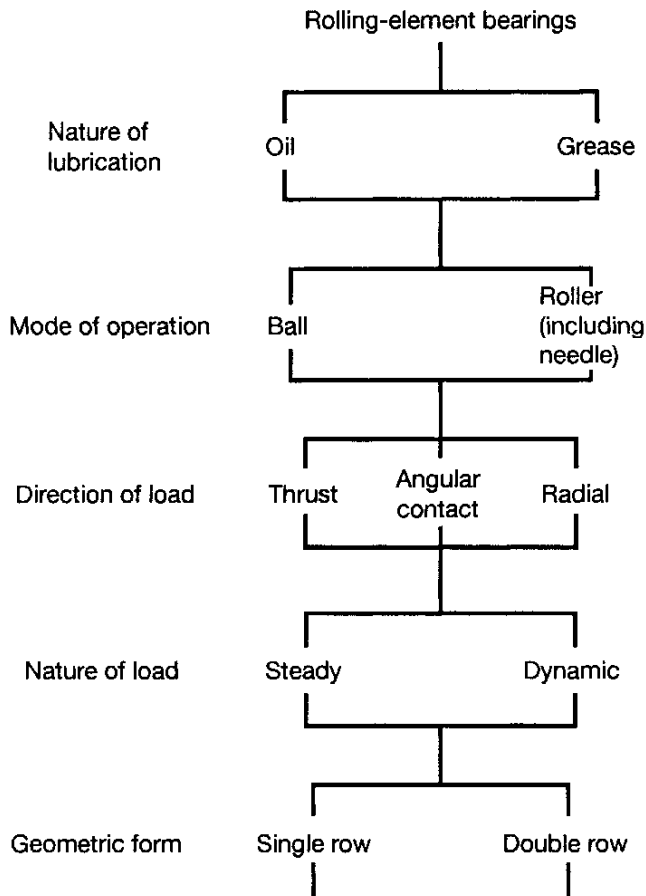


Figure 2.2: Divisions of rolling-element bearings.

## 2.2.4 Rolling-Element Bearings

The machine elements in rolling element bearings are separated by elements in predominately rolling motion. Figure 2.2 shows the subgrouping of rolling-element bearings. The rolling elements might be balls, rollers, or needles (rollers with large width-to-diameter ratios). Relative motion between the machine elements is permitted by replacing the sliding action with a motion that is mainly rolling. Normally some slipping, sliding, or spinning also takes place, and the friction characteristics are determined by the relative motion, the loading conditions, and the lubricant properties. Rolling-element bearings may be lubricated by liquids (mineral oils or synthetic lubricants) or greases. The lubricant (normally a grease) is sometimes sealed into the bearing assembly, or it may be applied in a mist of fine droplets. There are innumerable types of rolling-element bearings designed to meet the varied operating conditions encountered in industry.

## 2.3 Bearing Selection

The designer is often confronted with decisions on whether a rolling-element or hydrodynamic bearing should be used in a particular application. The following characteristics make rolling-element bearings more desirable than hydrodynamic (conformal fluid film) bearings in many situations: (1) low starting and good operating friction, (2) the ability to support combined radial and thrust loads, (3) less sensitivity to interruptions in lubrication, (4) no self-excited instabilities, (5) good low-temperature starting, and (6) the ability to seal the lubricant within the bearing. Within reasonable limits, changes in load, speed, and operating temperature have but little effect on the satisfactory performance of rolling-element bearings.

The following characteristics make rolling-element bearings less desirable than hydrodynamic (conformal fluid film) bearings: (1) finite fatigue life subject to wide fluctuations, (2) larger space required in the radial direction, (3) low damping capacity, (4) higher noise level, (5) more severe alignment requirements, and (6) higher cost. Each type of bearing has its particular strong points, and care should be taken in choosing the most appropriate type of bearing for a given application. Useful guidance on the important issue of bearing selection has been presented by the Engineering Sciences Data Unit (ESDU). The ESDU documents (1965, 1967) are excellent guides to selecting the type of journal or thrust bearing that is most likely to give the required performance when considering the load, speed, and geometry of the bearing.

Figure 2.3, reproduced from ESDU (1965), shows the typical maximum load that can be carried at various speed, for a nominal life of 10,000 h at room temperature, by various types of journal bearings on shafts of the diameters quoted. The heavy curves indicate the preferred type of journal bearing for a particular load, speed, and diameter and thus divide the graph into distinctive regions. The applied load and speed are usually known, and this enables a preliminary assessment to be made of the type of journal bearing most likely to be suitable for a particular application. In many cases the shaft diameter will already have been determined by other considerations, and Fig. 2.3 can be used to find the type of journal bearing that will give adequate load-carrying capacity at the required speed.

These curves are based on good engineering practice and commercially available parts. Higher loads and speeds or smaller shaft diameters are possible with exceptionally high engineering standards or specially produced materials. Except for rolling-element bearings the curves are drawn for bearings with widths equal to their diameters. A medium-viscosity mineral oil lubricant is assumed for the hydrodynamic bearings.

Considerations other than the load and speed may often have an overriding importance in bearing selection. Table 2.1 gives the advantages and limitations of various bearings in relation to environmental conditions and particular requirements. It is emphasized that Fig. 2.3 and Table 2.1 are only intended as guides.

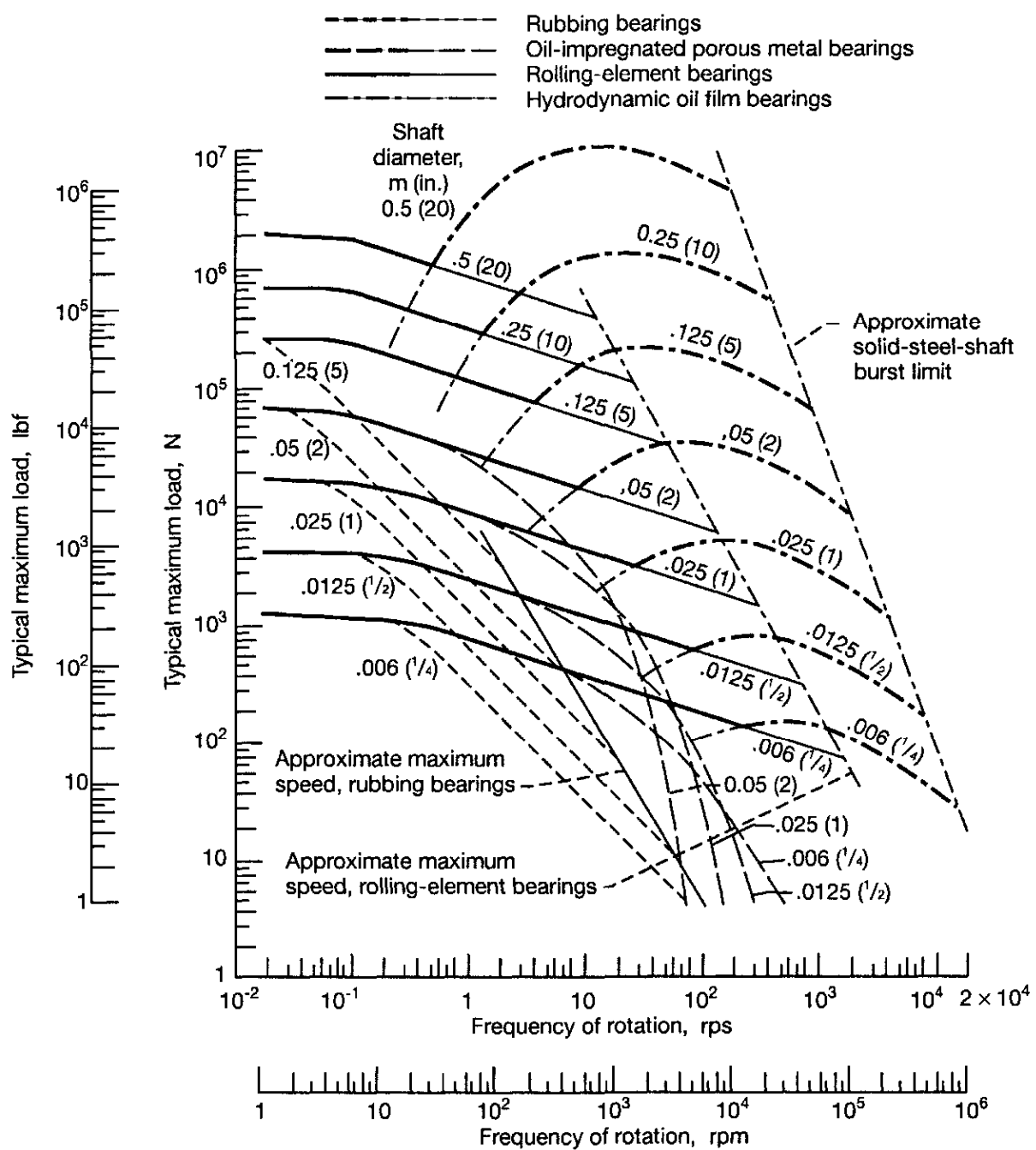


Figure 2.3: General guide to journal bearing type. Except for rolling-element bearings, curves are drawn for bearings with width equal to diameter. A medium-viscosity mineral oil is assumed for hydrodynamic bearings. [From ESDU (1965).]

Table 2.1: Advantages and limitations of journal bearings [(From ESDU 1965)]

Condition	General com- ments	Journal bearing type						
		Rubbing bearings	Oil- impregnated porous metal bearings	Rolling-element bearings	Hydrodynamic fluid film bearings	Hydrostatic fluid film bearings	Self-acting gas bear- ings	Externally pressurized gas bearings
High tem- perature	Attention to differential expansions and their effect on fits and clearances is necessary	Normally satis- factory de- pending on material	Attention to oxidation resistance of lubricant is necessary	Up to 100 °C no limitations; from 100 to 250°C stabilized bearings and special lubrication procedures are probably required	Attention to oxidation resistance of lubricant is necessary		Excellent	Excellent
Low tem- perature	Attention to differential expansions and starting torques is necessary		Lubricant may impose limitations; consideration of starting torque is necessary	Below -30 °C special lubricants are required; consideration of starting torque is necessary	Lubricant may impose limitations; consideration of starting torque is necessary	Lubricant may impose limitations	Excellent; thorough drying of gas is necessary	
External vibration	Attention to the possibility of fretting damage is necessary (except for hydrostatic bearings)	Normally satisfactory except when peak of impact load exceeds load-carrying capacity		May impose limitations; consult manufacturer	Satisfactory	Excellent	Normally satisfactory	Excellent
Space re- quirements		Small radial extent		Bearings of many different proportions; small axial extent	Small radial extent but total space requirement depends on the lubrication feed system		Small radial extent	Small radial extent, but total space requirement depends on the gas feed system
Dirt or dust		Normally satisfactory; sealing is advantageous	Sealing is important		Satisfactory; filtration of lubricant is important	Sealing im- portant	Satisfactory	
Vacuum		Excellent	Lubricant may impose limitations				Not normally applicable	Not applic- able when vacuum has to be maintained

Table 2.1: *Continued*

Condition	General comments	Journal bearing type						
		Rubbing bearings	Oil-impregnated porous metal bearings	Rolling-element bearings	Hydrodynamic fluid film bearings	Hydrostatic fluid film bearings	Self-acting gas bearings	Externally pressurized gas bearings
Simplicity of lubrication		Excellent		Excellent with self-contained grease or oil lubrication	Self-contained assemblies can be used with certain limits of load, speed, and diameter; beyond this, oil circulation is necessary	Auxiliary high pressure is necessary	Excellent	Pressurized supply of dry, clean gas is necessary
Availability of standard parts		Good to excellent depending on type	Excellent		Good	Not available		
Prevention of contamination product and surroundings		Improved performance can be obtained by allowing a process liquid to lubricate and cool the bearing, but wear debris may impose limitations	Normally satisfactory, but attention to sealing is necessary, except where a process liquid can be used as a lubricant			Excellent		
Frequent stop-starts		Excellent	Good	Excellent	Good	Excellent	Poor	Excellent
Frequent change of rotating direction			Generally good		Generally good			
Running costs		Very low			Depends on complexity of lubrication system	Cost of lubricant supply has to be considered	Nil	Cost of gas supply has to be considered

Table 2.1: *Concluded*

Condition	General comments	Journal bearing type						
		Rubbing bearings	Oil-impregnated porous metal bearings	Rolling-element bearings	Hydrodynamic fluid film bearings	Hydrostatic fluid film bearings	Self-acting gas bearings	Externally pressurized gas bearings
Wetness and humidity	Attention to possibility of metallic corrosion is necessary	Normally satisfactory depending on material	Normally satisfactory; sealing advantageous	Normally satisfactory, but special attention to sealing may be necessary	Satisfactory		Satisfactory	
Radiation		Satisfactory	Lubricant may impose limitations			Excellent		
Low starting torque		Not normally recommended	Satisfactory	Good	Satisfactory	Excellent	Satisfactory	Excellent
Low running torque								
Accuracy of radial location		Poor	Good			Excellent	Good	Excellent
Life		Finite but predictable			Theoretically infinite but affected by filtration and number of stops and starts	Theoretically infinite	Theoretically infinite but affected by filtration and number of stops and starts	Theoretically infinite
Combination of axial and load-carrying capacity		A thrust force must be provided to carry the axial loads	Most types capable of dual duty	A thrust force must be provided to carry the axial loads				
Silent running		Good for steady loading	Excellent	Usually satisfactory; consult manufacturer	Excellent	Excellent except for possible pump noise	Excellent	Excellent except for possible compressor noise

Table 2.2: Advantages and limitations of thrust bearings. [From ESDU (1967).]

Condition	General comments	Thrust bearing type						
		Rubbing bearings	Oil-impregnated porous metal bearings	Rolling-element bearings	Hydrodynamic fluid film bearings	Hydrostatic fluid film bearings	Self-acting gas bearings	Externally pressurized gas bearings
High temperature	Attention to differential expansions and their effect upon axial clearance is necessary	Normally satisfactory depending on material	Attention to oxidation resistance of lubricant necessary	Up to 100 °C no limitations; from 100 to 250 °C stabilized bearings and special lubrication procedures are probably required	Attention to oxidation resistance of lubricant is necessary		Excellent	
Low temperature	Attention to differential expansions and starting torques is necessary		Lubricant may impose limitations; consideration of starting torque is necessary	Below -30 °C special lubricants are required; consideration of starting torque is necessary	Lubricant may impose limitations; consideration of starting torque is necessary	Lubricant may impose limitations	Excellent; thorough drying of gas is necessary	
External vibration	Attention to the possibility of fretting damage is necessary (except for hydrostatic bearings)	Normally satisfactory except when peak of impact load exceeds load carrying capacity		May impose limitations; consult manufacturer	Satisfactory	Excellent	Normally satisfactory	Excellent
Space requirements		Small radial extent		Bearings of many different proportions are available	Small radial extent but total space requirement depends on the lubrication feed system		Small radial extent	Small radial total space requirement depends on gas feed system
Dirt or dust		Normally satisfactory; sealing advantageous		Sealing is important	Satisfactory; filtration of lubricant is important		Sealing important	Satisfactory
Vacuum		Excellent	Lubricant may impose limitations				Not normally applicable	Not applicable when vacuum has to be maintained

Table 2.2: *Continued.*

Condition	General comments	Thrust bearing type								
		Rubbing bearings	Oil-impregnated porous metal bearings	Rolling-element bearings	Hydrodynamic fluid film bearings	Hydrostatic fluid film bearings	Self-acting gas bearings	Externally pressurized gas bearings		
Wetness and humidity	Attention to possibility of metallic corrosion is necessary	Normally satisfactory depending on material	Normally satisfactory; sealing advantageous	Normally satisfactory, but special attention to sealing is perhaps necessary	Satisfactory					
Radiation		Satisfactory	Lubricant may impose limitations				Excellent			
Low starting torque		Not normally recommended	Satisfactory	Good	Satisfactory	Excellent	Satisfactory	Excellent		
Low running torque					Satisfactory		Excellent			
Accuracy of radial location		Good				Excellent	Good	Excellent		
Life		Finite but can be estimated			Theoretically infinite but affected by filtration and number of stops and starts	Theoretically infinite	Theoretically infinite but affected by number of stops and starts	Theoretically infinite		
Combination of axial and load-carrying capacity		A journal bearing surface must be provided to carry the radial loads		Some types capable of dual duty	A journal bearing surface must be provided to carry the radial loads					
Silent running		Good for steady loading	Excellent	Usually satisfactory; consult manufacturer	Excellent	Excellent, except for possible pump noise	Excellent	Excellent, except for possible compressor noise		
Simplicity of lubrication		Excellent		Excellent with self-contained grease lubrication; with large sizes or high speeds, oil lubrication might be necessary	Self-contained assemblies can be used with certain limits of load, speed, and diameter; beyond this, oil circulation is necessary	Auxiliary high pressure is necessary	Excellent	Pressurized supply of dry, clean gas is necessary		

Table 2.2: *Concluded.*

Condition		General comments	Thrust bearing type					
			Rubbing bearings	Oil-impregnated porous metal bearings	Rolling-element bearings	Hydrodynamic fluid film bearings	Hydrostatic fluid film bearings	Self-acting gas bearings
Availability of standard parts		Good to excellent depending on type	Excellent		Good	Poor		
Prevention of contamination of product and surroundings		Performance can be improved by allowing a process liquid to lubricate and cool the bearing, but wear debris may impose limitations	Normally satisfactory, but attention to sealing is necessary, except where a process liquid can be used as a lubricant				Excellent	
Tolerance to manufacturing and assembly inaccuracies		Good		Satisfactory	Poor	Satisfactory	Poor	Satisfactory
Type of motion	Frequent start-stops	Excellent			Good	Excellent	Excellent	
	Unidirectional	Suitable						
	Bidirectional	Suitable			Some types are suitable	Suitable	Some types are suitable	Suitable
	Oscillatory				Unsuitable		Unsuitable	
Running costs		Very low			Depends on complexity of lubrication system	Cost of lubricant supply has to be considered	Nil	Cost of gas supply has to be considered

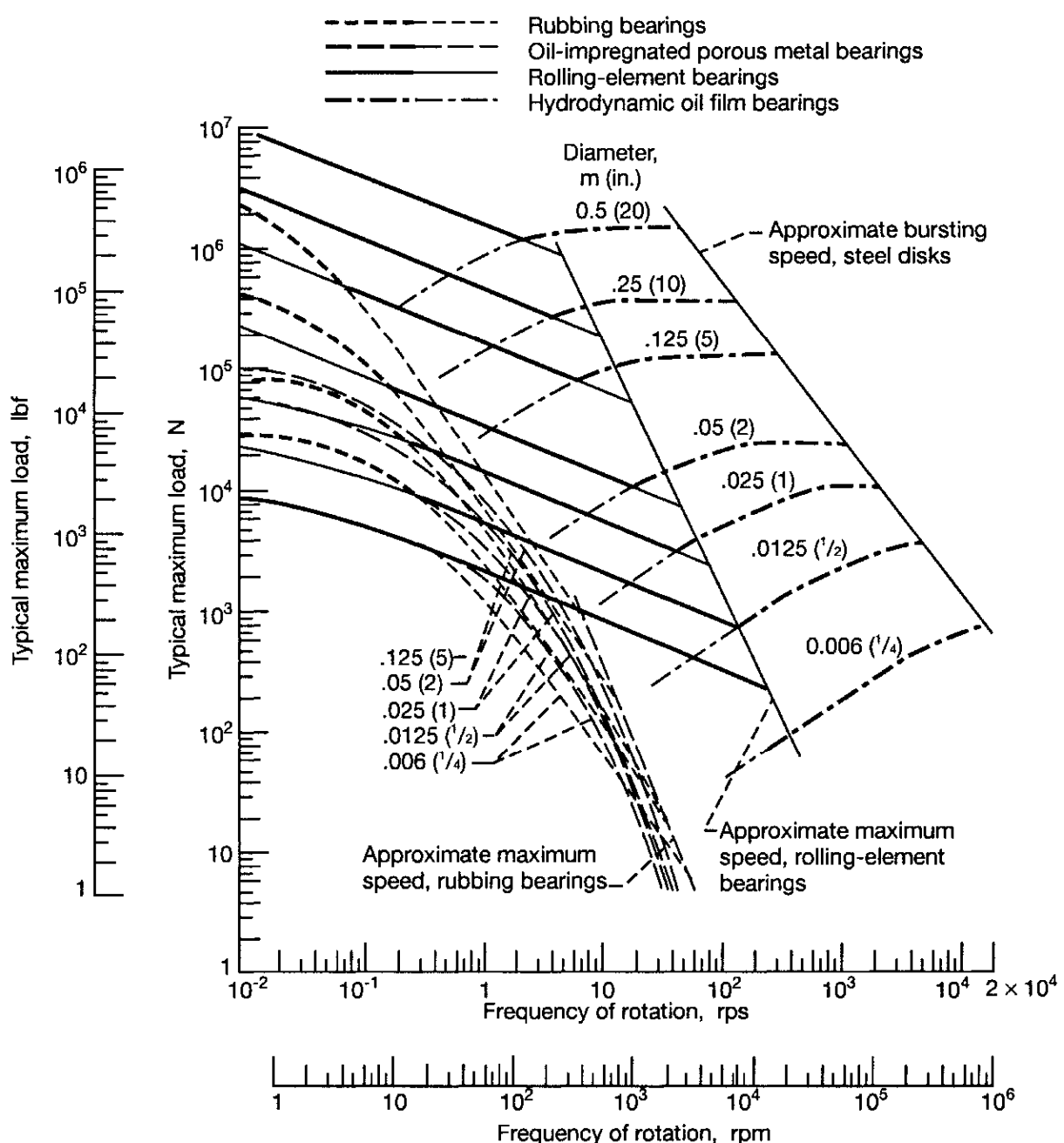


Figure 2.4: General guide to thrust bearing type. Except for rolling-element bearings, curves are drawn for typical ratios of inside diameter to outside diameter. A medium-viscosity mineral oil is assumed for hydrodynamic bearings. [From ESDU (1967).]

Similarly, Fig. 2.4, reproduced from ESDU (1967), shows the typical maximum load that can be carried at various speeds, for a nominal life of 10,000 h at room temperature, by various types of thrust bearings on shafts of the diameters quoted. The heavy curves again indicate the preferred type of bearing for a particular load, speed, and diameter and thus divide the graph into major regions. Considerations other than load and speed are given in Table 2.2 for thrust bearings.

## 2.4 Closure

This chapter began with a general discussion of the process of bearing design. The four primary steps used in bearing design are selecting a suitable type, estimating bearing size, analyzing performance, and modifying or fine-tuning. It was pointed out that the first two steps are the most difficult and require creative decisions, whereas the last two steps can be handled fairly easily by a person trained in analytical methods. After considering several options, it was decided that bearings would best be classified by considering their modes of operation. The four primary classes of bearing that were considered were dry or rubbing bearings, which use boundary lubrication if any; impregnated bearings, which use partial lubrication; rolling-element bearings, which use elastohydrodynamic lubrication; and hydrodynamic fluid film bearings, which use hydrodynamic lubrication. The Engineering Sciences Data Unit documents can be used as guides in selecting the type of journal or thrust bearing most likely to give the required performance when considering its load, speed, and geometry. Considerations other than load and speed are important in bearing selection. Thus, tables are presented that give the advantages and limitations of various bearings in relation to environmental conditions and particular requirements. It should be recognized that information on bearing selections given in this chapter is intended to be a guide to selecting a suitable type of bearing and to estimating a bearing size that is likely to be satisfactory.

## 2.5 Problems

- 2.1 Figures 2.3 and 2.4 show the relationship between load and speed for four different types of bearings. How would you use these figures to help you select the appropriate bearing for your particular application?
- 2.2 Suggest suitable types of bearing to meet the following situations: (a) High load, very low speed, very low friction; (b) Light load, very high speed, no liquid lubricant; (c) Light load, low speed, no liquid lubricant.
- 2.3 Explain why gas-lubricated bearings are appealing. Describe the limiting features of this type of bearing.

## References

- Cameron, A. (1976): *Basic Lubrication Theory*, 2d ed. Ellis Horwood Limited, Chichester, England.
- Engineering Sciences Data Unit (ESDU) (1965): General Guide to the Choice of Journal Bearing Type. Item 65007, Institution of Mechanical Engineers, London.
- Engineering Sciences Data Unit (ESDU) (1967): General Guide to the Choice of Thrust Bearing Type. Item 67033, Institution of Mechanical Engineers, London.

# Chapter 3

## Surface Topography

### Symbols

$\bar{b}$	intercept on $z$ axis, m	$z$	Cartesian coordinate in the direction of film, m
$\bar{d}$	difference in two methods of evaluating $z$ , m	$\bar{\alpha}$	skewness
$f$	friction force, N	$\bar{\beta}$	kurtosis
$h$	film thickness, m	$\Lambda$	dimensionless film parameter
$h_{\min}$	minimum film thickness, m	$\mu$	coefficient of sliding friction
$\ell^*$	bearing length, m	$\tilde{\rho}_k$	autocorrelation
$M_n$	$n$ th moment of distribution curve $\psi(z)$ about mean	$\bar{\sigma}$	standard deviation, m
$\bar{m}$	slope	$\tilde{\psi}$	probability density function, $\text{m}^{-1}$
$N$	number of measurements		
$R_a$	centerline average or arithmetic average, m		
$R_q$	root-mean-square (rms) surface roughness, m		
$R_t$	maximum peak-to-valley height, m		
$w_z$	normal load component, N	$a$	solid $a$
$x$	Cartesian coordinate in the direction of sliding, m	$b$	solid $b$
		$x, y, z$	coordinate

### Subscripts

### 3.1 Introduction

Increasing production speeds and new manufacturing methods, such as plasma cutting, spark erosion, chemical-mechanical polishing, and laser cutting, change the characteristics of machined surfaces. Requirements with regard to surface accuracy and surface refinement have also greatly increased. The importance of a fine-scale surface description is well demonstrated in tribology. The breakdown of lubrication layers of oil in engine cylinders or in bearings can be caused

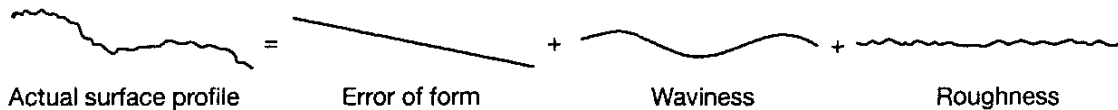


Figure 3.1: Geometric characteristics of solid surfaces [From Halling (1976).]

by improper microlevel surface shape.

Although bearing design theory relies heavily on fluid mechanics and kinematics, it is still ultimately a problem of two surfaces that are either in contact or separated by a thin fluid film. In either case the surface texture can be important in ensuring proper lubrication.

The first step in gaining insight into the lubrication of solid surfaces is to examine the surface profile, or topography. Smooth surfaces are not flat on an atomic scale. The roughness of manufactured surfaces used in lubrication is between 0.01 and 10  $\mu\text{m}$ , whereas typical atomic diameters are between 0.0001 and 0.001  $\mu\text{m}$ . Even a highly polished surface, when examined microscopically or with a profilometer, has an irregular nature. The surface consists of high and low spots. The high spots, or protuberances, are called "asperities."

Surface texture measurement and evaluation can be quite complex; only a few surface parameters and measurement issues are discussed here. Standardized nomenclature is contained in industry standards ASME B46.1 (ASME, 1995a) and ASME Y14.36M (ASME, 1995b).

A word of caution should be given that terms such as "rough", "fine", "smooth" and "super-smooth" should be avoided in describing the surface topography since the meaning is relative to the application being used. For example, a surface with  $R_q = 40 \text{ nm}$  is considered "very rough" by people working in the field of optics, whereas a  $R_q=40 \text{ nm}$  is considered "very smooth" for a machined surface.

## 3.2 Geometric Characteristics of Surfaces

The geometric characteristics, or texture, of surfaces as shown in Fig. 3.1 may conveniently be divided into three main categories:

1. *Error of form.* The surface deviates from a well-defined pattern because of errors inherent in the manufacturing process.
2. *Waviness.* Relatively long waves in a surface profile are often associated with unwanted vibrations that always occur in machine tool systems.
3. *Roughness.* Irregularities, excluding waviness and error of form, are inherent in the cutting and polishing process during production.

In the study of lubricated surfaces, roughness is the geometric variation that is generally of interest. Although often no sharp distinction can be drawn between

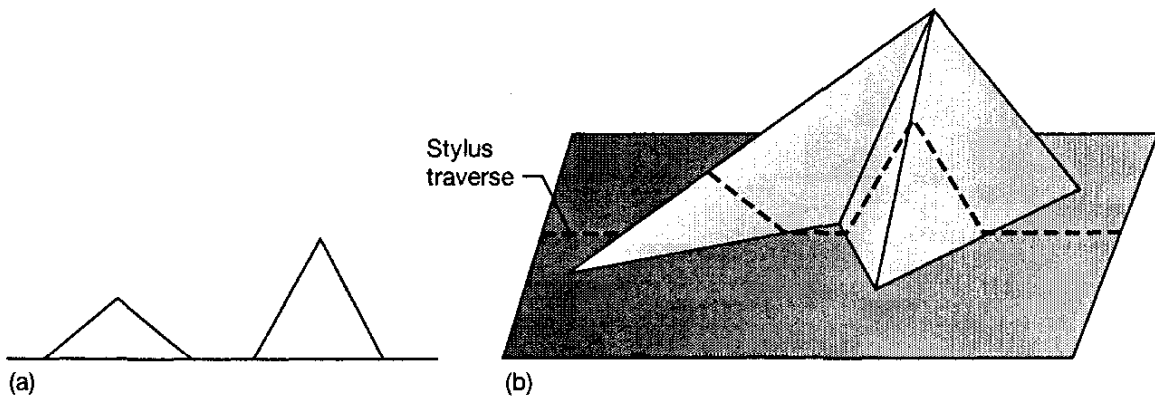


Figure 3.2: Difficulty in interpreting profilometer traces. (a) Surface profile; (b) surface asperity.

these categories, roughness simply concerns the horizontal spacing (wavelength) of the surface features. From a practical point of view, in characterizing surfaces used in tribology both the vertical direction (or amplitude parameter) and the horizontal direction (or wavelength) are important.

### 3.3 Contacting Measurement Methods

Two general classes of hardware are commonly used for measuring surface finish: contacting methods using stylus techniques and noncontacting methods. Contacting measurements are discussed in this section. Contacting measurements are based on transforming the vertical motion of a stylus tip as it traverses a surface into an electrical analog voltage. This voltage is then processed either by using analog circuitry or by converting it to digital information for processing. The method was introduced by Abbot and Firestone in 1933

#### 3.3.1 Stylus Profilometry

Stylus profilometry is by far the most common method of measuring surface roughness because of the flexibility and comparatively low cost of profilometers. The stylus is normally made of diamond and has a tip radius of  $2 \mu\text{m}$  and a static load of less than  $0.0007 \text{ N}$  ( $0.00256 \text{ oz}$ ). The tip radius is relatively large in comparison with the typical roughness. Therefore, it is often difficult to obtain a true picture of a surface from a stylus measurement. Features that appear to be asperity peaks on a single profile may in fact be local ridges on the flank of a true summit, as shown in Fig. 3.2. Moreover, many real surfaces of practical interest to tribologists have highly anisotropic surface textures. Thus, profiles taken in different traverse directions look quite different.

However, the main limitation of stylus measurements is the finite size of the stylus tip, which distorts the surface profile, as shown in Fig. 3.3, broadening peaks and narrowing valleys. The magnification in the vertical direction is

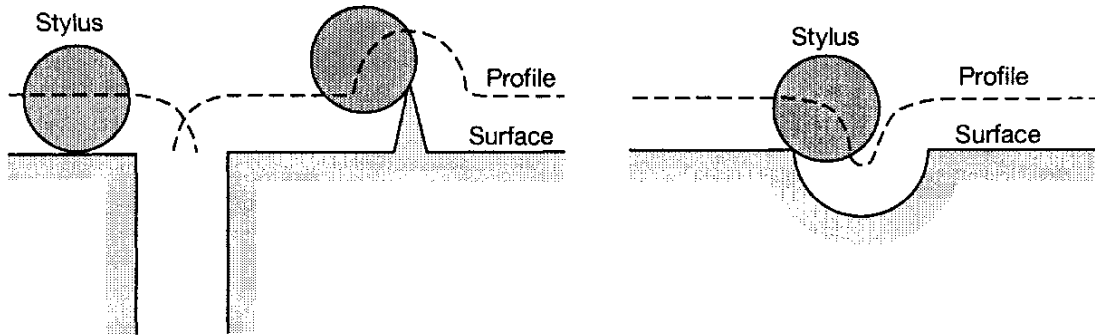


Figure 3.3: Error due to stylus radius.

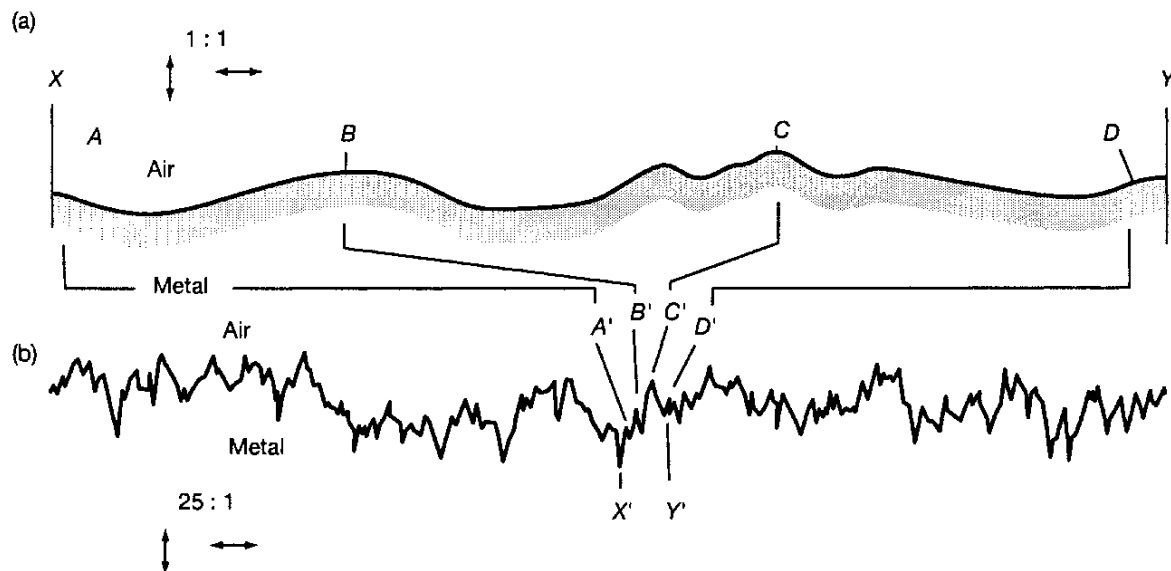


Figure 3.4: True (a) and compressed (b) profile. [From Thomas (1982).]

generally 100 to 100,000 and that in the horizontal direction is 10 to 5000. A typical ratio of vertical to horizontal magnification is 50:1. It is therefore important to take into account this difference in magnification. This is often not done, and thus a false impression of the nature of surfaces has become prevalent. Figure 3.4 attempts to illustrate this. In Fig. 3.4 the shape of a real surface is shown in the (a) portion of the figure and is compared with profilometer readings of the same surface in the (b) portion of the figure at a magnification ratio (vertical to horizontal) of 25:1.

Profilometers can measure single traces of surfaces, or else they can index across a surface to obtain a three dimensional contour.

### 3.3.2 Atomic Force Microscopy

Very smooth surfaces are difficult to characterize by standard stylus profilometry because they lack the vertical resolution and because of stylus size issues.

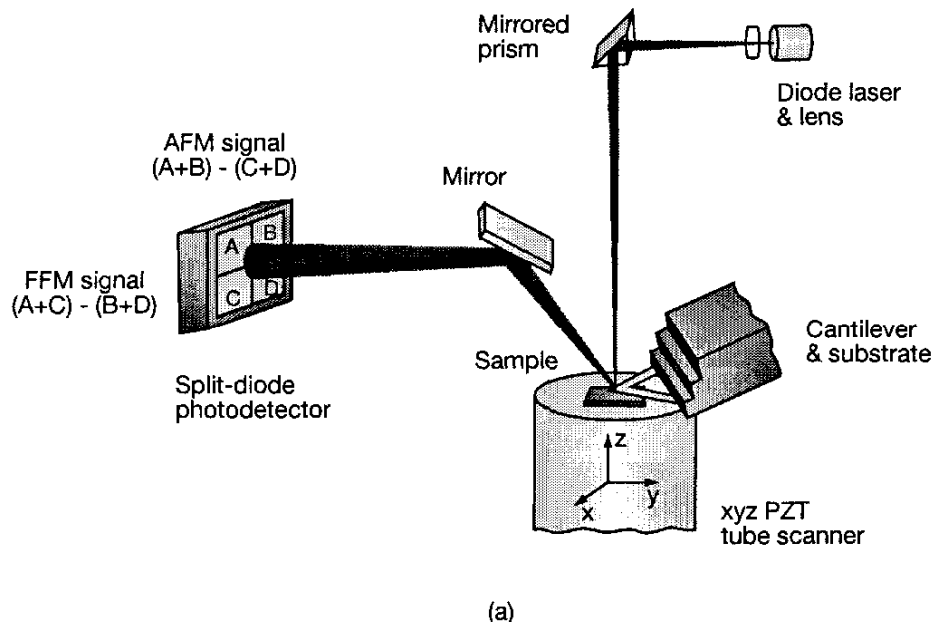
An instrument available for the characterization of three dimensional, exceptionally smooth surfaces is the atomic force microscope (AFM). There are a number of AFM designs, but each involves moving the cantilever or specimen in raster fashion and recording the height distribution of a surface. As shown in Fig. 3.5, a laser is focused onto the end of the cantilever and then reflected onto a series of four photodetectors. The position of the cantilever end can then be accurately measured by comparing the voltage registered by each photodetector.

There are two common modes for surface measurement in an AFM: contact mode and tapping mode. In contact mode, the sample and cantilever are displaced relative to one another and the associated cantilever displacement yields a surface profile. In tapping mode, the cantilever is vibrated to near its natural frequency, and it is placed close enough to the surface so that it taps the sample. The surface height profile is then recorded as the maximum vertical deflection of the cantilever. Typical cantilevers used in AFM surface measurements are shown in Fig. 3.5b. Further information regarding the utility of AFM operation can be found in Bhushan (1998, 2002).

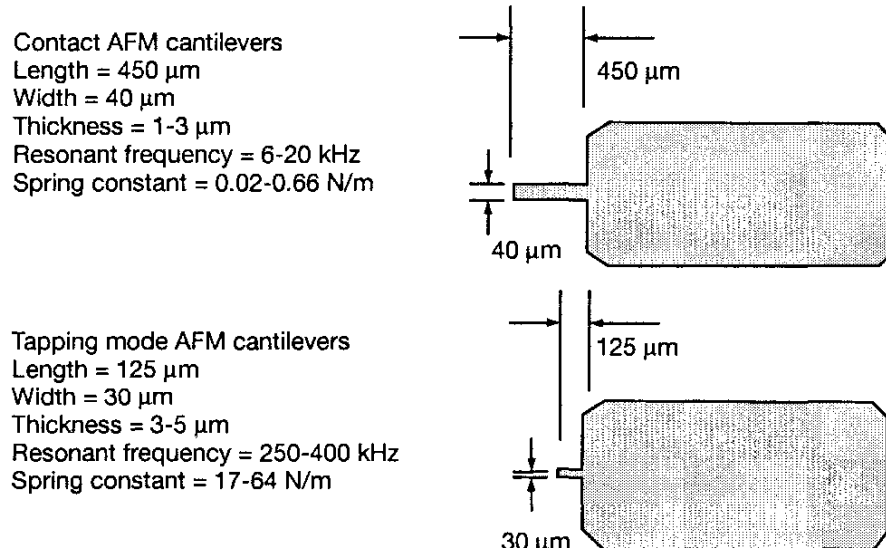
## 3.4 Noncontacting Measurement Devices

The noncontacting methods for determining the characteristics of surfaces use a number of different measurement principles and devices:

1. *Laser-based devices.* With these devices, a sample is placed under the sensor and is accurately positioned and rastered while the sensor transmits the height data to the measurement control unit. The sensor uses light focused from a laser diode onto the specimen surface. The reflected light is directed to a focus detector, which measures deviations from the ideal focus to within a few nanometers. The deviation in focus generates an error, which is used to refocus. The position of the objective represents an absolute measurement of the height.
2. *Pneumatic devices.* This method is based on the measurement of air leakage. A flat and finely finished measurement head has an orifice of air. Measuring the airflow when the head is placed on the surface indicates changes in surface roughness. Pneumatic devices provide a simple, inexpensive, portable, quick, and robust way of assessing surface roughness, well-suited for use in determining the quality of surfaces on the shop floor.
3. *Optical devices.* The intensity of reflected laser light defines the surface texture, producing an average over a surface area. The result is often called gloss, and attempts to correlate gloss to surface roughness have been only partially successful. This method is not well established in terms of the number of people who use it routinely.



(a)



(b)

Figure 3.5: Schematic illustration of an atomic force microscope. (a) Principle of operation for an AFM. (b) Typical cantilevers for use in an atomic force microscope. [Source: *Digital Instruments Corp.*]

4. *Electron microscope devices.* This method offers better resolution and depth of field than optical methods, chiefly because of the extremely short wavelength of electron microscope beams in comparison with that of light. Sherrington and Smith (1988) point out the two types of electron microscopy:

- (a) *Transmission electron microscopy* (TEM). Electrons are incident on a thin specimen (less than 10 nm thick) that deflects and scatters the electrons as they pass through it. A lens system magnifies and focuses scattered electrons to form an image on a screen or photographic film. To examine the surface of a metal component by TEM, it is usually necessary to fabricate a replica of the specimen surface. TEM is typically able to resolve features down to a separation of around 0.3 nm and has been used to study the changes in surface structure during wear.
- (b) *Reflection electron microscopy* (REM). Electrons are scattered from the surface of the specimen and strike a collector, which generates an electrical signal. This signal is subsequently processed and used to form an image representing the specimen surface on a monitor screen. Scattered electrons are produced by a beam of finely focused electrons that scans the specimen in a raster pattern, a process called "scanning electron microscopy" (SEM). Scanning electron microscopes can be adjusted to have a maximum resolution of about 10 nm, a little less than that available in TEM. However, this disadvantage is compensated for by the fact that specimen preparation is considerably easier.

Besides these noncontacting devices, scanning tunneling microscopy is also available but beyond the scope of this book. Sherrington and Smith (1988) give an excellent description of this device as well as describe in general the modern measurement techniques used in determining the characteristics of tribological surfaces.

Several methods of measuring surface topography have been described in this section as well as in the preceding section. Of these methods the stylus measurement device is the most widely used. Table 3.1, obtained from Sherrington and Smith (1988) and Stout et al. (1993), summarizes the specifications of a number of the devices described in this section as well as in the preceding section. From this table the resolution, the depth of field, and the measurable area are described for four different devices.

## 3.5 Reference Lines

In computing the parameters that define the surface texture all height measurements are made from some defined reference line. Several methods have been used. They are summarized below and shown graphically in Fig. 3.6.

Table 3.1: Summary of typical specifications of devices used for surface topography measurement. From Sherrington and Smith (1988).

Device	Resolution				Vertical measurement range or depth of field		Measurable area	
	Lateral		Vertical		At lowest resolution	At highest resolution		
	Lowest	Highest	Lowest	Highest				
Stylus instrument	a	a	0.5 $\mu\text{m}$	0.25 nm	500 $\mu\text{m}$	0.25 $\mu\text{m}$	Depends on transverse length; typically a few millimeters	
Optical light microscope	2.5 $\mu\text{m}$	0.1 $\mu\text{m}$	b	b	42 $\mu\text{m}$	0.04 $\mu\text{m}$	Depends on magnification	
Transmission electron microscope	2.5 nm	0.5 nm	c	c	400 nm	80 nm	Depends on magnification	
Scanning electron microscope	5 $\mu\text{m}$	10 nm	d	d	1 mm	2 $\mu\text{m}$	Depends on magnification	

<sup>a</sup> Not easily defined.

<sup>b</sup> Not applicable.

<sup>c</sup> Approximately the same as the lateral resolution.

<sup>d</sup> Not available.

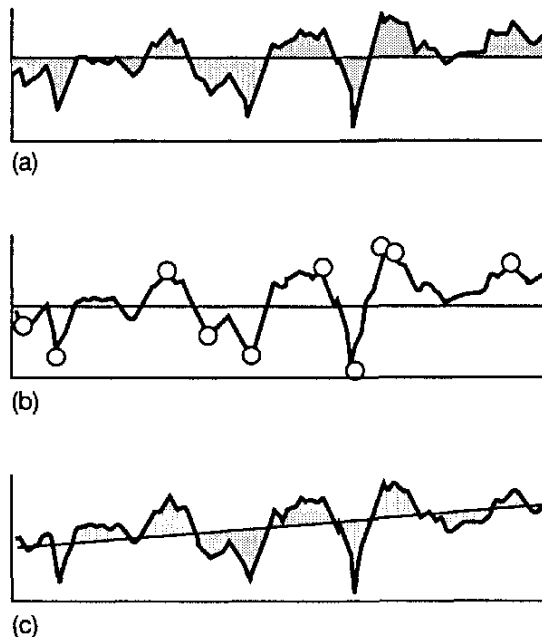


Figure 3.6: Comparison of three types of reference line: (a) M system; (b) ten-point average; (c) least squares.

### 3.5.1 Mean, or M System

The mean, or M system, method is based on selecting the mean line as the centroid of the profile. Thus, the areas above and below this line are equal. If for discrete profiles the area of each profile is a rectangle, this method turns out to be simply finding the average of the measured heights. This method gives a “horizontal” reference that does not compensate for errors of form or tilt.

### 3.5.2 Ten-Point Average

The ten-point average method is based on finding the five highest peaks and the five lowest valleys. The average of these 10 points gives the reference line. For deeply pitted surfaces this method can lead to a reference line that is below the major surface features.

### 3.5.3 Least Squares

The least-squares method is based on postulating a sloping reference line instead of a horizontal line as is the case for the M system. Therefore, the major advantage of this approach is that it can be used to compensate for the linear error of form, or tilt. The following will attempt to describe mathematically the least-squares reference lines. From the equation of a line,

$$z = \bar{m}x + \bar{b}$$

where

$\bar{m}$  = slope

$\bar{b}$  = intercept on  $z$  axis, m

Given a set of points  $P_1(x_1, z_1), P_2(x_2, z_2), \dots, P_n(x_n, z_n)$  corresponding to each value of  $x$ , consider two values of  $z$ : (1)  $z$  measured and (2)  $z$  obtained from  $\bar{m}x + \bar{b}$ . Call the difference  $\bar{d}$  such that

$$\bar{d}_1 = [z_1 - (\bar{m}x_1 + \bar{b})], \dots, \bar{d}_n = [z_n - (\bar{m}x_n + \bar{b})]$$

The set of all deviations gives a picture of how well the observed data fit a line. If  $\sum_{i=1}^n \bar{d}_i^2 = 0$ , the fit is perfect. This never occurs in real situations, and that is where the method of least squares comes in.

Not only is it important to establish a reference line or mean line in the  $z$  direction, it is also important to establish a sampling length or distance in the  $x$  direction that adequately differentiates between roughness and waviness.

$$\bar{f}(\bar{m}, \bar{b}) = \sum_{i=1}^n \bar{d}_i^2$$

or

$$\bar{f}(\bar{m}, \bar{b}) = (z_1 - \bar{m}x_1 - \bar{b})^2 + (z_2 - \bar{m}x_2 - \bar{b})^2 + \dots + (z_n - \bar{m}x_n - \bar{b})^2$$

Finding the values of  $\bar{m}$  and  $\bar{b}$  that give the smallest  $\bar{f}(\bar{m}, \bar{b})$  requires finding values of  $\bar{m}$  and  $\bar{b}$  that satisfy

$$\frac{\partial \bar{f}}{\partial \bar{m}} = \frac{\partial \bar{f}}{\partial \bar{b}} = 0$$

Solving these two equations for the two unknowns produces the reference line that gives the slope-intercept form.

Once the method of selecting a reference line is agreed upon, all surface height measurements are made relative to it. The centroid (or M system) and the least-squares reference line methods are the easiest to deal with analytically, because the sum of all the profile height deviations is always zero.

### 3.6 Computation of Surface Parameters

Measurements made with a stylus instrument are assumed. The reference line used is obtained by either the M system or the least squares method so that the average of  $z_i$  is zero. Samples taken at uniform length intervals are assumed. The  $\Delta$  is defined as small. Resulting discretized height values are denoted by  $z_i, i = 1, 2, \dots, N$ .

Three different surface parameters may be computed:

1. Centerline average (CLA) or arithmetic average (AA), denoted by  $R_a$ ,

$$R_a = \frac{1}{N} \sum_{i=1}^N |z_i| \tag{3.1}$$

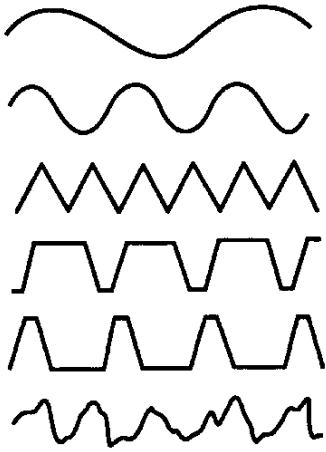


Figure 3.7: Geometric profiles having same values of arithmetic average. [From Halling (1976).]

From  $\partial \bar{f} / \partial \bar{b} = 0$  it immediately follows that  $\sum \bar{d}_i = 0$  so  $z'_i = z_i - \bar{m}x_i - \bar{b}$  has zero mean.

2. Root mean square (rms), denoted by  $R_q$ ,

$$R_q = \left( \frac{1}{N} \sum_{i=1}^N z_i^2 \right)^{1/2} \quad (3.2)$$

If a Gaussian height distribution is assumed, the  $R_q$  has the advantage of being the standard deviation of the profile.

3. Maximum peak-to-valley height, denoted by  $R_t$ ,

$$R_t = \max(z) - \min(z) \quad (3.3)$$

In general,

$$R_a < R_q < R_t \quad (3.4)$$

Also for a simple sine distribution the ratio of  $R_q$  to  $R_a$  is

$$\frac{R_q}{R_a} = \frac{\pi}{2\sqrt{2}} = 1.11 \quad (3.5)$$

Table 3.2 gives typical values of the arithmetic mean  $R_a$  for various processes and components. Figure 3.7 shows six different surface profiles, all with the same  $R_a$ , or arithmetic average roughness. The  $R_a$  is thus an ambiguous parameter, since it does not indicate whether the  $R_a$  value is the mean of many small deviations from the mean value or of a few large ones. For this reason tribologists seek additional surface parameters that are rather more informative.

Thus far, the discussion of surface roughness has been on defining the profile in the  $z$  direction. To incorporate the length of the asperities, the bearing length is introduced. The profile bearing length is obtained by cutting the profile peaks by a line parallel to the mean line within the sampling length at a given section

Table 3.2: Typical arithmetic averages for various processes and components.

Processes	Arithmetic average $R_a$	
	$\mu\text{m}$	$\mu\text{in.}$
Sand casting; hot rolling	12.5–25	500–1000
Sawing	3.2–25	128–1000
Planing and shaping	0.8–25	32–1000
Forging	3.2–12.5	128–500
Drilling	1.6–6.3	64–250
Milling	0.8–6.3	32–250
Boring; turning	0.4–6.3	16–250
Broaching; reaming; cold rolling; drawing	0.8–3.2	32–128
Die casting	0.8–1.6	32–64
Grinding, coarse	0.4–1.6	16–64
Grinding, fine	0.1–0.4	4–16
Honing	0.1–0.8	4–32
Polishing	0.05–0.4	2–16
Lapping	0.025–0.4	1–16
Components		
Gears	0.25–10	10–400
Plain bearings - journal (runner)	0.12–0.5	5–20
Plain bearings - bearing (pad)	0.25–1.2	10–50
Rolling bearings - rolling elements	0.025–0.12	1–5
Rolling bearings - tracks	0.1–0.3	4–12

level. Figure 3.8 is helpful in describing the bearing length  $\ell^*$ . Mathematically, it is defined as

$$\ell^* = \ell_1^* + \ell_2^* + \cdots + \ell_n^* \quad (3.6)$$

The profile bearing length ratio  $t_p$  is defined as

$$t_p = \frac{\ell^*}{\ell} \quad (3.7)$$

where  $\ell$  = sampling length, m.

The Abbot curve (also known as the “bearing length curve”) is shown in Fig. 3.9. The vertical axis is the bearing length ratio multiplied by 100. These curves describe how much of the profile protrudes a given distance above the surface. During running-in, a certain amount of the surface will be removed by plastic deformation. These curves also calculate the peakedness and the amount of material between given heights. In the top profile the asperities have steeper peaks than in the bottom profile.

The texture of a surface can be described in terms of the distribution function of its profile heights. In statistical terms the cumulative distribution of the all-ordinate distribution curve can be written as

$$\bar{F}(z) = \int_{-\infty}^z \tilde{\psi} dz$$

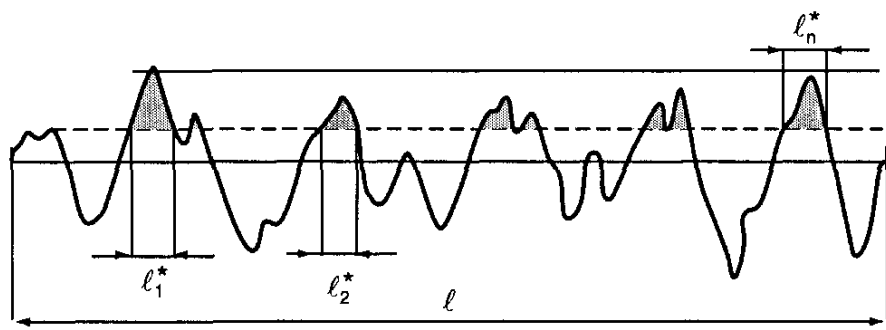


Figure 3.8: Surface profile showing bearing length. [From Persson (1992).]

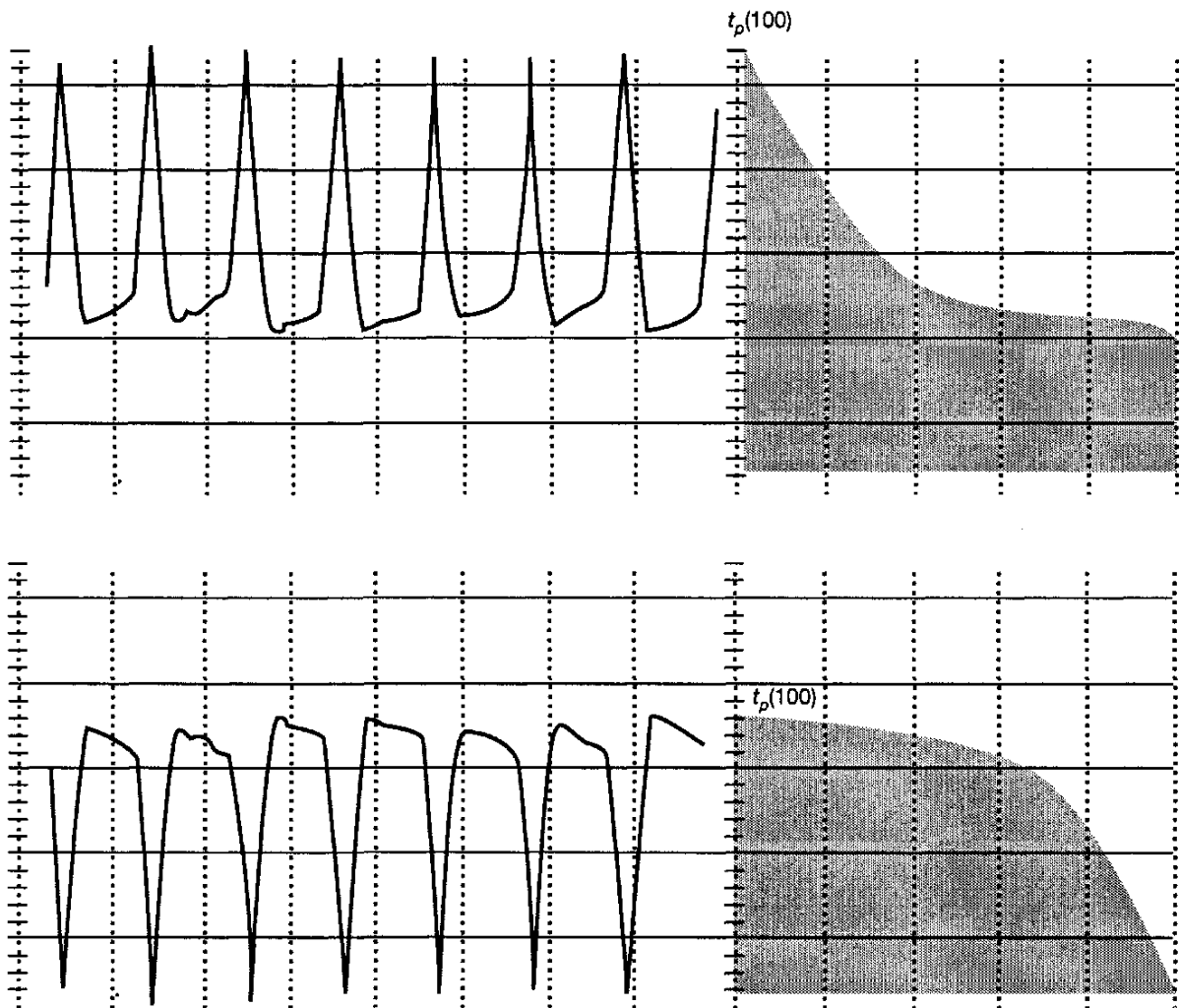


Figure 3.9: Abbot curves for two different profiles. [From Persson (1992).]

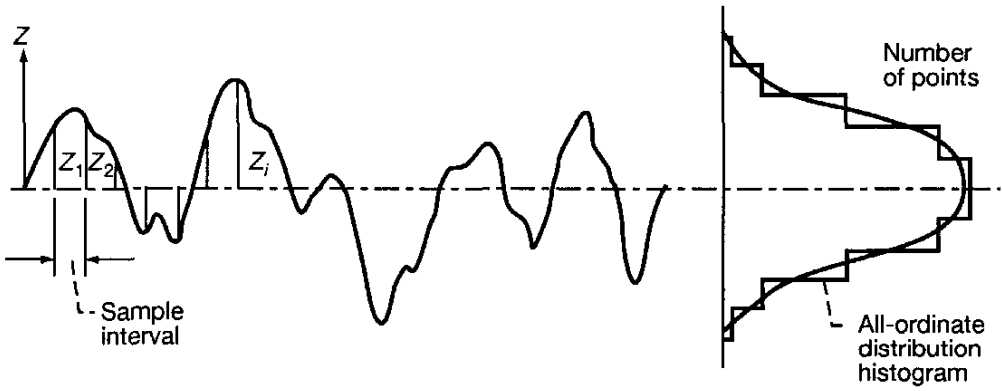


Figure 3.10: Method of deriving all-ordinate distribution. [From Halling (1975).]

where  $z$  refers to the profile height and  $\tilde{\psi}$  is the probability density function of the distribution of these heights. The probability density function may be viewed as the fraction of heights in a given interval. Therefore, the practical derivation of such a distribution curve involves taking measurements of  $z_1, z_2$ , etc., at some discrete interval and summing the number of ordinates at any given height level. Figure 3.10 illustrates the method used in obtaining the all-ordinate distribution. The distribution curve in Fig. 3.10 is the smoothest curve that can be drawn through the histogram produced by such a sampling procedure. This smooth curve for many surfaces tends to exhibit a Gaussian distribution of surface texture heights.

If these ideas of height distribution are introduced, the empirical probability density, or histogram, can be used to evaluate  $R_a$  and  $R_q$ . If the fraction of heights in an interval  $z_j - \Delta \leq z_j \leq z_j + \Delta$  is denoted by  $\tilde{\psi}_j$  for  $j = -L, \dots, 0, \dots, L$ , then approximately the same values as those given in Eqs. (3.1) and (3.2) can be expressed as

$$R_a = \int_{-L}^L |z| \tilde{\psi} dz \quad (3.8)$$

$$R_q = \left( \int_{-L}^L z^2 \tilde{\psi} dz \right)^{1/2} \quad (3.9)$$

From the Gauss-Laplace law a general expression for the probability density function while assuming a Gaussian distribution is

$$\tilde{\psi} = \frac{1}{\bar{\sigma} (2\pi)^{1/2}} \exp \frac{-(z - z^*)^2}{2\bar{\sigma}^2} \quad (3.10)$$

where  $\bar{\sigma}$  is the standard deviation and  $z^*$  is the distance of the mean from the value chosen as the origin. The values of the ordinate  $\tilde{\psi}$  of the Gaussian

distribution curve for  $z^* = 0$  are found in most books on statistics. The form of the Gaussian distribution necessitates a spread of  $-\infty$  to  $\infty$ , which cannot happen with practical surfaces. In practice the distribution curve is truncated to  $\pm 3\bar{\sigma}$ . Because approximately 99.9% of all events occur within this region, the truncation leads to negligible error while providing useful simplification.

The  $n$ th moment of the distribution curve  $\tilde{\psi}dz$  about the mean is defined as

$$M_n = \int_{-\infty}^{\infty} z^n \tilde{\psi} dz \quad (3.11)$$

It can be observed that twice the first moment of half  $\tilde{\psi}dz$  is equivalent to the centerline average  $R_a$  defined in Eq. (3.8) or

$$R_a = 2 \int_0^{\infty} z \tilde{\psi} dz = \text{twice the first moment of half } \tilde{\psi} dz$$

The first moment of the whole  $\tilde{\psi}dz$  about the mean reference line is zero. Likewise, comparing the second moment of  $\tilde{\psi}dz$  with the root mean square  $R_q$  expressed in Eq. (3.9) gives

$$R_q = \bar{\sigma} = \left( \int_{-\infty}^{\infty} z^2 \tilde{\psi} dz \right)^{1/2} = \left( \text{second moment of } \tilde{\psi} dz \right)^{1/2}$$

The third moment of  $\tilde{\psi}dz$  relates to the skewness of a curve, or the departure of a curve from symmetry. The mathematical expression for the normalized skewness is

$$\bar{\alpha} = \frac{1}{R_q^3} \int_{-\infty}^{\infty} z^3 \tilde{\psi} dz \quad (3.12)$$

If the peaks and valleys deviate from the reference line by approximately the same amount, the skewness will be zero. If, on the other hand, the surfaces are deeply pitted, the skewness will be some negative value.

The fourth moment of  $\tilde{\psi}dz$  relates to the peakedness, or kurtosis, of the curve and is expressed as

$$\bar{\beta} = \frac{1}{R_q^4} \int_{-\infty}^{\infty} z^4 \tilde{\psi} dz \quad (3.13)$$

The kurtosis always has a positive value and measures the sharpness of a symmetric distribution. For a Gaussian distribution the curve has a kurtosis of 3. When most of the profile heights are close to the reference line,  $\bar{\beta}$  is quite large; a relatively flat height distribution will have a  $\bar{\beta}$  near zero. Curves with values of  $\bar{\beta}$  less than 3 are called "platykurtic," and those with  $\bar{\beta}$  greater than 3 are called "leptokurtic." Figure 3.11 illustrates the various types of kurtosis curves.

For a Gaussian distribution where the curve is represented by  $\tilde{\psi}$ , as expressed in Eq. (3.10), the general expression for the  $n$ th moment is given by

$$M_n = \frac{1}{\bar{\sigma} (2\pi)^{1/2}} \int_{-\infty}^{\infty} z^n \exp \frac{-z^2}{2\sigma^2} dz \quad (3.14)$$

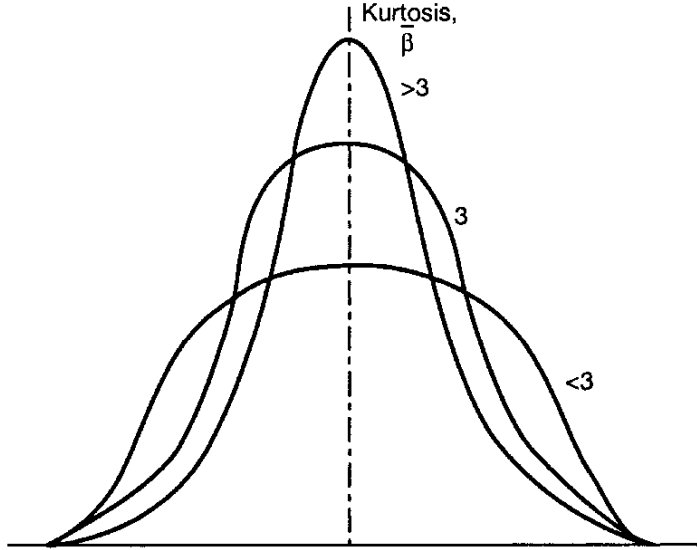


Figure 3.11: Illustration of three different kurtosis values. [From Halling (1975).]

where the standard deviation  $\bar{\sigma} = R_q$ . From Eq. (3.14) it is observed that, if  $n$  is odd,  $M_n$  vanishes and the curve must be symmetrical. If  $n$  is even, then

$$M_n = \frac{n!}{2^{n/2} (n/2)!} \bar{\sigma}^n \quad (3.15)$$

Note that the second moment becomes  $\bar{\sigma}^2$ , the variance.

$$\therefore M_2 = \bar{\sigma}^2 = R_q^2 = \text{variance} \quad (3.16)$$

Some additional parameters used to define surfaces utilized in fluid film lubrication as well as the range of values normally found are listed below:

- Density of asperities,  $10^2$  to  $10^6$  peaks/mm<sup>2</sup>
- Asperity spacing, 1 to 75  $\mu\text{m}$
- Asperity slopes, 0 to  $25^\circ$ , but mainly 5 to  $10^\circ$
- Radii of peaks, mostly 10 to 30  $\mu\text{m}$

These additional surface definitions better define the surface texture used in fluid film lubrication.

Fractals have not been used by researchers to characterize fluid film lubrication surfaces thus far, but they might be useful in the future. Fractals are geometric structures that have a similar appearance regardless of the scale on which they are being observed. If a surface profile exhibits self-similarity independent of the scales, the concept of fractal dimension can be used to characterize the profile.

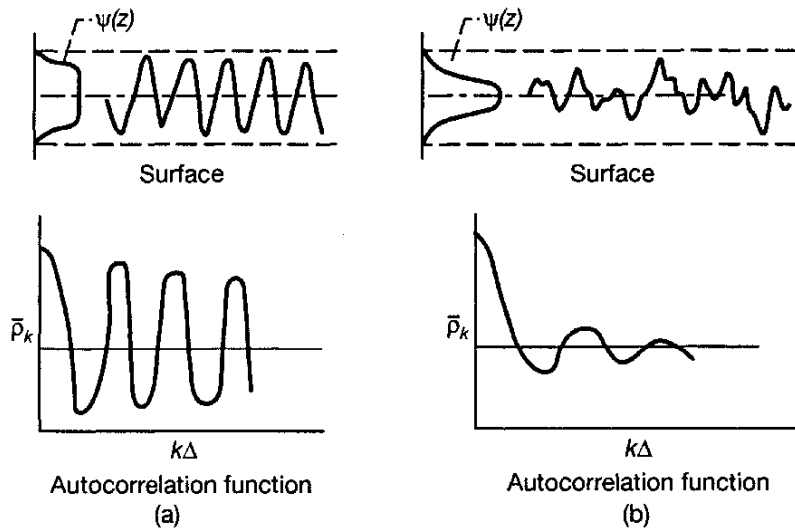


Figure 3.12: Two different surfaces and resulting autocorrelation functions. (a) Periodicity profile; (b) decay profile. [From Halling (1975).]

### 3.7 Autocorrelation Parameter

The previously discussed parameters ( $R_a$ ,  $R_q$ , and  $R_t$ ) depend only on the profile heights, not on the spacing between heights. As a result they do not truly reflect the shape of the profile, as illustrated in Fig. 3.10. The autocorrelation does incorporate the spacing between heights and is obtained by multiplying each profile height by the height of the point at some fixed horizontal distance farther along the profile. After averaging the product over a representative profile length and normalizing by the variance  $R_q^2$ , the expression for the autocorrelation is

$$\tilde{\rho}_k = \frac{1}{R_q^2(N-k)} \sum_{i=1}^{N-k} z_i z_{i+k} \quad (3.17)$$

The autocorrelation depends on  $k$  and is a measure of the similarity of heights separated by the distance  $k\Delta$  (where  $\Delta$  is the sample interval, assumed to be constant). In machining processes such as turning or milling, where there are pronounced feed marks, the autocorrelation will have a maximum where  $k\Delta$  is some integer multiple of the linear feed. This distance is often called the "characteristic wavelength."

Typical plots of the autocorrelation function for two different profiles are shown in Fig. 3.12. The variance is defined as  $\bar{\sigma}^2$ . The shape of this function is most useful in revealing some of the characteristics of the profile. The general decay of the function is the random component of the surface profile and indicates a decrease in correlation as  $k\Delta$  increases, as shown in Fig. 3.12b. The oscillatory component of the function indicates any inherent periodicity of the profile, as shown in Fig. 3.12a.

### 3.8 Distribution of Slope and Curvature

A basic geometric description of a profile can be given, considering the profile as a random function, with first and second derivatives. Each of the derivatives also has a statistical distribution associated with it. The most straightforward way of estimating this information is to use differences in the profile to represent the derivatives, or

$$\left( \frac{dz}{dx} \right)_i = \frac{z_{i+1} - z_i}{\Delta} \quad (3.18)$$

$$\left( \frac{d^2z}{dx^2} \right)_i = \frac{z_{i+1} - 2z_i + z_{i-1}}{\Delta^2} \quad (3.19)$$

Equation (3.18) defines the slope of the profile and Eq. (3.19) defines its curvature. However, because the profile is a random function with “noise,” differencing is not the best way, since it makes this noise greater. Some sort of smoothing of the data should be done to minimize this effect. One way of doing this is to use Eqs. (3.18) and (3.19) with samples taken at intervals of  $\Delta$ ,  $2\Delta$ ,  $3\Delta$ , ... and then to make weighted averages of these expressions. For example, by choosing weights of 1.5, -0.6, and 0.1 for derivatives formed at  $\Delta$ ,  $2\Delta$ , and  $3\Delta$ , respectively, the following expressions are obtained:

$$\left( \frac{dz}{dx} \right)_i = \frac{1}{60\Delta} [45(z_{i+1} - z_{i-1}) - 9(z_{i+2} - z_{i-2}) + (z_{i+3} - z_{i-3})] \quad (3.20)$$

$$\begin{aligned} \left( \frac{d^2z}{dx^2} \right)_i &= \frac{1}{180\Delta^2} \\ &\times [-490z_i + 270(z_{i+1} - z_{i-1}) - 27(z_{i+2} - z_{i-2}) + 2(z_{i+3} - z_{i-3})] \end{aligned} \quad (3.21)$$

A slope and curvature profile can be generated in this way from the height profile, and by using the same relations as for the heights, a mean or average slope and curvature can be found as well as the respective standard deviation of the distributions. Likewise, the skewness and the kurtosis can be computed to characterize the shape of these distributions.

The previously defined properties are a few of the parameters that can be found from analyzing a profile. These characteristics may be important in relating function to manufactured surfaces or in analyzing how a surface interacts with another surface. They illustrate some of the efforts at extracting more information from the surface measurement than simply the height sensitive parameters.

Finally, the relation between function and surface geometry has to be more fully understood. This will require closer interaction between the manufacturing engineer who makes the surface and the designer who specifies the surface.

### 3.9 Film Parameters for Different Lubrication Regimes

If a machine element is adequately designed and fluid film lubricated, the lubricated surfaces are completely separated by a lubricant film. Endurance testing of ball bearings, for example, as reported by Tallian et al. (1967) has demonstrated that when the lubricant film is thick enough to separate the contacting bodies, the fatigue life of the bearing is greatly extended. Conversely, when the film is not thick enough to provide full separation between the asperities in the contact zone, the life of the bearing is adversely affected by the high shear resulting from direct metal-to-metal contact.

The four lubrication regimes were defined in Sec. 1.3, and calculation methods for determining the rms surface finish were introduced in Sec. 3.6. This section introduces a film parameter and describes the range of values for the four lubrication regimes. The relationship between the dimensionless film parameter  $\Lambda$  and the minimum film thickness  $h_{\min}$  is

$$\Lambda = \frac{h_{\min}}{\left(R_{q,a}^2 + R_{q,b}^2\right)^{1/2}} \quad (3.22)$$

where

$R_{q,a}$  = rms surface finish of surface *a*

$R_{q,b}$  = rms surface finish of surface *b*

The film parameter is used to define the four important lubrication regimes. The range of  $\Lambda$  for these four regimes is

1. Hydrodynamic lubrication,  $5 < \Lambda < 100$
2. Elastohydrodynamic lubrication,  $3 < \Lambda < 10$
3. Partial lubrication,  $1 < \Lambda < 5$
4. Boundary lubrication,  $\Lambda < 1$

These values are rough estimates. The great differences in geometric conformity in going from hydrodynamically lubricated conjunctions to elastohydrodynamically lubricated conjunctions make it difficult for clear distinctions to be made.

Running-in is a process that affects the film parameter. This process allows wear to occur so that the mating surfaces can adjust to each other to provide for smooth running. This type of wear may be viewed as beneficial. The film parameter will increase with running-in, since the composite surface roughness will decrease. Running-in also has a significant effect on the shape of the asperities that is not captured by the composite surface roughness. With running-in, the peaks of the asperities in contact become flattened.

## Example 3.1

**Given:** Two equally rough surfaces are lubricated and loaded together ( $R_{qa} = R_{qb}$ ). The film parameter is two.

**Find:** The value of  $\Lambda$  if one of the surfaces is polished so that  $R_q \rightarrow 0$  (i.e., the surface becomes absolutely smooth).

**Solution:** From Eq. (3.22) the initial condition is

$$\Lambda_1 = \frac{h_{\min}}{(R_q^2 + R_q^2)^{1/2}} = \frac{h_{\min}}{\sqrt{2}R_q} = 2 \quad (a)$$

When one of the surfaces becomes absolutely smooth,

$$\Lambda_2 = \frac{h_{\min}}{(R_q^2 + 0)^{1/2}} = \frac{h_{\min}}{R_q} \quad (b)$$

$\therefore \Lambda$  increases from 2 to  $2\sqrt{2}$ .

---

## Example 3.2

**Given:** Gears for an excavator are manufactured by sand casting. The surface roughness is measured to have a centerline average of  $18 \mu\text{m}$ . This high surface roughness makes the gear wear rapidly. The film thickness for the grease-lubricated gears is calculated to be  $1.6 \mu\text{m}$ .

**Find:** The method of manufacture for the gears to produce a film parameter of 10.

**Solution:** Using Eq. (3.22) while assuming that the roughnesses are equal on the two surfaces gives

$$\Lambda = \frac{h_{\min}}{R_q\sqrt{2}} \quad \text{or} \quad R_q = \frac{h_{\min}}{\Lambda\sqrt{2}} = \frac{1.6}{10\sqrt{2}} = 0.1131 \mu\text{m}$$

Table 3.2 shows that for a surface roughness of  $0.1 \mu\text{m}$ , grinding is the fastest and cheapest method of achieving these surface finishes. Smoother surfaces can be manufactured by honing, polishing, and lapping, but these processes are considerably more expensive and do not lend themselves well to the intricate geometry of gear teeth.

---

## 3.10 Transition Between Lubrication Regimes

As the severity of loading is decreased, there is no sharp transition from boundary to fluid film lubrication; rather an increasing proportion of the load is carried by pressures within the film that fills most of the space between the

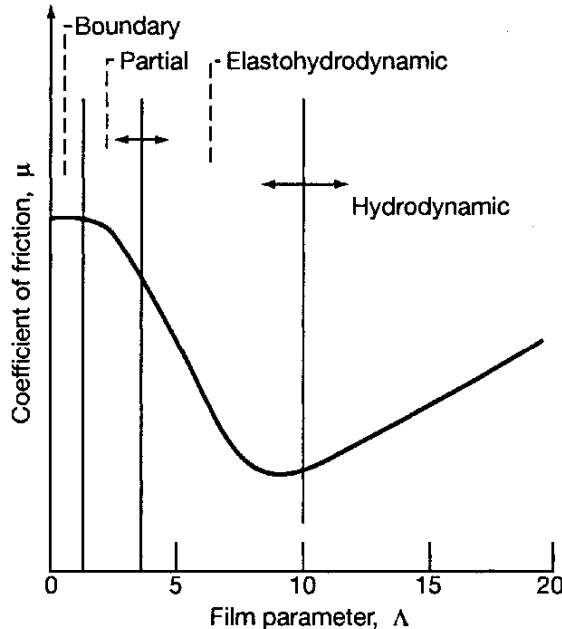


Figure 3.13: Variation of friction coefficient with film parameter [From Hamrock and Dowson (1981).]

opposing solids. Indeed, it is often difficult to eliminate fluid film lubrication effects so that true boundary lubrication can occur, and there is evidence to suggest that micro-fluid-film lubrication formed by surface irregularities is an important effect.

The variation of the friction coefficient  $\mu$  with the film parameter  $\Lambda$  is shown in Fig. 3.13. This can be compared to the Stribeck curve of Fig. 1.16. The friction coefficient is defined as

$$\mu = \frac{f}{w_z} \quad (3.23)$$

where  $f$  is the tangential (friction) force and  $w_z$  is the normal applied load. In Fig. 3.13 the approximate locations of the various lubrication regimes discussed in Sec. 3.9 are shown. This figure shows that as the film parameter  $\Lambda$  increases, the friction coefficient initially decreases in the elastohydrodynamic regime and then increases in the hydrodynamic regime. In explaining this phenomenon let us assume the surface roughness is the same in both lubrication regimes.

In hydrodynamic lubrication of conformal surfaces as found in journal and thrust bearings,  $w_z \propto 1/h^2$ . In elastohydrodynamic lubrication of nonconformal surfaces the normal applied load has little effect on the film thickness. Therefore,  $w_z$  is essentially proportional to a constant. In both hydrodynamic and elastohydrodynamic lubrication the frictional force is due to lubricant shearing and can be expressed in both lubrication regimes as  $f \propto 1/h$ . Making use of this,

$$\mu_{HL} \propto \frac{1/h}{(1/h)^2} \propto h \quad (3.24)$$

$$\mu_{EHL} \propto \frac{1/h}{\text{constant}} \propto \frac{1}{h} \quad (3.25)$$

This then explains the reversing of the slope of the friction coefficient in Fig. 3.13.

## 3.11 Closure

Since fluid film lubrication is concerned with the lubrication between solids separated by small film thicknesses, it is essential that the physical nature of the solid's surface topography be understood. To obtain this understanding, this chapter investigated surface measurement hardware. The contact method of stylus measurement is based on transforming the vertical motion of the stylus tip as it traverses a surface into an electrical analog voltage. The main limitation of this approach is the finite size of the stylus tip, which distorts the surface profile (broadening peaks and narrowing valleys). Atomic force microscopy allows more surface roughness measurement with higher resolution than profilometry. The following noncontacting measurement devices were presented.

1. Laser interferometers that move a lens in order to maintain focus on a sample surface. The laser can be focused at different locations in order to obtain a three-dimensional surface profile.
2. Pneumatic devices measure the airflow when a finely finished head is placed on the surface and indicate changes in surface roughness.
3. Optical devices use the intensity of reflected laser light to define the surface texture.
4. Electron microscopic devices produce images when electrons are incident on the specimen.

In computing the parameters that define the surface texture, all height measurements were made from some defined reference line. Two methods of defining the reference line are

1. Mean, or M system, based on selecting the mean line as the centroid of the profile. The area above this line equals the area below this line.
2. Least squares, based on postulating a slope-intercept form for the reference line. This can compensate for errors of form or tilt.

Methods of computing surface parameters were also discussed. The following two important parameters were presented:

1. Centerline average (CLA), or arithmetic average (AA), denoted by  $R_a$ .
2. Root mean square (rms) roughness, denoted by  $R_q$ . In general,  $R_a < R_q$ .

The film parameter  $\Lambda$  was defined as the ratio of the minimum film thickness to the composite surface roughness. The film parameter was used to define four important lubrication regimes: hydrodynamic, elastohydrodynamic, partial, and boundary.

## 3.12 Problems

- 3.1 Show that for a Gaussian distribution and a zero mean ( $z^* = 0$ ) from the reference line (determined by the M system) the theoretical skewness is zero and the kurtosis is 3.
- 3.2 Show that the skewness for a deeply pitted surface is less than zero ( $\bar{\alpha} < 0$ ) and that the kurtosis for a relatively flat height distribution approaches zero ( $\bar{\beta} \rightarrow 0$ ).
- 3.3 Find  $R_a/R_q$  for a Gaussian distribution with zero mean ( $z^* = 0$ ).
- 3.4 Prove that  $R_a < R_q$ .
- 3.5 What profile would produce an  $R_a = R_q$ ?
- 3.6 Prove that the kurtosis is greater than or equal to 1.
- 3.7 What is the skewness-kurtosis inequality? That is, when plotting skewness versus kurtosis, describe the critical curve that separates where the results are allowed and where they are forbidden.
- 3.8 Show that for a Gaussian distribution with a nonzero mean ( $z^* \neq 0$ ) from the reference line (determined by the M system), the theoretical skewness is 0 and the kurtosis is 3.
- 3.9 A surface with a triangular sawtooth roughness pattern has a peak-to-valley height of  $5 \mu\text{m}$ . Find the  $R_a$  value and the  $R_q$  value.
- 3.10 A precision ball bearing has a race root mean square surface roughness of  $0.07 \mu\text{m}$  and a ball root mean square surface roughness of  $0.02 \mu\text{m}$ . Changing the roughness of the components may give a higher  $\Lambda$  value. Determine which component to smooth if it costs equally as much to halve the roughness of the race as it costs to halve the roughness of the balls. Note that  $h_{\min}=0.2 \mu\text{m}$ .
- 3.11 Consider a two-dimensional surface in the shape of a sine wave with an amplitude of  $1 \mu\text{m}$ . Obtain the first four moments of the distribution curve for this surface. Repeat the problem assuming that this surface has encountered wear, so that the top half of the sine wave has been flattened.
- 3.12 Plot the cumulative distribution function and the Abbott-Firestone curve for the two surfaces in Problem 3.11.

## References

Abbot, E. J., and Firestone, F. A. (1933): Specifying Surface Quality. *J. Mech. Eng.*, vol. 55, no. 9, pp. 569-572.

- ASME (1995a): Surface Texture (Surface Roughness, Waviness, and Lay). American National Standard *ASME B46.1-1995*. New York.
- ASME (1995b): Surface Texture Symbols. American National Standard *ASME Y14.36-1995*. New York.
- Bhushan, B., ed., (1998): *Handbook of Nano/Micro Tribology*. CRC Press, Boca Raton (FL).
- Bhushan B., (2002): *Introduction to Tribology*. Wiley, New York.
- Halling, J. (ed.) (1975): *Principles of Tribology*. Macmillan Press, London and Basingstoke.
- Halling, J. (1976): *Introduction to Tribology*. Wykeham Publications, London.
- Hamrock, B. J., and Dowson, D. (1981): *Ball Bearing Lubrication-The Elasto-hydrodynamics of Elliptical Contacts*. Wiley-Interscience, New York.
- Persson, U. (1992): "Surface Topography-Speckle Technique and Image Analysis Applied to Surface Roughness Measurement on Machined Surfaces." Ph.D. Thesis. Instrumentation Laboratory, Royal Institute of Technology, Stockholm, TRITA-ILA 92.06.
- Sherrington, I., and Smith, E. H. (1988): Modern Measurement Techniques in Surface Metrology: Part I: Stylus Instruments, Electron Microscopy and Non-Optical Comparators. *Wear*, vol. 125, pp. 271-288.
- Stout, K.J., Sullican, P.J., Dong, W.P., Mainsah, E., Luo, N., Mathia, T., and Zahouni, H. (1993): The Development of Methods for the Characterization of Roughness in Three Dimensions. Commission of the European Communities, Report EUR 15178 EN.
- Tallian, T. E., et al. (1967): On Computing Failure Modes in Rolling Contacts. *ASLE Trans.*, vol. 10. no. 4, pp. 418-435.
- Thomas, R.R., (1982): *Rough Surfaces*. Longman, New York.

# Chapter 4

## Lubricant Properties

### Symbols

$A$	area, $\text{m}^2$	$t_m$	temperature, $^\circ\text{C}$
$\mathcal{A}$	experimentally determined constant, $\text{cm}^2/\text{s}$	$u$	velocity of moving surface, $\text{m}/\text{s}$
$\mathcal{B}$	experimentally determined constant, $\text{cm}^2$	$\bar{x}$	SUV of unknown oil
$E$	modulus of elasticity, $\text{N}/\text{m}^2$	$Z_1$	viscosity-pressure index, a dimensionless constant
$E'$	effective modulus of elasticity, $E' = 2 \left( \frac{1 - \nu_a^2}{E_a} + \frac{1 - \nu_b^2}{E_b} \right)^{-1}, \text{ N}/\text{m}^2$	$\gamma^*$	limiting-shear-strength proportionality constant, $\partial\tau_L/\partial p$
$f$	friction force, $\text{N}$	$\eta$	absolute viscosity, $\text{N}\cdot\text{s}/\text{m}^2$
$G_0$	dimensionless constant indicative of viscosity grade of liquid	$\eta_0$	absolute viscosity at $p = 0$ and at a constant temperature, $\text{N}\cdot\text{s}/\text{m}^2$
$\bar{H}$	SUV of reference oil of high VI	$\eta_e$	effective viscosity, $\text{N}\cdot\text{s}/\text{m}^2$
$h$	film thickness, $\text{m}$	$\eta_k$	kinematic viscosity, $\text{m}^2/\text{s}$
$L$	Saybolt universal viscosity (SUV) of reference oil of low VI	$\nu$	Poisson's ratio
$p$	pressure, $\text{N}/\text{m}^2$	$\xi$	pressure-viscosity coefficient of the lubricant dependent on temperature, $\text{m}^2/\text{N}$
$p_{iv,as}$	asymptotic isoviscous pressure, $\text{N}/\text{m}^2$	$\rho$	density, $\text{kg}/\text{m}^3$
$S_0$	dimensionless constant from slope of viscosity-temperature relationship	$\bar{\rho}$	dimensionless density
$s$	shear strain rate, $\text{s}^{-1}$	$\rho_0$	density when $p = 0$ , $\text{kg}/\text{m}^3$
$t$	time, $\text{s}$	$\tau$	shear stress, $\text{N}/\text{m}^2$
		$\tau_0$	shear stress at zero pressure, $\text{N}/\text{m}^2$
		$\tau_E$	shear stress when fluid starts to behave nonlinearly, $\text{N}/\text{m}^2$
		$\tau_L$	limiting shear stress, $\text{N}/\text{m}^2$

### 4.1 Introduction

The primary function of a lubricant is to control friction and wear. Liquid lubricants, however, also have desirable secondary properties and characteristics:

1. They can be drawn between moving parts by hydraulic action.
2. They have relatively high heat-sink capacity to cool the contacting parts.
3. They are easily mixed with chemicals to give a variety of properties such as corrosion resistance, detergency, or surface-active layers.
4. They can remove wear particles.

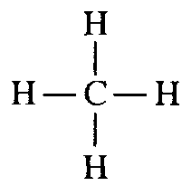
Lubricants can be divided into those of petroleum origin, known as “mineral oils,” and those of animal or vegetable origin, known as “fatty oils.” Synthetic oils are often grouped with the latter. In order for a lubricant to be effective, it must be viscous enough to maintain a lubricant film under operating conditions but should be as fluid as possible to remove heat and to avoid power loss due to viscous drag. A lubricant should also be stable under thermal and oxidation stresses, have low volatility, and possess some ability to control friction and wear by itself. As can be seen, quite a bit is expected from a lubricant, and to better understand the role of a lubricant some basic chemistry is needed.

## 4.2 Basic Chemistry

Since some lubricants are derived from petroleum, which consists of compounds of carbon and hydrogen, a brief discussion of hydrocarbon chemistry is needed. This discussion can also serve as a basis for the study of alcohols, fatty acids, and cyclic hydrocarbons. Much of this section was obtained from two sources, Pugh (1970) and Hess (1981).

### 4.2.1 Hydrocarbons

Hydrocarbons are compounds of carbon and hydrogen. Carbon has a valency, or chemical bonding power, of 4; hydrogen has a valency of 1. The simplest hydrocarbon can be represented diagrammatically as



and is named methane, with a chemical formula of  $\text{CH}_4$ . Carbon atoms have the unique property of being able to link together, and each can join further hydrogen atoms as in ethane ( $\text{C}_2\text{H}_6$ ), given as

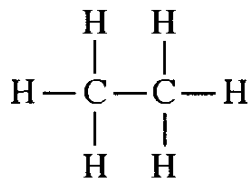


Table 4.1: Straight-chain paraffins. [From Pugh (1970).]

Number of carbon atoms	Name	Formula	Boiling point, °C	Specific gravity	Physical state at NTP <sup>a</sup>
1	Methane	CH <sub>4</sub>	-161.5	—	Gas
2	Ethane	C <sub>2</sub> H <sub>6</sub>	-88.3	—	Gas
3	Propane	C <sub>3</sub> H <sub>8</sub>	-44.5	—	Gas
4	Butane	C <sub>4</sub> H <sub>10</sub>	-0.5	—	Gas
5	Pentane	C <sub>5</sub> H <sub>12</sub>	36.2	0.626	Liquid
6	Hexane	C <sub>6</sub> H <sub>14</sub>	69	0.660	Liquid
7	Heptane	C <sub>7</sub> H <sub>16</sub>	98.4	0.684	Liquid
8	Octane	C <sub>8</sub> H <sub>18</sub>	125.8	0.704	Liquid
9	Nonane	C <sub>9</sub> H <sub>20</sub>	150.6	0.718	Liquid
10	Decane	C <sub>10</sub> H <sub>22</sub>	174	0.730	Liquid

<sup>a</sup>Normal temperature and pressure.

Note that the chain is symmetrical.

By varying the number of carbon atoms in the molecule, it is possible to present "straight-chain hydrocarbons." This family is known as "alkanes," or "paraffins," and has the general formula C<sub>n</sub>H<sub>2n+2</sub>, where n is the total number of carbon atoms present in the molecule. This forms a series in which such physical characteristics as boiling point and specific gravity increase as the value of n increases. Table 4.1, which lists the first 10 members of the series, shows that an increase in the number of carbon atoms increases the boiling point of the compounds, thus reducing their chemical activity. Such families of hydrocarbons are known as "homologous series," and all the members have formulas that fit the general formula of the series. The principal homologous series of hydrocarbons is summarized in Table 4.2.

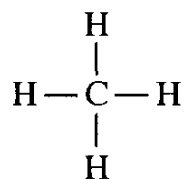
Much of the remainder of this section on basic chemistry concerns more details of the members of the homologous series given in Table 4.2. The main difference in the series is the type of bonding. A single covalent bond consists of a single pair of electrons shared between two atoms, as in methane. Double bonds involve two shared pairs of electrons, and triple bonds involve three shared pairs. The bonding in organic compounds is usually indicated by dashes,

Table 4.2: Homologous series of hydrocarbons. [From Hess (1981).]

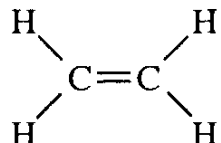
Name	Formula	Sample of familiar member
Alkane or paraffin	C <sub>n</sub> H <sub>2n+2</sub>	Methane (CH <sub>4</sub> )
Olefin or alkene	C <sub>n</sub> H <sub>2n</sub>	Ethylene (C <sub>2</sub> H <sub>4</sub> )
Acetylene or alkyne	C <sub>n</sub> H <sub>2n-2</sub>	Acetylene (C <sub>2</sub> H <sub>2</sub> )
Cycloparaffin or naphthene	C <sub>n</sub> H <sub>2n</sub>	Cyclopentane (C <sub>5</sub> H <sub>10</sub> )
Aromatic	C <sub>n</sub> H <sub>2n-6</sub>	Benzene (C <sub>6</sub> H <sub>6</sub> )

as shown for the following examples:

1. Single (methane, CH<sub>4</sub>):



2. Double (ethylene, C<sub>2</sub>H<sub>4</sub>):



3. Triple (acetylene, C<sub>2</sub>H<sub>2</sub>):

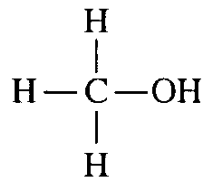


Although the olefin or alkene and the cycloparaffin or naphthene series in Table 4.2 have the same formula, they behave quite differently. In the alkene series the double bond present between two carbon atoms greatly increases the chemical reactivity of these hydrocarbons. In the cycloparaffin series the carbon atoms are joined to each other, forming a ring. Such a structure is relatively inert.

In the refining of petroleum many useful mixtures of hydrocarbons are made available. The basic process in refining is fractional distillation, which separates the various products according to ranges of boiling points. The products formed by the initial distillation of crude petroleum are known as "straight-run products." Table 4.3 gives the main products formed, together with other pertinent information about them.

#### 4.2.2 Alcohols

If in the structure of methane one hydrogen atom is replaced by the monovalent hydroxyl group OH, one gets methanol, or methyl alcohol,



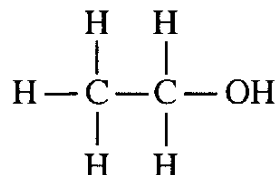
with a chemical formula of CH<sub>3</sub>OH. This volatile liquid is also known as "wood alcohol" because it is an important byproduct from the destructive distillation of wood to produce charcoal. Methanol is an important solvent and is used as

Table 4.3: Petroleum products with boiling point range and number of carbon atoms present.

Petroleum product	Boiling point range, °C	Number of carbon atoms present
Natural gas	< 32	1–4
Gasoline	40–200	4–12
Naphtha (benzine)	50–200	7–12
Kerosene	175–275	12–15
Fuel oil	200–300	15–18
Lubricating oil	> 300	16–20
Wax	> 300	20–34
Asphalt	Residue	Large

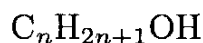
an antifreeze and as a denaturant for ethyl alcohol. It is the starting point in the production of many synthetic chemicals.

The structure of ethane can be modified in the same way as was done for methane to give ethanol, or ethyl alcohol ( $C_2H_5OH$ ),



Ethanol is also known as “grain alcohol.” It is produced from fermentation of carbohydrate compounds contained in molasses, corn, rye, barley, and potatoes. Enzymes in yeast cause the fermentation. Ethanol has the property of absorbing moisture from the atmosphere until it has a composition of 95% alcohol and 5% water. It is used extensively in industries preparing drugs, medicinals, and cosmetics. Ethanol is present in a variety of beverages, causing them to be intoxicating.

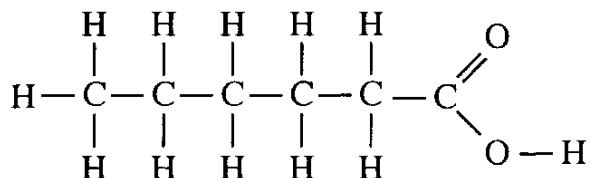
From observing the structures of methanol and ethanol, the family compounds of alcohol may be written in a general formula as



Each is named after the hydrocarbon from which it is derived, the terminal “e” being replaced by “ol.”

### 4.2.3 Fatty Acids

The fatty acids may be considered from the appearance of their molecular structure to be derived from the paraffins by replacing an end methyl ( $CH_3$ ) group with a carboxyl ( $CO_2H$ ) group. The corresponding acid is named after the root hydrocarbon, and the terminal “e” in the name is changed to “oic.” For example, hexanoic acid contains six carbon atoms and its structure is



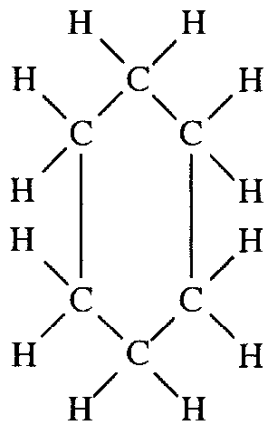
This could be expressed as  $\text{CH}_3(\text{CH}_2)_4\text{CO}_2\text{H}$ . Table 4.4 lists the straight-chain fatty acids that result when the number of carbon atoms present in the molecule is varied from 1 to 20. Note that the molecular structures of the fatty acids are no longer symmetrical as was true for the hydrocarbons, since in all cases one end methyl group has been replaced by the  $\text{CO}_2\text{H}$ , or carboxyl, group.

If a straight-chain hydrocarbon has a formula suggesting that it is short two hydrogen atoms, it is called an “olefin,” as pointed out in Table 4.2. The olefins form a family series of unsaturated hydrocarbons. They are called unsaturated because the valences of some of the carbon atoms in the molecule are not completely satisfied by the hydrogen atoms, and consequently the compound is particularly chemically active. The main feature of the olefin family is the double bonding of the carbon atom, which is easily broken and is a source of weakness in the molecule. The family, whose formula is  $\text{C}_n\text{H}_{2n}$ , starts with ethylene.

As pointed out by Pugh (1970), the olefins are not of direct interest from the lubrication point of view, although their reactivity is exploited in the manufacture of synthetic lubricants, but unsaturation in fatty acids is of definite interest, since a number of fatty acids present in animal and vegetable oils have some degree of unsaturation. The unsaturated fatty acids of primary interest in the study of lubricating oils are listed in Table 4.5.

#### 4.2.4 Cyclic Hydrocarbons

Cyclic hydrocarbons form two distinct groups, the cycloparaffins, or naphthenes, and the aromatics. An example of a naphthene is cyclohexane, which has the structure:



It is a saturated compound, and the molecule contains six carbon atoms and twelve hydrogen atoms. The naphthene family formula is  $\text{C}_n\text{H}_{2n}$ . Recall

Table 4.4: Formulas for straight-chain hydrocarbons and fatty acids. [From Pugh (1970)]

Number of carbon atoms in molecule	Hydrocarbon		Fatty acid		
	Formula	Name	Formula	Chemical name	Common name
1	HCH <sub>3</sub> or CH <sub>4</sub>	Methane	HCO <sub>2</sub> H	Methanoic	Formic
2	H(CH <sub>2</sub> )CH <sub>3</sub> or C <sub>2</sub> H <sub>6</sub>	Ethane	CH <sub>3</sub> CO <sub>2</sub> H	Ethanoic	Acetic
3	CH <sub>3</sub> (CH <sub>2</sub> )CH <sub>3</sub>	Propane	CH <sub>3</sub> CH <sub>2</sub> CO <sub>2</sub> H	Propanoic	Propionic
4	CH <sub>3</sub> (CH <sub>2</sub> ) <sub>2</sub> CH <sub>3</sub>	Butane	CH <sub>3</sub> (CH <sub>2</sub> ) <sub>2</sub> CO <sub>2</sub> H	Butanoic	Butyric
6	CH <sub>3</sub> (CH <sub>2</sub> ) <sub>4</sub> CH <sub>3</sub>	Hexane	CH <sub>3</sub> (CH <sub>2</sub> ) <sub>4</sub> CO <sub>2</sub> H	Hexanoic	Caprioc
8	CH <sub>3</sub> (CH <sub>2</sub> ) <sub>6</sub> CH <sub>3</sub>	Octane	CH <sub>3</sub> (CH <sub>2</sub> ) <sub>6</sub> CO <sub>2</sub> H	Octanoic	Caprylic
10	CH <sub>3</sub> (CH <sub>2</sub> ) <sub>8</sub> CH <sub>3</sub>	Decane	CH <sub>3</sub> (CH <sub>2</sub> ) <sub>8</sub> CO <sub>2</sub> H	Decanoic	Capric
12	CH <sub>3</sub> (CH <sub>2</sub> ) <sub>10</sub> CH <sub>3</sub>	Dodecane	CH <sub>3</sub> (CH <sub>2</sub> ) <sub>10</sub> CO <sub>2</sub> H	Dodecanoic	Lauric
14	CH <sub>3</sub> (CH <sub>2</sub> ) <sub>12</sub> CH <sub>3</sub>	Tetradecane	CH <sub>3</sub> (CH <sub>2</sub> ) <sub>12</sub> CO <sub>2</sub> H	Tetradecanoic	Myristic
16	CH <sub>3</sub> (CH <sub>2</sub> ) <sub>14</sub> CH <sub>3</sub>	Hexadecane	CH <sub>3</sub> (CH <sub>2</sub> ) <sub>14</sub> CO <sub>2</sub> H	Hexadecanoic	Palmitic
18	CH <sub>3</sub> (CH <sub>2</sub> ) <sub>16</sub> CH <sub>3</sub>	Octadecane	CH <sub>3</sub> (CH <sub>2</sub> ) <sub>16</sub> CO <sub>2</sub> H	Octadecanoic	Stearic
20	CH <sub>3</sub> (CH <sub>2</sub> ) <sub>18</sub> CH <sub>3</sub>	Eicosane	CH <sub>3</sub> (CH <sub>2</sub> ) <sub>18</sub> CO <sub>2</sub> H	Eicosanoic	Arachidic

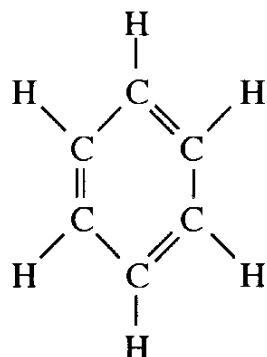
Table 4.5: Formulas for some unsaturated fatty acids. [Pugh (1970)]

Number of carbon atoms in molecule	Common name	Chemical name	Formula
16	Palmitoleic	Hexadec-9-enoic	CH <sub>3</sub> (CH <sub>2</sub> ) <sub>5</sub> CH:CH(CH <sub>2</sub> ) <sub>7</sub> CO <sub>2</sub> H
18	Oleic	Octadec-9-enoic	CH <sub>3</sub> (CH <sub>2</sub> ) <sub>7</sub> CH:CH(CH <sub>2</sub> ) <sub>7</sub> CO <sub>2</sub> H
18	Ricinoleic	12-Hydroxyoctadec-9-enoic	CH <sub>3</sub> (CH <sub>2</sub> ) <sub>5</sub> CH(OH)CH <sub>2</sub> CH:CH(CH <sub>2</sub> ) <sub>7</sub> CO <sub>2</sub> H
18	Linoleic	Octadeca-9:12-dienoic	CH <sub>3</sub> (CH <sub>2</sub> ) <sub>4</sub> (CH:CHCH <sub>2</sub> ) <sub>2</sub> (CH <sub>2</sub> ) <sub>6</sub> CO <sub>2</sub> H
18	Linolenic	Octadeca-9:12:15-trienoic	CH <sub>3</sub> CH <sub>2</sub> (CH:CHCH <sub>2</sub> ) <sub>3</sub> (CH <sub>2</sub> ) <sub>6</sub> CO <sub>2</sub> H
20	Arachidonic	Eicosa-5:8:11:14-tetraenoic	CH <sub>3</sub> (CH <sub>2</sub> ) <sub>4</sub> (CH:CHCH <sub>2</sub> ) <sub>4</sub> (CH <sub>2</sub> ) <sub>2</sub> CO <sub>2</sub> H

that the olefins have the same formula but that their structure differs considerably from the naphthene family's. One difference is that the olefins have double-bonded carbon atoms, whereas the naphthenes have single-bonded carbon atoms.

The cycloparaffins are named after the corresponding straight-chain paraffins containing the same number of carbon atoms, but since it takes at least three carbon atoms to form a ring, the series starts with cyclopropane. The physical properties of the cycloparaffins are different from those of the corresponding straight-chain paraffins, but they are chemically quite similar.

The last member of the homologous series given in Table 4.2 is the aromatics. They form a separate, distinct, and peculiar group of compounds, and much time has been spent studying their general structure. Aromatics have a basic ring structure containing three double bonds per molecule. A member of this family is benzene, which is represented structurally as:



The other aromatics can be derived from this basic structure by replacing one or more of the hydrogen atoms with a  $CH_3$  or more complex group of atoms. The ring system is exceptionally stable. Observe from the preceding discussion that there is an appreciable difference between a lubricating oil made from a naphthenic base and one made from an aromatic base.

### 4.3 Petroleum or Mineral Oil Base Stocks

Petroleum or mineral oils are generally complex mixtures of hydrocarbons but can roughly be divided according to the chemical family to which their predominating constituents belong, as paraffins or naphthenes (sometimes referred to as cycloparaffins). Paraffinic oils are characterized by their pour points, usually  $-17.8$  to  $-6.7^\circ C$ , and by a moderate change in viscosity with an increase in temperature. In general, their viscosity index will range from 85 to 100. Paraffinic oils have a lower density than naphthenic oils. Naphthenic oils are characterized by pour points from  $-50$  to  $-12^\circ C$  and a larger change in viscosity with an increase in temperature. In general, their viscosity index will range from 0 to 60. Both naphthenic and paraffinic oils have a wide range of flash and fire points.

Paraffinic oils are high in paraffin hydrocarbons and contain some wax. Naphthenic oils are high in naphthenic hydrocarbons and contain little wax. In

applications that operate over a wide range of temperatures, a naphthenic oil would generally be less suitable than a paraffinic oil. Naphthenic products are usually used in applications exhibiting a limited range of operating temperatures and requiring a relatively low pour point. Also, naphthenic oils tend to swell seal materials more than most paraffinic oils.

## 4.4 Synthetic Oil Base Stocks

Synthetic lubricants have the potential of satisfying a wide range of requirements, since they can be formulated with nearly any desired range of a specific property. However, certain other properties fixed by the chemical structures must be accepted in many cases. Applications must be considered in terms of all properties associated with the proposed synthetic fluid. Choosing the right synthetic fluid can be tricky because to get special characteristics the user usually must trade off some other performance feature. Generally, synthetics have good thermal and oxidation stability, but a common weakness is limited lubricity (the ability of the lubricant to reduce wear and friction other than by its purely viscous properties). In general, synthetic oils cost considerably more per unit volume than the petroleum oils they replace. However, the real value of the lubricant must be calculated on a price-for-performance basis. Much of the remainder of this section summarizes papers by Hatton (1973) and Wu (1993).

The field of synthetic lubricants comprises hundreds of organic and semiorganic compounds that cannot be easily classified within the scope of this book. Therefore, synthetic oils will be grouped here by chemical structure. This section briefly summarizes the properties of some of the more popular synthetics (see Table 4.6).

### 4.4.1 Synthetic Hydrocarbons

Synthetic hydrocarbons are compounds containing only carbon and hydrogen that are prepared by chemical reactions starting with low-molecular-weight materials. Synthetic hydrocarbons typically possess narrower boiling point ranges for a given viscosity than petroleum oils. In compatibility with other fluids, corrosivity, etc., they are similar to mineral oils.

The primary reasons for preparing synthetic hydrocarbons for use as lubricants are that chemical synthesis provides specific structures and characteristics and that molecular weight can be controlled within narrow ranges. Therefore, properties that are functions of molecular weight, such as vapor pressure, boiling point, viscosity, and low-temperature characteristics, can be controlled within narrow ranges.

The most important commercial synthetic hydrocarbon lubricants are based on poly-alpha-olefin (PAO) and have wide application in automotive and industrial lubrication areas. PAOs have high viscosity indexes, allowing for a wider operating temperature range, especially given its generally better oxidation stability and lower volatility than hydrocarbon fluids. PAOs can have varied per-

Table 4.6: Comparative rating of synthetic lubricants. [From Hatton (1973).]

Class	Property <sup>a</sup>											
	Viscosity-temperature relationship	Liquid range	Low-temperature properties	Thermal stability	Oxidative stability	Hydrolytic stability	Fire resistance	Lubricating ability	Bulk modulus	Volatility	Radiation resistance	Density
Petroleum oils	G	G	G	F	F	E	L	G	A	A	H	L
Superrefined hydrocarbons	E	G	G	G	F	E	L	G	A	L	H	L
Synthetic hydrocarbons	G	G	G	G	F	E	L	G	A	L	H	L
Organic esters	G	E	G	F	F	F	L	G	A	A	A	A
Polyglycols	G	G	G	F	F	G	L	G	H	A	H	H
Polyphenyl esters	P	G	P	E	G	E	L	G	H	A	H	H
Phosphate esters, alkyl	G	G	G	F	G	F	H	G	H	A	L	H
Phosphate esters, aryl	F	P	P	G	G	F	H	G	H	L	L	H
Silicate esters and polysiloxanes	E	E	E	G	F	P	L	F	A	A	L	A
Silicones	E	E	E	G	G	G	L	P	L	L	L	A
Silanes	G	G	G	G	F	E	L	F	A	H	L	L
Halogenated polyaryls	G	G	F	G	G	E	H	G	H	H	L	H
Fluorocarbons	F	G	F	G	G	F	H	P	L	A	L	H
Perfluoropolyglycols	F	G	G	G	G	G	H	G	L	A	L	H

<sup>a</sup>Ratings: E = excellent, G = good, F = fair, P = poor, H = high, L = low, A = average.

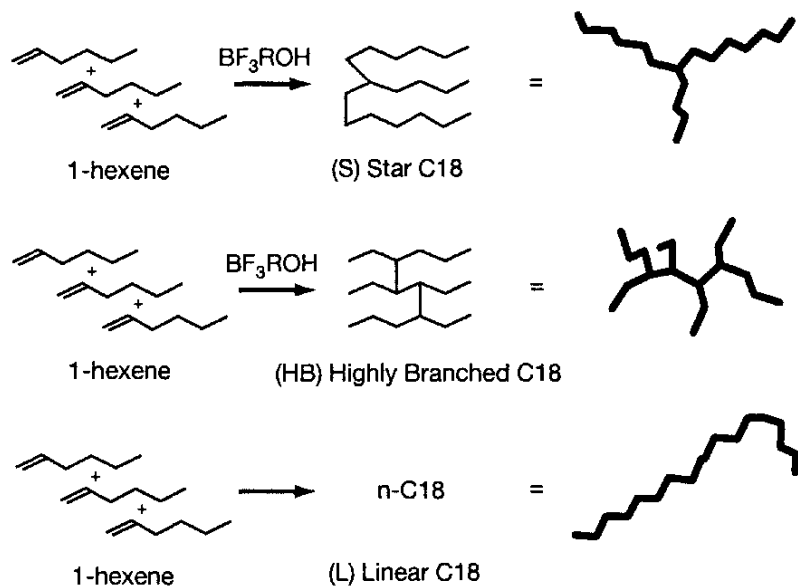


Figure 4.1: Poly-alpha-olefin (PAO) structures. The “star” orientation displays superior lubrication properties. [From Kioupis and Maginn (1999).]

formance depending on the structure of the particular molecule. For example, three different molecular structures of PAO molecules synthesized from hexane molecules to form C18 alkanes are shown in Fig. 4.1. Of these structures, the C18 alkane in the “star” orientation displays superior lubrication properties (Kioupis and Maginn 1999, 2000).

Polyisobutylene (PIB) is another common synthetic hydrocarbon lubricant, especially as a metalworking fluid, but has limited applications because of somewhat poor thermal stability. Organic esters and polyethers are also useful lubricants, often used in combination with PAO.

#### 4.4.2 Organic Esters

The term “organic esters” is applied to those materials that consist of carbon, hydrogen, and oxygen and contain an ester or carboxyl linkage in the molecule. The most widely used as lubricants are those that contain two ester groups and are made from dibasic acids. They are commonly called “diesters.” Diesters are the most widely used synthetic lubricants.

The esters have a good overall balance of properties, particularly in liquid range and in viscosity-volatility characteristics. They possess fair lubricity because they respond well to additives. Aliphatic diesters are thermally stable to about 260°C but are exceedingly vulnerable to oxidation above 149°C. This results in increased viscosity and the generation of oil insolubles and large amounts of acid or corrosive material.

Polyol esters were developed to improve upon the thermal stability of the

diesters while maintaining other desirable properties. However, they give poorer low-temperature performance. The polyol esters are used in other applications requiring enhanced thermal stability.

#### **4.4.3 Polyglycols**

The polyalkylene glycols are the most widely used of this class. They are high-molecular-weight polymers of ethylene or propylene oxide that are available in a wide range of viscosities. Some polymers are completely soluble in water and are often diluted and used as fire-resistant hydraulic fluids or lubricants. Another type of polyglycol is insoluble in water and is used as a lubricant base stock.

The polyglycols are excellent lubricants and respond well to additives. They have high flash points, good viscosity-temperature properties, low wax-free pour points, and shear stability. They have little or no adverse effect on many of the common seal materials but have a strong solvent action on nonresistant paints. Volatility can be a problem, particularly under severe thermal and oxidative conditions. Their stability characteristics, even when improved with appropriate additives, are not outstanding among the synthetics. Their rust-preventing characteristics are generally poor.

Polyglycols are used as industrial lubricants in rubber-processing applications, as machining lubricants, as lubricants for rubber seals, and in heat transfer applications.

#### **4.4.4 Phosphate Esters**

The phosphate esters are a diverse group of chemical compounds varying widely in physical and chemical characteristics. The oxidative stability of most phosphate esters is good; their thermal stability is excellent at medium temperatures but poorer at higher temperatures. In severe environments extensive thermal, oxidative, or hydrolytic breakdown of the phosphate esters can form acidic substances that may corrode metals. The outstanding properties of phosphate esters are their ability to lubricate moving surfaces and their good fire resistance. They are used as the sole component or as the major component of synthetic lubricants and hydraulic fluids. They are also widely used as an additive in both synthetic lubricants and petroleum oils. The phosphate esters require special consideration with respect to material compatibility—proper material matching is critical to successful performance.

#### **4.4.5 Silicon-Containing Compounds**

One of the more fruitful areas of research in modifying carbon, hydrogen, and oxygen compounds has been the inclusion of silicon in the molecule.

## Silicate Esters

These synthetics have found use as base stocks for wide-temperature-range fluids and lubricants. They have excellent viscosity-temperature characteristics and good lubricating properties.

## Silicones

Properly called “siloxane polymers” silicones are characterized by the nature of the substituents that are attached directly to the silicon atoms. Dimethyl silicones are characterized by low freezing points and probably the best viscosity-temperature properties of any synthetic lubricant. They have better thermal and oxidative properties than corresponding hydrocarbons, polyglycols, or aliphatic diesters; they can form gels when permitted to degrade excessively, particularly above 200°C. Stabilization is possible, permitting properly inhibited fluids to be used at temperatures as high as 315°C.

The dimethyl silicones are chemically inert, noncorrosive, and inert to most common plastics, elastomers, and paints. They have low surface tension and are shear stable. Their major shortcoming is their lack of steel-on-steel lubricating ability. They show relatively weak response to the usual lubricant additives. The lubricating properties of silicones can be improved by incorporating chlorine or fluorine into the molecule.

## Silanes

The silanes are compounds that contain only carbon-silicon bonds. These products possess wide liquid ranges and thermal stabilities up to 370°C, but they are poor lubricants for sliding surfaces.

### 4.4.6 Halogen-Containing Compounds

The incorporation of halogen atoms into organic molecules results in higher densities and reduced flammability relative to the parent compound. Chlorine tends to increase the pour point and the viscosity. Fluorine has little influence on the pour point or the viscosity but greatly decreases surface tension.

Because chlorine-aliphatic carbon bonds are generally weak, chlorinated aliphatic compounds have found little use as synthetic lubricants, *per se*. They are used as additives in lubricants to provide a source of chlorine that can be reacted with the surface and thus improve boundary lubrication.

Fluorine-containing materials have not found particular application as lubricants because on a price-for-performance basis the desired properties can better be obtained by using other materials.

#### **4.4.7 Halogenated Polyaryls**

The chlorine-containing biphenyls and polyphenyls have found some use as lubricants. These products range from mobile liquids to tacky solids. In the past they have found use as lubricant base stocks, heat transfer agents, industrial lubricants, and additives. However, these uses are now prohibited because of potential environmental problems. The common term for these materials is "PCB."

#### **4.4.8 Fluorocarbons**

Fluorocarbons are compounds containing only fluorine and carbon. Such compounds have been made and proposed as synthetic lubricant base stocks. In general, they are thermally and oxidatively stable and have physical properties quite similar to those of the corresponding hydrocarbons, but they have a higher density and a lower surface tension. They tend to creep over surfaces but do not appear to wet them in terms of boundary lubrication. Such compounds are particularly useful because of their extreme chemical inertness. These compounds are resistant to ignition by any source and represent some of the most fire-resistant organic compounds known.

Recent studies have been concentrated on the tetrafluoroethylene polymers. These have been used as liquid-oxygen-resistant fluids, lubricants, and greases.

Although not strictly fluorocarbons, the chlorotrifluoroethylene polymers have found some applications and are better lubricants than fluorocarbons because chlorine is more reactive with metals than fluorine. These materials generally have properties similar to those of the fluorocarbons but are significantly less stable.

#### **4.4.9 Perfluoropolyglycols**

The perfluoropolyglycols are polyalkylene glycols in which all the hydrogens have been replaced with fluorines. These types of products derived from propylene oxide are under consideration for a number of applications. Their primary advantages are high thermal stability, extreme fire resistance, relatively good liquid range, and moderate lubricating characteristics. However, they lack stability in the presence of certain commonly used high-temperature metals, have high specific gravities, and do not respond to common additives. Studies are under way to improve performance in these areas.

### **4.5 Grease Base Stocks**

A petroleum grease is a lubricating oil to which a thickener has been added, usually a metallic soap. The type of thickener added determines the characteristics of the grease. Greases are preferred to liquid lubricants when the application of a continuous supply of lubricant is impractical. Greases are also preferred

when equipment is not readily accessible and when a sufficiently tight enclosure for retaining a liquid lubricant does not exist.

#### **4.5.1 Thickeners**

A major factor influencing the properties of a lubricating grease is the thickener employed in it. Thickeners compose 5 to 17% of a simple grease formulation. Ninety percent of all greases sold in the United States are based on what is termed "metallic soap." Soaps utilized in lubricating greases are produced during grease manufacturing by saponifying (neutralizing) fats; the compounds (neutralizers) most commonly used are the hydroxides of lithium, calcium, sodium, barium, and aluminum. The saponifiable compounds include tallow, lard oil, hydrogenated fats and oils, fish oil, fatty acids, and vegetable oils. The two most commonly used fatty acids are stearic and 12-hydroxystearic.

During the grease manufacturing process the oil and the fatty acids are heated to 100°C, at which time the alkaline compound is added and saponification occurs. The water resulting from the chemical reaction is boiled off.

The amount of fatty acid and metal hydroxide added to the oil determines the amount of soap formed. The soap is the thickener. The resultant thickening action is referred to in the grease industry as "consistency." Consistency is a measure of the hardness or softness of the grease.

The major thickener types and the properties associated with them are detailed in the following text. The properties described for each thickener are typical; however, in some formulations they may be radically altered owing to the influence of other grease components.

#### **Water-Stabilized Calcium Soap (Cup-Type Thickener)**

Typically, this thickener is based on calcium stearate stabilized with water. It yields a buttery grease with excellent water resistance. However, service is limited to about 80°C because at higher temperatures the stabilizing water is lost, causing the soap to separate from the oil. This type of grease is chiefly used for mild service applications.

#### **Anhydrous-Calcium Soap**

Typically, this thickener is calcium 12-hydroxystearate. Greases with this thickener are similar to the cup-type products. However, because they do not need water to stabilize the system, they have a higher operating temperature range, typically about 120°C. At about 145°C they melt, often separating into their soap and oil phases. Commonly, such greases are used on rolling-element bearings, for applications such as excavators and other large equipment where temperature extremes do not occur.

## **Sodium Soap**

Sodium soap greases usually employ sodium stearate or similar materials. They tend to be fibrous relative to other types of thickener. Typically, they are usable to about 120°C with melting points in the range 150 to 230°C. Although the thickener provides some inherent rust protection, large amounts of water contamination cause these greases to wash out. Sodium soap greases also generally lack the oxidation resistance of lithium and clay greases. They are typically used in plain journal and slider bearings and gears. Certain short-fiber products may be used in greases for rolling-element bearings.

## **Lithium Soap**

This thickener is usually lithium 12-hydroxystearate. Lithium soaps are the most versatile and widely used greases. They are buttery and have a dropping point of around 180-190°C (and up to 210°C for extreme applications). When melted and recooled, they generally return to a grease texture (although the properties of the resulting recooled grease are usually changed from those of the unmelted grease). Lithium soap greases are also resistant to water, oxidation, and mechanical working. Most formulations will operate for long times at 120°C; some will function for extended times to about 165°C. They are widely used as multipurpose greases and are particularly suited for rolling-element bearings. The use of lithium soap greases has substantially reduced the number of complex specialty lubricating greases that would otherwise be required in modern manufacturing plants.

## **Complex Soaps**

Complex soap thickeners are generally formed by reacting several distinctly different acids with the alkali. For example, calcium-complex soap greases may be formed from calcium 12-hydroxystearate and calcium acetate. Calcium-complex soap, lithium-complex soap, and aluminum-complex soap thickened greases are fairly common, with some other types being used occasionally. The principal advantage of most complex soap thickeners is their high melting point, typically about 260°C or higher. This permits their use in applications in which the temperature may at times exceed the melting point of the simple soap thickeners and thus is the reason why they are much used today. Generally, if these greases are used in sustained service above about 120°C, frequent relubrication is needed unless the product is specially formulated for sustained high-temperature service.

## **Polyureas**

Polyureas are nonsoap thickeners that are polymerized substituted ureas. Like the complex soaps they typically melt at about 260°C and are used in similar types of service.

## **Clay Thickeners**

These thickeners are generally bentonite or hectorite clay that has been chemically treated to make it thicken oil. The chief feature of clay-thickened greases is that the thickener does not melt; hence, these greases can be used in operations in which temperatures occasionally exceed the melting points of other thickeners. Their oxidation stability is generally no better than that of other petroleum products. Therefore, if these greases are used in sustained service at temperatures above about 120°C, frequent relubrication is necessary unless the product has been explicitly formulated for sustained service at higher temperatures.

### **4.5.2 Lubricating Oil**

Lubricating oil is the largest single component of a lubricating grease and is the component that provides the grease with its ability to lubricate. Simple greases, only oil and thickener, usually contain 65 to 95% oil. Although the retentive properties of grease, as well as its resistance to heat, water, and extreme loads, depend upon the proportion and type of soap, the frictional characteristics of grease are based on its oil content. The more important oil properties affecting overall grease performance are as follows:

1. Viscosity and viscosity-temperature characteristics, which influence the ability of a grease to form a lubricating film in service and also influence its behavior at low temperatures
2. Oxidation resistance and evaporation characteristics, which influence the ability of a grease to lubricate for extended times, especially at higher temperatures
3. Characteristics affecting elastomers, which influence the compatibility of a grease with seal materials used in bearings and other devices

Most greases employ a petroleum-based oil as the lubricating oil, but some use synthetic fluids. Diesters, silicones, polyol esters, polyalkylene glycols, and fluorosilicones are most commonly used. These fluids offer special characteristics, such as high-temperature performance, chemical resistance, and low-temperature performance, that elude refined petroleum oils. Their cost is substantially higher than that of the refined petroleum oils.

The typical characteristics of some greases are shown in Table 4.7. The knowledge of these characteristics is important in establishing which grease is to be used in a specific application. Within the table the dropping point of the various greases is given. This characteristic is obtained from a test (ASTM D-566 and D-2265, IP-132, and DIN 51801) that indicates the temperature at which the thickener deteriorates (melts, loses water of stabilization, etc.). Greases generally should not be used above their dropping point temperatures, but many greases cannot be used even near them because of limits of base-oil

Table 4.7: Typical characteristics of lubricating greases

Thickener type	Thickener content, mass-%	Dropping point °C	Mechanical stability	Maximum temperature °C	Relative cost <sup>a</sup>
<b>Soap Thickeners</b>					
Lithium 12 HS	8–10	180–190	Good	120	2
Lithium complex	12–20	> 250	Good	150	3–4
Calcium, hydrated	7–12	80–100	Poor to good	< 70	1
Calcium, 12 HS (anhydrous)	7–12	140–150	Fair to good	110	2–3
Calcium complex	15–30	> 250	Poor to good	150	3–4
Sodium	8–10	150–170	Poor to fair	110–120	1
Sodium complex	10–20	> 250	Fair to good	150	3
Aluminum	8–10	90	Poor	< 70	1
Aluminum complex	10–20	> 250	Good	150	3
Barium	7–17	180	Fair to good		
Barium complex	10–20	> 250	Good		
<b>Non-soap Thickeners</b>					
Clays <sup>b</sup>	7–12	—	Poor to good	120	2–3
Silica, methylated <sup>b</sup>	7–12	—	Fair to good	120	3
Polyurea <sup>c</sup>	7–12	> 230	Good	150	4

<sup>a</sup>Cost: 1 = low; 5 = high.

<sup>b</sup>Sensitive to pressure and thermal separation.

<sup>c</sup>Often in combination with soap complex.

oxidation stability, additive stability, etc. The test designation of ASTM is for tests developed in the United States, IP for Britain, and DIN for Germany.

## 4.6 Gases

Just as liquids and greases are used as lubricants, so too can gases be used as lubricants, as explained more fully in Chapters 14 and 15. In this section some of the properties of gases will be described. As shown in Fig. 4.2 a most interesting aspect of gases is their viscosity-temperature relationship. That is, the viscosity of gases increases with temperature and is only moderately affected by changes in temperature and pressure. In contrast to this situation, as mentioned earlier in this chapter, liquids vary inversely with temperature and are strongly sensitive to temperature and pressure variations.

Figure 4.3 shows the viscosity of common gases as a function of temperature. The viscosity of air is midrange of the gases; hydrogen has the lowest and neon the highest value. The information given in Fig. 4.3 is tabulated in Table 4.8 for a complete range of temperatures. Besides the viscosity data, Table 4.8 also gives the boiling temperature and the gas constant. Table 4.9 shows how the properties of gases and liquids differ. Only a small number of quite different

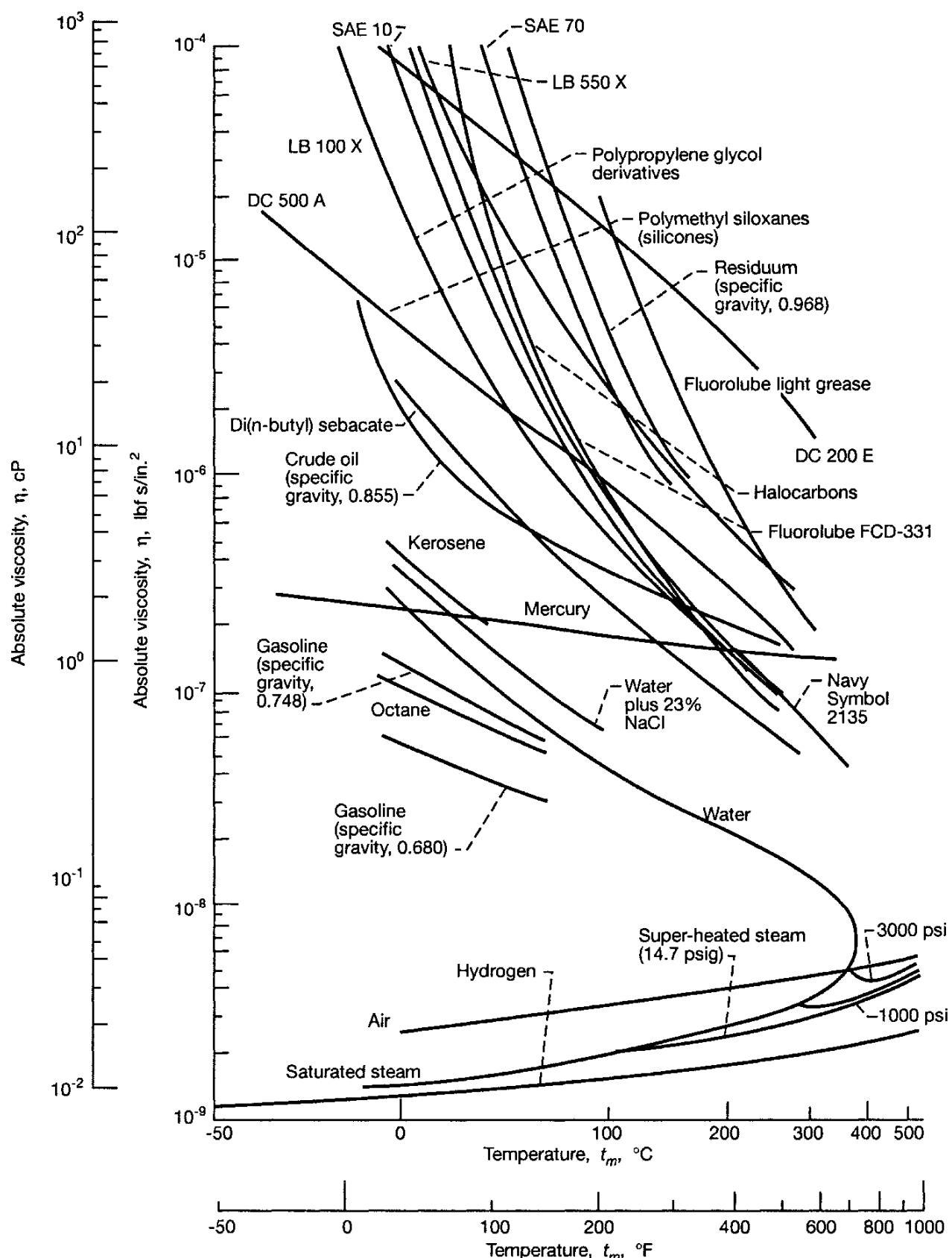


Figure 4.2: Absolute viscosities of a number of fluids for a wide range of temperatures.

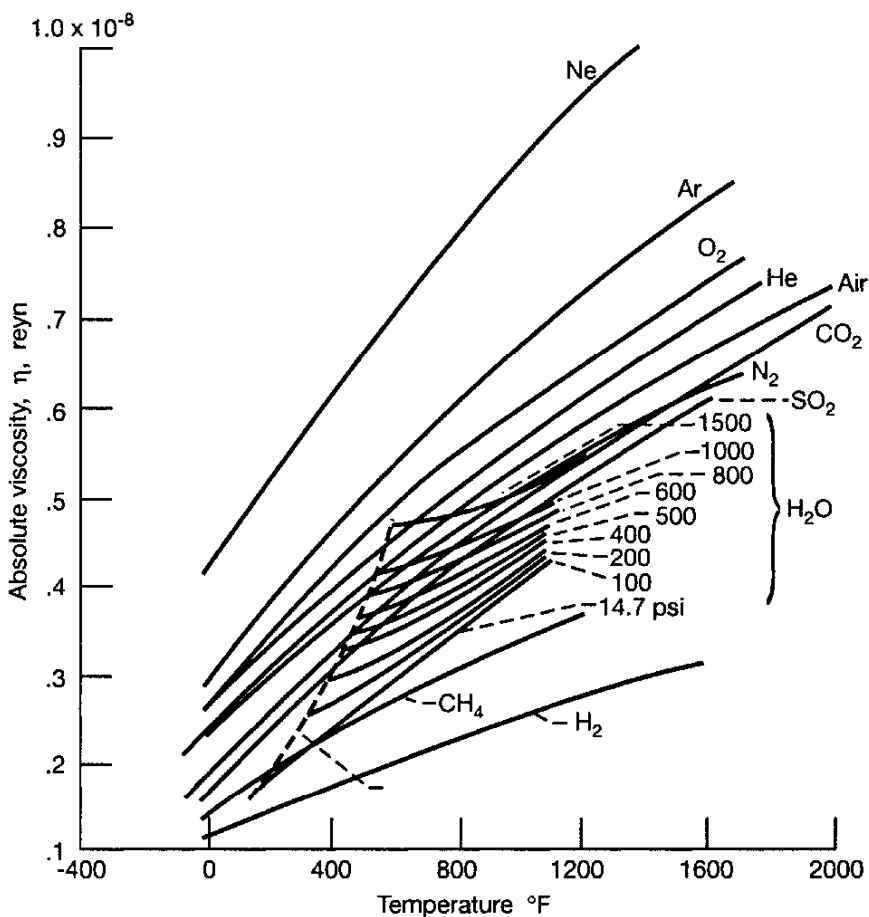


Figure 4.3: Viscosity of common gases as a function of temperature. [From Cameron (1976).]

liquids and gases are shown to illustrate the differences. Note that Tables 4.8 and 4.9 as well as Fig. 4.3 are in English units rather than SI units.

## 4.7 Emulsions

Lubricants serve many functions, only one of which is the generation of a load-bearing fluid film between surfaces. One other important function is associated with the removal of heat from bearing surfaces. Emulsions combine the lubricating effectiveness of oils with the cooling ability of water, and are therefore popular for some demanding applications. Also, because of the high water content, emulsions have been applied for applications where nonflammability is required.

An emulsion is a mixture of two immiscible liquids, where one is suspended in the other in the form of droplets that are larger than  $1 \mu\text{m}$  in diameter. Emulsions typically consist of 1-5% oil phase, with the remainder water. The oil phase contains 80-90% base oil with assorted additives making up the remainder of the formulation. Since oil is less dense than water, the emulsion will separate

Table 4.8: Viscosity of various gases at 14.7 psia. [From Svehla (1962).]

Temperature		Air	Ar	CO <sub>2</sub>	H <sub>2</sub> O	He	Kr	N <sub>2</sub>	Ne	Xe
°F	°R	Absolute viscosity $\times 10^{-9}$ , $\eta$ , lbf·s/in. <sup>2</sup> (reyn)								
-280	180	1.07	1.27	0.74	—	1.45	—	1.05	2.12	—
-100	360	1.97	2.41	1.49	—	2.27	2.50	1.91	3.48	2.24
80	540	2.68	3.32	2.20	—	2.96	3.67	2.57	4.56	3.35
260	720	3.29	4.10	2.84	2.08	3.56	4.69	3.15	5.50	4.38
440	900	3.84	4.80	3.41	2.59	4.11	5.61	3.66	6.35	5.29
620	1080	4.34	5.44	3.93	3.12	4.62	6.46	4.14	7.16	6.15
800	1260	4.80	6.04	4.41	3.64	5.11	7.23	4.57	7.91	6.93
980	1440	5.24	6.59	4.86	4.17	5.56	7.95	4.99	8.64	7.67
1160	1620	5.64	7.11	5.29	4.69	6.00	8.65	5.39	9.31	8.36
1340	1800	6.05	7.60	5.70	5.20	6.43	9.30	5.75	9.96	9.03
1520	1980	6.44	8.09	6.09	5.70	6.84	9.92	6.13	10.60	9.66
1700	2160	6.80	8.55	6.45	6.19	7.23	10.52	6.49	11.19	10.26
2600	3060	8.55	11.82	8.14	8.41	9.05	13.26	8.14	14.00	13.00
Boiling temperature, °R		—	147.2	—	67.2	7.9	219.2	139	48.7	298.4
Gas constant, in. <sup>2</sup> /(s <sup>2</sup> ·°R) $\times 10^{-5}$		2.47	1.79	1.63	39.8	17.9	0.85	2.55	3.54	0.55

Table 4.9: Some properties of common liquids and gases at 68°F and 14.7 psia. [From Gross (1980)]

Liquid or gas	Force density $\rho$ , lbf s <sup>2</sup> /in. <sup>4</sup>	Absolute viscosity $\eta$ , lbf s/in. <sup>2</sup> (reyn)	Kinematic viscosity $\eta_k$ , in. <sup>2</sup> /s	Specific heat $C_p$ , in./°F	Thermal conductivity $K_f$ , lbf/s °F
Liquids					
Carbon tetrachloride	$1.48 \times 10^{-4}$	$1.41 \times 10^{-7}$	$9.52 \times 10^{-4}$	$1.87 \times 10^3$	$2.4 \times 10^{-2}$
Glycerine	$1.18 \times 10^{-4}$	$1.21 \times 10^{-4}$	1.06	$5.4 \times 10^3$	$3.54 \times 10^{-2}$
Olive oil	$8.49 \times 10^{-5}$	$1.22 \times 10^{-5}$	$1.44 \times 10^{-1}$	$4.4 \times 10^3$	$2.10 \times 10^{-2}$
Lubricating oil	$8.02 \times 10^{-5}$	$4.44 \times 10^{-5}$	5.54	$4.7 \times 10^3$	$1.83 \times 10^{-2}$
Water	$9.33 \times 10^{-5}$	$1.46 \times 10^{-7}$	$1.56 \times 10^{-3}$	$9.32 \times 10^3$	$7.50 \times 10^{-2}$
Gases					
Air	$1.15 \times 10^{-7}$	$2.62 \times 10^{-9}$	$2.28 \times 10^{-2}$	$2.24 \times 10^3$	$3.22 \times 10^{-3}$
Helium	$1.61 \times 10^{-8}$	$2.85 \times 10^{-9}$	$1.77 \times 10^{-1}$	$1.17 \times 10^3$	$2.4 \times 10^{-2}$
Hydrogen	$8.08 \times 10^{-9}$	$1.31 \times 10^{-9}$	$1.62 \times 10^{-1}$	$3.20 \times 10^4$	$2.29 \times 10^{-2}$
Nitrogen	$1.12 \times 10^{-7}$	$2.56 \times 10^{-9}$	$2.28 \times 10^{-2}$	$2.32 \times 10^3$	$3.11 \times 10^{-3}$

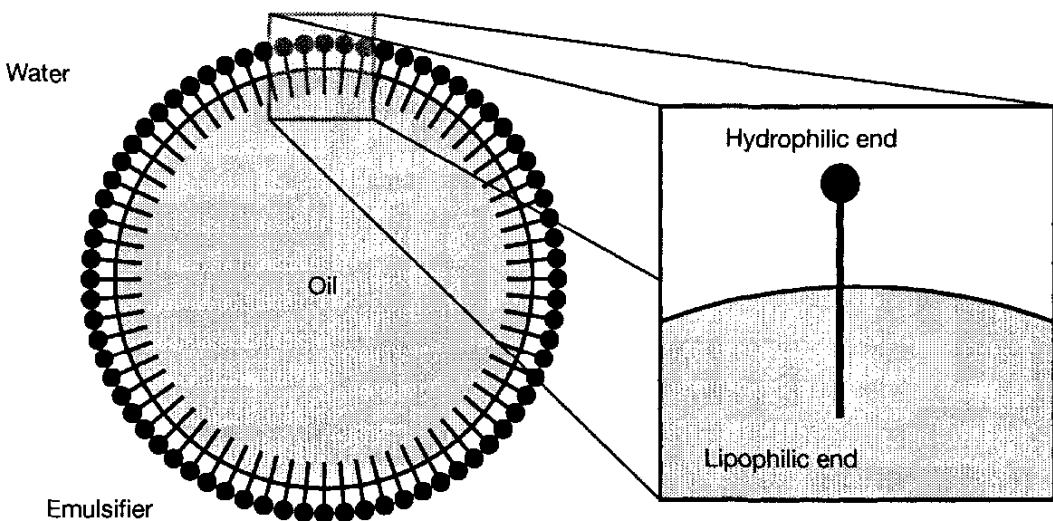


Figure 4.4: An oil-in-water emulsion stabilized by an emulsifier.

into two phases and have limited use as a lubricant. Increased stability can be achieved in an emulsion through the addition of an emulsifier. An emulsifier is a long chain paraffinic molecule with a polar end, with one end preferring water (hydrophilic end) and the other preferring oil (lipophilic). An oil droplet stabilized by an emulsifier is shown in Fig. 4.4. This natural orientation of the emulsifier molecules generates a surface tension through the attraction or repulsion of the ends of the emulsifier molecule and the water and oil.

Commercially available emulsions are formulated by the supplier and shipped in a form ready for mixing with water. Usually, deionized water is preferred because of adverse affects of hard water on emulsifiers and hence emulsion stability. The mixing procedure varies with user, but typically a prescribed agitation is applied for a certain number of fixed intervals, with pauses allowed for foams to dissipate.

## 4.8 Lubricant Additives

Industrial lubricants consist of 75-90% by volume base oil, the remainder additives. A wide variety of additives are applied in lubricant formulation, the most common of which are summarized here.

- *Boundary and extreme pressure lubricant (lubricity) additives.* When asperity contact takes place, it is beneficial to have a protective lubricant coating to reduce friction and wear. Boundary lubrication is discussed in Section 1.3.4.
- *Biocides.* Oil and additives such as emulsifiers are subject to biological attack in solution. For this reason, biocides are added to the base oil to control the activity of microorganisms and extend the useful life of

lubricants. The development of biocides is the topic of ongoing research, since the environmental implications of lubricant disposal conflict with the need for biodegradation resistance during use.

- *Alkalinity additives.* In naval applications, it is common to use a high-sulfur fuel, which results in  $\text{SO}_2$  and  $\text{SO}_3$  combustion products. These can cause acidic corrosion of machine elements, which is avoided through additives that increase the alkalinity of the lubricant. See Schmid and Schmid (2001) for details.
- *Detergents.* Especially in diesel engines, carbon particulate can become suspended in the lubricant and can coat and foul machine elements. Detergent additives maintain a suspension of particles, prolonging lubricant life.
- *Antifoaming additives.* Antifoaming additives are added to ensure proper flooding of contacts and pump operation.
- *Demulsibility (water-shedding) additives.* For marine applications, it is possible that lubricant can become contaminated with water. Additives that force rapid separation of the water from the lubricant are utilized for these applications.
- *Antioxidants.* Antioxidants decrease the rate of oxidation of oil, which is especially important at elevated temperatures.
- *Viscosity additives, viscosity index additives and emulsifiers* are also incorporated into certain industrial lubricants as described above.

## 4.9 Newtonian Fluids

The friction between surfaces that are completely separated (no asperity contact) is due solely to the internal friction of the liquid, namely, its viscosity. Newton in 1687 found that the absolute viscosity of a liquid  $\eta$  can be defined as

$$\eta = \frac{\tau}{s} \quad (4.1)$$

where

$$\begin{aligned}\tau &= \text{shear stress, N/m}^2 \\ s &= \text{shear strain rate, } du/dz, \text{ s}^{-1} \\ \eta &= \text{absolute viscosity, N}\cdot\text{s/m}^2\end{aligned}$$

The viscosity of a fluid may be associated with its resistance to flow, that is, with the resistance arising from intermolecular forces and internal friction as the molecules move past each other. Thick fluids such as molasses have relatively high viscosity; they do not flow easily. Thinner fluids such as water have lower

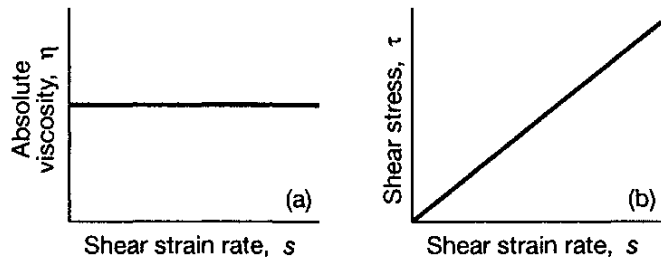


Figure 4.5: Properties of a Newtonian fluid. (a) Effect of viscosity on shear strain rate; (b) effect of shear stress on shear strain rate.

viscosity; they flow very easily. The flow characteristics of Newtonian liquids as a function of shear strain rate are shown in Fig. 4.5.

## 4.10 Newton's Postulate

Let us relook at Eq. (4.1) in the way Newton did, while making use of the sketch shown in Fig. 4.6. Oil molecules were visualized as small balls that roll along in layers between flat planes. Since the oil will "wet" and cling to the two surfaces, the bottommost layer will not move at all, the uppermost layer will move with a velocity equal to the velocity of the upper plane, and the layer in between will move with a velocity directly proportional to the distance between the two planes. This type of orderly movement in parallel layers is known as "streamline," "laminar," or "viscous" flow.

Newton went on to define

$$s = \text{shear strain rate} = \frac{u}{h} = \frac{u_1}{h_1} = \frac{u_2}{h_2} = \dots$$

Newton correctly deduced that the force required to maintain a constant velocity  $u$  of the upper layer was proportional to the area  $A$  and the velocity

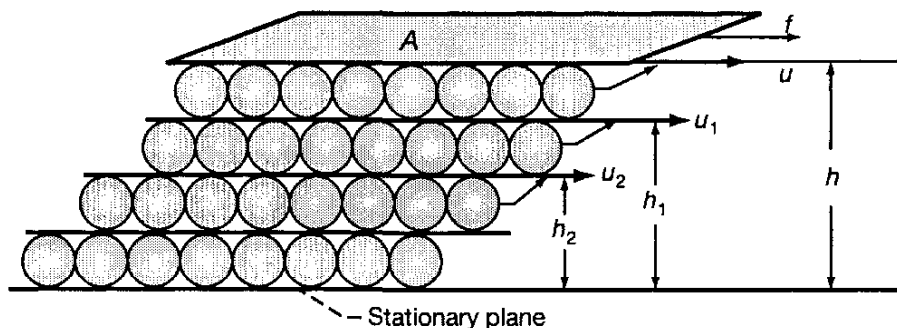


Figure 4.6: Physical illustration of Newton's postulate, where  $f$  = friction force, N;  $A$  = area,  $\text{m}^2$ ;  $u$  = velocity,  $\text{m/s}$ ;  $h$  = film thickness, m.

Table 4.10: Viscosity conversion factors.

To convert from —	To —			
	cP	kgf·s/m <sup>2</sup>	N·s/m <sup>2</sup>	lbf·s/in. <sup>2</sup>
	Multiply by —			
cP	1	$1.02 \times 10^{-4}$	$10^{-3}$	$1.45 \times 10^{-7}$
kgf·s/m <sup>2</sup>	$9.807 \times 10^3$	1	9.807	$1.422 \times 10^{-3}$
N·s/m <sup>2</sup>	$10^3$	$1.02 \times 10^{-1}$	1	$1.45 \times 10^{-4}$
lbf·s/in. <sup>2</sup>	$6.9 \times 10^6$	$7.03 \times 10^2$	$6.9 \times 10^3$	1

gradient or shear strain rate ( $s = u/h$ ):

$$f = \eta A \frac{u}{h} \quad (4.2)$$

where  $\eta$  is the proportionality constant, the viscosity coefficient, or the absolute viscosity. Viscosity, absolute viscosity, and dynamic viscosity all mean the same as defined above. By rearranging Eq. (4.2), absolute viscosity can be written as

$$\eta = \frac{f/A}{u/h} = \frac{\text{shear stress}}{\text{shear strain rate}} \quad (4.3)$$

## 4.11 Units of Absolute Viscosity

It follows from Eq. (4.3) that the units of viscosity must be the units of shear stress divided by the units of shear rate. The units of viscosity  $\eta$  for three different systems are

1. SI system: N·s/m<sup>2</sup> or, since a newton per square meter is also called a pascal, Pa·s
2. cgs system: dyn·s/cm<sup>2</sup> (dyne-second per square centimeter) or poise, where  $1 \text{ cP} = 10^{-2} \text{ P}$
3. English system: lbf·s/in.<sup>2</sup> (pound-force-second per square inch), called a reyn in honor of Osborne Reynolds

Conversion of absolute viscosity from one system to another can be facilitated by Table 4.10. To convert from a unit in the column on the left side of the table to a unit at the top of the table, multiply by the corresponding value given in the table.

### Example 4.1

**Given** An absolute viscosity of 0.04 N·s/m<sup>2</sup>.

**Find** The absolute viscosity in reyn, centipoise, and poise.

**Solution** Using Table 4.10 while recognizing that  $1 \text{ reyn} = 1 \text{lbf}\cdot\text{s}/\text{in.}^2$  gives

$$\eta = 0.04 \text{ N}\cdot\text{s}/\text{m}^2 = (0.04) 1.45 \times 10^{-4} \text{ lbf}\cdot\text{s}/\text{in.}^2 = 5.8 \times 10^{-6} \text{ lbf}\cdot\text{s}/\text{in.}^2$$

Note also that

$$\eta = 0.04 \text{ N}\cdot\text{s}/\text{m}^2 = 0.04 \text{ Pa}\cdot\text{s} = 5.8 \times 10^{-6} \text{ lbf}\cdot\text{s}/\text{in.}^2$$

and

$$\eta = 0.04 \text{ N}\cdot\text{s}/\text{m}^2 = (0.04) (10^3) \text{ cP} = 40 \text{ cP} = 0.4 \text{ P}$$

---

## Example 4.2

**Given** An absolute viscosity of 1 reyn.

**Find** The absolute viscosity in centipoise.

**Solution**

$$1 \text{ reyn} = 1 \text{ lbf}\cdot\text{s}/\text{in.}^2 = 7.03 \times 10^2 \text{ kgf}\cdot\text{s}/\text{m}^2 = 6.9 \times 10^6 \text{ cP}$$

$$1 \mu\text{reyn} = 1 \times 10^{-6} \text{ reyn} = 6.9 \text{ cP}$$

---

## 4.12 Kinematic Viscosity

In many situations it is convenient to use kinematic viscosity rather than absolute viscosity. The kinematic viscosity  $\eta_k$  is defined as

$$\eta_k = \frac{\text{absolute viscosity}}{\text{density}} = \frac{\eta}{\rho} = \frac{\text{N}\cdot\text{s}/\text{m}^2}{\text{N}\cdot\text{s}^2/\text{m}^4} = \text{m}^2/\text{s} \quad (4.4)$$

The ratio given in Eq. (4.4) is literally kinematic, all trace of force or mass canceling out. The units of kinematic viscosity are

1. SI units: square meters per second ( $\text{m}^2/\text{s}$ )
2. cgs units: square centimeters per second ( $\text{cm}^2/\text{s}$ ), called a stoke (St)
3. English units: square inches per second ( $\text{in.}^2/\text{s}$ )

Table 4.11 shows the difference between absolute and kinematic viscosity with increasing temperature for two types of lubricating oil. Because of the decrease in density, the difference between absolute and kinematic viscosity increases with increasing temperature. Absolute viscosity is required for calculating elastohydrodynamic lubrication as related to rolling-element bearings and gears. However, kinematic viscosity can be determined experimentally more easily and with great precision and is therefore preferred for characterizing lubricants.

Table 4.11: Divergence between kinematic and absolute viscosity data with increasing temperature. [From Klaman (1984).]

Temper- ature $t_m$ , °C	Paraffinic base oil			Naphthenic base oil		
	Kinematic viscosity $\eta_k$ , mm <sup>2</sup> /s	Absolute viscosity $\eta$ , mPa·s	Viscosity difference $\Delta$ , percent	Kinematic viscosity $\eta_k$ , mm <sup>2</sup> /s	absolute viscosity $\eta$ , mPa·s	Viscosity difference $\Delta$ , percent
0	287	253	13.4	1330	1245	6.8
20	78.4	68	15.3	218	201.0	8.5
40	30.2	25.8	17.1	60.5	55.0	10.0
60	14.7	12.33	19.2	23.6	21.2	11.3
80	8.33	6.91	20.5	11.6	16.2	13.7
100	5.3	4.32	22.7	6.66	5.80	14.8
120	3.65	2.93	24.6	4.27	3.66	16.7
150	2.33	1.83	27.3	2.53	2.12	19.3

## 4.13 Viscosity Grade System

The International Organization for Standardization (ISO) system is based on the kinematic viscosity of the oil, in centistokes, at 40°C. Each viscosity grade is numerically equal to the kinematic viscosity at the midpoint of the range. To fall into a given viscosity grade, the oil must be within 10% of the midpoint kinematic viscosity.

Figure 4.7 shows the various viscosity grades. The intent of this figure is to show how the various designations and the grades within them compare. The lowest grades are not presented because of space limitations. The Saybolt universal viscosity unit given in this figure is a commercial measure of kinematic viscosity expressed as the time in seconds required for 60 cm<sup>3</sup> of a fluid to flow through the orifice of the standard Saybolt universal viscometer at a temperature of 38°C.

Herschel in 1918 found that the kinematic viscosity in centistokes can be expressed in terms of a Saybolt second by the general formula

$$\eta_k = \bar{A}t - \frac{\mathcal{B}}{t}$$

where  $\bar{A}$  and  $\mathcal{B}$  are experimentally determined constants having units of centimeters squared per second squared and centimeters squared, respectively. In this expression  $t$  is expressed in Saybolt seconds. Values of  $\bar{A}$  and  $\mathcal{B}$  were obtained from experiments, and the preceding equation became

$$\eta_k = 0.22t - \frac{180}{t} \quad (4.5)$$

This equation is helpful in converting Saybolt seconds into kinematic viscosity expressed in centistokes. The appropriate expression, if we know the kinematic

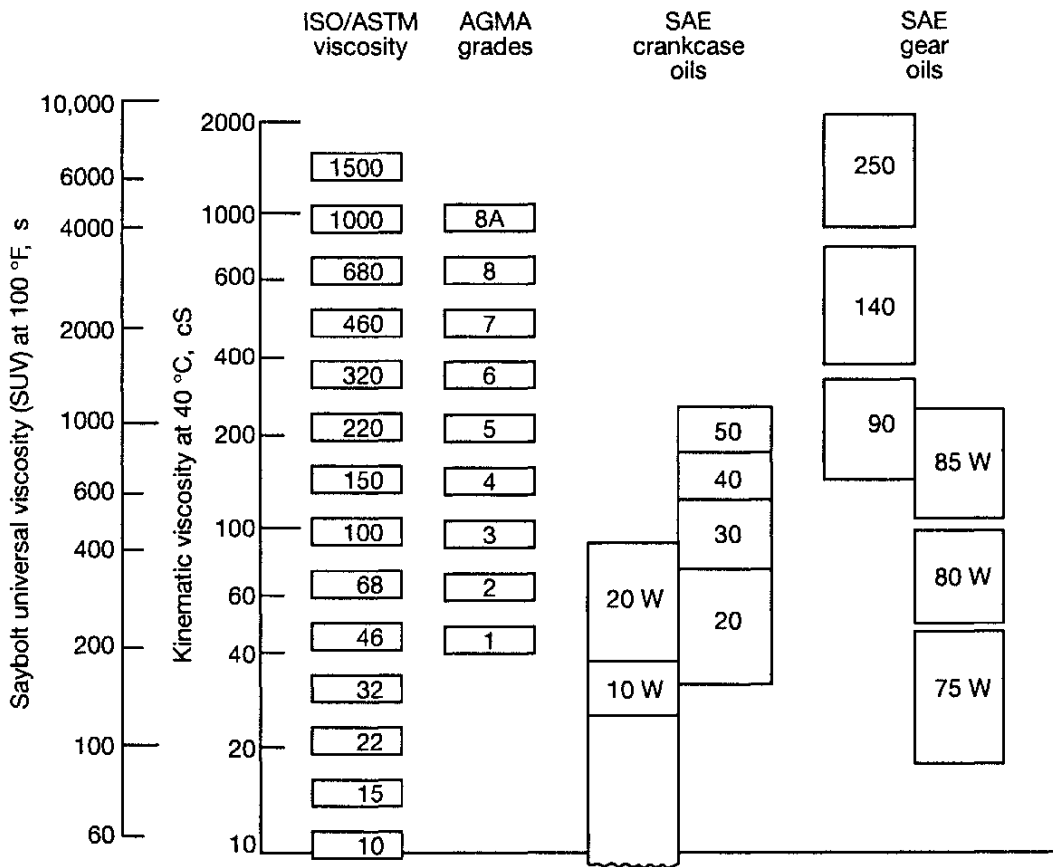


Figure 4.7: Viscosity grade comparisons. [From Litt (1986).]

viscosity and wish to know what the Saybolt seconds would be, can be determined from the equation

$$t = 2.27 \left[ \eta_k + (\eta_k^2 + 158.4)^{1/2} \right] \quad (4.6)$$

Equations (4.5) and (4.6) are only valid when the kinematic viscosity  $\eta_k$  is expressed in terms of centistokes and the time  $t$  in terms of Saybolt seconds.

Viscosity is the most important property of the lubricants employed in hydrodynamic and elastohydrodynamic lubrication. In general, however, a lubricant does not simply assume a uniform viscosity in a given bearing. This results from the nonuniformity of the pressure and/or the temperature prevailing in the lubricant film. Indeed, many elastohydrodynamically lubricated machine elements operate over ranges of pressure and/or temperature so extensive that the consequent variations in the viscosity of the lubricant may become substantial and, in turn, may dominate the operating characteristics of the machine element. Consequently, an adequate knowledge of the viscosity-pressure and viscosity-pressure-temperature relationships of lubricants is indispensable. The next three sections deal with such relationships.

Table 4.12: Absolute and kinematic viscosities of fluids at atmospheric pressure and three temperatures. [From Jones et al. (1975).]

Fluid	Temperature, $t_m$ , °C					
	38	99	149	38	99	149
	Absolute viscosity at $p = 0$ $\eta_0$ , cP			Kinematic viscosity at $p=0$ $\eta_k \times 10^5$ , m <sup>2</sup> /s		
Advanced ester	25.3	4.75	2.06	2.58	0.51	0.23
Formulated advanced ester	27.6	4.96	2.15	2.82	0.53	0.24
Polyalkyl aromatic	25.5	4.08	1.80	3.0	0.50	0.23
Synthetic paraffinic oil (lot 3)	414	34.3	10.9	49.3	4.26	1.4
Synthetic paraffinic oil (lot 4)	375	34.7	10.1	44.7	4.04	1.3
Synthetic paraffinic oil (lot 2) plus antiwear additive	370	32.0	9.93	44.2	4.0	1.29
Synthetic paraffinic oil (lot 4) plus antiwear additive	375	34.7	10.1	44.7	4.04	1.3
C-ether	29.5	4.67	2.20	2.5	0.41	0.20
Superrefined naphthenic mineral oil	68.1	6.86	2.74	7.8	0.82	0.33
Synthetic hydrocarbon (traction fluid)	34.3	3.53	1.62	3.72	0.40	0.19
Fluorinated polyether	181	20.2	6.68	9.66	1.15	0.4

## 4.14 Viscosity-Pressure Effects

As long ago as 1893, Barus proposed the following formula for the isothermal viscosity-pressure dependence of liquids:

$$\ln \frac{\eta}{\eta_0} = \xi p \quad (4.7)$$

where

$\ln$  = natural, or Napierian, logarithm,  $\log_e$

$\eta_0$  = absolute viscosity at  $p = 0$  and at a constant temperature, N·s/m<sup>2</sup>

$\xi$  = pressure-viscosity coefficient of the lubricant dependent on  
temperature, m<sup>2</sup>/N

$p$  = pressure, N/m<sup>2</sup>

Table 4.12 lists the kinematic viscosities in square meters per second and absolute viscosities in centipoise of 11 lubricants at zero pressure and three temperatures. These values of the absolute viscosity correspond to  $\eta_0$  in Eq. (4.8) for the particular fluid and temperature used. The manufacturer and the manufacturer's designation for these 11 lubricants are given in Table 4.13 and the pressure-viscosity coefficients  $\xi$ , expressed in square meters per newton, in Table 4.14. The values correspond to  $\xi$  used in Eq. (4.7).

Although Eq. (4.7) is extensively used, it is not generally applicable and is valid as a reasonable approximation only at moderate pressures. Because of this shortcoming of Eq. (4.7), several isothermal viscosity-pressure formulas have

been proposed that usually fit experimental data better than that suggested by Barus (1893). One of these approaches, which is used in this book, was developed by Roelands, who undertook a wide-ranging study of the effect of pressure on lubricant viscosity. For isothermal conditions the Roelands (1966) formula can be written as

$$\log \eta + 1.200 = (\log \eta_0 + 1.200) \left(1 + \frac{p}{2000}\right)^{Z_1} \quad (4.8)$$

where

$\log$  = common, or Briggsian, logarithm,  $\log_{10}$

$\eta$  = absolute viscosity, cP

$\eta_0$  = absolute viscosity at  $p = 0$  and a constant temperature, cP

$p$  = gage pressure, (kg)<sub>force</sub>/cm<sup>2</sup>

$Z_1$  = viscosity-pressure index, a dimensionless constant

Taking the antilog of both sides of Eq. (4.8) and rearranging terms gives

$$\bar{\eta} = \frac{\eta}{\eta_0} = 10^{-(1.2+\log \eta_0)[1-(1+p/2000)^{Z_1}]} \quad (4.9)$$

Rearranging this equation gives

$$\bar{\eta} = \frac{\eta}{\eta_0} = \left(\frac{\eta_\infty}{\eta_0}\right)^{1-(1+p/c_p)^{Z_1}} \quad (4.10)$$

where

$$\eta_\infty = 6.31 \times 10^{-5} \text{ N}\cdot\text{s}/\text{m}^2 (9.15 \times 10^{-9} \text{ lbf}\cdot\text{s}/\text{in.}^2)$$

$$c_p = 1.96 \times 10^8 \text{ N/m}^2 (28,440 \text{ lbf/in.}^2)$$

In Eq. (4.10) care must be taken to use the same dimensions in defining the constants  $\eta_\infty$  and  $c_p$  as are used for  $\eta_0$  and  $p$ .

Figure 4.8 compares the Barus equation [Eq. (4.7)] with the Roelands equation [Eq. (4.10)] for three different fluids presented in Tables 4.12 to 4.15. The temperature is fixed at 38°C. This figure indicates that for pressures normally experienced in elastohydrodynamically lubricated conjunctions ( $\sim 1$  GPa), the difference between the two formulas is appreciable. Figure 4.8 shows that the viscosity rises more rapidly for the Barus formula than for the Roelands formula for oils 1 and 2, but for oil 3 the Roelands formula rises more rapidly than the Barus formula. The difference between the formulas varies with the lubricant, the difference being less for the traction fluid. When the pressure approaches zero, the two formulas produce the same viscosity.

Table 4.15 gives values of the viscosity-pressure index  $Z_1$  as obtained from Jones et al. (1975) for the same lubricants considered in Tables 4.12 to 4.14. Roelands (1966) found that for most fluids  $Z_1$  is usually constant over a wide temperature range. This is confirmed in Table 4.15, the only exceptions being the synthetic hydrocarbon (traction fluid) and the C-ether.

Table 4.13: Fluids with manufacturer and manufacturer's designation. [From Jones *et al.* (1975).]

Fluid	Manufacturer	Designation
Advanced ester	Shell Oil Co.	Aeroshell turbine oil 555 (base oil)
Formulated advanced ester	Shell Oil Co.	Aeroshell turbine oil 555 (WRGL - 358)
Polyalkyl aromatic	Continental Oil Co.	DN-600
Synthetic paraffinic oil (lot 3)	Mobil Oil Co.	XRM 109-F3
Synthetic paraffinic oil (lot 4)	Mobil Oil Co.	XRM 109-F4
Synthetic paraffinic oil (lot 2) plus antiwear additive	Mobil Oil Co.	XRM 177-F2
Synthetic paraffinic oil (lot 4) plus antiwear additive	Mobil Oil Co.	XRM 177-F4
C-ether superrefined naphthenic mineral oil	Humble Oil and Refining Co.	FN 2961
Synthetic hydrocarbon (traction fluid)	Monsanto Co.	MCS-460
Fluorinated polyether	DuPont Co.	PR 143 AB (lot 10)

Table 4.14: Pressure-viscosity coefficients for fluids at three temperatures. [From Jones *et al.* (1975).]

Fluid	Temperature $t_m$ , °C		
	38	99	149
	Pressure-viscosity coefficient, $\xi$ , m <sup>2</sup> /N		
Advanced ester	$1.28 \times 10^{-8}$	$0.987 \times 10^{-8}$	$0.851 \times 10^{-8}$
Formulated advanced ester	$1.37 \times 10^{-8}$	$1.00 \times 10^{-8}$	$0.874 \times 10^{-8}$
Polyalkyl aromatic	$1.58 \times 10^{-8}$	$1.25 \times 10^{-8}$	$1.01 \times 10^{-8}$
Synthetic paraffinic oil (lot 3)	$1.77 \times 10^{-8}$	$1.51 \times 10^{-8}$	$1.09 \times 10^{-8}$
Synthetic paraffinic oil (lot 4)	$1.99 \times 10^{-8}$	$1.51 \times 10^{-8}$	$1.29 \times 10^{-8}$
Synthetic paraffinic oil (lot 2) plus antiwear additive	$1.81 \times 10^{-8}$	$1.37 \times 10^{-8}$	$1.13 \times 10^{-8}$
Synthetic paraffinic oil (lot 4) plus antiwear additive	$1.96 \times 10^{-8}$	$1.55 \times 10^{-8}$	$1.25 \times 10^{-8}$
C-ether	$1.80 \times 10^{-8}$	$0.980 \times 10^{-8}$	$0.795 \times 10^{-8}$
Superrefined naphthenic mineral oil	$2.51 \times 10^{-8}$	$1.54 \times 10^{-8}$	$1.27 \times 10^{-8}$
Synthetic hydrocarbon (traction fluid)	$3.12 \times 10^{-8}$	$1.71 \times 10^{-8}$	$0.939 \times 10^{-8}$
Fluorinated polyether	$4.17 \times 10^{-8}$	$3.24 \times 10^{-8}$	$3.02 \times 10^{-8}$

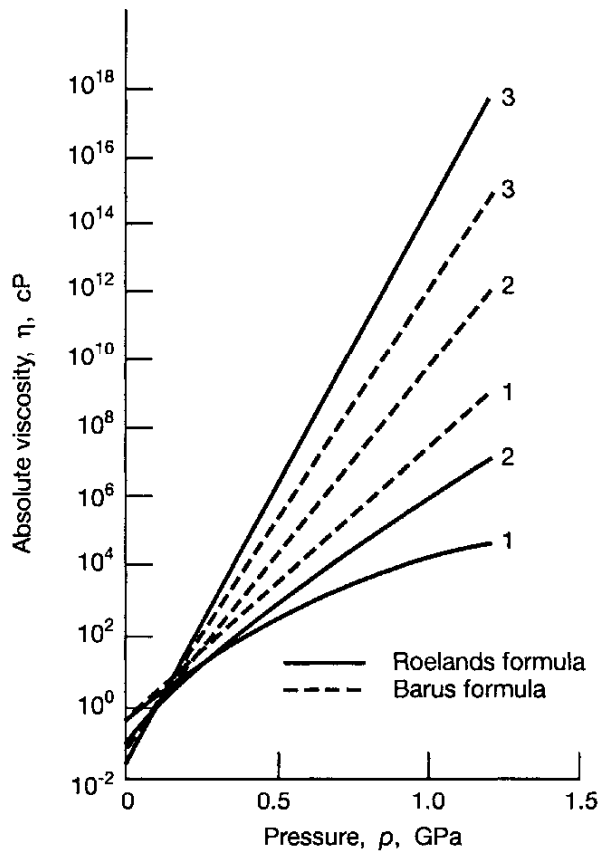


Figure 4.8: Comparison of absolute viscosity obtained from Barus' and Roelands' formulas for a wide range of pressure. Results are shown for three different lubricants at 38°C; oil 1 — synthetic paraffinic oil (lot 3); oil 2 — superrefined naphthenic mineral oil; oil 3 — synthetic hydrocarbon (traction fluid).

Blok (1965) arrived at the important conclusion that all elastohydrodynamic lubrication results achieved from the Barus formulas [Eq. (4.7)] can be generalized, to a fair approximation, simply by substituting the reciprocal of the asymptotic isoviscous pressure  $1/p_{iv,as}$  for the pressure-viscosity coefficient occurring in those results. This implies

$$\xi = \frac{1}{p_{iv,as}}$$

where

$$p_{iv,as} = \eta_0 \int_0^\infty \frac{dp}{\eta} \quad (4.11)$$

Substituting Eq. (4.7) into (4.11) quickly proves that  $\xi = 1/p_{iv,as}$ .

The preceding can be used to find a tie between the pressure-viscosity coefficient  $\xi$  used in the Barus formula [Eq. (4.7)] and the viscosity-pressure index  $Z_1$  used in the Roelands formula [Eq. (4.10)]. Making use of the fact

Table 4.15: Dimensionless viscosity pressure index for fluids at three temperatures. [From Jones et al. (1975).]

Fluid	Temperature $t_m, ^\circ\text{C}$					
	38	99	149	38	99	149
	Dimensionless viscosity-pressure index, $Z_1$					
	From Jones et al. (1975)			From Eq. (4.12)		
Advanced ester	0.48	0.48	0.48	0.42	0.45	0.48
Formulated advanced ester	0.49	0.47	0.49	0.44	0.45	0.49
Polyalkyl aromatic	0.55	0.54	0.55	0.52	0.59	0.59
Synthetic paraffinic oil (lot 3)	0.43	0.44	0.39	0.40	0.47	0.42
Synthetic paraffinic oil (lot 4)	0.44	0.46	0.47	0.45	0.47	0.50
Synthetic paraffinic oil (lot 2) plus antiwear additive	0.43	0.44	0.43	0.41	0.43	0.44
Synthetic paraffinic oil (lot 4) plus antiwear additive	0.44	0.46	0.46	0.44	0.48	0.48
C-ether	0.72	0.50	0.50	0.57	0.45	0.44
Superrefined naphthenic mineral oil	0.67	0.67	0.64	0.71	0.64	0.66
Synthetic hydrocarbon (traction fluid)	1.06	0.85	0.69	0.97	0.83	0.57
Fluorinated polyether	0.77	0.79	0.80	1.03	1.10	1.27

that the two different formulas approach each other as the pressure approaches zero gives

$$\frac{\partial}{\partial p} (\ln \eta|_{\text{Roelands}})_{p \rightarrow 0} \equiv \frac{\partial}{\partial p} (\ln \eta|_{\text{Barus}})_{p \rightarrow 0} = \xi$$

Making use of Eq. (4.10) gives

$$Z_1 = \frac{\xi}{(1/c_p)(\ln \eta_0 - \ln \eta_\infty)} \quad (4.12)$$

But

$$\frac{1}{c_p} = \frac{1}{1.96 \times 10^8} \text{ m}^2/\text{N} = 5.1 \times 10^{-9} \text{ m}^2/\text{N}$$

$$\ln \eta_\infty = \ln (6.31 \times 10^{-5} \text{ N}\cdot\text{s}/\text{m}^2) = -9.67$$

$$\therefore Z_1 = \frac{\xi}{5.1 \times 10^{-9} (\ln \eta_0 + 9.67)}$$

This equation is unit sensitive and only applicable for SI units. Equation (4.12), which is general, thus enables one to quickly determine the viscosity-pressure index directly from knowing the pressure-viscosity coefficient, or vice versa.

Table 4.15 also compares the viscosity-pressure indexes as obtained from Jones et al. (1975) and from Eq. (4.12) for the same fluids considered in Tables 4.12 to 4.14. The agreement between the two methods of obtaining  $Z_1$  is quite good, the exception being the fluorinated polyether. Thus, Eq. (4.12) can be useful for relating the viscosity as obtained from the Roelands and Barus formulas.

---

## Example 4.3

**Given** Both mercury and water have an absolute viscosity of 1.5 cP at 5°C, but mercury has 13.6 times higher density than water. Assume that no change in density occurs when the temperature is increased.

**Find** The kinematic viscosities of mercury and water at 5°C and at 90°C.

**Solution** Figure 4.2 gives the absolute viscosities of various fluids as a function of temperature. At 90°C the absolute viscosity of water is 0.32 cP, and for mercury it is 1.2 cP. The kinematic viscosity of *mercury* at 5 °C is

$$\eta_k = \frac{\eta}{\rho} = \frac{1.2(10^{-3})}{13,600} = 0.110(10^{-6}) \text{ m}^2/\text{s}$$

At 90°C it is

$$\eta_k = \frac{\eta}{\rho} = \frac{0.32(10^{-3})}{13,600} = 0.0882(10^{-6}) \text{ m}^2/\text{s}$$

The kinematic viscosity of *water* at 5°C is

$$\eta_k = \frac{\eta}{\rho} = \frac{1.5(10^{-3})}{1000} = 1.5(10^{-6}) \text{ m}^2/\text{s}$$

At 90°C it is

$$\eta_k = \frac{\eta}{\rho} = \frac{0.32(10^{-3})}{1000} = 0.32(10^{-6}) \text{ m}^2/\text{s}$$

Although mercury has the same absolute viscosity as water at 5°C and 3.75 times higher absolute viscosity at 90°C, the kinematic viscosities for mercury are much lower than those for water because of mercury's high density.

---

## Example 4.4

**Given** A synthetic paraffin has an absolute viscosity of 32 cP at 99°C , and a fluorinated polyether has an absolute viscosity of 20.2 cP at 99°C.

**Find**

- The pressure at which the two oils have the same absolute viscosity.
- The pressure at which the paraffin is 100 times less viscous than the polyether.

**Solution**

(a) From Table 4.15 the pressure-viscosity coefficient at 99°C for the paraffin is  $1.37 \times 10^{-8} \text{ m}^2/\text{N}$  and for the polyether it is  $3.24 \times 10^{-8} \text{ m}^2/\text{N}$ . Using the Barus equation (Eq. 4.7) while equating the viscosity gives

$$32e^{1.37 \times 10^{-8} p} = 20.2e^{3.24 \times 10^{-8} p}$$

$$1.58e^{1.37 \times 10^{-8} p} = e^{3.24 \times 10^{-8} p}$$

But

$$1.58 = e^{0.46}$$

Therefore

$$e^{0.46+1.37 \times 10^{-8} p} = e^{3.24 \times 10^{-8} p}$$

$$p = 24.6 \times 10^6 \text{ Pa} = 24.6 \text{ MPa}$$

(b) Using the Barus equation [Eq. (4.7)] while letting the paraffin be 100 times less viscous than the polyether gives

$$1.58 (100) e^{1.37 \times 10^{-8} p} = e^{3.24 \times 10^{-8} p}$$

But

$$158 = e^{5.063}$$

Therefore

$$e^{5.063+1.37 \times 10^{-8} p} = e^{3.24 \times 10^{-8} p}$$

$$p = 2.71 \times 10^8 \text{ Pa} = 0.271 \text{ GPa}$$

---

## 4.15 Viscosity-Temperature Effects

The viscosity of mineral and synthetic oils decreases with increasing temperature. Therefore, the temperature at which the viscosity was measured must be quoted with every viscosity reported. Figures 4.2 and 4.9 show how absolute viscosity varies with temperature. The absolute viscosity of a number of different fluids for a wide range of temperatures is presented in Fig. 4.2. The interesting point of this figure is how drastically the slope and the level of viscosity change for different fluids. The viscosity varies five orders of magnitude, with the slope being highly negative for the SAE oils and positive for gases. Figure 4.9 gives the viscosity-temperature effect for the SAE Oils.

The expression used by Roelands (1966) to describe the effect of temperature on viscosity is given as

$$\log(\log \eta + 1.200) = -S_0 \log\left(1 + \frac{t_m}{135}\right) + \log G_0 \quad (4.13)$$

where

$\eta$  = absolute viscosity, cP

$t_m$  = temperature, °C

$G_0$  = dimensionless constant indicative of viscosity grade of liquid

$S_0$  = dimensionless constant that establishes slope of viscosity-temperature relationship

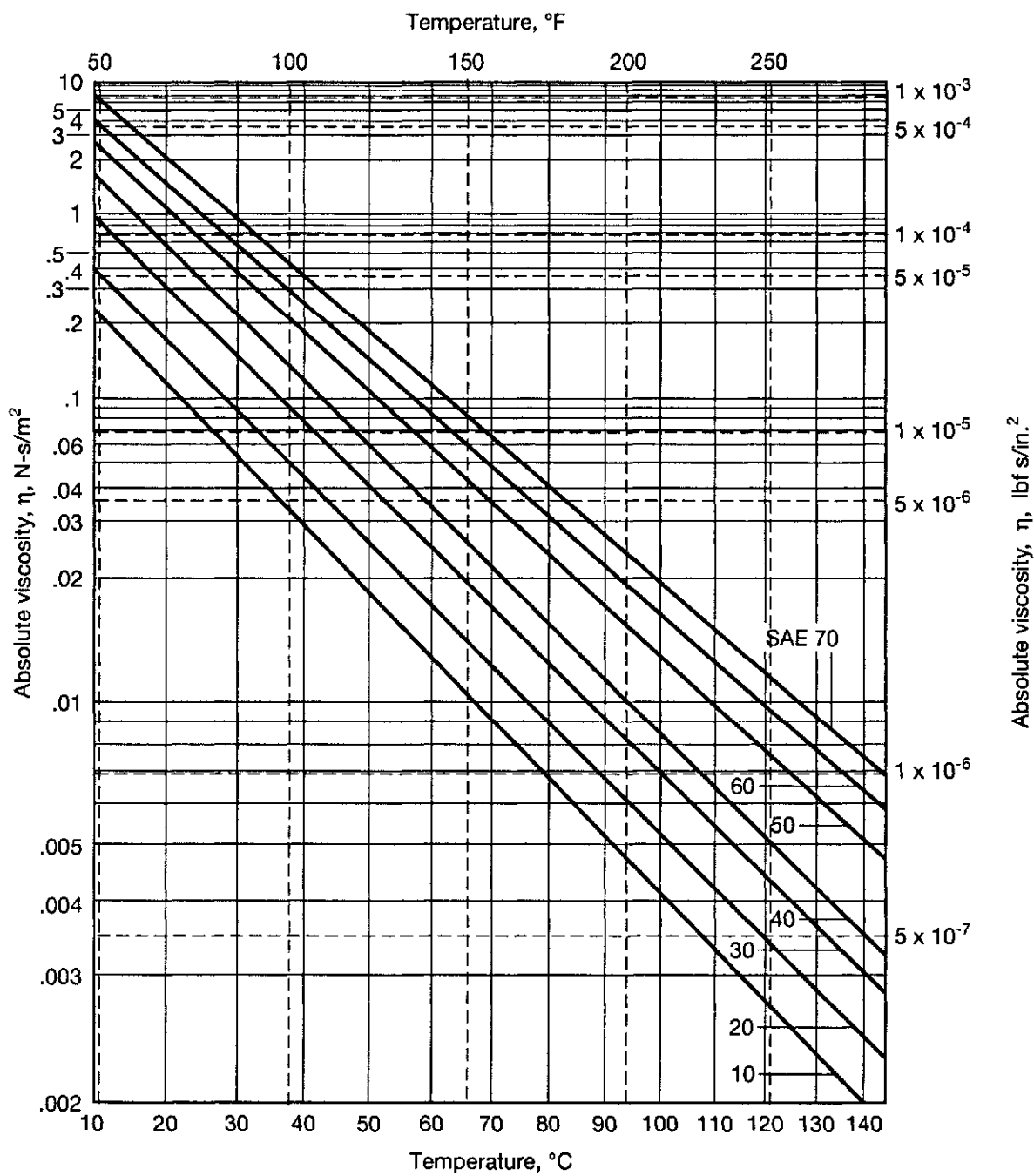


Figure 4.9: Absolute viscosities of SAE lubricating oils at atmospheric pressure.

Taking the antilog of Eq. (4.13) gives

$$\log \eta + 1.2 = G_0 \times 10^{-S_0 \log(1+t_m/135)} \quad (4.14)$$

Equation (4.14) can be expressed in dimensionless terms as

$$\bar{\eta} = \frac{\eta}{\eta_0} = \left( \frac{\eta_\infty}{\eta_0} \right) 10^{G_0(1+t_m/135)-S_0} \quad (4.15)$$

where

$$\eta_\infty = 6.31 \times 10^{-5} \text{ N}\cdot\text{s}/\text{m}^2 \left( 9.15 \times 10^{-9} \text{ lbf}\cdot\text{s}/\text{in.}^2 \right)$$

Besides the variations of viscosity with temperature, a number of other thermal properties of fluids are important in lubrication. Some of these are specific heat, volumetric specific heat, thermal conductivity, and thermal diffusivity. The volumetric specific heat  $C_s$  is defined as the density multiplied by the specific heat ( $C_s = \rho C_p$ ) and therefore has the units of kilojoules per degree Celsius per cubic meter ( $\text{kJ}/^\circ\text{C} \cdot \text{m}^3$ ). Winer and Cheng (1980) point out that  $C_s$  is relatively constant for classes of fluids based on chemical composition.

Winer and Cheng (1980) also point out that the thermal conductivity  $K_f$ , like the volumetric specific heat, is relatively constant for classes of lubricants based on chemical composition. For mineral oils the thermal conductivity is between 0.12 and 0.15  $\text{W}/\text{m}\cdot^\circ\text{C}$ . Recall that a watt is equivalent to a joule per second ( $\text{W} = \text{J}/\text{s}$ ), a joule is equivalent to a newton-meter ( $\text{J} = \text{N}\cdot\text{m}$ ), and a newton is equivalent to a kilogram-meter per second squared ( $\text{N} = \text{kg}\cdot\text{m}/\text{s}^2$ ). Typical values of thermal properties of other fluids are shown in Table 4.16. In this table the thermal diffusivity is defined as  $K_f/\rho C_p$ .

## Example 4.5

**Given** An SAE 10 oil is used in a car motor where the working temperature is  $110^\circ\text{C}$ .

**Find** How many times more viscous would the oil be if the motor were used in arctic conditions where the working temperature is  $-30^\circ\text{C}$ ?

**Solution** Figure 4.9 gives the viscosity at  $110^\circ\text{C}$  to be 3.3 cP and, by extrapolation, to be  $10^4$  at  $-30^\circ\text{C}$ . The viscosity ratio is  $10^4/3.3 = 3030$ . The oil is 3030 times more viscous at  $-30^\circ\text{C}$  than at  $110^\circ\text{C}$ .

## 4.16 Viscosity-Pressure-Temperature Effects

Viscosity is extremely sensitive to both pressure and temperature. This extreme sensitivity forms a considerable obstacle to the analytical description

Table 4.16: Typical thermal properties of some liquids. [From Winer and Cheng (1980).]

Temperature $t_m$ °C	Density $\rho$ , kg/m <sup>3</sup>	Specific heat $C_p$ , kJ/kg °C	Kinematic viscosity $\eta_k = \eta/\rho$ , m <sup>2</sup> /s	Thermal conductivity $K_f$ , W/m °C	Thermal diffusivity $\alpha_t = K_f/\rho \cdot C_p$ , m <sup>2</sup> /s
Glycerin ( $C_3H_5(OH)_3$ )					
0	1276	2.261	0.00831	0.282	$0.983 \times 10^{-7}$
10	1270	2.319	0.00300	0.284	$0.965 \times 10^{-7}$
20	1264	2.386	0.00118	0.286	$0.947 \times 10^{-7}$
30	1258	2.445	0.00050	0.286	$0.929 \times 10^{-7}$
40	1252	2.512	0.00022	0.286	$0.914 \times 10^{-7}$
Ethylene glycol ( $C_2H_4(OH)_2$ )					
0	1130	2.294	$57.53 \times 10^{-6}$	0.242	$0.934 \times 10^{-7}$
20	1116	2.382	$19.18 \times 10^{-6}$	0.249	$0.939 \times 10^{-7}$
40	1101	2.474	$8.69 \times 10^{-6}$	0.256	$0.939 \times 10^{-7}$
60	1087	2.562	$4.75 \times 10^{-6}$	0.260	$0.932 \times 10^{-7}$
80	1077	2.650	$2.98 \times 10^{-6}$	0.261	$0.921 \times 10^{-7}$
Engine oil (unused) <sup>a</sup>					
0	899	1.796	0.00428	0.147	$0.911 \times 10^{-7}$
20	888	1.880	0.00090	0.145	$0.872 \times 10^{-7}$
40	876	1.964	0.00024	0.144	$0.834 \times 10^{-7}$
60	864	2.047	$0.839 \times 10^{-4}$	0.140	$0.800 \times 10^{-7}$
80	852	2.131	$0.375 \times 10^{-4}$	0.138	$0.769 \times 10^{-7}$
100	840	2.219	$0.203 \times 10^{-4}$	0.137	$0.738 \times 10^{-7}$
120	828	2.307	$0.124 \times 10^{-4}$	0.135	$0.710 \times 10^{-7}$
140	816	2.395	$0.080 \times 10^{-4}$	0.133	$0.686 \times 10^{-7}$
160	805	2.483	$0.056 \times 10^{-4}$	0.132	$0.663 \times 10^{-7}$
Mercury (Hg)					
0	13,628	0.1403	$0.1240 \times 10^{-6}$	8.20	$42.99 \times 10^{-7}$
20	13,579	0.1394	$0.1140 \times 10^{-6}$	8.69	$46.06 \times 10^{-7}$
50	13,505	0.1386	$0.1040 \times 10^{-6}$	9.40	$50.22 \times 10^{-7}$
100	13,384	0.1373	$0.0928 \times 10^{-6}$	10.51	$57.16 \times 10^{-7}$
150	13,264	0.1365	$0.0853 \times 10^{-6}$	11.49	$63.54 \times 10^{-7}$
200	13,144	0.1570	$0.0802 \times 10^{-6}$	12.34	$69.08 \times 10^{-7}$
Diester					
30	910	1.93	—	0.151	$0.860 \times 10^{-7}$
Phosphate ester					
30	1060	1.76	—	0.125	$0.670 \times 10^{-7}$
Polyglycol					
30	1000	1.97	—	0.125	$0.670 \times 10^{-7}$
Polyphenylether					
30	1180	1.80	—	0.132	$0.621 \times 10^{-7}$
Dimethyl silicone					
30	970	1.42	—	0.142	$1.03 \times 10^{-7}$
Chlorofluorocarbon					
30	1900	1.22	—	0.069	$0.298 \times 10^{-7}$
Fluorinated polyether					
30	1870	0.96	—	0.093	$0.518 \times 10^{-7}$

<sup>a</sup>The viscosity values should only be used if no other information on the particular lubricant is available. The thermal properties ( $\rho$ ,  $C_p$ ,  $K_f$ ,  $\alpha_t$ ) should be representative of most mineral oils.

of the consequent viscosity changes. Roelands (1966) noted that at constant pressure the viscosity increases more or less exponentially with the reciprocal of absolute temperature. Similarly, at constant temperature the viscosity increases more or less exponentially with pressure as shown earlier in this chapter. In general, however, the relevant exponential relationships constitute only first approximations and may be resorted to only in moderate-temperature ranges.

From Roelands (1966) the viscosity-temperature-pressure equation can be written as

$$\log \eta + 1.200 = G_0 \frac{(1 + p/2000)^{C_2 \log(1+t_m/135)+D_2}}{(1 + t_m/135)^{S_0}} \quad (4.16)$$

Comparing Eqs. (4.10) and (4.14) with the preceding equation reveals the contribution of the pressure and temperature effects that are contained in Eq. (4.16). Equation (4.16) can also be expressed as

$$\bar{\eta} = \frac{\eta}{\eta_0} = \frac{\eta_\infty}{\eta_0} 10^{G_0(1+t_m/135)^{-S_0}(1+p/2000)^{D_2-C_2 \log(1+t_m/135)}} \quad (4.17)$$

According to Eq. (4.17), four parameters ( $G_0$ ,  $S_0$ ,  $C_2$ , and  $D_2$ ) that are determined experimentally are sufficient to enable the viscosity  $\eta$  to be expressed in centipoise as a function of temperature  $t_m$  in degrees Celsius and gage pressure  $p$  in kilograms per square centimeter.

## 4.17 Viscosity-Shear Rate Effects

Liquids whose viscosities are independent of the shear rate are known as “Newtonian.” Liquids whose viscosities vary with shear rate are known as “non-Newtonian.” Figure 4.10 shows viscosity and shear stress versus shear rate for Newtonian and non-Newtonian fluids. In Fig. 4.10a the pseudoplastic fluids show a decrease in viscosity with increasing shear rate. This behavior may be restricted to ranges of shear rate. The dilatant fluid shows an increase in viscosity with increasing shear rate.

In Fig. 4.10b the shear stress is shown as a function of shear rate for a Newtonian, a pseudoplastic, and a dilatant fluid and a Bingham solid. A Bingham solid is a plastic solid such as a grease that flows only above a certain yield shear stress. The pseudoplastic fluids are characterized by linearity at extremely low and extremely high shear rates. The dilatant fluid exhibits an increase in apparent viscosity with increasing shear rate. An explanation of this behavior in the case of suspensions is that particles in a concentrated suspension will be oriented at rest so that the void space is a minimum. The suspending liquid is just sufficient to fill the voids in this state. The increase in voidage caused by shearing a dilatant material means that the space between particles becomes incompletely filled with liquid. Under these conditions of inadequate lubrication the surfaces of adjacent particles come into direct contact, causing an increase in apparent viscosity with increasing shear rate.

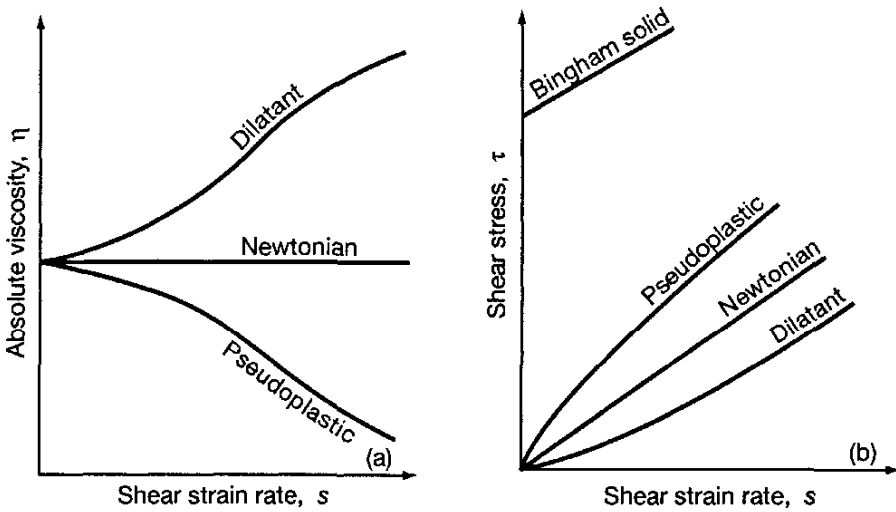


Figure 4.10: Characteristics of different fluids as a function of shear rate: (a) viscosity; (b) shear stress.

## 4.18 Viscosity Index

To better evaluate the relationship between viscosity and temperature, Dean and Davis (1929) developed an arbitrary system of comparison called a “viscosity index” (VI). The standard of comparison is based on Pennsylvania oils refined by the sulfuric acid method and on Texas or California oils refined by the same process. The Pennsylvania oils thinned (became less viscous) less rapidly than other types of mineral oils when subjected to increases in temperature. Those oils were rated 100 for this property. The Texas naphthenic oils were rated 0.

Although oils have changed considerably since 1929, the interest in expressing the relative change of viscosity with temperature has not. As far as evaluating between two limits is concerned, there is no question as to the sense and meaning of the viscosity index. A viscosity index of 75 means that the quality of an oil with regard to viscosity has reached 75% of the range from the poorest naphthenic oil ( $VI = 0$ ) to the best Pennsylvania oil ( $VI = 100$ ). When the limiting oils were selected, no allowance was made for development in manufacturing methods and the introduction of synthetic lubricants. As a result, lubricants are produced today with viscosity indices that are considerably higher than 100 [Mishra and Saxton (1995) report VI up to 170 for some multigrade oils]. It is nevertheless customary to compute the viscosity index according to the formula

$$VI\% = \left( \frac{\bar{L} - \bar{x}}{\bar{L} - \bar{H}} \right) 100 \quad (4.18)$$

where

$\bar{L}$  = Saybolt universal viscosity (SUV) of reference oil of low VI

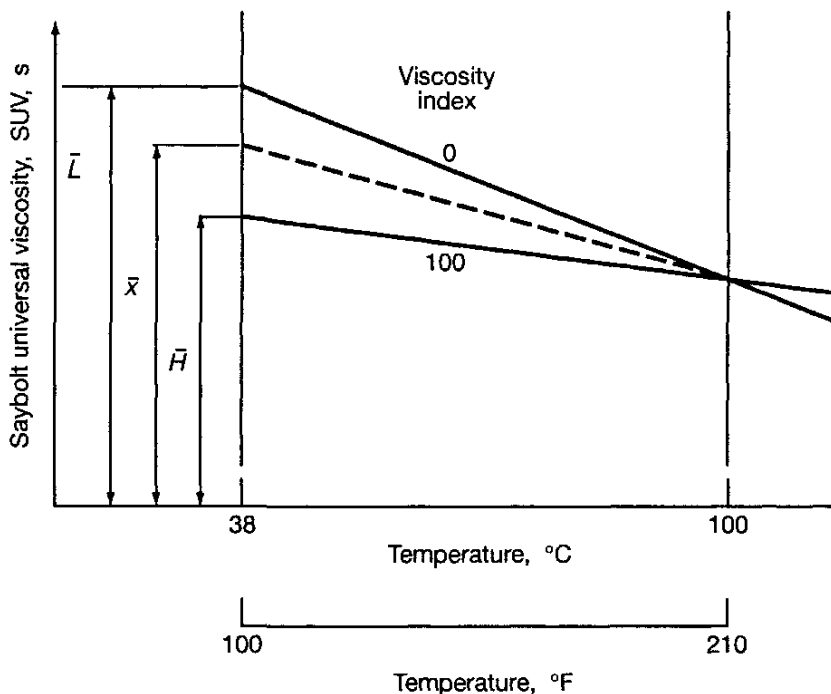


Figure 4.11: Graphical explanation of viscosity index, where  $\bar{L}$  = low VI oil,  $\bar{x}$  = unknown oil, and  $\bar{H}$  = high VI oil.

$$\begin{aligned}\bar{H} &= \text{SUV of reference oil of high VI} \\ \bar{x} &= \text{SUV of unknown oil}\end{aligned}$$

Note that the values of  $\bar{L}$ ,  $\bar{H}$ , and  $\bar{x}$  are assumed to be equal at 100°C. Equation (4.18) is expressed graphically in Fig. 4.11.

Figure 4.11 shows how the viscosity index is obtained. The figure shows that the two reference oils and the unknown oil have the same Saybolt viscosity at 100°C. At 38°C the Saybolt viscosities are different, and these values of  $\bar{L}$ ,  $\bar{H}$ , and  $\bar{x}$  are then used in Eq. (4.18).

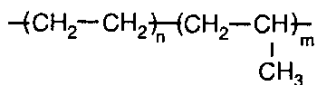
Table 4.17 gives tabular values of  $\bar{H}$  and  $\bar{L}$  at 38°C for given values of the Saybolt universal viscosity of the unknown oil at 100°C. These values are to be used in Eq. (4.18).

Viscosity index improvers are often added to automotive oils to reduce the loss of viscosity at high temperatures. These are usually soluble polymers, summarized in Fig. 4.12, whose structure is temperature dependent. At low temperatures, the polymer molecules coil into a ball-like shape, providing very little additional resistance to lubricant shear. However, at elevated temperatures, the molecules uncoil and provide considerable resistance to shear; the effect is that the viscosity does not fall as much with a VI improver in the formulation.

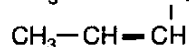
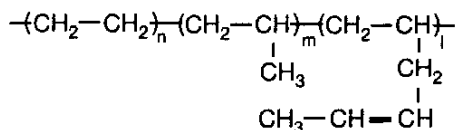
Table 4.17: Viscosity-index data to be used in Eq. (4.18) [From: An abridgement from ASTM D567, "Standard Method for Calculating Viscosity Index".]

SUV at 100 °C $\bar{x}$	SUV at 38 °C		SUV at 100 °C $\bar{x}$	SUV at 38 °C		SUV at 100 °C $\bar{x}$	SUV at 38 °C	
	$\bar{H}$	$\bar{L}$		$\bar{H}$	$\bar{L}$		$\bar{H}$	$\bar{L}$
40	93	107	—	—	—	—	—	—
41	109	137	81	810	1674	121	1643	3902
42	124	167	82	829	1721	122	1665	3966
43	140	197	83	849	1769	123	1688	4031
44	157	228	84	868	1817	124	1710	4097
45	173	261	85	888	1865	125	1733	4163
46	189	291	86	907	1914	126	1756	4229
47	205	325	87	927	1964	127	1779	4296
48	222	356	88	947	2014	128	1802	4364
49	238	389	89	966	2064	129	1825	4430
50	255	422	90	986	2115	130	1848	4498
51	272	456	91	1006	2166	131	1871	4567
52	288	491	92	1026	2217	132	1894	4636
53	305	525	93	1046	2270	133	1918	4705
54	322	561	94	1066	2322	134	1941	4775
55	339	596	95	1087	2375	135	1965	4845
56	356	632	96	1107	2428	136	1988	4915
57	374	669	97	1128	2481	137	2012	4986
58	391	706	98	1148	2536	138	2036	5058
59	408	743	99	1168	2591	139	2060	5130
60	426	781	100	1189	2646	140	2084	5202
61	443	819	101	1210	2701	141	2108	5275
62	461	857	102	1231	2757	142	2132	5348
63	478	897	103	1252	2814	143	2156	5422
64	496	936	104	1273	2870	144	2180	5496
65	514	976	105	1294	2928	145	2205	5570
66	532	1016	106	1315	2985	146	2229	5645
67	550	1057	107	1337	3043	147	2254	5721
68	568	1098	108	1358	3102	148	2278	5796
69	586	1140	109	1379	3161	149	2303	5873
70	604	1182	110	1401	3220	150	2328	5949
71	623	1225	111	1422	3280	151	2353	6026
72	641	1268	112	1444	3340	152	2378	6104
73	660	1311	113	1466	3400	153	2403	6182
74	678	1355	114	1488	3462	154	2428	6260
75	697	1399	115	1510	3524	155	2453	6339
76	716	1444	116	1532	3585	156	2478	6418
77	734	1489	117	1554	3648	157	2503	6498
78	753	1534	118	1576	3711	158	2529	6578
79	772	1580	119	1598	3774	159	2554	6659
80	791	1627	120	1620	3838	160	2580	6740

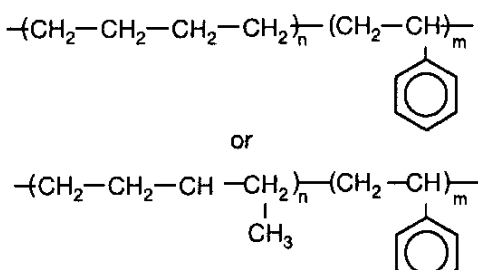
Ethylene-propylene copolymer



Ethylene-propylene-diene terpolymer



Hydrogenated diene-styrene copolymer



Polymethacrylate copolymer

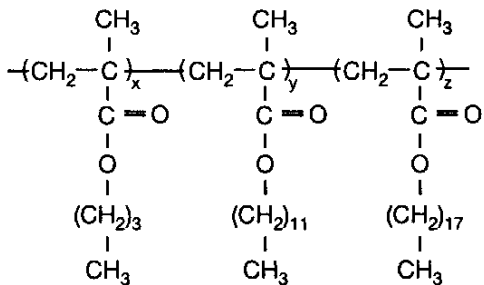


Figure 4.12: Summary of common viscosity index improver molecules.

## Example 4.6

**Given** Suppose that an unknown oil has a Saybolt universal viscosity of 2730 SUV at 38°C and 120 SUV at 100°C.

**Find** What is the VI of the oil?

**Solution**

From the first column of Table 4.17, find the two oils that will have Saybolt universal viscosity of 120 SUV at 100°C. Therefore,

$$\bar{H} = 1620 \text{ SUV at } 38^\circ\text{C}$$

$$\bar{L} = 3838 \text{ SUV at } 38^\circ\text{C}$$

Thus, making use of Eq. (4.17) for  $\bar{x}=2730$  SUV gives

$$\text{VI} = \left( \frac{3838 - 2730}{3838 - 1620} \right) 100 = 50$$

## 4.19 Oxidation Stability

The chemical reaction whereby oxygen in air combines with hydrocarbon in an oil is called “oxidation.” Straight mineral oils possess a certain resistance to oxidation during the early stages of service, but subsequently deterioration due to oxidation tends to accelerate. Operating conditions where oxidation can occur are

1. High temperature
2. Presence of metallic wear particles
3. Presence of moisture and other contaminants, such as sludge, dirt, rust, and other corrosion products
4. Churning and agitation

Oxidation of straight mineral oils proceeds very slowly at room temperature; at 140°F (60°C) oxidation is still slow but significant; and above 200°F (93°C) it is greatly accelerated.

Oil oxidation products are undesirable for the following reasons: Insoluble products (sludge) may prevent effective lubrication due to clogging. Soluble products circulating with the oil tend to be acidic and eventually either lead to corrosion or pitting of bearing surfaces or form varnish deposits on parts operating at high temperatures.

## 4.20 Pour Point

The pour point is the lowest temperature at which a lubricant can be observed to flow under specified conditions. Oils, especially those used in automotive lubricants, generally contain some paraffinic wax that was not removed during refining. At low temperatures, these waxes crystallize and form three-dimensional lattices that interfere with normal oil flow. Pour point is related to viscosity, since its concern is if the oil will flow at low temperatures or just barely flow under prescribed conditions.

Oils used under low-temperature conditions must have low pour points. Oils must have pour points (1) below the minimum operating temperature of the system and (2) below the minimum surrounding temperature to which the oil will be exposed.

While removal of the residue waxes from the oil is somewhat expensive, pour point depressants are an economical alternative to reduce the pour point of lubricants. The most common pour point depressants are the same additives used for viscosity index improvement. The mechanism through which these molecules reduce pour point is still poorly understood and somewhat controversial. It has been suggested that these molecules adsorb into the wax crystals and redirect their growth, forming smaller and more isotropic crystals that interfere less with oil flow.

## 4.21 Density

The effects of temperature on viscosity were found in Sec. 4.15 to be important. For a comparable change in pressure, temperature, or both, the density change is small relative to the viscosity change. However, extremely high pressure exists

in elastohydrodynamic films, and the lubricant can no longer be considered as an incompressible medium, it is therefore necessary to consider the dependence of density on pressure.

The variation of density with pressure is roughly linear at low pressures, but the rate of increase falls off at high pressures. The limit of the compression of mineral oils is only 25%, for a maximum density increase of about 33%. From Dowson and Higginson (1966) the dimensionless density for mineral oil can be written as

$$\bar{\rho} = \frac{\rho}{\rho_0} = 1 + \frac{0.6p}{1 + 1.7p} \quad (4.19)$$

where

$\rho_0$  = density when  $p = 0$ , kg/m<sup>3</sup>

$p$  = gage pressure, GPa

Therefore, the general expression for the dimensionless density can be written as

$$\bar{\rho} = 1 + \frac{0.6E'P}{1 + 1.7E'P} \quad (4.20)$$

where

$$E' = 2 \left( \frac{1 - \nu_a^2}{E_a} + \frac{1 - \nu_b^2}{E_b} \right)^{-1}$$

$E$  = modulus of elasticity, Pa

$\nu$  = Poisson's ratio

and where  $E'$  in Eq. (4.20) must be expressed in gigapascals and  $P = p/E'$ .

Equation (4.20) states that the variation of density with pressure is roughly linear at low pressures but that its rate of increase falls off at high pressures. The maximum density increase from atmospheric pressure is 35%. The data used in obtaining Eq. (4.20) were restricted to relatively low pressures (<0.4 GPa).

Hamrock et al. (1987) obtained experimental data showing the effect of pressure on density for a range of pressures from 0.4 to 2.2 GPa and for six base fluids at an assumed constant temperature of 20°C. The six base fluids tested are listed in Table 4.18 along with corresponding kinematic viscosity and average molecular weight. An important parameter used to describe the results is the change of relative volume with change of pressure,  $dV_r/dp$ . For pressures less than the solidification pressure ( $p < p_s$ ), a small change in pressure results in a large change in  $dV_r/dp$ . For pressures greater than the solidification pressure ( $p > p_s$ ), there is little change in  $dV_r/dp$ . Once the molecules of the lubricant become closely packed, increasing the pressure fails to alter the value of  $dV_r/dp$ .

In elastohydrodynamic lubrication, which is covered more fully later in the text, the rate of pressure increase is extremely high, typically  $10^{13}$  Pa/s. The lubricant under these conditions will not have time to crystallize but will be compressed to an amorphous solid. Physically, this means that as the lubricant is compressed, the distance between the molecules of the lubricant becomes

Table 4.18: Base fluids tested, with corresponding kinematic viscosity and average molecular weight. [From Hamrock et al. (1987).]

Base fluid	Kinematic viscosity at 40°C $\eta_k$ , mm <sup>2</sup> /s	Average molecular weight
Naphthenic distillate	26	300
Naphthenic raffinate	23	320
Polypropylene glycol 1	175	2000
Polypropylene glycol 2	80	2000
Ditridecyl adipate	26	520
Polyalphaolefin	450	500

smaller and smaller. There exists a point where the molecules are not free to move and any further compression will result in deformation of the molecules. The pressure where this first starts to occur is the solidification pressure, which varies considerably for the different lubricants.

Figure 4.13 shows change in relative volume with changing pressure for six base fluids. The solidification pressure varies considerably for the different base fluids tested. Furthermore, for  $p < p_s$  the experimental data assume different slopes for the different base fluids. A new pressure-density formula was developed by Hamrock et al. (1987) that describes the effect of pressure on density in terms of four constants. It is given here.

$$\bar{\rho} = \begin{cases} \frac{1}{1 - C_1 p^2 - C_2 p} & \text{for } p \leq p_s \\ \frac{1}{1 - C_3 p + C_4} & \text{for } p > p_s \end{cases} \quad (4.21)$$

$$C_1 = \frac{\bar{m}}{2C} \quad (\text{GPa})^{-2} \quad (4.22)$$

$$C_2 = \frac{n_2 - \bar{m}p_s}{C} \quad (\text{GPa})^{-1} \quad (4.23)$$

$$C_3 = \frac{n_2}{C} \quad (\text{GPa})^{-1} \quad (4.24)$$

$$C_4 = \frac{\bar{m}p_s^2}{2C} \quad (4.25)$$

where

$$C = 1 + \frac{\bar{m}}{2} (\bar{p}_i)^2 + (n_2 - \bar{m}p_s) \bar{p}_i \quad (4.26)$$

and  $\bar{p}_i$  is the initial pressure in gigapascals. Experimentally obtained values of  $\bar{m}$ ,  $n_2$ , and  $p_s$  for each base fluid are given in Table 4.19; Table 4.20 gives corresponding values of  $C_1$ ,  $C_2$ ,  $C_3$ , and  $C_4$ .

Hamrock et al. (1987) used their derived formula in obtaining Fig. 4.14, which shows the effect of pressure on density for two of the fluids. Also in this

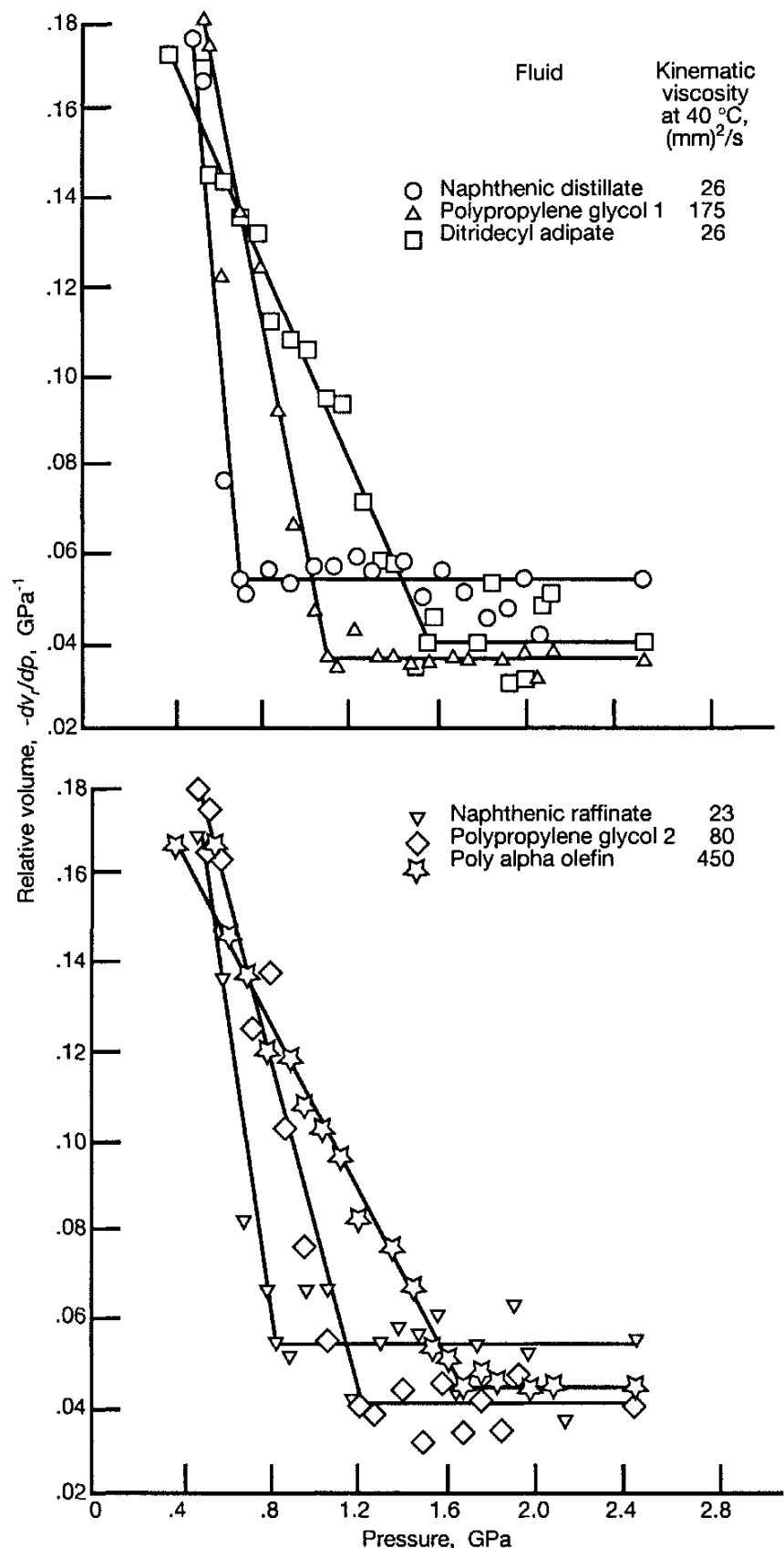


Figure 4.13: Effect of pressure on relative volume for six base fluids. Constant temperature of 20°C assumed. [From Hamrock et al. (1987).]

Table 4.19: Parameters obtained from least-squares fit of experimental data. [From Hamrock et al. (1987).]

Base fluid	Slope $\bar{m}$ , (GPa) $^{-2}$	Asymptote $n_2$ , (GPa) $^{-1}$	Solidification pressure $p_s$ , GPa
Naphthenic distillate	-0.626	0.0538	0.706
Naphthenic raffinate	-0.336	0.0542	0.839
Polypropylene glycol 1	-0.271	0.0360	1.092
Polypropylene glycol 2	-0.195	0.0395	1.213
Ditridecyl adipate	-0.115	0.0395	1.561
Polyalphaolefin	-0.0958	0.0439	1.682

figure is the pressure-density curve obtained from Dowson and Higginson (1966). As the pressures increased above 2 GPa, the deviation between the Dowson and Higginson (1966) formula and the present results also increased. For pressures to 2 GPa for the naphthenic distillate there was good agreement with the Dowson and Higginson (1966) formula. The same cannot be said for the poly alpha olefin. It is anticipated that these deviations from the normally used Dowson and Higginson pressure-density formula will significantly influence the definition of the pressure profile in elastohydrodynamically lubricated conjunctions.

Furthermore, it can be observed from Fig. 4.14 that for fluids other than mineral oils the Dowson and Higginson (1966) formula is not valid, as demonstrated with polyalphaolefin. Therefore, Hamrock et al. (1987) claim that Eqs. (4.21) and (4.22) are valid for any lubricant as long as there are measured values for the constants  $C_1$ ,  $C_2$ ,  $C_3$ , and  $C_4$  as well as for  $\bar{m}$ ,  $n_2$ , and  $p_s$ .

## 4.22 Limiting Shear Stress

For most fluid film lubrication analyses the lubricant is assumed to behave in a Newtonian manner. This implies from Eq. (4.1) that the shear stress  $\tau$  is

Table 4.20: Constants used in defining effect of pressure on density. [From Hamrock et al. (1987).]

Base fluid	Pressure-density constants			
	$C_1$ , (GPa) $^{-2}$	$C_2$ , (GPa) $^{-1}$	$C_3$ , (GPa) $^{-1}$	$C_4$
Naphthenic distillate	-0.271	0.430	0.0466	-0.135
Naphthenic raffinate	-0.151	0.302	0.0487	-0.106
Polypropylene glycol 1	-0.121	0.297	0.0323	-0.145
Polypropylene glycol 2	-0.0887	0.251	0.0395	-0.131
Ditridecyl adipate	-0.0531	0.202	0.0365	-0.129
Poly alpha olefin	-0.0444	0.190	0.0407	-0.126

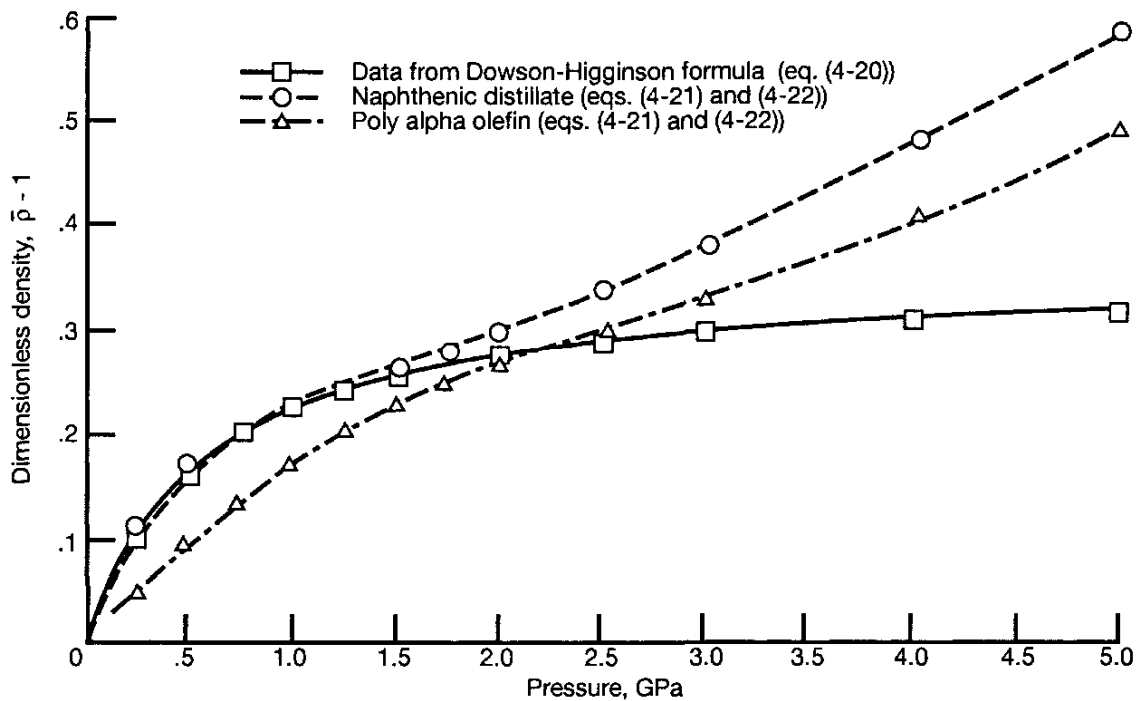


Figure 4.14: Effect of pressure on density. [From Hamrock *et al.* (1987).]

linearly related to the shear strain rate  $s$ , or

$$s = \frac{\tau}{\eta} \quad (4.27)$$

where  $\eta$  is the absolute viscosity or proportionality constant and may vary with both pressure and temperature. However, the lubricant in elastohydrodynamically lubricated conjunctions experiences rapid and extremely large pressure variations, a rapid transit time, possibly large temperature changes, and particularly in sliding contacts, high shear rates. The great severity of these conditions has called into question the normal assumptions of Newtonian behavior of the fluids in elastohydrodynamically lubricated conjunctions. This implies that the lubrication shear stress is still a function of the shear strain rate but that the relationship is no longer linear as shown in Eq. (4.27). For a fluid having non-Newtonian characteristics, the shear rate increases more rapidly than the shear stress.

Figure 4.15 shows the relationship between the dimensionless shear strain rate and the dimensionless shear stress for three nonlinear, viscous rheological fluid models. Isothermal conditions are assumed. The two limiting-shear-stress models shown in Fig. 4.15 were obtained from Bair and Winer (1979) and can be expressed as

$$s = \frac{\tau_L}{\eta} \ln \left( 1 - \frac{\tau}{\tau_L} \right)^{-1} \quad (4.28)$$

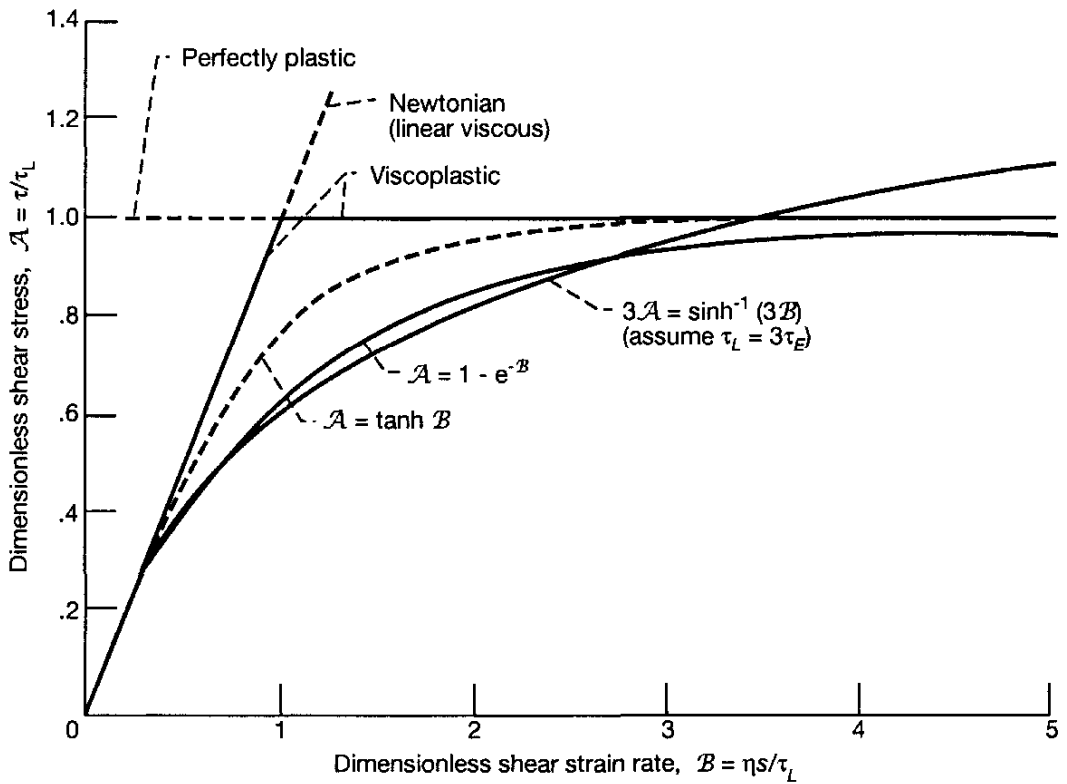


Figure 4.15: Comparison of rheological models for isothermal conditions.

$$s = \frac{\tau_L}{\eta} \tanh^{-1} \frac{\tau}{\tau_L} \quad (4.29)$$

where

$\tau_L$  = limiting shear stress,  $\tau_0 + \gamma^* p$ , Pa

$\tau_0$  = limiting shear stress at zero pressure, Pa

$\gamma^*$  = limiting-shear-strength proportionality constant,  $\partial\tau_L/\partial p$

Rewriting these equations in dimensionless form gives

$$\mathcal{A} = 1 - e^{-\mathcal{B}} \quad (4.30)$$

and

$$\mathcal{A} = \tanh \mathcal{B} \quad (4.31)$$

where

$$\mathcal{A} = \frac{\tau}{\tau_L} \quad (4.32)$$

$$\mathcal{B} = \frac{\eta s}{\tau_L} \quad (4.33)$$

The other nonlinear viscous model shown in Fig. 4.15 is that attributed to Eyring (1936) and can be expressed as

$$s = \frac{\tau_E}{\eta} \sinh \frac{\tau}{\tau_E} \quad (4.34)$$

where  $\tau_E$  is the shear stress at which the fluid first starts to behave nonlinearly when stress is plotted against shear strain rate. In comparing this model with the limiting-shear-stress models, the following relationship between  $\tau_E$  and  $\tau_L$  will be assumed:

$$\tau_E = \frac{\tau_L}{3} \quad (4.35)$$

Making use of Eq. (4.35) while rewriting Eq. (4.34) in dimensionless form gives

$$3A = \sinh^{-1}(3B) \quad (4.36)$$

Figure 4.15 shows that for the Eyring model the shear stress increases monotonically with increasing strain rate.

Bair and Winer (1979), Jacobson (1985), and Höglund and Jacobson (1986) observe that at a given pressure and temperature there is a critical shear stress at which the lubricant will shear plastically with no further increase in shear stress with increasing shear strain rate. Jacobson and Hamrock (1984) used the limiting-shear-stress concept so that, when the shear stress at the bearing surfaces exceeded the limiting shear stress, the shear stress was set equal to the limiting shear stress. As their model was isothermal, slip planes developed at the bearing surfaces if the shear stress was too high. Depending on the shear stress at the bearing surfaces, three different pressure equations were used. As discussed earlier, Houpert and Hamrock (1985) used the Eyring model in developing a new Reynolds equation that shows the nonlinear viscous effects.

The various properties of lubricants having been described in the preceding sections, the next four sections will describe how these properties vary for three different types of lubricant, namely, liquids, greases, and gases. Liquid lubricants will be separated into petroleum or mineral oils and synthetic oils.

## 4.23 Fluid Rheology Models

With the exception of Sec. 4.22 in which the limiting shear stress was introduced, the text will deal strictly with the assumption that the fluid behaves in a Newtonian fashion. That is, the shear stress is linearly related to the shear strain rate by the fluid viscosity. In elastohydrodynamically lubricated conjunctions the lubricant experiences rapid and very large temperature changes, elongational viscosity, and, particularly in sliding contacts, high shear rates. As a result of high fluid film pressures and shear heating, the viscosity changes drastically within the lubricating film. In addition, the existence of very high shear rates may result in shear stresses that are well beyond the limiting shear stress of the lubricant. In elastohydrodynamically lubricated conjunctions the shear rates can range up to  $10^7 \text{ s}^{-1}$ . The maximum temperature within the conjunction can be as high as  $500^\circ\text{C}$ . Furthermore, the transit time required for the fluid to go from the inlet through the high-pressure zone to the outlet is between  $10^{-3}$  and  $10^{-4}$  s. The great severity of these conditions has called into question the normal assumption of Newtonian behavior.

Hirst and Moore (1974) presented an experimental investigation of the dependence between shear stress and shear strain rate and proposed an Eyring type of relationship. Johnson and Tevaarwerk (1977) found the same type of relationship as did Hirst and Moore (1974). Houpert and Hamrock (1985), as well as Conry et al. (1987), incorporated Eyring's model (see Sec. 4.22) into the analysis of elastohydrodynamically lubricated line contacts by using a system approach to get a full numerical solution. It has been observed that the Eyring model does not exhibit limiting-shear-strength properties. In Eyring's model the rate at which shear stress increases with increasing shear strain rate is significantly smaller than the Newtonian linear rate at high shear strain rates. An upper limit to the shear stress increase can only be achieved for Eyring's model by resorting to a plastic transition.

The non-Newtonian property of limiting shear strength imposes that the lubricant does not experience shear stress exceeding this limit. The limiting shear strength is usually considered as an asymptotic limit. Should the fluid model, however, allow the shear stress to reach the limiting shear strength, slippage will occur either within the oil film or at the interface between the oil and one of the bounding surfaces. A fluid model that allows for such a slip phenomenon will be referred to as "a viscoplastic fluid model." The distinction between asymptotic and viscoplastic limiting-shear-strength behavior is an important one because the latter requires the replacement of the traditional velocity boundary conditions by stress boundary conditions. This means that there will be transitions in the type of boundary conditions imposed if the shear stress reaches the plastic limit inside the conjunction, a condition that may introduce singularities in the solution.

Bair and Winer (1979) and Gecim and Winer (1980) proposed alternative expressions for the relationship between shear stress and shear strain rate that do exhibit asymptotic limiting-shear-stress behavior. Both Bair and Winer (1979) and Gecim and Winer (1980) incorporated their models into the analysis of elastohydrodynamically lubricated line contacts by using a Grubin-like inlet analysis. In attempts to obtain a full numerical solution of the problem of elastohydrodynamically lubricated line contacts, Bair and Winer's model has been approximated into simple forms such as the linear model proposed by Trachman (1971), which was used in elastohydrodynamic lubrication by Wang and Zhang (1988) and Iivonen and Hamrock (1989), or the circular model proposed by Lee and Hamrock (1990). Both the linear and the circular fluid models allow the establishment of a modified Reynolds equation by using an approach similar to the one that applies for a Newtonian fluid. The circular model is, however, not as severe a non-Newtonian fluid model as is the linear model, and it is therefore in better agreement with experimental observations. The modified Reynolds equation for the circular fluid model was solved by Lee and Hamrock (1990) by using the fast system approach developed by Houpert and Hamrock (1986). This approach was later refined by Hsiao and Hamrock (1992) and used to investigate thermal effects in non-Newtonian elastohydrodynamic lubrication, which will be considered in the next chapter. The existence of the solution for

a circular fluid model allows the most significant non-Newtonian feature to be incorporated into the analysis of elastohydrodynamic lubrication, namely, the limiting shear strength. It is, however, restrictive not to be able to model more freely the transition between Newtonian behavior at low shear strain rate and limiting-shear-strength behavior at high shear strain rate.

## 4.24 Formulation of Fluid Rheology Models

An alternative way of showing the non-Newtonian effect is to use the effective viscosity, defined as

$$\eta_e = \frac{\tau}{s} \quad (4.37)$$

where  $\tau$  is the shear stress and  $s$  is the shear strain rate ( $\partial u / \partial z$ ). This then defines the viscosity that is actually experienced within elastohydrodynamically lubricated conjunctions. Using this form, the non-Newtonian models given by Eqs. (4.28), (4.29), and (4.34) can be written as

$$\frac{\eta_e}{\eta} = -\frac{\tau/\tau_L}{\ln(1 - \tau/\tau_L)} \quad (4.38)$$

$$\frac{\eta_e}{\eta} = \frac{\tau/\tau_L}{\tanh^{-1}(\tau/\tau_L)} \quad (4.39)$$

$$\frac{\eta_e}{\eta} = \frac{\tau/\tau_E}{\sinh(\tau/\tau_L)} \quad (4.40)$$

where  $\tau_E$  is the shear stress at which the fluid first starts to behave nonlinearly when stress is plotted against shear strain rate.

A highly non-Newtonian fluid model was introduced by Iivonen and Hamrock (1989) that can be expressed as

$$\frac{\eta_e}{\eta} = 1 - \frac{\tau}{\tau_L} \quad (4.41)$$

This model is referred to as “a straight-line model.”

Another new non-Newtonian fluid rheology model developed by Lee and Hamrock (1990) that shows considerable promise is

$$\frac{\eta_e}{\eta} = \left[ 1 - \left( \frac{\tau}{\tau_L} \right)^2 \right]^{1/2} \quad (4.42)$$

This model is referred to as “the circular model.”

Elsharkawy and Hamrock (1991) proposed a general nonlinear viscous model in which the limiting shear strength has already been incorporated as

$$\frac{\partial u}{\partial z} = \frac{\tau}{\eta} \left[ 1 - \left( \frac{\tau}{\tau_L} \right)^n \right]^{-1/n} \quad (4.43)$$

where

$$\tau_l = \tau_0 + \gamma^* p \quad (4.44)$$

Equation (4.44) can be written as

$$\frac{\tau}{\tau_L} = \frac{\frac{\eta}{\tau_L} \frac{\partial u}{\partial z}}{\left[ 1 + \left( \frac{\eta}{\tau_L} \frac{\partial u}{\partial z} \right)^n \right]^{1/n}} \quad (4.45)$$

Equation (4.45) is plotted in Fig. 4.16 for different values of  $n$ . In Fig. 4.16a the conventional way of describing the various models is used. Using the alternative representation given in Eq. (4.38) this non-Newtonian model can be expressed as

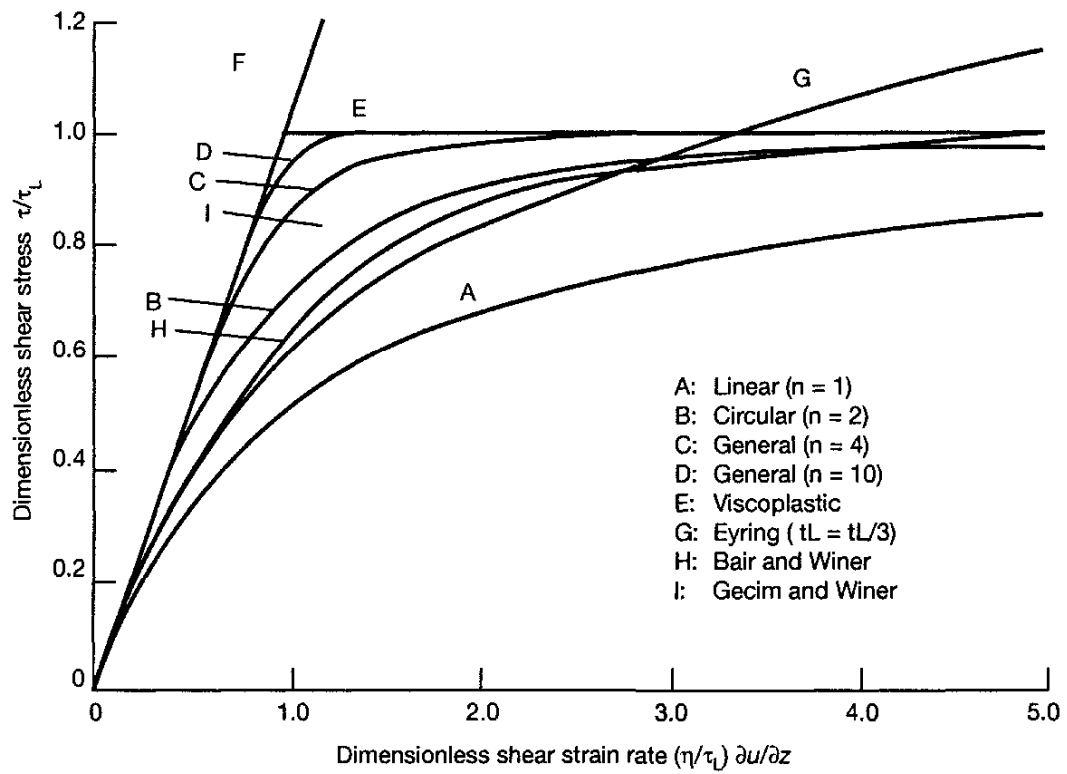
$$\eta_e = \tau \left( \frac{\partial u}{\partial z} \right)^{-1} = \eta \left[ 1 - \left( \frac{\tau}{\tau_L} \right)^n \right]^{1/n} \quad (4.46)$$

This relationship between shear stress and effective viscosity is shown in Fig. 4.16b for various values of the shape exponent  $n$ .

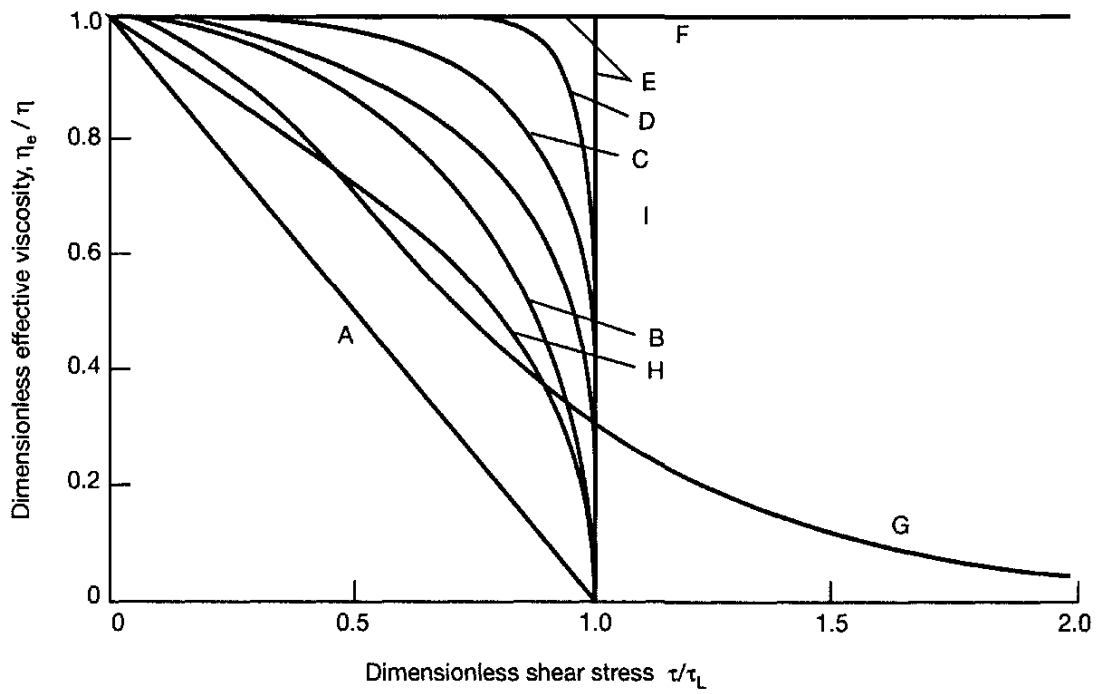
The main advantage of the general model is that all the other nonlinear viscous models with the limiting-shear-strength property are readily derived or closely approximated by appropriate choice of the exponent  $n$ . As shown in Fig. 4.16,  $n = 1$  results in the linear model, and  $n = 2$  in the circular model. The general fluid model will, in fact, if incorporated into the analysis of elastohydrodynamic lubrication, allow a given relationship between shear strain rate and shear stress to also be simulated in the transition zone. In the general case of arbitrary  $n$  it is not possible to derive a modified Reynolds equation directly as was the case for  $n = 1$  and  $n = 2$ .

In Fig. 4.16b the straight-line model is strongly non-Newtonian and thus probably overexaggerates the fluid effect. The straight-line model may be viewed as a limiting solution; the viscoplastic model is the other limit. An actual lubricant behaves somewhere between these two extremes. Table 4.21 shows the expression for the dimensionless effective viscosity and the shear strain rate for the various rheological models.

The circular model of Lee and Hamrock (1990) and the  $\tanh^{-1}$  model of Gecim and Winer (1980), shown in Fig. 4.16, behave more like a Newtonian model for dimensionless shear stresses less than 0.5 and then become highly non-Newtonian for dimensionless shear stresses greater than 0.5. This behavior is more like what one would expect for actual fluids used in elastohydrodynamically lubricated conjunctions. The major advantage that the circular model offers over the  $\tanh^{-1}$  model is that the analytical expressions can be obtained for the elements of the Jacobian by using the approach of Houpert and Hamrock (1986). Thus, the circular model is used in this chapter because it offers easy implementation of the numerical approach presented in Chap. 21, and yet the stress-strain relation agrees with the  $\tanh^{-1}$  model of Gecim and Winer (1980) for which there is experimental evidence.



(a)



(b)

Figure 4.16: Non-Newtonian rheological models represented by (a) effect of shear strain rate on dimensionless shear stress and (b) effect of dimensionless shear stress on dimensionless effective viscosity. [From Myllerup et al. (1993).]

Table 4.21: Dimensionless effective viscosity for different viscosity models.  
[From Hamrock *et al.* (1987).]

Fluid model	Shear strain rate $s$	Dimensionless effective viscosity $\eta_e/\eta$
Newtonian	$\frac{\tau}{\eta}$	1
Eyring (1936) (sinh model)	$\frac{\tau_E}{\eta} \sinh \frac{\tau}{\tau_E}$	$\frac{\tau}{\tau_E \sinh(\tau/\tau_E)}$
Bair and Winer (1979) (ln model)	$\frac{\tau_L}{\eta} \ln(1 - \bar{\tau})^{-1}$	$-\frac{\bar{\tau}}{\ln(1 - \bar{\tau})}$
Gecim and Winer (1980) (tanh <sup>-1</sup> model)	$\frac{\tau_L}{\eta} \tanh^{-1} \tau$	$\frac{\bar{\tau}}{\tanh^{-1} \bar{\tau}}$
Iivonen and Hamrock (1989) (straight-line model)	$\frac{\tau_L}{\eta} [(1 - \bar{\tau})^{-1} - 1]$	$1 - \bar{\tau}$
Elsharkawy and Hamrock (1991) (general model)	$\frac{\tau}{\eta} [1 - (\bar{\tau})^n]^{-1/n}$	$[1 - (\bar{\tau})^n]^{1/n}$
Lee and Hamrock (1990) (circular model)	$\frac{\tau}{\eta} [1 - (\bar{\tau})^2]^{-1/2}$	$(1 - \bar{\tau})^{1/2}$

For the Eyring (1936), or sinh, model given in Eq. (4.40) and shown in Fig. 4.16 and Table 4.21, it was assumed that  $\tau_E = \tau_L/3$ . The Eyring (1936) model was found to have shear stress that increases monotonically with increasing strain rate as shown in Fig. 4.14. In Fig. 4.16(a) the dimensionless shear stress decreases monotonically with decreasing effective viscosity. The sinh model was used by Houpert and Hamrock (1985) in applying the elastohydrodynamic lubrication analysis to the problem of scuffing. Furthermore, the viscoplastic model shown in Fig. 4.16(a) was used by Jacobson and Hamrock (1984) in solving the elastohydrodynamic lubrication problem. That is, when the shear stress at the bearing surfaces exceeded the limiting shear stress, the shear stress was set equal to the limiting shear stress.

## 4.25 Closure

This chapter described the properties of lubricants that are important in fluid film lubrication. Since lubricating oils are derived from petroleum, which consists of compounds of carbon and hydrogen, basic chemistry has been briefly discussed. In fluid film lubrication the most important physical property of a lubricant is its viscosity. The viscosity of a fluid is associated with its resistance to flow, that is, with the resistance arising from intermolecular forces and internal friction as the molecules move past each other. Newton deduced that the force required to maintain a constant velocity  $u$  of an upper plane while the bottom plane is stationary was proportional to the area  $A$  and the velocity

gradient or rate of shear. Therefore,

$$f = \eta A \frac{u}{h}$$

where  $\eta$  is the proportionality constant or absolute viscosity.

It was also shown in this chapter that the viscosity is greatly affected by temperature, pressure, and shear rate. Appropriate expressions that describe these relationships were presented. Density-pressure effects were also discussed, and the concept of solidification pressure was introduced.

It was found in this chapter that the lubricant in elastohydrodynamically lubricated conjunctions experiences rapid and extremely large pressure variations, a rapid transit time, possibly large temperature changes, and particularly in sliding contacts, high shear rates. The great severity of these conditions has called into question the normal assumption of Newtonian fluid behavior. The concept of a limiting shear stress was introduced, and some non-Newtonian fluid models were presented. The chapter included discussions of synthetic oil base stocks, greases, and gases, all of which are used as lubricants in fluid film lubrication. Lubricant formulation was introduced, and the large variety of additives incorporated into industrial lubricants were described.

Non-Newtonian fluid rheology effects were considered in this chapter. Various non-Newtonian models were presented in terms of the effective viscosity, which defines the actual viscosity experienced in elastohydrodynamically lubricated conjunctions. The circular model behaves more like a Newtonian model for dimensionless shear stresses less than 0.5 and then becomes highly non-Newtonian for dimensionless shear stresses greater than 0.5.

## 4.26 Problems

4.1 Given the absolute viscosity of a given fluid at atmospheric conditions to be  $6 \times 10^{-3} \text{ (kg)}_{\text{force}} \cdot \text{s/m}^2$ , what would this absolute viscosity be in

- (a) reyn
- (b) P
- (c) lbf·s/in<sup>2</sup>
- (d) N·s/m<sup>2</sup>

4.2 Given a fluid with an absolute viscosity  $\eta$  between two 1-m<sup>2</sup> surfaces spaced 1 mm apart, find how fast the surfaces will move relative to each other if a 10-N force is applied in the direction of the surfaces when  $\eta$  is

- (a) 0.001 N·s/m<sup>2</sup> (water)
- (b) 0.100 N·s/m<sup>2</sup> (a thin oil at room temperature)
- (c) 10.0 N·s/m<sup>2</sup> (syrup; cold oil)
- (d) 10<sup>8</sup> N·s/m<sup>2</sup> (asphalt)

- 4.3 A silicon fluid has a Saybolt universal viscosity of 1000 SUV at 38°C and 130 SUV at 100°C. What is the VI of the oil?
- 4.4 Given that a machine element is elastohydrodynamically lubricated with an oil, describe some of the properties you would like to see for that oil. Give an indication whether high or low values are desirable.
- 4.5 Given the general non-Newtonian fluid model in Eq. (4.43), establish to the first decimal place the value of  $n$  in the general model that approximates the Bair and Winer (1979) model as well as the Gecim and Winer (1980) model.

## References

- Bair, S., and Winer, W. O. (1979): Shear Strength Measurements of Lubricants at High Pressure. *J. Lubr. Technol.*, vol. 101, no. 3, pp. 251-257.
- Barus, C. (1893): Isothermals, Isopiestic, and Isometrics Relative to Viscosity. *Am. J. Sci.*, vol. 45, pp. 87-96.
- Blok, H. (1965): Inverse Problems in Hydrodynamic Lubrication and Design Directions for Lubricated Flexible Surfaces. *Proceedings of International Symposium on Lubrication and Wear*. D. Muster and B. Sternlicht (eds.). McCutchan, Berkeley, pp. 1-151.
- Cameron, A. (1976): *Basic Lubrication Theory*, 2d ed. Ellis Harwood Limited, Chichester, England.
- Conry, T. F., Wang, S., and Cusano, C. (1987): "A Reynolds-Eyring Equation for Elastohydrodynamic Lubrication in Line Contacts," *ASME J. of Tribol.*, vol. 109, pp. 648-658.
- Dean, E. W., and Davis, G. H. B. (1929): Viscosity Variations of Oils With Temperature. *J. Chem. Met. Eng.*, vol. 36, no. 10, pp. 618-619.
- Dowson, D., and Higginson, G. R. (1966): *Elastohydrodynamic Lubrication: The Fundamentals of Roller and Gear Lubrication*. Pergamon, Oxford.
- Elsharkawy, A. A., and Hamrock, B. J. (1991): Subsurface Stresses in Micro-EHL, Line Contacts. *J. Tribol.*, vol. 113, no. 3, pp. 645-656.
- Eyring, H. (1936): Viscosity, Plasticity, and Diffusion as Examples of Absolute Reaction Rates. *J. Chem. Phys.*, vol. 4, no. 4, pp. 283-291.
- Gecim, B., and Winer, W.O., (1980): Lubricant Limiting Shear Stress Effect on EHD Film Thickness. *J. Lubr. Technol.*, v. 102, p. 213.
- Gross, W. A. (1980): *Fluid Film Lubrication*. Wiley-Interscience, New York.
- Hamrock, B. J., Jacobson, B. O., and Bergstrom, S. I. (1987): Measurement of the Density of Base Fluids at Pressures to 2.2 GPa. *ASLE Trans.*, vol. 30, no 2, Apr., pp. 196-202.
- Hatton, R. E. (1973): Synthetic Oils. Interdisciplinary Approach to Liquid Lubricant Technology. *NASA Spec. Publ. 318*, P. M. Ku (ed.), pp. 101-135.

- Herschel, W. F.. (1918): Standardization of the Saybolt Universal Viscometer. *Tech. Pap. 112, Nat. Bur. Stands.*
- Hess, F. C. (1981): Chemistry Made Simple. Heinemann, London.
- Hirst, W., and Moore, A.J. (1974): "Non-Newtonian Behavior in Elastohydrodynamic Lubrication" *Proc. Roy. Soc. London*, v. 33, pp. 101-113.
- Höglund, E., and Jacobson, B. (1986): Experimental Investigations of the Shear Strength of Lubricants Subjected to High Pressure and Temperature. *J. Tribology*, vol. 108, no. 4, pp. 571-578.
- Houpert, L. G., and Hamrock, B. J. (1985): Elastohydrodynamic Lubrication Calculations Used as a Tool to Study Scuffing. *Mechanisms and Surface Distress: Global Studies of Mechanisms and Local Analyses of Surface Distress Phenomena*, D. Dowson et al. (eds.), Butterworths. England, pp. 146-162.
- Hsiao, H. S., and Hamrock, B. J. (1992): "A Complete Solution for Thermal-Elastohydrodynamic Lubrication of Line Contacts Using the Circular Non-Newtonian Fluid Model," *ASME J. Tribol.*, vol. 114, no. 3, pp. 540-552.
- Iivonen, H. T., and Hamrock, B. J. (1989): A Non-Newtonian Fluid Model for Elastohydrodynamic Lubrication of Rectangular Contacts. *Proceedings of the Fifth International Congress on Tribology*. Helsinki, Finland, June 1989. pp. 178-183.
- Jacobson, B. O. (1985): A High Pressure-Short Time Shear Strength Analyzer for Lubricants. *J. Tribology*, vol. 107, no. 2, pp. 220-223.
- Jacobson, B. O., and Hamrock, B. J. (1984): Non-Newtonian Fluid Model Incorporated into Elastohydrodynamic Lubrication of Rectangular Contacts. *J. Tribology*, vol. 106, no. 2, pp. 275-284.
- Johnson, K. L., and Tevaarwerk, J. L. (1977): "Shear Behavior of MID Oil Films." *Proc. Roy. Soc.. London*, vol. 356, pp. 215-236.
- Jones, W. R., et al. (1975): Pressure-Viscosity Measurements for Several Lubricants to  $5.5 \times 10^8$  Newtons Per Square Meter ( $8 \times 10^4$  psi) and 149°C (300°F). *ASLE Trans.*, vol. 18, no. 4. pp. 249-262.
- Klamann, D. (Killer, A., transl.) (1984): *Lubricants and Related Products*. Verlag Chemie. Weinheim.
- Kioupis, L. I., and Maginn, E.J., "Molecular Simulation of Poly- $\alpha$ -olefin Synthetic Lubricants: Impact of Molecular Architecture on Performance Properties," *J. Phys. Chem. B.*, v. 103, 1999, pp. 10781-10790.
- Kioupis, L. I., and Maginn, E.J., "Impact of Molecular Architecture on the High-Pressure Rheology of Hydrocarbon Fluids," *J. Phys. Chem. B.*, v. 104, 2000, pp. 7774-7783.
- Lee, R. T., and Hamrock, B. J. (1990): A Circular Non-Newtonian Fluid Model: Part 1-Used in Elastohydrodynamic Lubrication. *J. Tribol.*, vol. 112, no. 3, pp. 486-496.
- Litt, F. A. (1986): Viscosity Index Calculations. *Lubr. Eng.*, vol. 42, no. 12, pp. 752-753.
- Mishra, M.K., and Saxton. R.G., "Polymer Additives for Engine Oils," *Chemtech*, 1995, pp. 35-41.

- Newton, I. (1687): *Philosophiae Naturales Principia Mathematica*. Revised and supplied with a historical and explanatory appendix by F. Cajori, edited by R. T. Crawford (1934), and published by the University of California Press, Berkeley and Los Angeles (1966).
- Pugh, B. (1970): *Practical Lubrication*. Newnes-Butterworths, London.
- Roelands, C. J. A. (1966): *Correlational Aspects of the Viscosity-Temperature-Pressure Relationship of Lubricating Oils*. Druk, V. R. B., Groingen, Netherlands.
- Schmid, S.R., and Schmid. K.J., "Marine Equipment Tribology," in Bhushan, B., ed., *Modern Tribology Handbook*. CRC Press, 2001, pp. 1371-1384.
- Svehla, R. A. (1962): Estimated Viscosities and Thermal Conductivities of Gases at High Temperatures. *NASA Tech. Rep. R-132*.
- Trachman, E. G. (1971): "The Rheological Effects of Friction in EHL," Ph.D. thesis, Northwestern University, Evanston, IL.
- Wang, J., and Zhang, H. H. (1992): "A Higher Order Perturbational Approach in Lubricated EHL Contacts with Non-Newtonian Lubricant," *ASME J. of Tribol.*, vol. 114, pp. 95-99.
- Winer, W. O., and Cheng, H. S. (1980): Film Thickness, Contact Stress and Surface Temperatures. *Wear Control Handbook*, ASME, New York, pp. 81-141.
- Wu, M., "Synthetic Lubricants", *MESD Newsletter*, v. 24, 1993, pp. 7-12.

# Chapter 5

# Bearing Materials

## Symbols

$\bar{a}$	linear thermal expansion coefficient, m/mK	$\hat{Q}$	quantity of heat, J
$C_p$	specific heat, J/(kgK)	$\Delta t_m$	temperature change, K
$d_b$	bore diameter, mm	$V$	surface velocity, m/s
$E$	modulus of elasticity, N/m <sup>2</sup>	$\epsilon_1$	strain in axial direction
$K_f$	thermal conductivity, W/mK	$\nu$	Poisson's ratio
$m_a$	mass, kg	$\rho$	density, kg/m <sup>3</sup>
$N_a$	rotational speed, rev/min	$\sigma_1$	stress in axial direction, N/m <sup>2</sup>
$P$	pressure, N/m <sup>2</sup>		

## 5.1 Introduction

Another factor that can affect the successful operation of tribological elements is the solid materials used. Bearing materials must have special characteristics if the bearings are to operate successfully. Some desirable characteristics that will be explored in this chapter are compatibility with rubbing counterface materials; embeddability for dirt particles and wear debris; conformability to enable the bearing to accommodate misalignment, geometrical errors, and deflection in the structure; thermal stability; corrosion resistance; and fatigue resistance.

## 5.2 Material Characteristics

The selection of the bearing material for a particular application depends on (1) the type of bearing (journal, thrust, ball, etc.), (2) the type of lubricant (grease, oil, water, gas, etc.), and (3) the environmental conditions (temperature, pressure, etc.). No single material has been developed that can satisfy all

the requirements of a good bearing material. Therefore, the selection must be made on the basis of the characteristics considered of primary importance in the application.

1. *Compatibility.* Although a properly performing hydrodynamic bearing is one in which the shaft and the bearing are separated by a lubricant film, there are times during the operation when the shaft and the bearing come into contact. High spots on the shaft and the bearing rub, localized heating occurs, the high spots can weld, and the microscopic welds can fracture. This sequence of events results in scoring damage to both the shaft and bearing materials. The ability of these material combinations to resist welding and scoring is a measure of their compatibility.
2. *Embeddability.* In the operation of bearings dirt or other foreign debris is carried into the bearing clearance by the lubricant and by the rotation of the shaft. If this dirt cannot be embedded in the bearing material, scoring damage results. The ability to embed or absorb this dirt determines the embeddability characteristic of the bearing material.
3. *Conformability.* As the term implies, conformability is a measure of the ability of the bearing material to conform to misalignment between the shaft and the bearing or to other geometric inaccuracies produced in manufacturing the parts. Usually, bearing materials having a low modulus of elasticity (low  $E$ ) are readily conformable.
4. *Corrosion resistance.* The bearing material should be resistant to attack by the lubricant or any of the oxidation products produced during lubricant degradation. For example, lubricating oils without oxidation inhibitors produce organic acids, which attack and corrode certain bearing materials. The selection of materials for use with water as the lubricant is of necessity limited to corrosion-resistant materials.
5. *Fatigue resistance.* High fatigue resistance is necessary in applications in which the load changes direction or in which the load intensity varies cyclically. Fatigue failures appear initially as cracks in the bearing surface. These cracks propagate throughout the bearing material, interconnecting with other cracks and resulting in loose pieces of bearing material. Fatigue strength is particularly important where cyclic loading is present.
6. *Dimensional and thermal stability.* The thermal characteristics of the bearing material are important with regard to both heat dissipation and thermal distortion. The thermal conductivity  $K_f$  of the bearing material should be high to ensure maximum dissipation of the frictional heat generated if hydrodynamic lubrication conditions cannot be maintained. The linear thermal expansion coefficient  $\bar{a}$  should be acceptable within the overall design so that the effects of temperature variation are not detrimental. Values of  $K_f$  and  $\bar{a}$  are given in Sec. 5.7. Even if a material has

these desirable characteristics, additional constraints of acceptable cost and material availability need to be satisfied.

The properties and characteristics of several bearing materials are shown in Table 5.1. Brinell hardness number, load-carrying capacity, and maximum operating temperature are given. Also in this table ratings of fatigue strength, antiseizure property, conformability, and embeddability are given based on an arbitrary scale, with 1 being the most desirable or best.

## 5.3 Metallics

Bearing materials for conformal surfaces fall into two major categories:

1. *Metallics*: babbitts, bronzes, aluminum alloys, porous metals, and metal overlays such as silver, babbitts, and indium
2. *Nonmetallics*: plastics, rubber, carbon-graphite, wood, ceramics, cemented carbides, metal oxides (e.g., aluminum oxide), and glass

The principal metallic materials will now be covered in more detail.

### 5.3.1 Tin- and Lead-Base Alloys

The babbitts are among the most widely used materials for hydrodynamically lubricated bearings. Babbitts are either tin or lead-base alloys having excellent embeddability and conformability characteristics. They are unsurpassed in compatibility and thus prevent shaft scoring.

Tin- and lead-base babbitts have relatively low load-carrying capacity. This capacity is increased by metallurgically bonding these alloys to stronger backing materials such as steel, cast iron, or bronze. Babbitt linings are either still cast or centrifugally cast onto the backing material. Fatigue strength is increased by decreasing the thickness of the babbitt lining. Dowson (1998) points out that at the beginning of the century babbitt linings were rarely less than 3 mm thick and not infrequently at least 6.4 mm thick. The need to provide adequate compressive and fatigue strength gradually brought the thickness of the lining down to 500  $\mu\text{m}$ , at the expense of other desirable features such as embeddability and conformability. The optimum thickness of the bearing layer varies with the application but is generally between 0.02 and 0.12 mm.

Tables 5.2 and 5.3 show the composition and physical properties of some of the tin- and lead-base alloys presently used. Table 5.2 shows the significant effect of temperature in decreasing the strength properties of these alloys. The alloys in more general use are shown in Table 5.3. The effect of various percentages of the alloying elements on the mechanical and physical properties of tin- and lead-base alloys can be significant. Increasing the copper or the antimony increases the hardness and the tensile strength and decreases the ductility. However, increases beyond the percentages shown in Table 5.3 can result in decreased fatigue strength.

Table 5.1: Properties and characteristics of various conformal bearing metals [From Clauser (1948)]

Bearing metal	Brinell hardness number		Load-carrying capacity		Maximum operating temperature		Fatigue strength <sup>a</sup>	Antiseizure property <sup>a</sup>	Conformability and embeddability <sup>a</sup>
	Room temperature	149°C (300°F)	MPa	psi	°C	°F			
Tin-base babbitt	20-30	6-12	5.5-10.4	800-1500	149	300	3	1	1
Lead-base babbitt	15-20	6-12	5.5-8.3	800-1200	149	300	3	1	1
Alkali-hardened lead	22-26	11-17	8.3-10.4	1200-1500	260	500	3	1	1
Cadmium base	30-40	15	10.4-13.8	1500-2000	260	500	3	1	1
Copper lead	20-30	20-23	10.4-17.2	1500-2500	177	350	2	2	2
Tin bronze	60-80	60-70	> 27.6	> 4000	260+	500+	1	3	3
Lead bronze	40-70	40-60	20.7-31.1	3000-4500	232-260	450-500	1	3	3
Phosphor bronze	75-100	65-100	>27.6	> 4000	260+	500+	1	3	3
Aluminum alloy	45-50	40-45	>27.6	> 4000	107-149	225-300	2	2	3
Silver (overplated)	25	25	>27.6	> 4000	260+	500+	1	2	3
Copper-nickel matrix	10	7	13.8	2000	177	350	2	1	2
Trimetal and plated	b	b	>27.6	> 4000	107-149	225-300	2	1	2
Grid type	b	b	>27.6	> 4000	107-149	225-300	2	1	2
Thin babbitt overlay, 0.051-0.178 mm (0.002-0.007 in.)	b	b	13.8	2000	149	300	2	1	2
Conventional babbitt overlays, 0.51 mm (0.0020 in.)	b	b	10.4	1500	149	300	2	1	2

<sup>a</sup>This is an arbitrary scale with 1 being the highest rating.

<sup>b</sup>Approximately the same as the babbitts.

Table 5.2: Composition and physical properties of white metal bearing alloys<sup>a</sup> [From ASTM B23-83.  
Reprinted by permission of the American Society for Testing and Materials.]

Alloy number <sup>b</sup>	Tin	Antimony	Lead	Copper	Arsenic	Specific gravity <sup>c</sup>	Tin	Antimony	Lead	Copper	20°C (68°F)	100°C (212°F)	Yield point <sup>d</sup>			
	Specified nominal composition of alloys, percent						Composition of alloys tested, percent					MPa	psi	MPa	psi	
	1	91.0	4.5	—	4.5	—	7.34	90.9	4.52	None	4.56	30.3	4400	18.3	2650	
2	89.0	7.5	—	3.5	—	7.39	89.2	7.4	0.03	3.1	42.0	6100	20.6	3000		
3	84.0	8.0	—	8.0	—	7.46	83.4	8.2	.03	8.3	45.5	6600	21.7	3150		
7	10.0	15.0	Remainder	—	.45	9.73	10.0	14.5	75.0	.11	24.5	3550	11.0	1600		
8	5.0	15.0	Remainder	—	.45	10.04	5.2	14.9	79.4	.14	23.4	3400	12.1	1750		
15	1.0	16.0	Remainder	—	1.0	10.05	—	—	—	—	—	—	—	—	—	
Alloy number <sup>b</sup>	20°C (68°F)		100°C (212°F)		20°C (68°F)		100°C (212°F)		20°C (68°F)	100 °C (212°F)	Melting point		Temperature of complete liquefaction		Proper pouring temperature	
	Johnson's apparent elastic limit <sup>e</sup>				Ultimate strength in compression <sup>f</sup>											
	MPa	psi	MPa	psi	MPa	psi	MPa	psi	MPa	psi	°C	°F	°C	°F	°C	°F
1	16.9	2450	7.2	1050	88.6	12,850	47.9	6950	8.0	17.0	223	433	371	700	441	825
2	23.1	3350	7.6	1100	102.7	14,900	60.0	8700	12.0	24.5	241	466	354	669	424	795
3	36.9	5350	9.0	1300	121.3	17,600	68.3	9900	14.5	27.0	240	464	422	792	491	915
7	17.2	2500	9.3	1350	107.9	15,650	42.4	6150	10.5	22.5	240	464	268	514	338	620
8	18.3	2650	8.3	1200	107.6	15,600	42.4	6150	9.5	20.0	237	459	272	522	341	645
15	—	—	—	—	—	—	—	—	13.0	21.0	248	479	281	538	350	662

<sup>a</sup>Compression test specimens were cylinders 1.5 in. (38 mm) in length and 0.5 in. (13 mm) in diameter, machined from chill castings 2 in. (51 mm) in length and 0.75 in (19 mm) in diameter. The Brinell tests were made on the bottom of parallel machined specimens cast in a mold 2 in. (51 mm) in diameter and 0.0625 in. (16 mm) deep at room temperature.

<sup>b</sup>Data not available on alloys 11 and 13.

<sup>c</sup>The specific gravity multiplied by 0.0361 equals the mass density in pounds per cubic inch.

<sup>d</sup>The values for yield point were taken from stress-strain curves at a deformation of 0.125 percent of gage length.

<sup>e</sup>Johnson's apparent elastic limit is taken as the unit stress at the point where the slope of the tangent to the curve is two-thirds its slope at the origin.

<sup>f</sup>The ultimate strength values were taken as the unit load necessary to produce a deformation of 25 percent of the specimen length.

<sup>g</sup>These values are the average Brinell number of three impressions on each alloy, using a 10-mm (0.39-in) ball and a 500-kg (1102.3 lb) load applied for 30 s.

Table 5.3: Chemical composition of alloys in more general use. [From ASTM B23-83. Reprinted by permission of the American Society for Testing and Materials.]

Element	Alloy number <sup>a,b</sup>							
	Tin base				Lead base			
	1	2	3	11	7	8	13	15
	Chemical composition, percent							
Tin	90.0-92.0	88.0-90.0	83.0-85.0	86.0-89.0	9.3-10.7	4.5-5.5	5.5-6.5	0.8-1.2
Antimony	4.0-5.0	7.0-8.0	7.5-8.5	6.0-7.5	14.0-16.0	14.0-16.0	9.5-10.5	14.5-17.5
Lead	.35	.35	.35	.50	Remainder <sup>c</sup>	Remainder	Remainder	Remainder
Copper	4.0-5.0	3.0-4.0	7.5-8.5	5.0-6.5	.50	.50	.50	.6
Iron	.08	.08	.08	.08	.10	.10	.10	.10
Arsenic	.10	.10	.10	.10	.30-.60	.30-.60	.25	.8-1.4
Bismuth	.08	.08	.08	.08	.10	.10	.10	.10
Zinc	.005	.005	.005	.005	.005	.005	.005	.005
Aluminum	.005	.005	.005	.005	.005	.005	.005	.005
Cadmium	.05	.05	.05	.05	.05	.05	.05	.05
Total named elements, minimum	99.80	99.80	99.80	99.80	—	—	—	—

<sup>a</sup>All values not given as ranges are maximum values unless shown otherwise.

<sup>b</sup>Alloy 9 was discontinued in 1946 and 4,5,6,10,11,12,16, and 19 were discontinued in 1959. A new number 11, similar to SAE grade 11, was added in 1966.

<sup>c</sup>To be determined by difference.

### **5.3.2 Copper-Lead Alloys**

Two alloys, one consisting of 60% copper and 40% lead and the other of 70% copper and 30% lead, or slight variations, are used as lining materials on steel-backed bearings. These alloys are either strip cast or sintered onto the backing strip, thus providing a bearing with a higher load-carrying capacity than one lined with the babbitt alloys. They also have higher fatigue resistance and can operate at higher temperatures, but they have poor antiseizure properties. They are used in automotive and aircraft internal combustion engines and in diesel engines. Their high lead content provides a good bearing surface but makes them susceptible to corrosion. Their corrosion resistance and antiseizure properties are improved when they are used as trimetal bearings with a lead-tin or lead-indium overlay electrodeposited onto the copper-lead surface.

### **5.3.3 Bronzes**

Several bronze alloys, including lead, tin, and aluminum bronzes, are used extensively as bearing materials. Some are described in Table 5.4. Because of their good structural properties, they can be used as cast bearings without a steel backing. Bearings can also be machined from standard bar stock.

Lead bronzes, which contain up to 25% lead, provide higher load-carrying capacity and fatigue resistance and a higher temperature capability than the babbitt alloys. Tin contents up to about 10% are used to improve the strength properties. Higher-lead bronze (70% copper, 5% tin, and 25% lead) can be used with soft shafts, but harder shafts (300 BHN) are recommended with the harder lower-lead bronzes, particularly under conditions of sparse lubrication. Lead bronze bearings are used in pumps, diesel engines, railroad cars, home appliances, and many other applications.

Tin bronzes, which contain 9 to 20% tin and small quantities of lead (usually < 1%), are harder than lead bronzes and are therefore used in heavier-duty applications.

## **5.4 Nonmetallics**

Although nonmetallic materials such as rubber and graphite have found increasing application, polymeric and plastic materials have had the greatest recent impact in triboelements. These materials fall into two categories: thermosetting and thermoplastic materials. In thermosetting materials the fabrics of nonoriented fibers are generally set in phenolic, or occasionally cresylic, resins.

Of the thermoplastic materials nylon has been recognized as a valuable bearing material as has the remarkable low-friction polymer polytetrafluoroethylene (PTFE). The great merit of these materials is that they can operate effectively without lubricants, although their mechanical properties generally limit their application to lightly loaded conditions and often to low speeds and conforming surfaces.

Table 5.4: Typical bronze and copper alloy bearing materials [From Booser (1966)]

Designation	Material	Cu	Sn	Pb	Zn	Fe	Al	Brinell hardness number BNH	Tensile strength		Maximum operating temperature		Maximum load		
		Nominal composition, percent							MPa	ksi	°C	°F	MPa	ksi	
SAE 480	Copper lead	65	—	35	—	—	—	25	55.2	8	177	350	13.8	2	
AMS 4840	High-lead tin bronze	70	5	25	—	—	—	48	172.5	25	204+	400+	20.7+	3+	
SAE 67	Semiplastic bronze	78	6	16	—	—	—	55	207.0	30	232	450	20.7+	3+	
SAE 40	Leaded red brass	85	5	5	5	—	—	60	241.5	35	232	450	24.2	3.5	
SAE 660	Bronze	83	7	7	3	—	—	60	241.5	35	232+	450+	27.6	4	
SAE 64	Phosphor bronze	80	10	10	—	—	—	63	241.5	35	232+	450+	27.6	4	
SAE 62	Gunmetal	88	10	—	2	—	—	65	310.5	45	260+	500+	27.6	4	
SAE 620	Navy G	88	8	—	4	—	—	68	276.0	40	260	500	27.6+	4+	
SAE 63	Leaded gunmetal	88	10	2	—	—	—	70	276.0	45	260	500	27.6+	4+	
ASTM B148- 52-9c	Aluminum bronze	85	—	—	—	4	11	195	621.0	90	260+	500+	31.1+	4.5+	

Table 5.5: Limits of application of nonmetallic bearing materials. [Revised from O'Connor et al. (1968).]

Material	Load-carrying capacity		Maximum temperature		Maximum speed		$PV$ limit <sup>a</sup>
	MPa	psi	°C	°F	m/s	ft/min	
Carbon graphite	4.1	600	399	750	12.7	2500	$15 \times 10^3$
Phenolics	41.4	6000	93	200	12.7	2500	$15 \times 10^3$
Nylon	6.9	1000	93	200	5.1	1000	$3 \times 10^3$
PTFE (Teflon)	3.4	500	260	500	0.51	100	$1 \times 10^3$
Reinforced PTFE	17.2	2500	260	500	5.1	1000	$10 \times 10^3$
PTFE fabric	414.0	60,000	260	500	0.25	50	$25 \times 10^3$
Polycarbonate (Lexan)	6.9	1000	104	220	5.1	1000	$3 \times 10^3$
Acetal resin (Delrin)	6.9	1000	82	180	5.1	1000	$3 \times 10^3$
Rubber	0.34	50	66	150	7.6	1500	$15 \times 10^3$
Wood	13.8	2000	66	150	10.2	2000	$15 \times 10^3$

<sup>a</sup>  $P$  = load (psi);  $V$  = surface speed (ft/min).

The limits of applying nonmetallic materials are shown in Table 5.5. The specific limits shown in this table are load-carrying capacity, maximum temperature, maximum speed, and  $PV$  limit, where  $P$  is the pressure expressed in pounds force per square inch and  $V$  is the surface speed expressed in feet per minute.

#### 5.4.1 Carbon Graphites

In addition to their excellent self-lubricating properties, carbon graphites have several advantages over conventional materials and lubricants. They can withstand temperatures of approximately 370°C in an oxidizing atmosphere such as air and can be used in inert atmospheres to 700°C or at cryogenic temperatures. They can be used in equipment in which lubricant contamination must be prevented, such as textile machinery and food-handling machinery. Carbon graphites are highly resistant to chemical attack and are used in applications where the chemicals attack conventional lubricants. They can be used with low-viscosity lubricants, such as water, gasoline, or air.

Carbon graphites are used for pump shaft bearings, impeller wear rings in centrifugal pumps, and journal and thrust bearings in covered motor pumps and for many other applications. Because of its low expansion coefficient of  $2.7 \times 10^{-6}$  mm/mm·°C, a carbon graphite liner is shrunk-fit into a steel sleeve. The steel backing provides mechanical support, improves heat transfer, and helps to maintain shaft clearance. The mating shaft should be made of harder metals. Chromium plates, hardened tool steels, or even some ceramics are used.

A  $PV$  value of 15,000 is used when lubricant is present. Depending on the material grade and the application, friction coefficients ranging from 0.04 to 0.25 are obtainable. Absorbed water vapor enhances film formation and reduces the friction and wear of carbon graphite. With no water vapor present

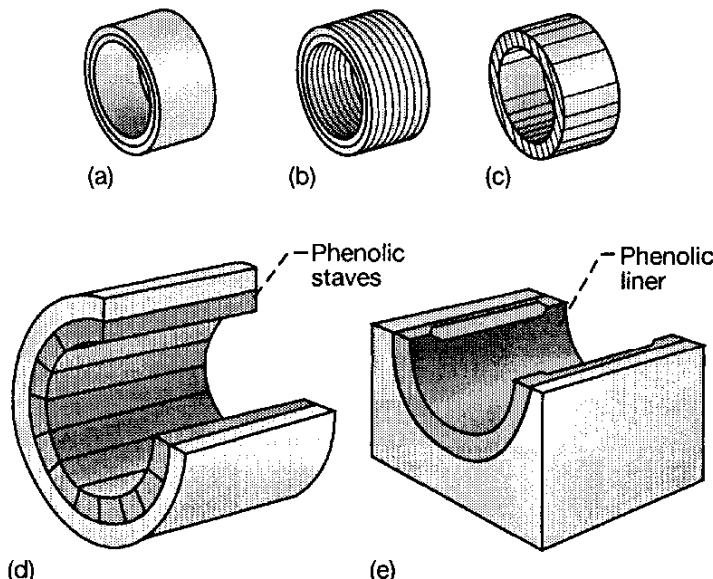


Figure 5.1: Phenolic laminate bearings. (a) Tubular bearing; (b) circumferentially laminated bearing; (c) axially laminated bearing; (d) stave bearing; (e) molded bearing. [From Kaufman (1980).]

(low humidity), wear increases. In general, low speeds and light loads should be used in nonlubricated applications.

#### 5.4.2 Phenolics

Among several types of plastic bearings presently in use are the phenolics. These are in the form of laminated phenolics, made by treating sheets of either paper or fabric with phenolic resin, stacking the desired number of sheets, and curing with heat and pressure to bond them together and set the resin. Other filling materials, such as graphite and molybdenum disulfide, are added in powdered form to improve lubrication qualities and strength.

Figure 5.1 shows the various orientations of the phenolic laminates used in bearings. Tubular bearings (Fig. 5.1a) are used where complete bushings are required. Bearings in which the load is taken by the edges of the laminations (Fig. 5.1b and c) are used in light-duty service. Stave bearings (Fig. 5.1d) are used mainly for stern-tube and rudder-stock bearings on ships and for guide bearings on vertical waterwheel turbines. Molded bearings (Fig. 5.1e) are used for roll-neck bearings in steel mills or for ball-mill bearings. Table 5.6 gives some typical applications of phenolic bearings.

Laminated phenolics operate well with steel or bronze journals when lubricated with oil, water, or other liquids. They have good resistance to seizure. One main disadvantage of these materials is their low thermal conductivity ( $0.35 \text{ W/m} \cdot ^\circ\text{C}$ , about  $1/150$  that of steel), which prevents them from dissipating frictional heat readily and can result in their failure by charring. In large roll-neck bearings the heat is removed by providing a large water flow through the bearing.

Laminated phenolics have good resistance to chemical attack and can be used with water, oil, diluted acid, and alkali solutions. They have good conformability, having an elastic modulus of 3.45 to 6.90 GPa, in comparison with

Table 5.6: Typical applications of laminated phenolic bearings [*From Kaufman (1980)*].

Bearing application	Type <sup>a</sup>	Size range		Fabric weight		Resin	Lubricant	Diametral clearance <sup>b</sup>		Principal reasons for using laminated phenolic bearing material
		mm	in.	g/m	oz/yd			mm	in.	
Roll neck	(e)	76-762	3-30	466-1552	15-50	40-60	Water or emulsion	0-13	0-0.5	Longer life, power savings due to lower friction, lower-cost water lubrication, greater cleanliness of operation, better holding of gage due to less water.
Ship, stern tube	(d)	76-660	3-26	248	8	60	Water	0.001/mm diameter over 127 mm	0.001/in. diameter over 5 in.	Longer life, greater ease of handling and installing, higher load-carrying capacity particularly with impact loads, lower friction, greater corrosion and decay resistance, lower journal wear, greater local availability
Rudder, pintle	(a), (d)	76-660	3-26	93-248	3-8	55-60	Grease or water	0.001/mm diameter over 127 mm	0.001/in. diameter over 5 in.	
Small craft, stern tube	(c)	13-76	.5-3	248	8	60	Water	.127	.005	
Centrifugal pump	(a),(b),(c)	13-102	.5-4	93-248	3-8	60	Pumped liquid	.127	.005	Longer life, better lubrication with pumped liquid (water, gasoline, chemical solutions, etc.)
Water wheel, turbine, guide bearing	(d)	102-610	4-24	248	8	60	Water	.127	.005	Longer life, lower friction, no decay, less journal wear
Ball mill	(a),(e)	381-1219	15-49	202-466	6.5-15	55-60	Water or emulsion of water and grease	.381-.762	.015-0.30	Longer life, higher load-carrying capacity, lower friction, lower lubricant cost
Aircraft, landing gear	(a)	51-381	2-12	93	3	60	Oil	0.001/mm diameter over 127 mm	0.001/in. diameter over 5 in.	Lighter weight, satisfactory dimensional stability and load-carrying capacity
Railway, bolster cup	Molded cone	—	—	202	6.5	53	Grease	—	—	Longer life, lower noise and vibration transmission

about 3.45 GPa for babbitts. Laminated phenolics also have a high degree of embeddability. This property is advantageous in ship stern-tube bearings, which are lubricated by water that contains sand and other sediment. Because of their good resilience, they are highly resistant to damage by fatigue and shock loading. They do not hammer out or extrude under shock loading as do some babbitt alloys. Because laminated phenolics are made up of organic fibers that absorb certain liquids and expand, small changes in dimensions can occur. Water or lubricants containing water have a greater measurable effect on the dimensional stability of phenolics than do oils. Expansion is greater perpendicular to the laminations (2 to 3%) than parallel (0 to 0.3 percent).

#### **5.4.3 Nylon**

Nylon is one of the classes of thermoplastic materials, as differentiated from the thermosetting plastics, the phenolics. Nylon bearings can be molded, or nylon powders can be sintered in a manner similar to the manufacture of porous metals. Nylon is not affected by petroleum oils and greases, food acids, milk, photographic solutions, etc., and thus can be used in applications where these fluids are handled.

Nylon has good abrasion resistance, a low wear rate, and good embeddability. Like most plastics, it has good antiseizure properties and softens or chars rather than seizing. It has low thermal conductivity ( $0.24 \text{ W/m}\cdot\text{°C}$ ), and failure is usually the result of overheating. Cold flow (creep) under load is one of its main disadvantages. This effect can be minimized by supporting thin nylon liners in metal sleeves. Nylon bearings are used in household applications such as mixers and blenders and for other lightly loaded applications.

#### **5.4.4 Teflon**

Teflon is a thermoplastic material based on the polymer polytetrafluoroethylene (PTFE), which has a low friction coefficient. It has excellent self-lubricating properties and in many applications can be used dry. It is resistant to chemical attack by many solvents and chemicals and can be used in the temperature range -260 to 260°C. Like nylon, it has a tendency to cold-form under loads. Teflon in its unmodified form also has the disadvantages of low stiffness, a high thermal expansion coefficient, low thermal conductivity, and poor wear resistance. These poor properties are greatly improved by adding fibers such as glass, ceramics, metal powders, metal oxides, graphite, or molybdenum disulfide.

### **5.5 Form of Bearing Surfaces**

The metallic and nonmetallic materials described in the two preceding sections may be applied to bearing surfaces in several ways, (as shown in Fig. 5.2):

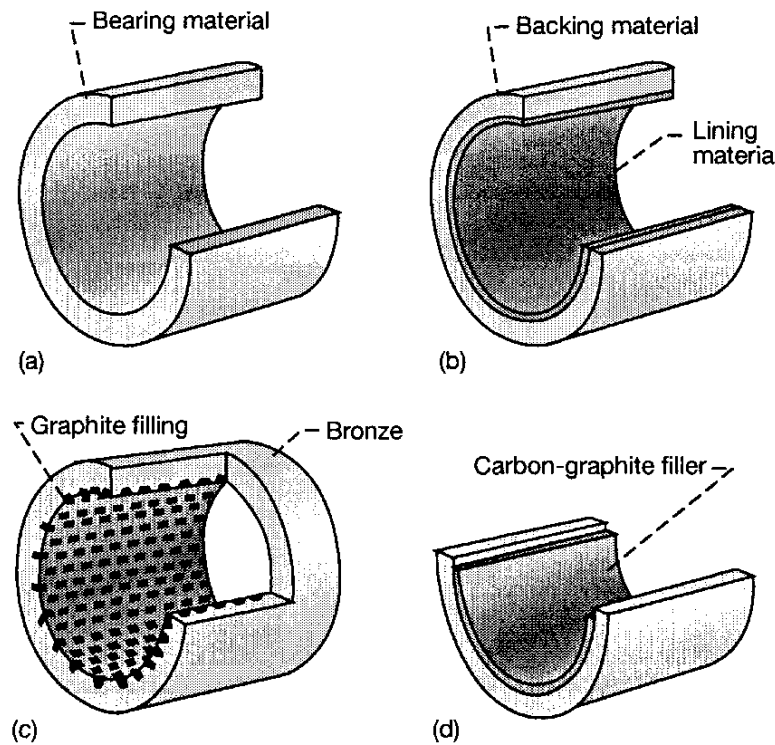


Figure 5.2: Different forms of bearing surfaces. (a) Solid bearing; (b) lined bearing; (c) filled bearing; (d) shrink-fit bearing.

- Solid bearing (Fig. 5.2a). Bearings are machined directly from a single material (cast iron, aluminum alloys, bronzes, porous metals, etc.).
- Lined bearing (Fig. 5.2b). Bearing material is bonded to a stronger backing material. The thickness of the bearing lining may range from 0.25 mm to as much as 13 mm. Most modern bonding techniques are metallurgical, although chemical and mechanical methods are also used. The lining material may be cast, sprayed, electrodeposited, or chemically applied.
- Filled bearing (Fig. 5.2c). A stronger bearing material is impregnated with a bearing material that has better lubricating properties (e.g., graphite impregnated into a bronze backing).
- Shrink-fit liner bearing Fig. 5.2d). Carbon-graphite or plastic liners are shrunk into a metal housing sleeve by retaining devices such as setscrews, dowels, and clamping flanges.

## 5.6 Materials and Manufacturing Processes Used for Rolling-Element Bearings

Nonconformal surfaces such as rolling-element bearings operate under conditions that impose high compressive stresses for millions of stress cycles as the

balls or the rollers rotate through the loaded zone of the bearing. For such applications the race and ball materials should be hard and have high fatigue resistance.

Until about 1955 the technology of rolling-element bearing materials did not receive much attention from materials scientists. Bearing materials were restricted to SAE 52100 and some carburizing grades such as AISI 4320 and AISI 9310, which seemed to be adequate for most bearing applications, despite the limitation in temperature of about 176°C for 52100 steel. A minimum acceptable hardness of Rockwell C 58 was specified. Experiments indicated that fatigue life increased with increasing hardness.

The advent of the aircraft gas turbine engine, with its need for advanced rolling-element bearings, provided the major impetus for advancements in the technology of rolling-element bearing materials. Higher temperatures, higher speeds and loads, and the need for greater durability and reliability all served as incentives for developing and evaluating a broad range of new materials and processing methods. The combined research efforts of bearing manufacturers, engine manufacturers, and government agencies over the past three decades have resulted in startling advances in rolling-element bearing life, reliability, and performance. The discussion here is narrow in scope. For a comprehensive treatment of the research status of current bearing technology and current bearing designs, refer to Bamberger et al. (1980).

### 5.6.1 Ferrous Alloys

The need for higher temperature capability led to the evaluation of several available molybdenum and tungsten alloy tool steels as bearing materials. These alloys have excellent high-temperature hardness retention. Such alloys melted and cast in an air environment were, however, generally deficient in fatigue resistance because of nonmetallic inclusions. Vacuum processing techniques can reduce or eliminate these inclusions. Techniques used include vacuum induction melting (VIM) and vacuum arc remelting (VAR). These have been extensively explored, not only with the tool steels now used as bearing materials but with SAE 52100 and some of the carburizing steels as well. Table 5.7 lists a fairly complete array of ferrous alloys, both fully developed and experimental, from which present-day bearings are fabricated. AISI M-50, usually VIM-VAR or consumable electrode vacuum melted (CEVM), has become a widely used quality bearing material. It is usable at temperatures to 315°C, and it is usually assigned a materials life factor of 3 to 5. T-1 tool steel has also come into fairly wide use in bearings, mostly in Europe. Its hot hardness retention is slightly superior to that of M-50 and approximately equal to that of M-1 and M-2. These alloys retain adequate hardness to about 400°C.

Surface-hardened or carburized steels are used in many bearings where, because of shock loads or cyclic bending stresses, the fracture toughness of through-hardened steels is inadequate. Some of the newer materials being developed, such as CBS 1000 and Vasco X-2, have hot hardness retention compa-

Table 5.7: Typical compositions of selected bearing steels [From Bamberger et al. (1980)]

Designation	C	P (max)	S (max)	Mn	Si	Cr	V	W	Mo	Co	Cb	Ni
	Alloying element, wt %											
SAE 52100 <sup>a</sup>	1.00	0.025	0.025	0.35	0.30	1.45	—	—	—	—	—	—
MHT <sup>b</sup>	1.03	0.025	0.025	0.35	0.35	1.50	—	—	—	—	—	—
AISI M-1	0.80	0.030	0.030	0.30	0.30	4.00	1.00	1.50	8.00	—	—	—
AISI M-2 <sup>a</sup>	0.83	0.030	0.030	0.30	0.30	3.85	1.90	6.15	5.00	—	—	—
AISI M-10	0.85	0.030	0.030	0.25	0.30	4.00	2.00	—	8.00	—	—	—
AISI M-50 <sup>a</sup>	0.80	0.030	0.030	0.30	0.25	4.00	1.00	—	4.25	—	—	—
T-1 (18-4-1) <sup>a</sup>	0.70	0.030	0.030	0.30	0.25	4.00	1.00	18.0	—	—	—	—
T15	1.52	0.010	0.004	0.26	0.25	4.70	4.90	12.5	0.20	5.10	—	—
440C <sup>a</sup>	1.03	0.018	0.014	0.48	0.41	17.30	0.14	—	0.50	—	—	—
AMS 5749	1.15	0.012	0.004	0.50	0.30	14.50	1.20	—	4.00	—	—	—
Vasco Matrix II	0.53	0.014	0.013	0.12	0.21	4.13	1.08	1.40	4.80	7.81	—	0.10
CRB-7	1.10	0.016	0.003	0.43	0.31	14.00	1.03	—	2.02	—	0.32	—
AISI 9310 <sup>c</sup>	0.10	0.006	0.001	0.54	0.28	1.18	—	—	0.11	—	—	3.15
CBS 600 <sup>c</sup>	0.19	0.007	0.014	0.61	1.05	1.50	—	—	0.94	—	—	0.18
CBS 1000M <sup>c</sup>	0.14	0.018	0.019	0.48	0.43	1.12	—	—	4.77	—	—	2.94
Vasco X-2 <sup>c</sup>	0.14	0.011	0.011	0.24	0.94	4.76	0.45	1.40	1.40	0.03	—	0.10

<sup>a</sup>Balance, iron.

<sup>b</sup>Also contains 1.36% Al.

<sup>c</sup>Carburizing grades.

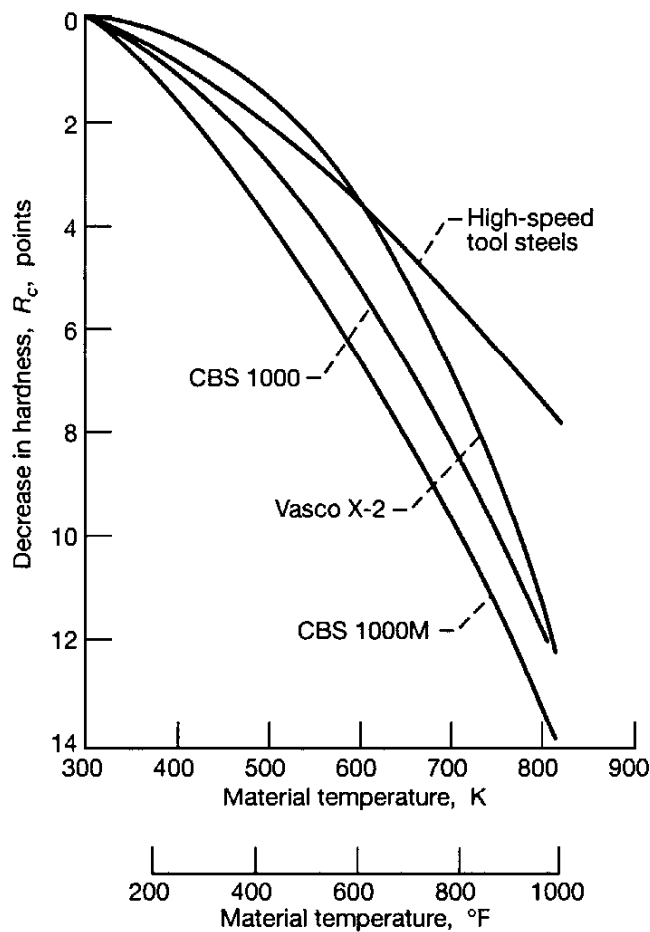


Figure 5.3: Hot hardness of CBS 1000, CBS 1000M, Vasco X-2, and high-speed tool steels. [From Anderson and Zaretsky (1975).]

rable to that of the tool steels (Fig. 5.3). They too are available as ultraclean, vacuum-processed materials and should offer adequate resistance to fatigue. Carburized steels may become of increasing importance in ultra-high-speed applications. Bearings with through-hardened steel races are currently limited to approximately 2.5 million  $d_b N_a$  (where  $d_b$  is bore diameter in millimeters and  $N_a$  is rotational speed in revolutions per minute). At higher  $d_b N_a$  values fatigue cracks propagate through the rotating race as a result of excessive hoop stress (Bamberger et al., 1976).

In applications where the bearings are not lubricated with conventional oils and protected from corrosion at all times, a corrosion-resistant alloy should be used. Dry-film-lubricated bearings, bearings cooled by liquefied cryogenic gases, and bearings exposed to corrosive environments such as high humidity and salt water are applications where corrosion-resistant alloys should be considered. Of the alloys listed in Table 5.7, both 440C and AMS 5749 are readily available in vacuum-melted heats.

Forging and forming methods that result in improved resistance to fatigue have also been developed. Experiments indicate that fiber or grain flow parallel to the stressed surface is superior to fiber flow that intersects the stressed surface (Bamberger, 1970; Zaretsky and Anderson, 1966). Forming methods that result in more parallel grain flow are now being used in the manufacture of many bearings, especially those for high-load applications.

## 5.6.2 Ceramics

Experimental bearings have been made from a variety of ceramics including alumina, silicon carbide, titanium carbide, and silicon nitride. The use of ceramics as bearing materials for specialized applications will probably continue to grow for several reasons. These include

- High-temperature capability. Because ceramics can exhibit elastic behavior to temperatures beyond 1000°C, they are an obvious choice for extreme temperature applications.
- Corrosion resistance. Ceramics are essentially chemically inert and able to function in many environments hostile to ferrous alloys.
- Low density. This can be translated into improved bearing capacity at high speeds, where centrifugal effects predominate.
- Low thermal expansion coefficient. Under severe thermal gradients, ceramic bearings exhibit less drastic changes in geometry and internal play than do ferrous alloy bearings.

Silicon nitride has been developed as a bearing material (Sibley, 1982; Cundill and Giordano, 1982). Silicon nitride bearings have exhibited fatigue lives comparable to and in some instances superior to that of high-quality vacuum-melted M-50 (Sibley, 1982). Two problems remain: (1) quality control and precise nondestructive inspection techniques to determine acceptability and (2) cost. Improved hot isostatic compaction, metrology, and finishing techniques are all being actively pursued.

## 5.7 Properties of Common Bearing Materials

This section provides representative values for a number of solid material properties required in evaluating fluid film bearings. The tables and figures presented in this section came from ESDU (1984). With many materials a wide range of property values is attainable by, for example, heat treatment or a small change in composition. The quoted values given in the tables are therefore only typical values likely to be met in fluid film lubrication applications. Unless otherwise stated, all material properties are quoted for room temperature (20°C).

Bearing materials have been conveniently grouped into three basic classifications: metals, ceramics, and polymers. This scheme is based primarily on chemical makeup and atomic structure, and most materials fall into one distinct grouping or another, although there are some intermediates. In addition to these three major classifications, there is one additional group of bearing materials that might be considered, namely, composites. A brief explanation of the material classifications and their representative characteristics is given here:

- *Metals.* Metallic materials are normally combinations of metallic elements. They have large numbers of nonlocalized electrons; that is, these electrons are not bound to particular atoms. Metals are extremely good conductors of electricity and heat and are not transparent to visible light; a polished metal surface has a lustrous appearance. Furthermore, metals are quite strong yet deformable.
- *Ceramics.* Ceramics are compounds of metallic and nonmetallic elements; they are most frequently oxides, nitrides, and carbides. The wide range of materials that fall within this classification includes ceramics that are composed of clay, cement, and glass. These materials are typically insulative to the passage of electricity and heat and are more resistant to high temperatures and harsh environments than metals and polymers. With regard to mechanical behavior, ceramics are hard but very brittle.
- *Polymers.* Polymers include plastic and rubber materials. Many polymers are organic compounds that are chemically based on carbon, hydrogen, and other nonmetallic elements. Furthermore, they have very large molecular structures. These materials typically have low density and may be extremely flexible.
- *Composites.* Composite materials include more than one material type. Fiberglass is an example, in which glass fibers are embedded within a polymeric material. A composite is designed to display a combination of the best characteristics of each of the component materials. Fiberglass acquires strength from glass and flexibility from the polymer.

Composites are beyond the scope of this book, but the properties of the other three main classifications of materials will be considered along with a number of materials within each classification.

### 5.7.1 Density

As pointed out in Sec. 4.12, the density  $\rho$  of a solid material is the mass divided by the volume and hence has metric units of kilograms per cubic meter. Typical values lie between  $10^3$  and  $10^4 \text{ kg/m}^3$ . Figure 5.4 illustrates the density ordering of various metals, polymers, and ceramics, and Table 5.8 gives quantitative density at room temperature ( $20^\circ\text{C}$ ).

Alloying changes the density only slightly. To a first approximation, the density of an alloy (metallic solid resulting from dissolving two or more molten metals in each other) is given by the “rule of mixtures” (i.e., by a linear interpolation between the densities of the alloy components).

Table 5.8: Densities of various metals, polymers, and ceramics at room temperature (20°C; 68°F) [From ESDU (1984).]

Material	Density, $\rho$	
	kg/m <sup>3</sup>	lbm/in. <sup>3</sup>
<b>Metals:</b>		
Aluminum and its alloys <sup>a</sup>	$2.7 \times 10^3$	0.097
Aluminum tin	$3.1 \times 10^3$	0.11
Babbitt, lead-based white metal	$10.1 \times 10^3$	0.36
Babbitt, tin-based white metal	$7.4 \times 10^3$	0.27
Brasses	$8.6 \times 10^3$	0.31
Bronze, aluminum	$7.5 \times 10^3$	0.27
Bronze, leaded	$8.9 \times 10^3$	0.32
Bronze, phosphor (cast) <sup>b</sup>	$8.7 \times 10^3$	0.31
Bronze, porous	$6.4 \times 10^3$	0.23
Copper	$8.9 \times 10^3$	0.32
Copper lead	$9.5 \times 10^3$	0.34
Iron, cast	$7.4 \times 10^3$	0.27
Iron, porous	$6.1 \times 10^3$	0.22
Iron, wrought	$7.8 \times 10^3$	0.28
Magnesium alloys	$1.8 \times 10^3$	0.065
Steels <sup>c</sup>	$7.8 \times 10^3$	0.28
Zinc alloys	$6.7 \times 10^3$	0.24
<b>Polymers:</b>		
Acetal (polyformaldehyde)	$1.4 \times 10^3$	0.051
Nylons (polyamides)	$1.14 \times 10^3$	0.041
Polyethylene, high quality	$0.95 \times 10^3$	0.034
Phenol, formaldehyde	$1.3 \times 10^3$	0.047
Rubber, natural <sup>d</sup>	$1.0 \times 10^3$	0.036
Rubber, silicone	$1.8 \times 10^3$	0.065
<b>Ceramics:</b>		
Alumina ( $\text{Al}_2\text{O}_3$ )	$3.9 \times 10^3$	0.14
Graphite, high strength	$1.7 \times 10^3$	0.061
Silicon carbide ( $\text{SiC}$ )	$2.9 \times 10^3$	0.10
Silicon nitride ( $\text{Si}_3\text{N}_4$ )	$3.2 \times 10^3$	0.12

<sup>a</sup>Structural alloys.

<sup>b</sup>Bar stock typically  $8.8 \times 10^3$  kg/m<sup>3</sup> (0.30 lbm/in.<sup>3</sup>).

<sup>c</sup>Excluding "refractory" steels.

<sup>d</sup>"Mechanical" rubber

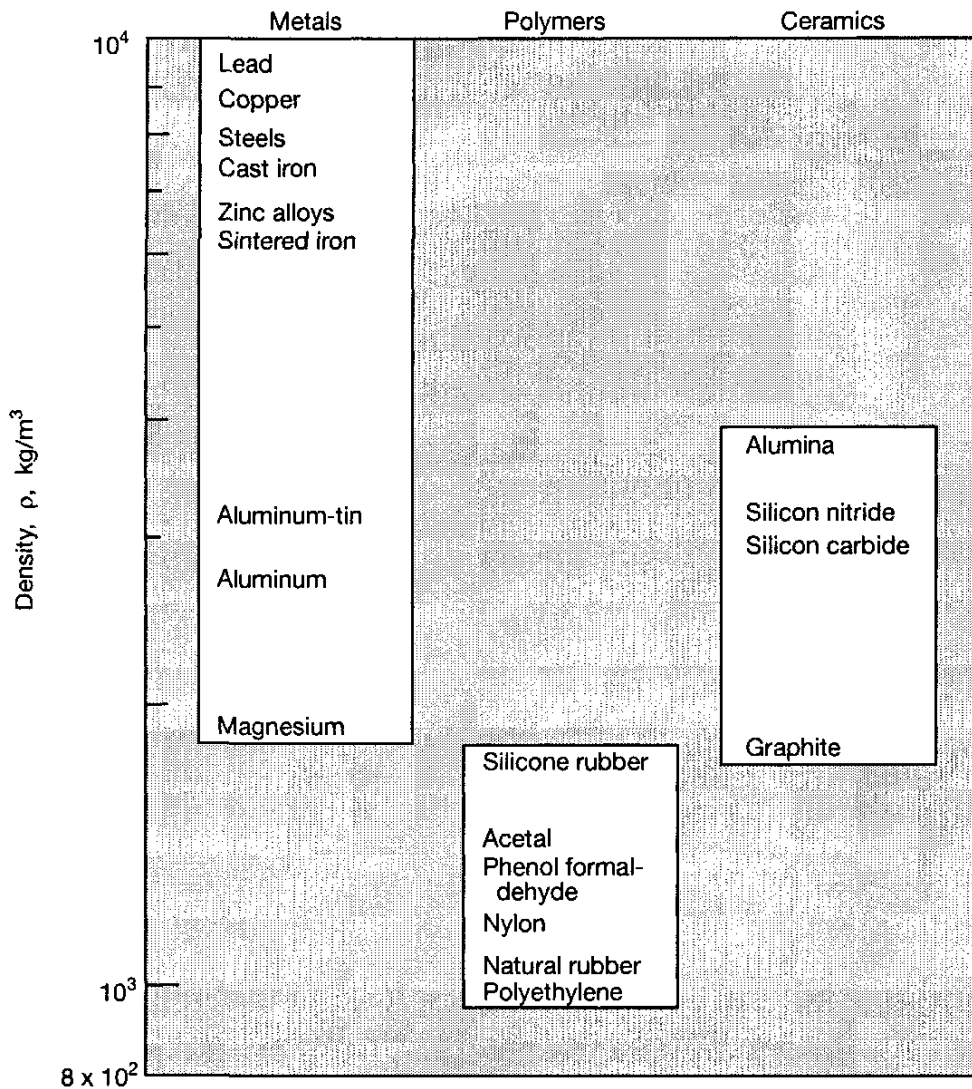


Figure 5.4: Illustration of density for various metals, polymers, and ceramics at room temperature (20°C; 68°F). [From ESDU (1984).]

### 5.7.2 Modulus of Elasticity and Poisson's Ratio

A simple tensile load applied to a bar produces a stress  $\sigma_1$  and a strain  $\epsilon_1$ , where

$$\sigma_1 = \frac{\text{load}}{\text{cross-sectional area}} = \text{stress in axial direction}$$

$$\epsilon_1 = \frac{\text{change in length}}{\text{original length}} = \text{strain in axial direction}$$

The elastic constant, or modulus of elasticity (sometimes referred to as "Young's modulus"), can be written as

$$E = \frac{\sigma_1}{\epsilon_1} \quad (5.1)$$

Although no stress acts transversely to the axial direction, there will nevertheless be dimensional changes in the transverse direction, for as a bar extends axially it contracts transversely. The transverse strains  $\epsilon_2$  are related to the axial strains by Poisson's ratio  $\nu$  such that

$$\epsilon_2 = -\nu\epsilon_1 \quad (5.2)$$

where the negative sign simply means that the transverse deformation will be in the opposite sense to the axial deformation. The metric unit of modulus of elasticity is newton per square meter, or pascal, and Poisson's ratio is dimensionless.

Figure 5.5 illustrates values of the modulus of elasticity for various metals, polymers, and ceramics at room temperature ( $20^\circ\text{C}$ ). The moduli of elasticity for metals and ceramics are quite similar, but those for the polymers are considerably lower. Tables 5.9 and 5.10 give quantitative values of the modulus of elasticity and Poisson's ratio, respectively, for various metals, polymers, and ceramics at room temperature.

### 5.7.3 Linear Thermal Expansion Coefficient

Different materials expand at different rates when heated. A solid object increases in length by a certain fraction for each degree rise in temperature. This result is accurate over a fairly large range of temperatures. It can be used for calculating how much an object will expand for a given change in temperature, once the extent of the material's expansion is measured. This value is given for each material by a number called "linear expansivity" or "linear thermal expansion coefficient"  $\bar{a}$ . The metric unit of  $\bar{a}$  is  $\text{Kelvin}^{-1}$ .

Figure 5.6 illustrates the linear thermal expansion coefficient for various metals, polymers, and ceramics applied over the temperature range 20 to  $200^\circ\text{C}$ . The polymers have the highest value, followed by the metals and then the ceramics. Table 5.11 gives quantitative values of the linear thermal expansion coefficient for various metals, polymers, and ceramics from 20 to  $200^\circ\text{C}$ .

### 5.7.4 Thermal Conductivity

When two bodies at different temperatures are brought together, the faster-moving molecules of the warmer body collide with the slower-moving molecules of the cooler body and transfer some of their motion to the latter. The warmer object loses energy (drops in temperature) while the cooler one gains energy (rises in temperature). The transfer process stops when the two bodies reach the same temperature. This transfer of molecular motion through a material is called "heat conduction." Materials differ in how fast they let this transfer go on. The metric units of thermal conductivity  $K_f$  are watts per meter-Kelvin.

Figure 5.7 illustrates the thermal conductivity of various metals, polymers, and ceramics. The metals and ceramics in general are good conductors, and the polymers are good insulators. Table 5.12 quantifies the thermal conductivity

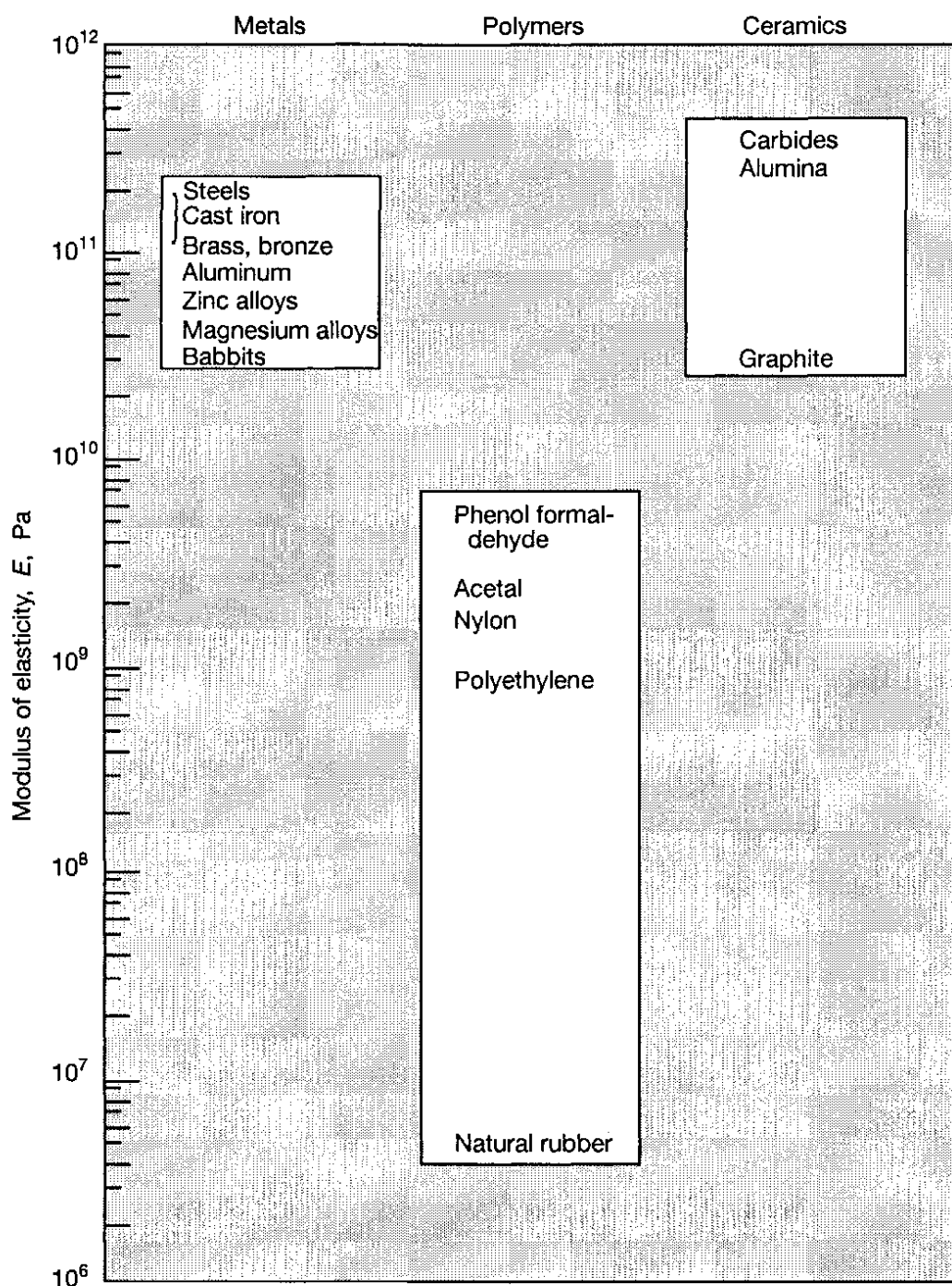


Figure 5.5: Illustration of modulus of elasticity for various metals, polymers, and ceramics at room temperature (20°C; 68°F). [From ESDU (1984).]

Table 5.9: Modulus of elasticity for various metals, polymers, and ceramics at room temperature (20°C; 68°F) [From ESDU (1984).]

Material	Modulus of elasticity, $E$	
	GPa	Mlb/in. <sup>2</sup>
<b>Metals</b>		
Aluminum	62	9.0
Aluminum alloys <sup>a</sup>	70	10.2
Aluminum tin	63	9.1
Babbitt, lead-base white metal	29	4.2
Babbitt, tin-base white metal	52	7.5
Brasses	100	14.5
Bronze, aluminum	117	17.0
Bronze, leaded	97	14.1
Bronze, phosphor	110	16.0
Bronze, porous	60	8.7
Copper	124	18.0
Iron, gray cast	109	15.8
Iron, malleable cast	170	24.7
Iron, spheroidal graphite <sup>b</sup>	159	23.1
Iron, porous	80	11.6
Iron, wrought	170	24.7
Magnesium alloys	41	5.9
Steel, low alloys	196	28.4
Steel, medium and high alloys	200	29.0
Steel, stainless <sup>c</sup>	193	28.0
Steel, high speed	212	30.7
Zinc alloys <sup>d</sup>	50	7.3
<b>Polymers</b>		
Acetal (polyformaldehyde)	2.7	0.39
Nylons (polyamides)	1.9	0.28
Polyethylene, high density	0.9	0.13
Phenol formaldehyde <sup>e</sup>	7.0	1.02
Rubber, natural <sup>f</sup>	0.004	0.0006
<b>Ceramics</b>		
Alumina ( $\text{Al}_2\text{O}_3$ )	390	56.6
Graphite	27	3.9
Cemented carbides	450	65.3
Silicon carbide ( $\text{SiC}$ )	450	65.3
Silicon nitride ( $\text{Si}_3\text{N}_4$ )	314	45.5

<sup>a</sup> Structural alloys.

<sup>b</sup> For bearings.

<sup>c</sup> Precipitation-hardened alloys up to 211 GPa (30 lbf/in.<sup>2</sup>).

<sup>d</sup> Some alloys up to 96 GPa (14 lbf/in.<sup>2</sup>).

<sup>e</sup> Filled.

<sup>f</sup> 25-Percent-carbon-black “mechanical” rubber.

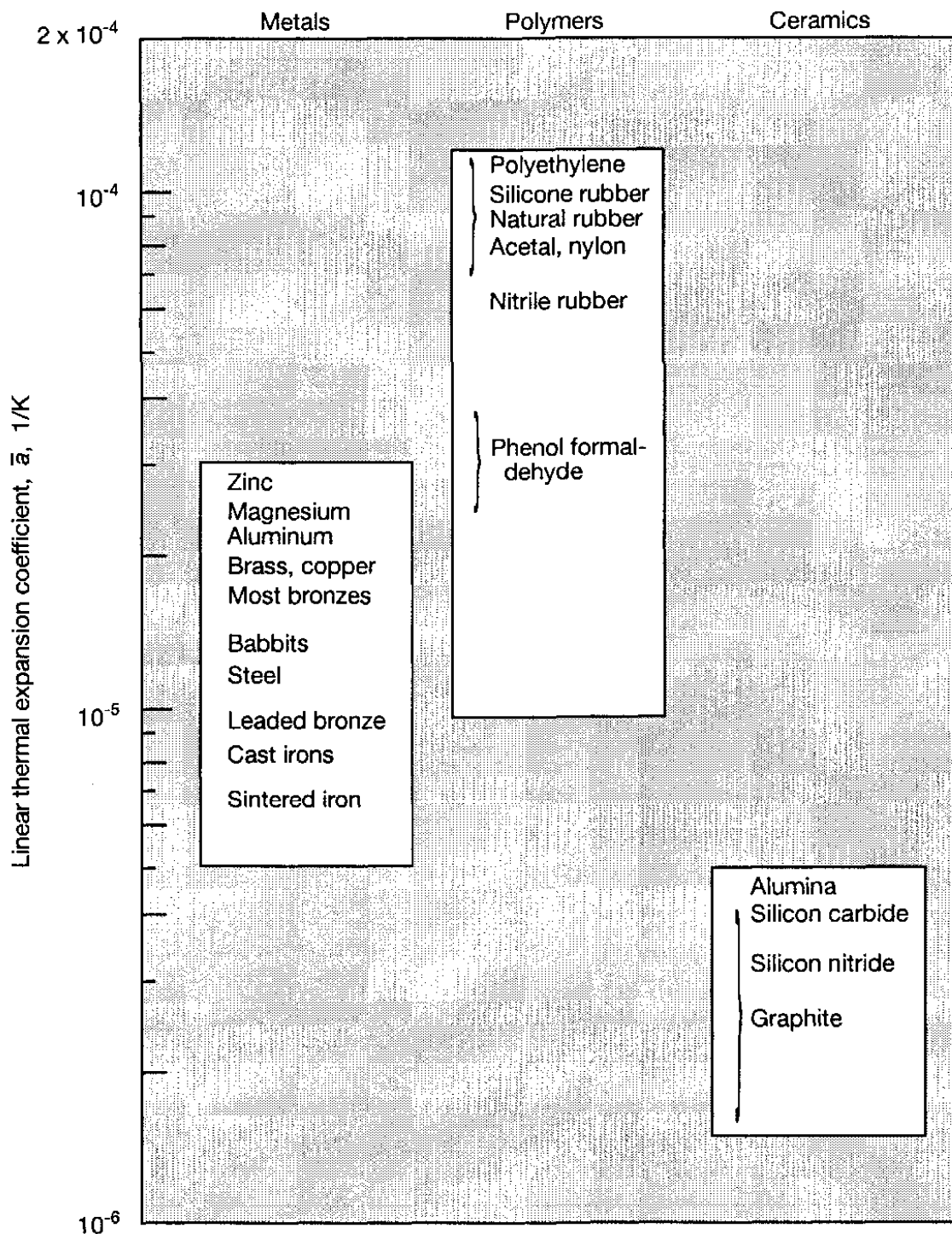


Figure 5.6: Illustration of thermal expansion coefficient for various metals, polymers, and ceramics applied over temperature range 20 to 200°C (68 to 392°F). [From ESDU (1984).]

Table 5.10: Poisson's ratio for various metals, polymers, and ceramics at room temperature (20°C; 68°F) [From ESDU (1984).]

Material	Poisson's ratio, $\nu$
<b>Metals:</b>	
Aluminum and its alloys	0.33
Aluminum tin	—
Babbitt, lead-base white metal	—
Babbitt, tin-base white metal	—
Brasses	0.33
Bronze	0.33
Bronze, porous	0.22
Copper	0.33
Iron, cast	0.26
Iron, porous	0.20
Iron, wrought	0.30
Magnesium alloys	0.33
Steels	0.30
Zinc alloys <sup>d</sup>	0.27
<b>Polymers:</b>	
Acetal (polyformaldehyde)	—
Nylons (polyamides)	0.40
Polyethylene, high density	0.35
Phenol formaldehyde <sup>e</sup>	—
Rubber	0.50
<b>Ceramics:</b>	
Alumina ( $\text{Al}_2\text{O}_3$ )	0.28
Graphite, high strength	—
Cemented carbides	0.19
Silicon carbide ( $\text{SiC}$ )	0.19
Silicon nitride ( $\text{Si}_3\text{N}_4$ )	0.26

<sup>a</sup>Structural alloys.

results given in Fig. 5.7. In Fig. 5.7 and Table 5.12, unless otherwise stated, the temperature is assumed to be room temperature (20°C; 68°F).

### 5.7.5 Specific Heat Capacity

The nature of a material determines the amount of heat transferred to or from a body when its temperature changes by a given amount. Imagine an experiment in which you take a cast iron ball and a babbitt (lead-based white metal) ball of the same size, heat them both to the temperature of boiling water, and then lay them on a block of wax. You would find that the cast iron ball melts a considerable amount of wax but the babbitt ball, in spite of its greater mass, melts hardly any. It therefore would seem that different materials, in cooling through the same temperature range, give up different amounts of heat.

The quantity of heat energy given up or taken on when a body changes its

Table 5.11: Linear thermal expansion coefficient for various metals, polymers and ceramics applied over temperature range 20 to 200° (68 to 392°) [From ESDU (1984)]

Material	Linear thermal expansion coefficient, $\bar{\alpha}$	
	$\mu\text{m}/\text{m}\cdot\text{K}$	$\mu\text{in./in.} \cdot {}^\circ\text{F}$
<b>Metals:</b>		
Aluminum	23	12.8
Aluminum alloys <sup>a</sup>	24	13.3
Aluminum tin	24	13.3
Babbitt, lead-based white metal	20	11
Babbitt, tin-based white metal	23	13
Brasses	19	10.6
Bronzes	18	10.0
Copper	18	10.0
Copper lead	18	10.0
Iron, cast	11	6.1
Iron, porous	12	6.7
Iron, wrought	12	6.7
Magnesium alloys	27	15
Steel, alloy <sup>b</sup>	11	6.1
Steel, stainless	17	9.5
Steel, high speed	11	6.1
Zinc alloys	27	15
<b>Polymers:</b>		
Thermoplastics <sup>c</sup>	60–100	35–56
Thermosets <sup>d</sup>	10–80	6–44
Acetal (polyformaldehyde)	90	50
Nylons (polyamides)	100	56
Polyethylene, high density	126	70
Phenol formaldehyde <sup>e</sup>	25–40	14–22
Rubber, natural <sup>f</sup>	80–120	44–67
Rubber, nitrile <sup>g</sup>	34	62
Rubber, silicone	57	103
<b>Ceramics:</b>		
Alumina ( $\text{Al}_2\text{O}_3$ ) <sup>h</sup>	5.0	2.8
Graphite, high strength	4.5	0.8–2.2
Silicon carbide ( $\text{SiC}$ )	4.3	2.4
Silicon nitride ( $\text{Si}_3\text{N}_4$ )	3.2	1.8

<sup>a</sup>Structural alloys.

<sup>b</sup>Cast alloys can be up to  $15\mu\text{m}/\text{m}\cdot\text{K}$ .

<sup>c</sup>Typical bearing materials.

<sup>d</sup>25  $\mu\text{m}/\text{m}\cdot\text{K}$  to 80  $\mu\text{m}/\text{m}\cdot\text{K}$  when reinforced.

<sup>e</sup>Mineral filled.

<sup>f</sup>Fillers can reduce coefficients.

<sup>g</sup>Varies with composition.

<sup>h</sup>0 to 200°C.

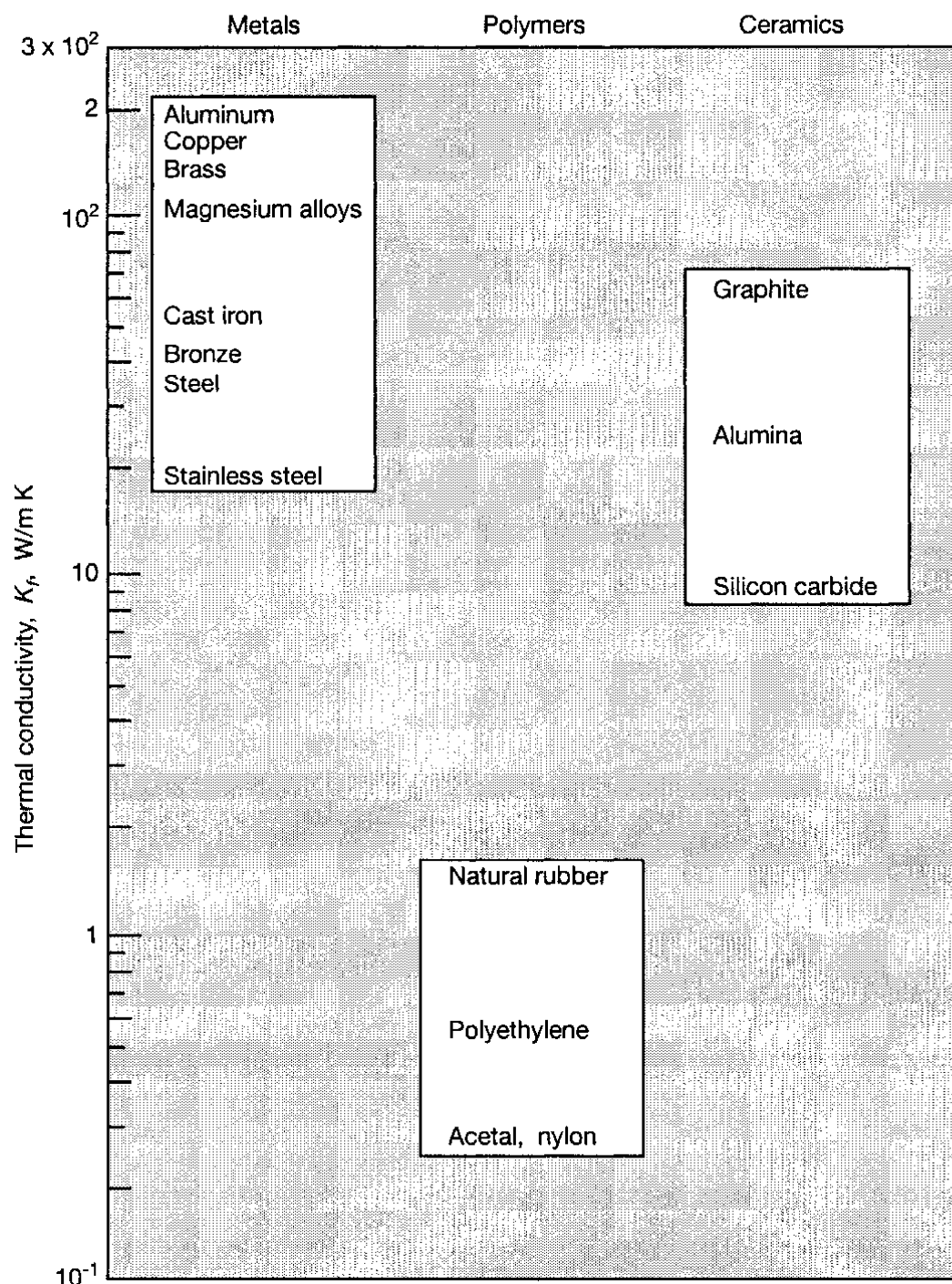


Figure 5.7: Illustration of thermal conductivity for various metals, polymers, and ceramics. [From ESDU (1984).]

Table 5.12: Thermal conductivity for various metals, polymers, and ceramics

Material	Thermal conductivity	
	W/m K	Btu/ft hr °F
<b>Metals:</b>		
Aluminum	209	120
Aluminum alloys, casting <sup>a</sup>	146	84
Aluminum alloys, silicon <sup>b</sup>	170	98
Aluminum alloys, wrought <sup>c</sup>	151	87
Aluminum tin	180	100
Babbitt, lead-based white metal	24	14
Babbitt, tin-based white metal	56	32
Brasses <sup>a</sup>	120	69
Bronze, aluminum <sup>a</sup>	50	29
Bronze, leaded	47	27
Bronze, phosphor (cast) <sup>d</sup>	50	29
Bronze, porous	30	17
Copper <sup>e</sup>	170	98
Copper lead	30	17
Iron, gray cast	50	29
Iron, spheroidal graphite	30	17
Iron, porous	28	16
Iron, wrought	70	40
Magnesium alloys	110	64
Steel, low alloy <sup>c</sup>	35	20
Steel, medium alloy	30	17
Steel, stainless <sup>f</sup>	15	8.7
Zinc alloys	110	64
<b>Polymers:</b>		
Acetal (polyformaldehyde)	0.24	0.14
Nylons (polyamides)	0.25	0.14
Polyethylene, high density	0.5	0.29
Rubber, natural	1.6	0.92
<b>Ceramics:</b>		
Alumina ( $\text{Al}_2\text{O}_3$ ) <sup>g</sup>	25	14
Graphite, high strength	125	72
Silicon carbide ( $\text{SiC}$ )	15	8.6

<sup>a</sup>At 100°C.<sup>b</sup>At 100°C (~150 W/m·K at 25°C.)<sup>c</sup>20 to 100°C.<sup>d</sup>Bar stock typically 69 W/m K.<sup>e</sup>Typically 22 W/m·K at 200°C.<sup>f</sup>Typically 12 W/m·K at 400°C.

Table 5.13: Specific heat capacity for various metals, polymers and ceramics at room temperature ( $20^\circ$ ;  $68^\circ\text{F}$ ) [From ESDU (1984).]

Material	Specific heat capacity, $C_p$	
	kJ/kg K	Btu/lb $^{\circ}\text{F}$
<b>Metals:</b>		
Aluminum and its alloys	0.9	0.22
Aluminum tin	0.96	0.23
Babbitt, lead-based white metal	0.15	0.036
Babbitt, tin-based white metal	0.21	0.05
Brasses	0.39	0.093
Bronzes,	0.38	0.091
Copper <sup>a</sup>	0.38	0.091
Copper lead	0.32	0.076
Iron, cast	0.42	0.10
Iron, porous	0.46	0.11
Iron, wrought	0.46	0.11
Magnesium alloys	1.0	0.24
Steels <sup>b</sup>	0.45	0.11
Zinc alloys	0.4	0.096
<b>Polymers:</b>		
Thermoplastics	1.4	0.33
Rubber, natural	2.0	0.48
<b>Ceramics:</b>		
Graphite	0.8	0.2
Cemented carbides	0.7	0.17

<sup>a</sup>Aluminum bronzes up to 0.48 kJ/kg K (0.12 Btu/lb  $^{\circ}\text{F}$ ).

<sup>b</sup>Rising to 0.55 kJ/kg K (0.13 Btu/lb  $^{\circ}\text{F}$ ) at  $200^\circ\text{C}$  ( $392^\circ\text{F}$ ).

temperature is proportional to the mass of the object, to the amount that its temperature changes, and to a characteristic number called the “specific heat capacity” of the material the body is made from.

$$\therefore \hat{Q} = C_p m_a (\Delta t_m) \quad (5.3)$$

where

$\hat{Q}$  = quantity of heat, J

$C_p$  = specific heat of material, J/(kg·K)

$m_a$  = mass of body, kg

$\Delta t_m$  = temperature change, K

Figure 5.8 illustrates the specific heat capacity of various metals, polymers, and ceramics at room temperature ( $20^\circ\text{C}$ ). Polymers have considerably higher specific heat than metals or ceramics. Table 5.13 quantifies the information presented in Fig. 5.8.

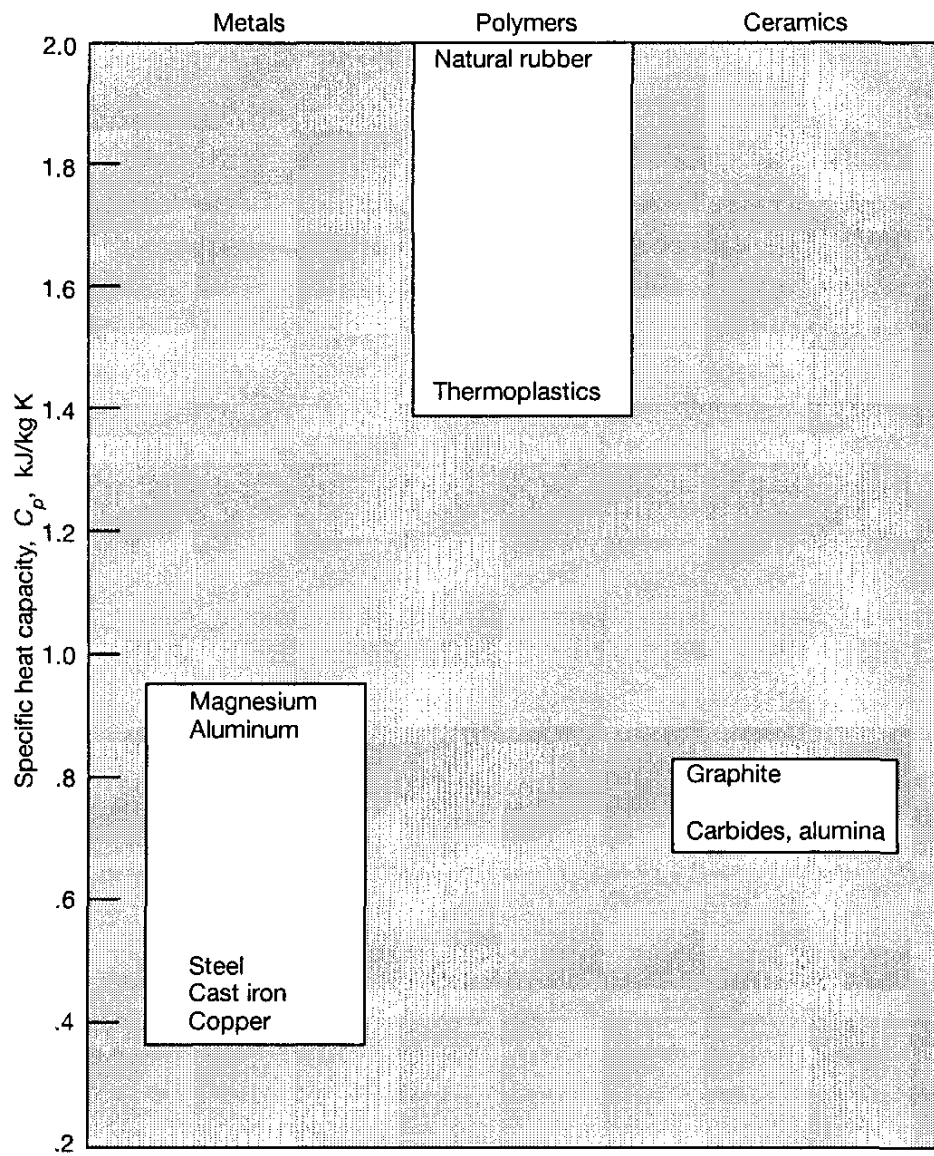


Figure 5.8: Illustration of specific heat capacity for various metals, polymers, and ceramics at room temperature (20°C; 68°F). [From ESDU (1984).]

## 5.8 Closure

In this chapter the general characteristics of bearing materials have been established and discussed. Some desirable characteristics covered in this chapter are compatibility with rubbing counterface materials; embeddability for dirt particles and wear debris; conformability to enable the bearing to accommodate misalignment, geometrical errors, and deflections in structure, strength, corrosion resistance, and fatigue resistance. The various types of bearing material that are now available have been evaluated in terms of these characteristics. These materials consist of metallics (babbitts, bronzes, aluminum alloys, porous metals, and metal overlays such as silver and indium) or nonmetallics (plastics, rubber, carbon-graphite, ceramics, cemented carbides, and metal ox-

ides). Bearing materials applicable to conformal surfaces, where hydrodynamic lubrication occurs, as well as to nonconformal surfaces, where elastohydrodynamic lubrication occurs, were discussed. The stresses acting on conformal and nonconformal surfaces differ considerably, and therefore the solid surface requirements are quite different. The last section listed representative values of a number of solid material properties required in evaluating fluid film bearings. These properties included density, modulus of elasticity, Poisson's ratio, linear thermal expansion coefficient, thermal conductivity, and specific heat capacity. Values of these parameters were given for a variety of metals, polymers, and ceramics at room temperature. The material developed in this chapter should prove useful in subsequent chapters.

## 5.9 Problem

- 5.1 Describe and compare the main types of materials that are available for use as a plain journal bearing when an oil or a grease is undesirable as a lubricant.

## References

- Anderson, N. E., and Zaretsky, E. V. (1975): Short-Term Hot-Hardness Characteristics of Five Case-Hardened Steels. *NASA Tech. Note D-8031*.
- Bamberger, E. N. (1970): Effect of Materials-Metallurgy Viewpoint. *Interdisciplinary Approach to the Lubrication of Concentrated Contacts*, P. M. Ku (ed.), NASA Spec. Publ. 237, pp. 409-437.
- Bamberger, E. N., Zaretsky, E. V., and Signer, H. (1976): Endurance and Failure Characteristics of Main-Shaft Jet Engine Bearing at  $3 \times 10^6$  DN. *J. Lubr. Technol.*, vol. 98, no. 4, pp. 580-585.
- Bamberger, E. N., et al. (1980): Materials for Rolling Element Bearings. *Bearing Design-Historical Aspects, Present Technology and Future Problems*, W. J. Anderson (ed.), ASME, New York, pp. 1-46.
- Booser, E. R. (1966): Bearing Materials and Properties. *Mach. Des.*, vol. 38, Mar., pp. 22-28.
- Clauser, H. R. (1948): Bearing Metals. (*Materials and Methods Manual 40*), *Mater. Methods*, vol. 28, no. 2, pp. 75-86.
- Cundill, R. T., and Giordano, F. (1982): Lightweight Materials for Rolling Elements in Aircraft Bearings. *Problems in Bearings and Lubrication, AGARD/Conf. Proc. 323*, pp. 6-1 to 6-11.
- Dowson, D. (1998): *History of Tribology*, 2nd. ed., Professional Engineering Publishing, London and Bury St. Edmunds.
- Engineering Sciences Data Unit (ESDU) (1984): *Properties of Common Engineering Materials*. Item 84041, London.
- Kaufman, H. N. (1980): Bearing Materials. *Tribology -Friction, Lubrication, and Wear*, A. Z. Szeri (ed.). Hemisphere Publishing Corp., Washington, D.

- C., pp. 477-505.
- O'Conner, J. J., Boyd, J.. and Avellone, E. A. (eds.) (1968): *Standard Handbook of Lubrication Engineering*. McGraw-Hill, New York.
- Sibley, L. B. (1982): *Silicon Nitride Bearing Elements for High-Speed High-Temperature Applications*. AGARD/Conf. Proc. 323, pp. 5-1 to 5-15.
- Zaretsky, E. V., and Anderson, W. J. (1966): Material Properties and Processing Variables and Their Effect on Rolling-Element Fatigue. *NASA Tech. Memo. X-52227*.

# Chapter 6

## Viscous Flow

### Symbols

$A$	area, $\text{m}^2$	$X_a, Y_a, Z_a$	directions of spherical polar coordinates, $\text{m}/\text{s}$
$a$	radius of pipe, $\text{m}$	$x, y, z$	Cartesian coordinates, $\text{m}$
$b$	width of journal, $\text{m}$	$\eta$	absolute viscosity, $\text{N}\cdot\text{s}/\text{m}^2$
$C_f$	correction for tube diameter	$\eta_0$	absolute viscosity at $p=0$ and constant temperature, $\text{N}\cdot\text{s}/\text{m}^2$
$c$	radial clearance, $\text{m}$	$\theta$	coordinate in cylindrical polar coordinates
$f$	friction force, $\text{N}$	$\lambda_a$	second viscosity coefficient, $\text{Ns}/\text{m}^2$
$g$	acceleration due to gravity ( $9.8 \text{ m/s}^2$ )	$\xi_a$	dilatation, $\text{s}^{-1}$
$h$	film thickness, $\text{m}$	$\rho$	density of lubricant, $\text{kg}/\text{m}^3$
$h_t$	height of liquid level, $\text{m}$	$\rho_s$	density of sphere, $\text{kg}/\text{m}^3$
$\bar{h}_t$	height that sphere falls, $\text{m}$	$\rho_f$	density of fluid, $\text{kg}/\text{m}^3$
$\ell_a$	length of annulus, $\text{m}$	$\rho_0$	density at $p=0$ , $\text{N}\cdot\text{s}^2/\text{m}^4$
$N_a$	rotational speed, rev/s	$\rho^*$	mean density, $\text{kg}/\text{m}^3$
$p$	pressure, $\text{N}/\text{m}^2$	$\sigma$	normal stress, $\text{N}/\text{m}^2$
$p_i$	inlet pressure, $\text{N}/\text{m}^2$	$\tau$	shear stress, $\text{N}/\text{m}^2$
$q$	volumetric flow rate, $\text{m}^3/\text{s}$	$\omega$	angular speed, $\text{rad}/\text{s}$
$r$	radius, $\text{m}$		
$r_i$	inner radius, $\text{m}$		
$r_o$	outer radius, $\text{m}$		
$t$	time, $\text{s}$		
$t_q$	torque, $\text{N}\cdot\text{m}$		
$u$	velocity in $x$ direction, $\text{m}/\text{s}$		
$u_a$	surface $a$ velocity, $\text{m}/\text{s}$		
$u_b$	surface $b$ velocity, $\text{m}/\text{s}$		
$v$	velocity in $y$ direction, $\text{m}/\text{s}$		
$w$	velocity in $z$ direction, $\text{m}/\text{s}$		
$v_r, v_z, v_\theta$	velocity in $r$ , $z$ , and $\theta$		
	directions of cylindrical polar coordinates, $\text{m}/\text{s}$		
$v_r, v_\theta, v_\phi$	velocity in $r$ , $\theta$ , and $\phi$		

### Subscripts

$a$	solid $a$
$b$	solid $b$
$x, y, z$	Cartesian coordinates
$r, z, \theta$	cylindrical coordinates
$r, \theta, \phi$	spherical coordinates

## 6.1 Introduction

This chapter focuses on aspects of fluid mechanics that are important in understanding fluid film lubrication. Four aspects of viscous flow are important:

1. A fluid's viscous resistance increases with the deformation rate. Making a fluid flow fast requires a greater force than making it flow slowly.
2. Molecules do not go back to their original positions when the applied force is removed. The flow involves a nonreversible change, and the work done in producing viscous flow appears as heat in the liquid.
3. A liquid becomes less viscous as its temperature is raised. The greater thermal energy enables the molecules to escape from their neighbors (less external force is required to hurry them on).
4. The viscosity of a liquid in nonconformal conjunctions generally increases as the pressure increases. The viscosity may increase by several orders of magnitude. This is a fortunate state of affairs, for it implies that the harder one tries to squeeze out a lubricant, the higher will be its viscosity and the greater its resistance to extrusion.

## 6.2 Petrov's Equation

Here Newton's postulate (Sec. 4.10) is applied to a full journal running concentrically with the bearing, as shown in Fig. 6.1. It is shown later that the journal will run concentrically with the bearing only when one of the following conditions prevails: (1) the radial load acting on the bearing is zero, (2) the viscosity of the lubricant is infinite, or (3) the speed of the journal is infinite. None of these conditions are practically possible. However, if the load is light enough, if the journal has a sufficiently high speed, and if the viscosity is sufficiently high, the eccentricity of the journal relative to the bearing may be so small that the oil film around the journal can be considered practically to be of uniform thickness.

The oil film in a journal bearing is always thin relative to the radius of the bearing. Therefore, the curvature of the bearing surface may be ignored, and the film may be considered as an unwrapped body having a thickness equal to the radial clearance, a length equal to  $2\pi r$ , and  $b$  equal to the width of the bearing. Assume that the viscosity throughout the oil film is constant. In Fig. 6.2 the bottom surface is stationary and the top surface is moving with constant velocity  $u_a$ . Petrov (1883) assumed no slip at the interface between the lubricant and the solids.

Making use of Newton's postulate as expressed in Eq. (4.2) gives the friction force in a concentric journal bearing as

$$f = \eta_0 A \frac{u_a}{c} = \eta_0 2\pi r b \frac{2\pi r N_a}{c} = \frac{4\pi^2 \eta_0 r^2 b N_a}{c} \quad (6.1)$$

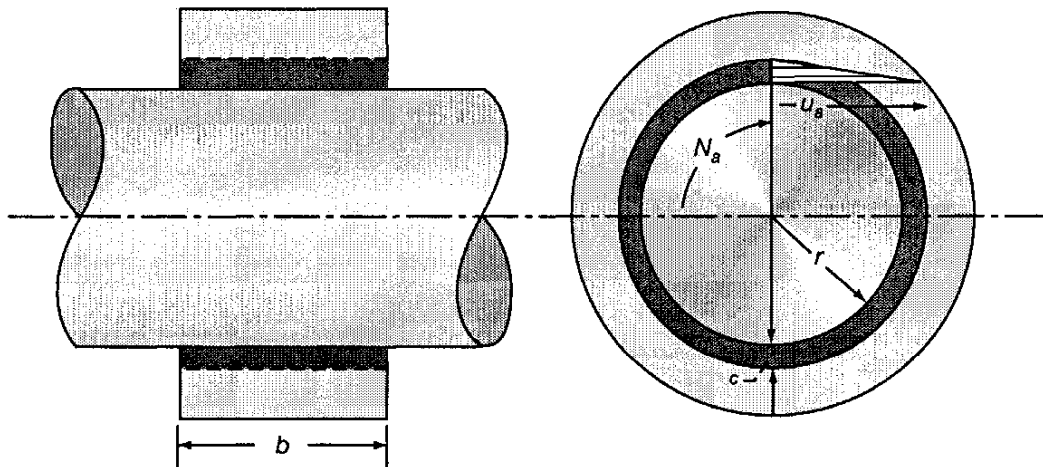


Figure 6.1: Concentric journal bearing.

where  $N_a$  is in revolutions per second and  $\eta_0$  is the viscosity at  $p = 0$  and at a constant temperature. The coefficient of friction for a concentric journal bearing can be written as

$$\mu = \frac{f}{w_z} = \frac{4\pi^2 \eta_0 r^2 b N_a}{c w_z} \quad (6.2)$$

where  $w_z$  is the normal applied load. The friction torque for a concentric journal bearing can be written as

$$t_q = fr = \frac{4\pi^2 \eta_0 r^3 b N_a}{c} = \frac{2\pi \eta_0 r^3 b \omega}{c} \quad (6.3)$$

where  $\omega = 2\pi N_a$ , the angular velocity in radians per second. Equation (6.3) is generally called “Petrov’s equation” (after N. Petrov, who suggested a similar equation for torque in his work published in 1883).

The power loss is just the velocity multiplied by the frictional force. The power loss for a concentric (lightly loaded) journal bearing can be expressed in

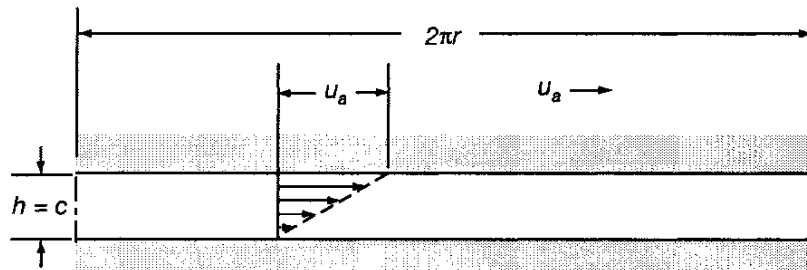


Figure 6.2: Developed journal and bearing surfaces for a concentric journal bearing.

horsepower as

$$H_p = \frac{8\pi^3}{(12)(550)} \frac{\eta_0 r^3 b N_a^2}{c} = (0.03758) \frac{\eta_0 r^3 b N_a^2}{c} \quad (6.4)$$

where

$\eta_0$  = viscosity at  $p = 0$  and at a constant temperature, lbf·s/in<sup>2</sup>

$r$  = radius of journal, in.

$b$  = width of journal, in.

$N_a$  = speed, r/s

$c$  = radial clearance, in.

Note that Eq. (6.4) is valid for only these units.

## 6.3 Navier-Stokes Equations

Lubricants in hydrodynamic lubrication analyses and in many elastohydrodynamic lubrication analyses are assumed to behave as Newtonian fluids. As given in Chapter 4 the shear rate is linearly related to the shear stress. Besides assuming that the fluid behavior is Newtonian, assume also that laminar flow exists. Navier (1823) derived the equations of fluid motion for these conditions from molecular considerations and by introducing Newton's postulate for a viscous fluid. Stokes (1845) also derived the governing equations of motion for a viscous fluid in a slightly different form, and the basic equations are thus known as "Navier-Stokes equations of motion."

The Navier-Stokes equations can be derived by considering the dynamic equilibrium of a fluid element. It is necessary to consider surface forces, body forces, and inertia forces.

### 6.3.1 Surface Forces

Figure 6.3 shows the stresses on the surface of a fluid element in a viscous fluid. Across each of the three mutually perpendicular surfaces there are three stresses, yielding a total of nine stress components. Of the three stresses acting on a given surface the normal stress is denoted by  $\sigma$  and the shear stress by  $\tau$ . The stresses on the surface perpendicular to the  $z$  axis have been omitted to avoid overcrowding, the first subscript on the shear stresses refers to the coordinate direction perpendicular to the plane in which the stress acts, and the second designates the coordinate direction in which the stress acts. The following five relationships should be noted in relation to the surface stresses:

1. For equilibrium of the moments of the fluid element the stresses must be symmetric; that is, the subscripts on the shear stresses can be reversed in order.

$$\tau_{xy} = \tau_{yx} \quad \tau_{xz} = \tau_{zx} \quad \tau_{yz} = \tau_{zy} \quad (6.5)$$

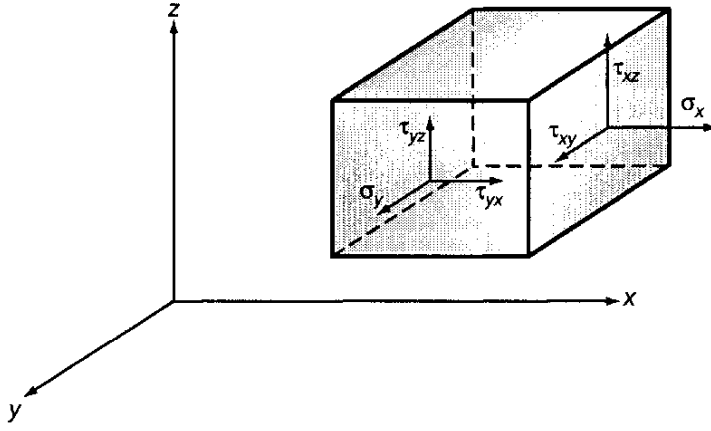


Figure 6.3: Stresses on two surfaces of a fluid element.

2. The hydrostatic pressure  $p$  in the fluid is considered to be the average of the three normal stress components

$$\sigma_x + \sigma_y + \sigma_z = -3p \quad (6.6)$$

The minus sign is used because hydrostatic pressures are compressive, whereas positive stresses are tensile.

3. The magnitude of the shear stresses depends on the rate at which the fluid is being distorted. For most fluids the dependence is of the form

$$\tau_{ij} = \eta \left( \frac{\partial u_i}{\partial x_j} + \frac{\partial u_j}{\partial x_i} \right) \quad (6.7)$$

where

$\eta$  = absolute viscosity, N·s/m<sup>2</sup>

$u_i$  = components of velocity vector, m/s ( $u_x = u, u_y = v, u_z = w$ )

$x_i$  = components of coordinate vector, m ( $x_x = x, x_y = y, x_z = z$ )

Note the similarity of Eq. (6.7) to Newton's postulate [Eq. (4.1)]. The terms in parentheses in Eq. (6.7) are a measure of the distortion of the fluid element.

4. The magnitude of the normal stresses can be written as

$$\sigma_i = -p + \lambda_a \xi_a + 2\eta \frac{\partial u_i}{\partial x_i} \quad (6.8)$$

where

$$\xi_a = \frac{\partial u}{\partial x} + \frac{\partial v}{\partial y} + \frac{\partial w}{\partial z} \quad (6.9)$$

and  $\lambda_a$  is a second viscosity coefficient. The divergence of the velocity vector, the dilatation  $\xi_a$ , measures the rate at which fluid is flowing out from each point; that is, it measures the expansion of the fluid.

5. From Eq. (6.8)

$$\begin{aligned}\sigma_x &= -p + \lambda_a \xi_a + 2\eta \frac{\partial u}{\partial x} \\ \sigma_y &= -p + \lambda_a \xi_a + 2\eta \frac{\partial v}{\partial y} \\ \sigma_z &= -p + \lambda_a \xi_a + 2\eta \frac{\partial w}{\partial z}\end{aligned}$$

Substituting these expressions into Eq. (6.6) gives

$$-3p + 3\lambda_a \xi_a + 2\eta \left( \frac{\partial u}{\partial x} + \frac{\partial v}{\partial y} + \frac{\partial w}{\partial z} \right) = -3p$$

or

$$\begin{aligned}3\lambda_a \xi_a + 2\eta \xi_a &= 0 \\ \lambda_a &= -2\eta/3\end{aligned}\tag{6.10}$$

Therefore, the second viscosity coefficient can simply be expressed in terms of the absolute viscosity.

The conclusions about the surface stresses can be expressed as

$$\tau_{ij} = \tau_{ji}\tag{6.11}$$

$$\tau_{ij} = \eta \left( \frac{\partial u_i}{\partial x_j} + \frac{\partial u_j}{\partial x_i} \right)\tag{6.12}$$

$$\sigma_i = -p + \lambda_a \xi_a + 2\eta \frac{\partial u_i}{\partial x_i}\tag{6.13}$$

The normal and shear stresses tend to move the element in the  $x$ ,  $y$ , and  $z$  directions. The surface forces resulting from these stresses can be expressed as

$$\frac{\partial \sigma_i}{\partial x_i} dx dy dz\tag{6.14a}$$

and

$$\frac{\partial \tau_{ij}}{\partial x_j} dx dy dz\tag{6.14b}$$

### 6.3.2 Body Forces

The forces needed to accelerate a fluid element may be supplied in part by an external force field, perhaps gravity, associated with the whole body of the element. If the components of the external force field per unit mass are  $X_a$ ,  $Y_a$ , and  $Z_a$ , these forces acting on an element are

$$X_a \rho dx dy dz \quad Y_a \rho dx dy dz \quad Z_a \rho dx dy dz\tag{6.15}$$

Note that the units of  $X_a$ ,  $Y_a$ , and  $Z_a$  are meters per second squared since  $\rho$ , the density, has units of Newton-seconds squared per meter to the fourth power ( $N \cdot s^2 / m^4$ ).

### 6.3.3 Inertia Forces

The three components of fluid acceleration are the three total derivatives  $Du/Dt$ ,  $Dv/Dt$ , and  $Dw/Dt$ . The significance of the total derivative can be seen from the following. Consider only the  $x$  component of velocity  $u$ .

$$u = f(x, y, z, t) \quad (6.16)$$

The change in  $u$  that occurs in time  $dt$  is

$$Du = \frac{\partial u}{\partial t} dt + \frac{\partial u}{\partial x} dx + \frac{\partial u}{\partial y} dy + \frac{\partial u}{\partial z} dz \quad (6.17)$$

in the limit as  $dt \rightarrow 0$ ,  $dx/dt = u$ ,  $dy/dt = v$ , and  $dz/dt = w$ . Therefore, if Eq. (6.17) is divided throughout by  $dt$  while making use of the preceding, the total derivative for the  $u$  component can be written as

$$\frac{Du}{Dt} = \frac{\partial u}{\partial t} + u \frac{\partial u}{\partial x} + v \frac{\partial u}{\partial y} + w \frac{\partial u}{\partial z} \quad (6.18)$$

Similarly, for the  $v$  and  $w$  components of velocity,

$$\frac{Dv}{Dt} = \frac{\partial v}{\partial t} + u \frac{\partial v}{\partial x} + v \frac{\partial v}{\partial y} + w \frac{\partial v}{\partial z} \quad (6.19)$$

$$\frac{Dw}{Dt} = \frac{\partial w}{\partial t} + u \frac{\partial w}{\partial x} + v \frac{\partial w}{\partial y} + w \frac{\partial w}{\partial z} \quad (6.20)$$

The total time derivative measures the change in velocity of one fluid element as it moves about in space. The term  $\partial/\partial t$  is known as the “local derivative,” since it gives the variation of velocity with time at a fixed point. The last three terms are grouped together under the heading “convective differential.”

The resultant forces required to accelerate the elements are

$$\rho \frac{Du}{Dt} dx dy dz \quad \rho \frac{Dv}{Dt} dx dy dz \quad \rho \frac{Dw}{Dt} dx dy dz \quad (6.21)$$

### 6.3.4 Equilibrium

The surface, body, and inertia forces acting on a fluid element having been defined, the requirement for dynamic equilibrium can now be stated mathematically. When the common factor  $dxdydz$  is eliminated from each term and the resultant inertia force is set equal to the sum of the body and surface forces,

$$\rho \frac{Du}{Dt} = \rho X_a + \frac{\partial \sigma_x}{\partial x} + \frac{\partial \tau_{xy}}{\partial y} + \frac{\partial \tau_{xz}}{\partial z} \quad (6.22)$$

$$\rho \frac{Dv}{Dt} = \rho Y_a + \frac{\partial \tau_{yx}}{\partial x} + \frac{\partial \sigma_y}{\partial y} + \frac{\partial \tau_{yz}}{\partial z} \quad (6.23)$$

$$\rho \frac{Dw}{Dt} = \rho Z_a + \frac{\partial \tau_{zx}}{\partial x} + \frac{\partial \tau_{zy}}{\partial y} + \frac{\partial \sigma_z}{\partial z} \quad (6.24)$$

Making use of Eqs. (6.11) to (6.13), the Navier-Stokes equations in Cartesian coordinates are

$$\begin{aligned} \rho \frac{Du}{Dt} &= \rho X_a - \frac{\partial p}{\partial x} - \frac{2}{3} \frac{\partial}{\partial x} (\eta \xi_a) + 2 \frac{\partial}{\partial x} \left( \eta \frac{\partial u}{\partial x} \right) \\ &\quad + \frac{\partial}{\partial y} \left[ \eta \left( \frac{\partial u}{\partial y} + \frac{\partial v}{\partial x} \right) \right] + \frac{\partial}{\partial z} \left[ \eta \left( \frac{\partial u}{\partial z} + \frac{\partial w}{\partial x} \right) \right] \end{aligned} \quad (6.25)$$

$$\begin{aligned} \rho \frac{Dv}{Dt} &= \rho Y_a - \frac{\partial p}{\partial y} - \frac{2}{3} \frac{\partial}{\partial y} (\eta \xi_a) + 2 \frac{\partial}{\partial y} \left( \eta \frac{\partial v}{\partial y} \right) \\ &\quad + \frac{\partial}{\partial x} \left[ \eta \left( \frac{\partial u}{\partial y} + \frac{\partial v}{\partial x} \right) \right] + \frac{\partial}{\partial z} \left[ \eta \left( \frac{\partial v}{\partial z} + \frac{\partial w}{\partial y} \right) \right] \end{aligned} \quad (6.26)$$

$$\begin{aligned} \rho \frac{Dw}{Dt} &= \rho Z_a - \frac{\partial p}{\partial z} - \frac{2}{3} \frac{\partial}{\partial z} (\eta \xi_a) + 2 \frac{\partial}{\partial z} \left( \eta \frac{\partial w}{\partial z} \right) \\ &\quad + \frac{\partial}{\partial x} \left[ \eta \left( \frac{\partial u}{\partial z} + \frac{\partial w}{\partial x} \right) \right] + \frac{\partial}{\partial y} \left[ \eta \left( \frac{\partial v}{\partial z} + \frac{\partial w}{\partial y} \right) \right] \end{aligned} \quad (6.27)$$

The terms on the left side of these equations represent inertia effects, and those on the right side are the body force, pressure gradient, and viscous terms in that order. Equations (6.25) to (6.27) are the most general form of the Navier-Stokes equations as expressed in Cartesian coordinates for a Newtonian fluid. These equations play a central role in fluid mechanics, and nearly all analytical work involving a viscous fluid is based on them. These equations so far have not been restricted to either constant density or constant viscosity. They are valid for viscous compressible flow with varying viscosity.

Note that if the inertia terms in Eqs. (6.25) to (6.27) are neglected (left side of these equations set equal to zero), this form of the equations is sometimes referred to as the "Stokes equations."

### 6.3.5 Standard Forms

For all the forms of the Navier-Stokes equations to be presented in this section, the viscosity is assumed to be constant ( $\eta = \eta_0$ ).

#### Cartesian Coordinates

If the viscosity is assumed to be constant ( $\eta = \eta_0$ ), the Navier-Stokes equations in Cartesian coordinates can be simplified and rearranged to give

$$\rho \frac{Du}{Dt} = \rho X_a - \frac{\partial p}{\partial x} + \eta_0 \left( \frac{\partial^2 u}{\partial x^2} + \frac{\partial^2 u}{\partial y^2} + \frac{\partial^2 u}{\partial z^2} \right) + \frac{\eta_0}{3} \frac{\partial \xi_a}{\partial x} \quad (6.28)$$

$$\rho \frac{Dv}{Dt} = \rho Y_a - \frac{\partial p}{\partial y} + \eta_0 \left( \frac{\partial^2 v}{\partial x^2} + \frac{\partial^2 v}{\partial y^2} + \frac{\partial^2 v}{\partial z^2} \right) + \frac{\eta_0}{3} \frac{\partial \xi_a}{\partial y} \quad (6.29)$$

$$\rho \frac{Dw}{Dt} = \rho Z_a - \frac{\partial p}{\partial z} + \eta_0 \left( \frac{\partial^2 w}{\partial x^2} + \frac{\partial^2 w}{\partial y^2} + \frac{\partial^2 w}{\partial z^2} \right) + \frac{\eta_0}{3} \frac{\partial \xi_a}{\partial z} \quad (6.30)$$

If, besides the viscosity being constant, the density is also constant ( $\rho = \rho_0$ ), the last term on the right side of these equations is zero. Earlier [Eq. (6.9)]  $\xi_a = \partial u / \partial x + \partial v / \partial y + \partial w / \partial z$  was defined as the dilatation, or the measure of the rate at which the fluid is flowing out from each point, that is, a measure of the fluid expansion. If the fluid density equals the density at  $p = 0$  and at a fixed temperature ( $\rho = \rho_0$ ), then  $\xi_a = 0$ .

### Cylindrical Polar Coordinates

In cylindrical polar coordinates with  $r, \theta, z$  such that  $x = r \cos \theta$ ,  $y = r \sin \theta$ , and  $z = z$ , the Navier-Stokes equations for constant viscosity and constant density can be expressed as

$$\begin{aligned} & \rho_0 \left( \frac{\partial v_r}{\partial t} + v_r \frac{\partial v_r}{\partial r} + \frac{v_\theta}{r} \frac{\partial v_r}{\partial \theta} + v_z \frac{\partial v_r}{\partial z} - \frac{v_\theta^2}{r} \right) \\ &= \rho_0 X_c - \frac{\partial p}{\partial r} + \eta_0 \left( \nabla^2 v_r - \frac{v_r}{r^2} - \frac{2}{r^2} \frac{\partial v_\theta}{\partial \theta} \right) \end{aligned} \quad (6.31)$$

$$\begin{aligned} & \rho_0 \left( \frac{\partial v_\theta}{\partial t} + v_r \frac{\partial v_\theta}{\partial r} + \frac{v_\theta}{r} \frac{\partial v_\theta}{\partial \theta} + v_z \frac{\partial v_\theta}{\partial z} + \frac{v_r v_\theta}{r} \right) \\ &= \rho_0 Y_c - \frac{1}{r} \frac{\partial p}{\partial \theta} + \eta_0 \left( \nabla^2 v_\theta - \frac{v_\theta}{r^2} + \frac{2}{r^2} \frac{\partial v_r}{\partial \theta} \right) \end{aligned} \quad (6.32)$$

$$\rho_0 \left( \frac{\partial v_z}{\partial t} + v_r \frac{\partial v_z}{\partial r} + \frac{v_\theta}{r} \frac{\partial v_z}{\partial \theta} + v_z \frac{\partial v_z}{\partial z} \right) = \rho_0 Z_c - \frac{\partial p}{\partial z} + \eta_0 \nabla^2 v_z \quad (6.33)$$

where

$$\nabla^2 = \frac{\partial^2}{\partial r^2} + \frac{1}{r} \frac{\partial}{\partial r} + \frac{1}{r^2} \frac{\partial^2}{\partial \theta^2} + \frac{\partial^2}{\partial z^2} \quad (6.34)$$

### Spherical Polar Coordinates

The comparable equations to (6.31) to (6.34) for the Navier-Stokes equations expressed in spherical polar coordinates  $r, \theta, \phi$ , where

$$\begin{aligned} x &= r \sin \theta \cos \phi \\ y &= r \sin \theta \sin \phi \\ z &= r \cos \theta \end{aligned} \quad (6.35)$$

are

$$\begin{aligned} \frac{\partial v_r}{\partial t} + v_r \frac{\partial v_r}{\partial r} + \frac{v_\theta}{r} \frac{\partial v_r}{\partial \theta} + \frac{v_\phi}{r \sin \theta} \frac{\partial v_r}{\partial \phi} - \frac{v_\theta^2 + v_\phi^2}{r} &= X_s + \frac{1}{\rho_0} \frac{\partial p}{\partial r} \\ + \frac{\eta_0}{\rho_0} \left( \nabla^2 v_r - \frac{2v_r}{r^2} - \frac{2}{r^2} \frac{\partial v_\theta}{\partial \theta} - \frac{2v_\theta \cot \theta}{r^2} - \frac{2}{r^2 \sin \theta} \frac{\partial v_\phi}{\partial \phi} \right) & \end{aligned} \quad (6.36)$$

$$\begin{aligned} \frac{\partial v_\theta}{\partial t} + v_r \frac{\partial v_\theta}{\partial r} + \frac{v_\theta}{r} \frac{\partial v_\theta}{\partial \theta} + \frac{v_\phi}{r \sin \theta} \frac{\partial v_\theta}{\partial \phi} + \frac{v_r v_\theta}{r} - \frac{v_\phi^2 \cot \theta}{r} &= Y_s \\ - \frac{1}{\rho_0} \frac{1}{r} \frac{\partial p}{\partial \theta} + \frac{\eta_0}{\rho_0} \left( \nabla^2 v_\theta + \frac{2}{r^2} \frac{\partial v_r}{\partial \theta} - \frac{v_\theta}{r^2 \sin^2 \theta} - \frac{2 \cos \theta}{r^2 \sin^2 \theta} \frac{\partial v_\phi}{\partial \phi} \right) & \end{aligned} \quad (6.37)$$

$$\begin{aligned} \frac{\partial v_\phi}{\partial t} + v_r \frac{\partial v_\phi}{\partial r} + \frac{v_\theta}{r} \frac{\partial v_\phi}{\partial \theta} + \frac{v_\phi}{r \sin \theta} \frac{\partial v_\phi}{\partial \phi} + \frac{v_\phi v_r}{r} + \frac{v_\theta v_\phi \cot \theta}{r} & \\ = Z_s - \frac{1}{\rho_0} \frac{1}{r \sin \theta} \frac{\partial p}{\partial \phi} & \\ + \frac{\eta_0}{\rho_0} \left( \nabla^2 v_\phi - \frac{v_\phi}{r^2 \sin^2 \theta} + \frac{2}{r^2 \sin \theta} \frac{\partial v_r}{\partial \phi} + \frac{2 \cos \theta}{r^2 \sin^2 \theta} \frac{\partial v_\theta}{\partial \phi} \right) & \end{aligned} \quad (6.38)$$

where

$$\nabla^2 = \frac{1}{r^2} \frac{\partial}{\partial r} \left( r^2 \frac{\partial}{\partial r} \right) + \frac{1}{r^2 \sin \theta} \frac{\partial}{\partial \theta} \left( \sin \theta \frac{\partial}{\partial \theta} \right) + \frac{1}{r^2 \sin^2 \theta} \frac{\partial^2}{\partial \phi^2} \quad (6.39)$$

### Cartesian Coordinates - Turbulent Flow

Up to this point laminar flow has been assumed. Most of the book will be concerned only with laminar flow. However, it is important to describe the Navier-Stokes equations when confronted with turbulent flow.

For laminar flow the velocity pattern is steady and very predictable, whereas for turbulent flow the velocity pattern changes where eddies and vortices and pressure show random variation with time and position. Because of this the instantaneous value has little practical significance, and it is the mean value that is of interest.

Thus, we may express the pressure and velocities as

$$\begin{aligned} p &= p^* + p' & v &= v^* + v' \\ u &= u^* + u' & w &= w^* + w' \end{aligned} \quad (6.40)$$

where asterisked values are mean and primed values are fluctuations.

Substituting Eq. (6.40) into Eqs. (6.28) to (6.30) and following the procedure given, for example, in Szeri (1980) gives

$$\begin{aligned} \rho^* \frac{\partial u^*}{\partial t} + \rho^* u^* \frac{\partial u^*}{\partial x} + \rho^* v^* \frac{\partial u^*}{\partial y} + \rho^* w^* \frac{\partial u^*}{\partial z} & \\ = \rho^* X_a - \frac{\partial p^*}{\partial x} + \eta_0 \frac{\partial^2 u^*}{\partial z^2} - \frac{\partial}{\partial x} [\rho^* (u' u')^*] & \\ - \frac{\partial}{\partial y} [\rho^* (u' v')^*] - \frac{\partial}{\partial z} [\rho^* (u' w')^*] & \end{aligned} \quad (6.41)$$

$$\begin{aligned}
\rho^* \frac{\partial v^*}{\partial t} + \rho^* u^* \frac{\partial v^*}{\partial x} + \rho^* v^* \frac{\partial v^*}{\partial y} + \rho^* w^* \frac{\partial v^*}{\partial z} \\
= \rho^* Y_a - \frac{\partial p^*}{\partial y} + \eta_0 \frac{\partial^2 v^*}{\partial z^2} - \frac{\partial}{\partial x} [\rho^* (u'v')^*] \\
- \frac{\partial}{\partial y} [\rho^* (v'v')^*] - \frac{\partial}{\partial z} [\rho^* (v'w')^*]
\end{aligned} \tag{6.42}$$

$$\begin{aligned}
\rho^* \frac{\partial w^*}{\partial t} + \rho^* u^* \frac{\partial w^*}{\partial x} + \rho^* v^* \frac{\partial w^*}{\partial y} + \rho^* w^* \frac{\partial w^*}{\partial z} \\
= \rho^* Z_a - \frac{\partial p^*}{\partial z} + \eta_0 \frac{\partial^2 w^*}{\partial z^2} - \frac{\partial}{\partial x} [\rho^* (u'w')^*] \\
- \frac{\partial}{\partial y} [\rho^* (v'w')^*] - \frac{\partial}{\partial z} [\rho^* (w'w')^*]
\end{aligned} \tag{6.43}$$

If we neglect inertia terms and body force terms and retain only dominant turbulent stresses, the above equations become

$$0 = -\frac{\partial p^*}{\partial x} + \eta_0 \frac{\partial^2 u^*}{\partial z^2} - \frac{\partial}{\partial z} [\rho^* (u'w')^*] \tag{6.44}$$

$$0 = -\frac{\partial p^*}{\partial y} + \eta_0 \frac{\partial^2 v^*}{\partial z^2} - \frac{\partial}{\partial z} [\rho^* (v'w')^*] \tag{6.45}$$

$$0 = -\frac{\partial p^*}{\partial z} + \eta_0 \frac{\partial^2 w^*}{\partial z^2} - \frac{\partial}{\partial z} [\rho^* (w'w')^*] \tag{6.46}$$

Equations (6.44) to (6.46) show that in turbulent flow the pressure distribution across the film is no longer hydrostatic, as it was in laminar flow.

## 6.4 Continuity Equation

The Navier-Stokes equations contain three equations and four unknowns:  $u$ ,  $v$ ,  $w$ , and  $p$ . The viscosity and density can be written as functions of pressure and temperature. A fourth equation is supplied by the continuity equation. The principle of mass conservation requires that the net outflow of mass from a volume of fluid must be equal to the decrease of mass within the volume. This is readily calculated with reference to Fig. 6.4. The flow of mass per unit time and area through a surface is a product of the velocity normal to the surface and the density. Thus, the  $x$  component of mass flux per unit area at the center of the volume is  $\rho u$ . This flux, however, changes from point to point as indicated in Fig. 6.4. The net outflow of mass per unit time therefore is

$$\begin{aligned}
& \left[ \rho u + \frac{1}{2} \frac{\partial (\rho u)}{\partial x} dx \right] dz + \left[ \rho w + \frac{1}{2} \frac{\partial (\rho w)}{\partial z} dz \right] dx \\
& - \left[ \rho u - \frac{1}{2} \frac{\partial (\rho u)}{\partial x} dx \right] dz - \left[ \rho w - \frac{1}{2} \frac{\partial (\rho w)}{\partial z} dz \right] dx
\end{aligned}$$

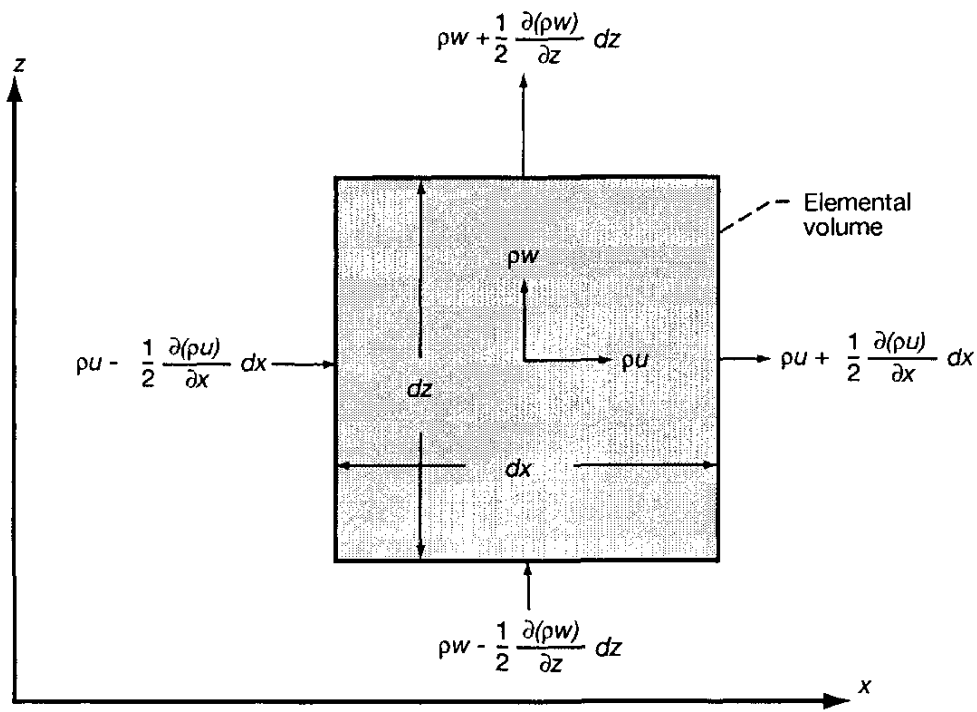


Figure 6.4: Velocities and densities for mass flow balance through a flux volume element in two dimensions.

and this must be equal to the rate of mass decrease within the element,

$$-\frac{\partial \rho}{\partial t} dx dz$$

Upon simplification this becomes

$$\frac{\partial \rho}{\partial t} + \frac{\partial}{\partial x} (\rho u) + \frac{\partial}{\partial z} (\rho w) = 0$$

When the  $y$  direction is included, the continuity equation results.

$$\frac{\partial \rho}{\partial t} + \frac{\partial}{\partial x} (\rho u) + \frac{\partial}{\partial y} (\rho v) + \frac{\partial}{\partial z} (\rho w) = 0 \quad (6.47)$$

If the density is a constant, the continuity equation becomes

$$\frac{\partial u}{\partial x} + \frac{\partial v}{\partial y} + \frac{\partial w}{\partial z} = 0 \quad (6.48)$$

This equation is valid whether or not the velocity is time dependent.

The continuity equation in cylindrical polar coordinates where  $z = z$ ,  $x = r \cos \theta$ , and  $y = r \sin \theta$  can be expressed as

$$\frac{\partial \rho}{\partial t} + \frac{1}{r} \frac{\partial}{\partial r} (\rho r v_r) + \frac{1}{r} \frac{\partial}{\partial \theta} (\rho v_\theta) + \frac{\partial}{\partial z} (\rho v_z) = 0 \quad (6.49)$$

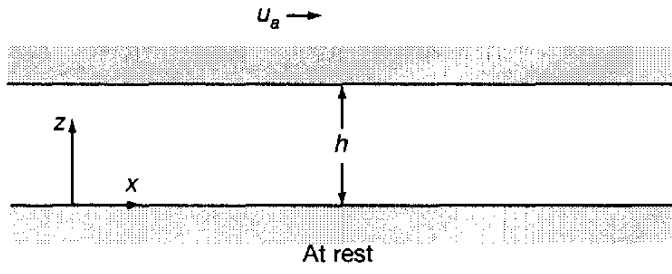


Figure 6.5: Flow between parallel flat plates.

The continuity equation in spherical polar coordinates  $(r, \theta, \phi)$  while making use of Eq. (6.35) is

$$\frac{\partial \rho}{\partial t} + \frac{1}{r^2} \frac{\partial}{\partial r} (\rho r^2 v_r) + \frac{1}{r \sin \theta} \frac{\partial}{\partial \theta} (\rho v_\theta \sin \theta) + \frac{1}{r \sin \theta} \frac{\partial}{\partial \phi} (\rho v_\phi) = 0 \quad (6.50)$$

The continuity equation for turbulent flow is

$$\frac{\partial \rho^*}{\partial t} + \frac{\partial (\rho^* u^*)}{\partial x} + \frac{\partial (\rho^* v^*)}{\partial y} + \frac{\partial (\rho^* w^*)}{\partial z} = 0 \quad (6.51)$$

Now that general expressions for the Navier-Stokes equations and the continuity equation have been developed, the next four sections will illustrate how these equations in simplified form can be used for some specific applications.

## 6.5 Flow Between Parallel Flat Plates

Consider the rate of flow through the clearance between two parallel surfaces shown in Fig. 6.5. The top surface is moving with a velocity  $u_a$  and the bottom surface is at rest. The following assumptions are imposed:

1. The inertia effect is small.
2. Body force terms can be neglected.
3. Viscosity and density can be considered constant.
4.  $dp/dz = dp/dy = 0$ .
5. The film thickness is much smaller than other dimensions.

For these considerations the reduced Navier-Stokes equation is

$$\frac{\partial^2 u}{\partial z^2} = \frac{1}{\eta_0} \frac{dp}{dx}$$

Integrating twice gives

$$u = \frac{1}{\eta_0} \frac{dp}{dx} \frac{z^2}{2} + \tilde{A}z + \tilde{B} \quad (6.52)$$

where  $\tilde{A}$  and  $\tilde{B}$  are integration constants. The no-slip boundary conditions are imposed:

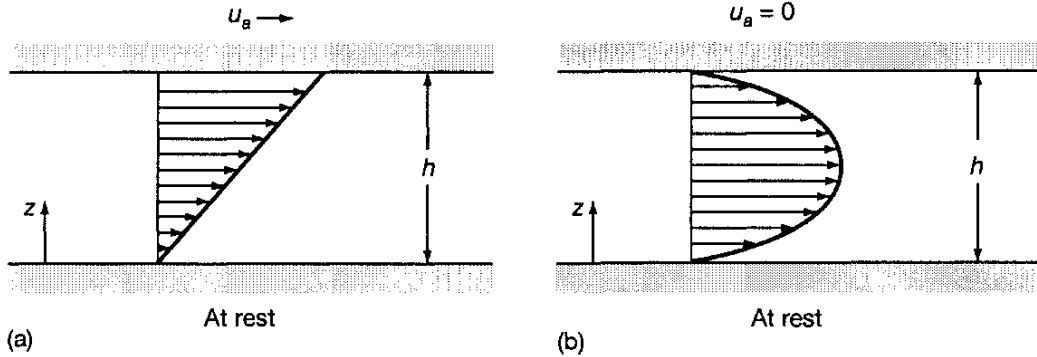


Figure 6.6: (a) Couette and (b) Poiseuille velocity profiles.

1.  $z = 0, u = 0$

2.  $z = h, u = u_a$

From boundary condition 1,  $\tilde{B} = 0$ . Boundary condition 2 gives

$$\begin{aligned}\tilde{A} &= \frac{u_a}{h} - \frac{h}{2\eta_0} \frac{dp}{dx} \\ \therefore u &= \frac{1}{2\eta_0} \frac{dp}{dx} (z^2 - zh) + \frac{u_a z}{h}\end{aligned}\quad (6.53)$$

For  $dp/dx = 0$  the *Couette term* is  $u = u_a z/h$ . For  $u_a = 0$  the *Poiseuille term* is  $u = -(dp/dx)z(h-z)/2\eta_0$ . Figure 6.6 shows the Couette and Poiseuille velocity profiles. The velocity gradient can be written as

$$\frac{du}{dz} = \frac{1}{2\eta_0} \frac{dp}{dx} (2z - h) + \frac{u_a}{h} \quad (6.54)$$

$$\left( \frac{du}{dz} \right)_{z=0} = -\frac{h}{2\eta_0} \frac{dp}{dx} + \frac{u_a}{h} \quad (6.55)$$

$$\left( \frac{du}{dz} \right)_{z=h} = \frac{h}{2\eta_0} \frac{dp}{dx} + \frac{u_a}{h} \quad (6.56)$$

Some other interesting velocity profiles are shown in Fig. 6.7.

The volume flow rate per unit width can be written as

$$q' = \int_0^h u dz \quad (6.57)$$

Substituting Eq. (6.53) into this equation gives

$$q' = \frac{1}{2\eta_0} \frac{dp}{dx} \left( \frac{z^3}{3} - \frac{z^2 h}{2} \right)_{z=0}^{z=h} + \frac{u_a}{h} \left( \frac{z^2}{2} \right)_{z=0}^{z=h} = \underbrace{-\frac{h^3}{12\eta_0} \frac{dp}{dx}}_{\text{Poiseuille}} + \underbrace{\frac{u_a h}{2}}_{\text{Couette}} \quad (6.58)$$

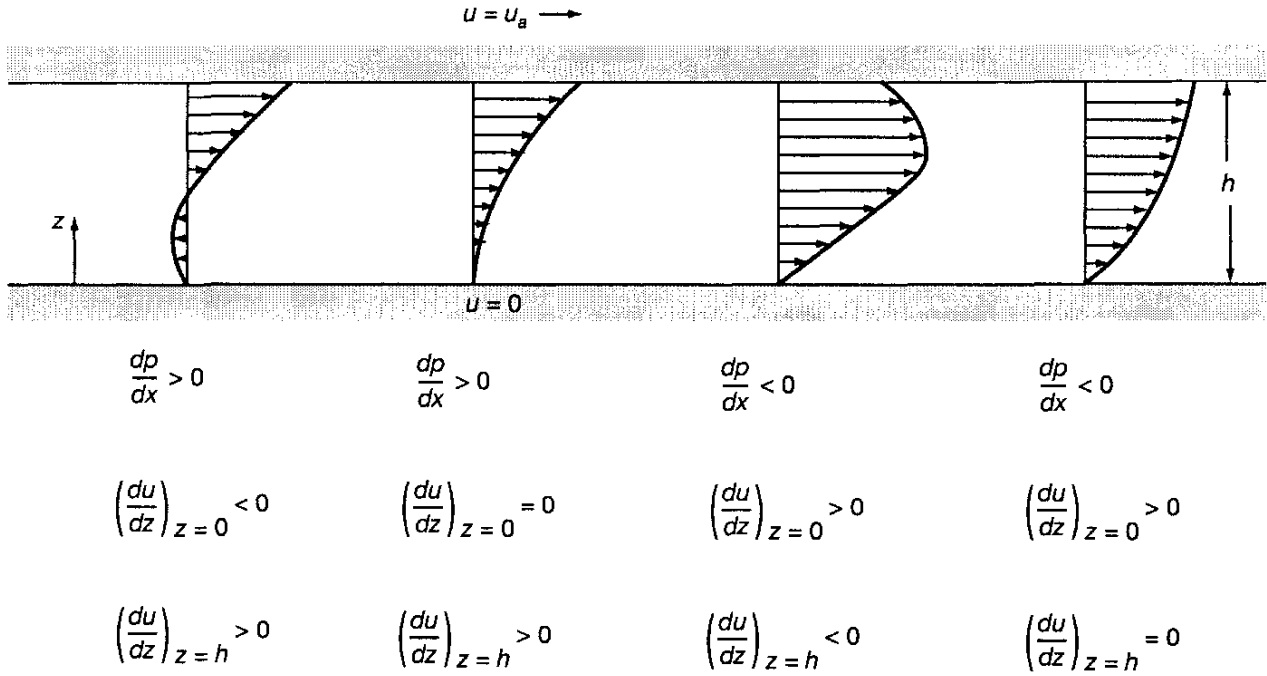


Figure 6.7: Some interesting velocity profiles.

## 6.6 Flow in a Circular Pipe

Consider the flow in a circular pipe as shown in Fig. 6.8. Cylindrical coordinates will be used with their origin at the tube center. The fluid velocity is zero at the pipe walls. The pressure at the left end of the tube is higher than that at the right end and drops gradually along the tube length. This pressure causes the fluid to flow from left to right.

The following assumptions are imposed:

1. Viscosity and density can be considered constant.
2. The inertia effect is small.
3. Body force terms can be neglected.
4.  $dp/dr = dp/d\theta = 0$ .
5.  $v_r = v_\theta = 0$  and  $v_z = f(r)$ .

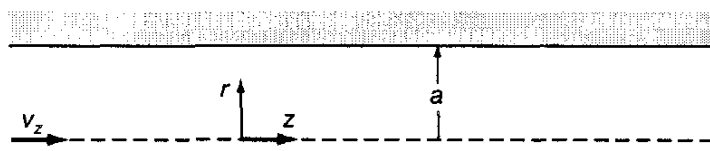


Figure 6.8: Flow in a circular pipe.

With these assumptions the Navier-Stokes equations in cylindrical polar coordinates as expressed in Eqs. (6.31) to (6.33) reduce to the following equations:

$$0 = -\frac{\partial p}{\partial z} + \eta_0 \left( \frac{d^2 v_z}{dr^2} + \frac{1}{r} \frac{dv_z}{dr} \right)$$

or

$$\frac{r}{\eta_0} \frac{dp}{dz} = r \frac{d^2 v_z}{dr^2} + \frac{dv_z}{dr} = \frac{d}{dr} \left( r \frac{dv_z}{dr} \right)$$

Integrating once gives

$$\frac{dv_z}{dr} = \frac{r}{2\eta_0} \frac{dp}{dz} + \frac{\tilde{A}}{r} \quad (6.59)$$

Integrating again gives

$$v_z = \frac{r^2}{4\eta_0} \frac{dp}{dz} + \tilde{A} \ln r + \tilde{B} \quad (6.60)$$

The boundary conditions are

1.  $v_z = 0$  when  $r = a$ .
2. From considerations of symmetry  $dv_z/dr = 0$  when  $r = 0$ .

Making use of boundary condition 2 and Eq. (6.59) results in  $\tilde{A} = 0$ . Making use of boundary condition 1 gives

$$\begin{aligned} \tilde{B} &= -\frac{a^2}{4\eta_0} \frac{dp}{dz} \\ \therefore v_z &= -\frac{1}{4\eta_0} \frac{dp}{dz} (a^2 - r^2) \end{aligned} \quad (6.61)$$

The volume flow rate can be written as

$$q = 2\pi \int_0^a v_z r dr$$

Substituting Eq. (6.61) into this equation gives

$$q = -\frac{\pi}{2\eta_0} \frac{dp}{dz} \int_0^a (a^2 r - r^3) dr$$

or

$$q = -\frac{\pi a^4}{8\eta_0} \frac{dp}{dz} \quad (6.62)$$

Note that a negative pressure gradient is required to get a positive flow in the  $z$  direction.

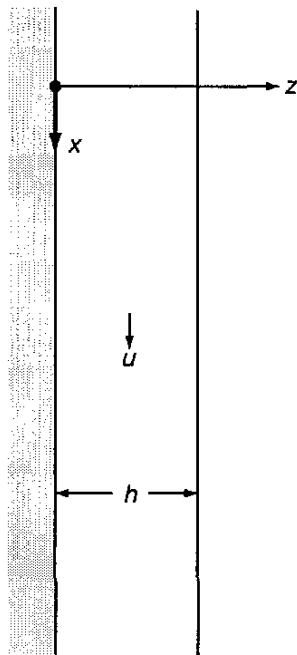


Figure 6.9: Flow down a vertical plane.

## 6.7 Flow Down a Vertical Plane

Consider a vertical plane and a fluid moving down the plane due to gravity. Figure 6.9 describes the physical situation. The fluid has a uniform thickness of  $h$  along the plane. The following assumptions are imposed:

1. Viscosity and density can be considered constant.
2. The inertia effect is small.
3. The body force term in the  $x$  direction contains gravitational acceleration; the body force terms in the  $y, z$  directions are zero ( $Y_a = Z_a = 0$ ).
4. There are no pressure gradients.
5. The fluid velocity varies only in the  $z$  direction.
6. The film thickness is much smaller than the other dimensions.

With these assumptions the Navier-Stokes equations as expressed in Eqs. (6.28) to (6.30) reduce to

$$\frac{d^2u}{dz^2} = -\frac{\rho_0 g}{\eta_0}$$

Integrating gives

$$\frac{du}{dz} = -\frac{\rho_0 g}{\eta_0} z + \tilde{A} \quad (6.63)$$

Integrating again gives

$$u = -\frac{\rho_0 g}{\eta_0} \frac{z^2}{2} + \tilde{A}z + \tilde{B} \quad (6.64)$$

The boundary conditions are

1.  $u=0$  when  $z = 0$ .
2. Assuming negligible air resistance, the shear stress at the free surface must be zero.

$$\therefore \frac{du}{dz} = 0 \quad \text{when } z = h$$

From boundary condition 2 and Eq. (6.63),

$$\begin{aligned} \tilde{A} &= \frac{\rho_0 gh}{\eta_0} \\ \therefore u &= -\frac{\rho_0 g}{\eta_0} \frac{z^2}{2} + \frac{\rho_0 ghz}{\eta_0} + \tilde{B} \end{aligned} \quad (6.65)$$

From boundary condition 1,  $\tilde{B} = 0$ ;

$$\therefore u = \frac{\rho_0 gz}{2\eta_0} (2h - z) \quad (6.66)$$

The volume flow rate per unit width can be expressed as

$$q' = \int_0^h u dz$$

Substituting Eq. (6.66) into this equation gives

$$q' = \frac{\rho_0 gh^3}{3\eta_0} \quad (6.67)$$

The main goal of presenting the three simple viscous flow examples just covered is to show the importance of the various terms in the Navier-Stokes equations. These simple solutions are also used in describing the various types of viscometer in the next section.

## 6.8 Viscometers

The viscosity of fluids can be measured by many methods based on different principles. Only the more typical or most important types of viscometers are discussed here. Also the emphasis is on the principles by which these viscometers operate. The following classifications of viscometers are considered: capillary, rotational, and falling sphere. Each of these is considered separately.

### 6.8.1 Capillary Viscometers

This type of viscometer (shown in Fig. 6.10) is based on measuring the rate at which a fluid flows through a small-diameter tube. Usually, this takes the form of measuring the time taken to discharge a given quantity of fluid. From the

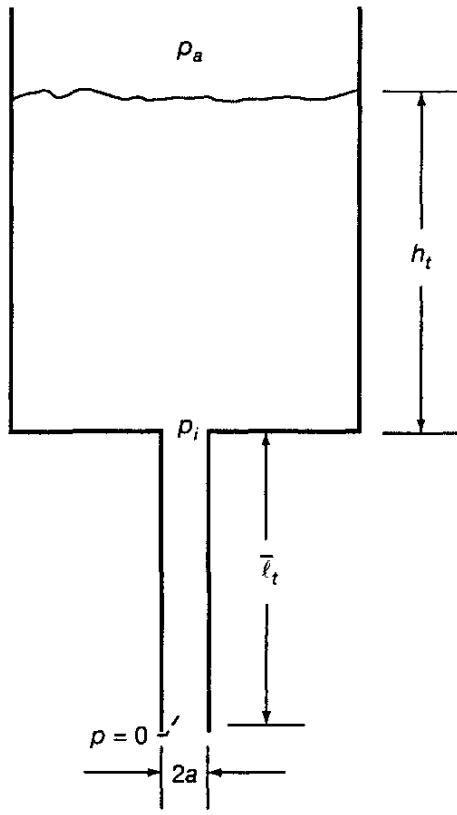


Figure 6.10: Important features of a capillary viscometer.

flow in a circular pipe covered earlier in this chapter [Eq. (6.62)],

$$\frac{dp}{dx} = -\frac{8\eta_0 q}{\pi a^4}$$

If  $p_i$  is the pressure at the inlet of the liquid contents and  $\bar{l}_t$  is the length of the capillary tube,

$$\begin{aligned} -\frac{dp}{dx} &= \frac{p_i}{\bar{l}_t} \\ \therefore p_i &= \frac{8\eta_0 q \bar{l}_t}{\pi a^4} \end{aligned}$$

But the pressure head developed is simply

$$p_i = \rho_0 g h_t$$

where  $h_t$  is the height of the capillary tube and  $\rho_0$  is the density at  $p = 0$  and a constant temperature.

$$\therefore \rho_0 g h_t = \frac{8\eta_0 q \bar{l}_t}{\pi a^4}$$

or

$$h_t = \frac{8\eta_0 q \bar{l}_t}{\pi a^4 \rho_0 g} = A^* q \eta_{k,0} \quad (6.68)$$

where  $\eta_{k,0} = \eta_0 / \rho_0$  is the kinematic viscosity at  $p = 0$  and a fixed temperature, and

$$A^* = \frac{8\bar{l}_t}{\pi g a^4}$$

Recall that  $q$  is the volume flow rate per unit time.

$$q \propto \frac{1}{t}$$

$$\therefore \eta_{k,0} = \frac{h_t}{A^* q} = B^* t \quad (6.69)$$

where  $B^*$  is a constant that is a function of the apparatus.

### 6.8.2 Rotational Viscometers

Two different types of rotational viscometer are considered: the rotational cylindrical viscometer and the cone-and-plate viscometer.

#### Rotational Cylindrical Viscometer

As shown in Fig. 6.11 the rotational cylindrical viscometer consists of two concentric cylinders with a fluid contained between them. The outer cylinder rotates and torque is measured at the inner cylinder. Let

- $r_i$  = inner cylinder radius
- $r_o$  = outer cylinder radius
- $\ell_a$  = length of annulus
- $c$  = radial clearance,  $r_o - r_i$  ( $c \ll r_i$ )
- $\omega$  = angular velocity

From Newton's postulate [Eq. (4.2)],

$$f = \eta_0 A \frac{u}{c}$$

where

$$A = \text{area, } 2\pi r_o \ell_a$$

$$u = \text{velocity, } r_o \omega$$

$$\therefore f = \eta_0 (2\pi r_o \ell_a) \frac{\omega r_o}{c}$$

The torque on the inner cylinder is

$$t_q = f r_i = \frac{2\pi \eta_0 \omega r_o^2 r_i \ell_a}{c}$$

or

$$\eta_0 = \frac{t_q c}{2\pi \omega r_o^2 r_i \ell_a} \quad (6.70)$$

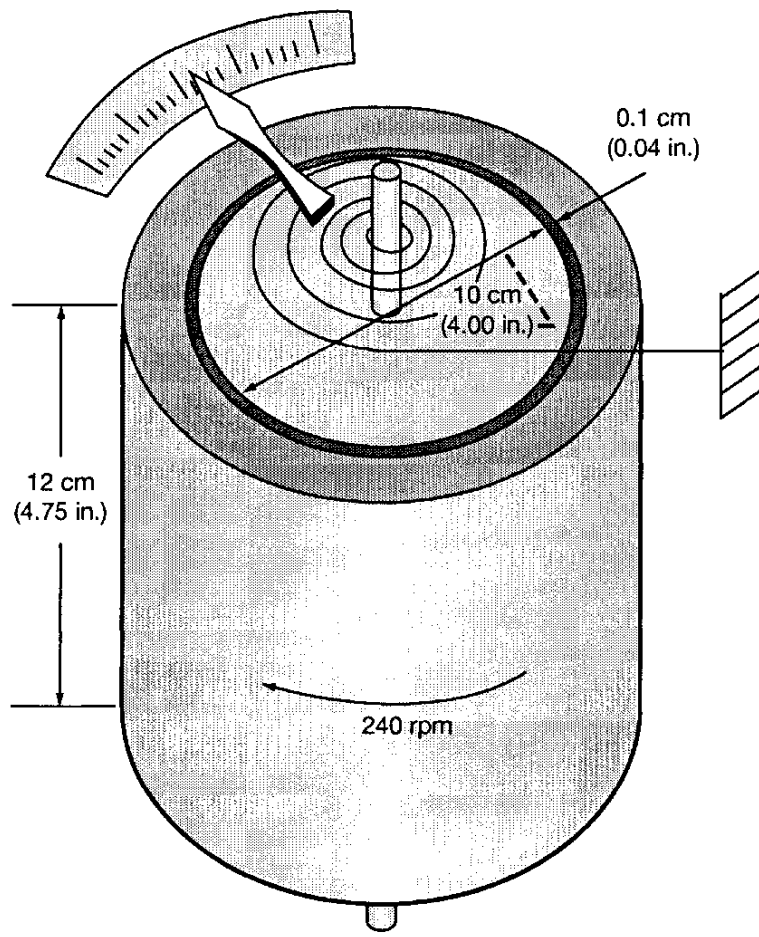


Figure 6.11: Rotational circular viscometer.

### Cone-and-Plane Viscometer

Figure 6.12 shows the essentials of a cone-and-plane viscometer. The angle  $\alpha$  is small. The surface speed of the cone at any radius  $r$  is  $u = \omega r$ . The film thickness is  $h = r \tan \alpha \approx r\alpha$ . From Newton's postulate,

$$f = \eta_0 A \frac{u}{h} = \int_0^R \eta_0 (2\pi r dr) \frac{\omega r}{r\alpha} = \int_0^R \frac{2\pi\eta_0\omega}{\alpha} r dr$$

The torque is

$$\begin{aligned} t_q &= \frac{2\pi\eta_0\omega}{\alpha} \int_0^R r^2 dr = \frac{2\pi\eta_0\omega R^3}{3\alpha} \\ \therefore \eta_0 &= \frac{3t_q\alpha}{2\pi\omega R^3} \end{aligned} \quad (6.71)$$

### 6.8.3 Falling-Sphere Viscometer

The absolute viscosity  $\eta_0$  of a fluid at  $p = 0$  and at a constant temperature can be determined by measuring the time it takes for a ball to fall through a tube (preferably of glass so that the ball can be easily observed). If a sphere is falling through a fluid under a constant force, it will assume a constant velocity.

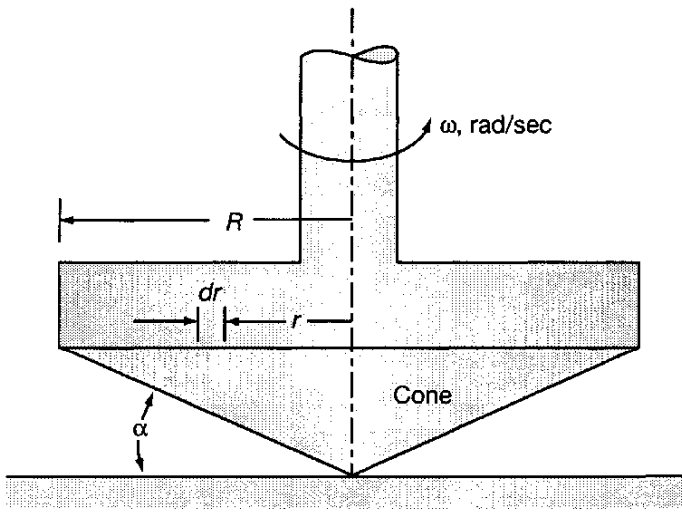


Figure 6.12: Cone-and-plane viscometer.

Stokes' formula can be applied for a sphere moving through an infinite fluid. A sphere falling freely under gravity in a liquid will be attaining a velocity  $u_a$  given by

$$u_a = \frac{2r^2 (\rho_s - \rho_f) g}{\eta_0} \quad (6.72)$$

where

$r$  = radius of sphere, m

$\rho_s$  = density of sphere, kg/m<sup>3</sup>

$\rho_f$  = density of fluid, kg/m<sup>3</sup>

$g$  = gravitational acceleration, m/s<sup>2</sup>

$\eta_0$  = absolute viscosity at  $p = 0$  and a fixed temperature, N·s/m<sup>2</sup>

The Stokes formula given in Eq. (6.72) is for an infinite fluid and not for a fluid in a glass tube as is the case in a falling-sphere viscometer. From Jacobson (1991) the correction to account for the tube diameter and the eccentric position of the sphere within the tube is

$$u_a = B_o r^2 (\rho_s - \rho_f) g \psi^{2.5} / \eta_0 \quad (6.73)$$

where

$$\psi = (R - r)/r$$

$R$  = radius of tube, m

and  $B_o$  is given by

$$B_o = \frac{2\sqrt{2}\epsilon^2}{27 \int_0^\pi \frac{\cos^2 \phi d\phi}{\sqrt{1 + \epsilon \cos \phi}}} + \frac{8\sqrt{2}}{27\pi^2} \int_0^\pi (1 + \epsilon \cos \phi)^{2.5} d\phi \quad (6.74)$$

where

$$\epsilon = \text{eccentricity ratio} = \frac{e}{(R - r)} \quad (6.75)$$

and  $e$  is the eccentricity of the sphere in the tube. It should be noted that when  $\epsilon = 0$  (sphere is concentric with tube),

$$B_o = \frac{8\sqrt{2}}{27\pi} = 0.1334 \quad (6.76)$$

and when  $\epsilon = 1$  (sphere is in contact with tube),

$$B_o = \frac{2^{10}}{3^4(5\pi^2)} = \frac{1024}{405\pi^2} = 0.2562 \quad (6.77)$$

For any other eccentric position, Eq. (6.74) needs to be evaluated.

If the sphere falls at a constant velocity, then

$$u_a = \bar{h}_t/t \quad (6.78)$$

where

$\bar{h}_t$  = height that sphere falls, m

$t$  = time it takes for sphere to fall, s

Using Eqs. (6.73) and (6.78) the absolute viscosity at  $p = 0$  and a fixed temperature can be expressed as

$$\eta_0 = B_o r^2 (\rho_s - \rho_f) g \psi^{2.5} \left( \frac{t}{\bar{h}_t} \right) \quad (6.79)$$

Note that for a falling-sphere viscometer the absolute viscosity is directly proportional to the time it takes for the sphere to travel a fixed distance.

## 6.9 Closure

This chapter focused on viscous fluid flow, which is important in understanding fluid film lubrication. Petrov's equation was derived and gave the friction torque in a concentric journal bearing. Navier-Stokes equations were derived in general form and gave the dynamic equilibrium of a fluid element. It was necessary to consider the surface forces, body forces, and inertia of a fluid element. The continuity equation was also derived by applying the principle of mass conservation to a fluid element. The Navier-Stokes equations and the continuity equations were expressed in Cartesian, cylindrical, and spherical polar coordinates.

Having the general expressions for the Navier-Stokes and continuity equations, the next development in this chapter was to illustrate how these equations can be applied to various physical conditions. Some of the physical conditions considered were flow between parallel flat plates, flow in a circular pipe, flow down a vertical plane, and various types of viscometers. The emphasis in considering these applications was to point out the significance of the various terms in the Navier-Stokes equations. The presence of the Couette and Poiseuille terms in the velocity and flow was emphasized.

## 6.10 Problems

- 6.1 A viscous fluid flows parallel to the axis in the annular space between two coaxial cylinders of radii  $R_1$  and  $R_2$  and infinite length. Show that the flow rate between these coaxial cylinders when both cylinders are at rest and there is an axial pressure gradient is

$$q = -\frac{\pi R_1^4}{8\eta_0} \frac{dp}{dz} \left[ \left( \frac{R_2}{R_1} \right)^4 - 1 - \frac{\left[ (R_2/R_1)^2 - 1 \right]^2}{\ln(R_2/R_1)} \right]$$

- 6.2 Two immiscible liquids of viscosities  $\eta_1$ , and  $\eta_2$  flow together down a vertical plane in distinct layers of thicknesses  $h_1$  and  $h_2$ . The thinner fluid is assumed to be closest to the plane. What are the boundary conditions that determine the velocity distribution? Determine the velocity and flow rate for the two regions. For the special case of  $\eta_2 = 2\eta_1$ ,  $\rho_1 = \rho_2$ , and  $h_1 = h_2$ , show that  $q_2/q_1 = 2$ .
- 6.3 Viscous fluid is contained between two parallel flat plates that are a distance  $h$  apart. One of the plates moves in its own plane with velocity  $3u_a$  and the other in the opposite direction with velocity  $u_a$ . If the flow in the direction of motion of the faster plate is  $u_a h/2$  per unit width, determine the pressure gradient.
- 6.4 A viscous fluid is contained between two parallel flat plates that are a distance  $h$  apart, one of which is fixed while the other moves in its own plane with velocity  $u_a$ . There is a pressure gradient  $dp/dx$  in the direction of motion.

Show that the velocity distribution can be expressed in the form

$$\frac{u}{u_a} = \lambda (\zeta - \zeta^2) + \zeta$$

where

$$\zeta = \frac{z}{h} \quad \lambda = 6 \frac{u_m}{u_a}$$

and  $u_m$  is the mean velocity due to the pressure gradient alone. Find the value of  $\lambda$  corresponding to

- (a) Couette flow
- (b) Poiseuille flow
- (c) A flow for which the volume flow rate is zero
- (d) Zero shear stress on the fixed plate
- (e) Zero shear stress on the moving plate

- 6.5 A laminar flow takes place along a pipe of radius  $a$  that is inclined at an angle of  $\alpha$  to the horizontal. Define the appropriate Navier-Stokes equation. Determine what the velocity ( $v_z$ ) mean velocity ( $\tilde{v}_z$ ), and volume flow rate are in the pipe. Show also that the pressure will remain constant along the pipe when

$$\alpha = \sin^{-1} \frac{8\eta_0 \tilde{v}_z}{\rho_0 g a^2}$$

The viscosity ( $\eta_0$ ) and density ( $\rho_0$ ) are assumed constant throughout the pipe.

- 6.6 Starting with the general Navier-Stokes equations in Cartesian coordinates [Eqs. (6.25), (6.26), and (6.27)] determine appropriate equations if  $\eta = \text{constant} = \eta_0$ . Express in terms of the dilatation.

- 6.7 Starting with the general Navier-Stokes equations [Eqs. (6.25), (6.26) and (6.27)] determine the appropriate equations if  $\eta=\text{constant}=\eta_0$  and  $\rho=\text{constant}=\rho_0$ .

- 6.8 Starting with Eq. (6.52) and with the boundary conditions  $z=0$ ,  $u=u_b$ , and  $z=h$ ,  $u=u_a$ , determine the equation for the velocity. If  $u_b = u_a/2$  show the velocity profile across the film for pressure gradients  $\frac{dp}{dx} > 0$  and  $\frac{dp}{dx} < 0$ .

- 6.9 Starting with Eqs. (6.31) to (6.33) and the boundary conditions given for flow in a circular pipe indicate which boundary condition is used for the various terms in reducing the equations to Eq. (6.59).

- 6.10 Starting with Eqs. (6.28) to (6.30) for flow down a vertical plane using boundary conditions given in Sec. 6.7 indicate which boundary condition is used in reducing the equations to Eq. (6.63).

- 6.11 A shaft of radius  $R_1$  is held concentric within a sleeve of radius  $R_2$ . If the shaft is stationary while the sleeve moves with an axial velocity of  $v_0$ , determine an equation for the volume flow rate. Also, what is the force per unit length required to move the sleeve? The pressure gradient in the direction of motion is assumed to be zero. Constant viscosity and density are assumed. Inertia and body force terms are neglected. Assume  $(R_2 - R_1)/R_1 \approx 1 \times 10^{-3}$ .

- 6.12 A journal bearing has a diameter of 200 mm and a width of 50 mm while rotating at 300 rpm and supporting a radial load of 10 kN. Calculate the oil viscosity from Petrov's law if  $r/c = 100$  and the coefficient of friction is 0.003.

- 6.13 A shaft is rotating at 1000 rpm and is supported by two journal bearings at the two ends of the shaft. The bearings are lubricated with SAE 40

oil at a temperature of 25°C. A 5 kN load is applied 0.5 m from the left bearing where the total shaft length is 2.5 m. The bearing width is 25 mm, the diameter is 50 mm, and the radial clearance is 0.0315 mm. Determine the coefficient of friction and power loss using Petrov's law.

- 6.14 A journal bearing has a diameter of 50 mm, a width of 100 mm, and rotates at 1000 rpm. The bearing is lubricated by SAE 10 oil at a temperature of 110°C and supports 5 kN. Calculate the coefficient of friction and power loss.

## References

- Jacobson, B.O. (1991): *Rheology and Elastohydrodynamic Lubrication*. Elsevier, Amsterdam, Tribology Series 19.
- Navier, C. L. M. H. (1823): Memoire sur les lois du mouvement des fluides. *Mem. Acad. Sci. Inst. Fr.*, vol. 6, pp. 389-416.
- Petrov. N. P. (1883): Friction in Machines and the Effect of the Lubricant. *Inzh. Zh. St. Petersburg*, vol. 1, pp. 71-140; vol. 2, pp. 227-279; vol. 3, pp. 377-463; vol. 4, pp. 535-564.
- Stokes, G. G. (1845): On the Theories of the Internal Friction of Fluids in Motion, and of the Equilibrium and Motion of Elastic Solids. *Trans. Cambridge Philos. Soc.*, vol. 8. pp. 287-341.
- Szeri, A. Z. (ed.) (1980): *Tribology -Friction, Lubrication, and Wear*. Hemisphere Publishing Corp., Washington, D.C.

# Chapter 7

## Reynolds Equation

### Symbols

$\tilde{A}, \tilde{B}$	integration constants	$\mathfrak{R}_z$	modified Reynolds number in $z$ direction, $\rho_0 w_0 h_0 / \eta_0$
$\tilde{C}, \tilde{D}$	integration constants	$\bar{R}$	gas constant
$b_0$	characteristic length in $y$ direction, m	$R_{eh}$	$rwh\rho/\eta$ as defined in Eq. (7.64)
$c$	radial clearance, m	$T$	dimensionless time, $t/t_0$
$g$	acceleration due to gravity (9.8 m/s <sup>2</sup> )	$t$	time, s
$h$	film thickness, m	$t_m$	temperature, °C
$h_m$	film thickness where $dp/dx = 0$ , m	$t_0$	characteristic time, s
$h_0$	characteristic length in $z$ direction, m	$u, v, w$	velocity in $x$ , $y$ , and $z$ directions, m/s
$k$	turbulent flow constant given in Eq. (7.65)	$u_0$	characteristic velocity in $x$ direction, m/s
$k_x, k_y$	turbulent flow constant given in Eqs. (7.62) and (7.63)	$v_0$	characteristic velocity in $y$ direction, m/s
$\ell_0$	characteristic length in $x$ direction, m	$w_0$	characteristic velocity in $z$ direction, m/s
$P$	dimensionless pressure, $h_0^2 p / \eta_0 u_0 \ell_0$	$\bar{u}, \bar{v}, \bar{w}$	dimensionless velocity in $x$ , $y$ , and $z$ -direction
$p$	pressure, N/m <sup>2</sup>	$\tilde{u}$	mean surface velocity in $x$ -direction, $(u_a + u_b)/2$ , m/s
$p_0$	characteristic pressure, N/m <sup>2</sup>	$\tilde{v}$	mean surface velocity in $y$ -direction, $(v_a + v_b)/2$ , m/s
$q$	volumetric flow rate, m <sup>3</sup> /s	$v_r, v_z, v_\theta$	velocities in $r$ , $z$ , and $\theta$ directions of cylindrical polar coordinates, m/s
$q'$	volumetric flow rate per unit width, m <sup>2</sup> /s	$v_r, v_\theta, v_\phi$	velocities in $r$ , $\theta$ , and $\phi$ directions of spherical polar coordinates, m/s
$\mathfrak{R}$	Reynolds number	$X$	dimensionless length parameter, $x/\ell_0$
$\mathfrak{R}_x$	modified Reynolds number in $x$ direction, $\rho_0 u_0 h_0^2 / \eta_0 \ell_0$		
$\mathfrak{R}_y$	modified Reynolds number in $y$ direction, $\rho_0 v_0 h_0^2 / \eta_0 b_0$		

$Y$	dimensionless length parameter, $y/b_0$	$\rho$	coordinates density, $\text{kg}/\text{m}^3$
$Z$	dimensionless length parameter, $z/h_0$	$\bar{\rho}$	dimensionless density, $\rho/\rho_0$
$\eta$	absolute viscosity, $\text{N}\cdot\text{s}/\text{m}^2$	$\rho_m$	density where $dp/dx = 0$ , $\text{kg}/\text{m}^3$
$\eta_0$	characteristic absolute viscosity, $\text{N}\cdot\text{s}/\text{m}^2$	$\sigma_s$	squeeze number, $\rho_0 h_0^2 / \eta_0 t_0$
$\bar{\eta}$	dimensionless absolute viscosity, $\eta/\eta_0$	$\tau$	viscous shear stress, $\text{N}/\text{m}^2$
$\theta$	coordinate in cylindrical polar	$\omega$	angular speed, $\text{rad}/\text{s}$

## 7.1 Introduction

The full Navier-Stokes equations presented in the last chapter, in which inertia, body, pressure, and viscous terms are included, are sufficiently complicated to prohibit analytical solutions to most practical problems. There is, however, a class of flow condition known as “slow viscous motion” in which the pressure and viscous terms predominate. Fluid film lubrication problems are in this class. It will first be demonstrated that indeed the pressure and viscous terms of the Navier-Stokes equations are the most important terms.

## 7.2 Dimensionless Numbers

The following characteristic parameters may be defined:

$b_0$	characteristic length in $y$ direction, m
$h_0$	characteristic length in $z$ direction, m
$\ell_0$	characteristic length in $x$ direction, m
$t_0$	characteristic time, s
$u_0$	characteristic velocity in $x$ direction, $\text{m}/\text{s}$
$v_0$	characteristic velocity in $y$ direction, $\text{m}/\text{s}$
$w_0$	characteristic velocity in $z$ direction, $\text{m}/\text{s}$
$\rho_0$	characteristic density, $\text{kg}/\text{m}^3$
$\eta_0$	characteristic absolute viscosity, $\text{N}\cdot\text{s}/\text{m}^2$

These characteristic parameters are used to define the following dimensionless parameters:

$$\begin{aligned} X &= \frac{x}{\ell_0} & Y &= \frac{y}{b_0} & Z &= \frac{z}{h_0} & T &= \frac{t}{t_0} & \bar{u} &= \frac{u}{u_0} \\ \bar{v} &= \frac{v}{v_0} & \bar{w} &= \frac{w}{w_0} & \bar{\rho} &= \frac{\rho}{\rho_0} & \bar{\eta} &= \frac{\eta}{\eta_0} & P &= \frac{h_0^2 p}{\eta_0 u_0 \ell_0} \end{aligned} \quad (7.1)$$

Substituting Eqs. (7.1) into the first Navier-Stokes equation expressed in Eq. (6.25), while making use of Eqs. (6.9) and (6.18) as well as  $X_a$  in the

body force term being equivalent to gravitational acceleration  $g$  gives

$$\begin{aligned} \frac{\ell_0}{u_0 t_0} \frac{\partial \bar{u}}{\partial T} + \bar{u} \frac{\partial \bar{u}}{\partial X} + \frac{\ell_0}{b_0} \frac{v_0}{u_0} \bar{v} \frac{\partial \bar{u}}{\partial Y} + \frac{\ell_0}{h_0} \frac{w_0}{u_0} \bar{w} \frac{\partial \bar{u}}{\partial Z} &= \frac{\ell_0 g}{u_0^2} - \frac{\eta_0}{\rho_0 u_0 \ell_0} \left( \frac{\ell_0}{h_0} \right)^2 \frac{1}{\bar{\rho}} \frac{\partial P}{\partial X} \\ &\quad - \frac{2}{3} \frac{\eta_0}{\rho_0 u_0 \ell_0} \frac{1}{\bar{\rho}} \frac{\partial}{\partial X} \left[ \bar{\eta} \left( \frac{\partial \bar{u}}{\partial X} + \frac{v_0}{u_0} \frac{\ell_0}{b_0} \frac{\partial \bar{v}}{\partial Y} + \frac{w_0}{u_0} \frac{\ell_0}{h_0} \frac{\partial \bar{w}}{\partial Z} \right) \right] \\ &+ 2 \frac{\eta_0}{\rho_0 u_0 \ell_0} \frac{1}{\bar{\rho}} \frac{\partial}{\partial X} \left( \bar{\eta} \frac{\partial \bar{u}}{\partial X} \right) + \frac{\eta_0}{\rho_0 u_0 \ell_0} \left( \frac{\ell_0}{b_0} \right)^2 \frac{1}{\bar{\rho}} \frac{\partial}{\partial Y} \left[ \bar{\eta} \left( \frac{\partial \bar{u}}{\partial Y} + \frac{v_0}{u_0} \frac{b_0}{\ell_0} \frac{\partial \bar{v}}{\partial X} \right) \right] \\ &\quad + \frac{\eta_0}{\rho_0 u_0 \ell_0} \left( \frac{\ell_0}{h_0} \right)^2 \frac{1}{\bar{\rho}} \frac{\partial}{\partial Z} \left[ \bar{\eta} \left( \frac{\partial \bar{u}}{\partial Z} + \frac{w_0}{u_0} \frac{h_0}{\ell_0} \frac{\partial \bar{w}}{\partial X} \right) \right] \end{aligned} \quad (7.2)$$

The inertia, pressure, viscous, and gravitational effects from Eq. (7.2) are compared in defining several dimensionless numbers.

### 7.2.1 Reynolds Number

The relative importance of inertia to viscous forces in any flow problem can be judged from the value of the Reynolds number  $\mathfrak{R}$ .

$$\mathfrak{R} = \frac{\text{inertia}}{\text{viscous}} = \frac{\rho_0 u_0 \ell_0}{\eta_0} \quad (7.3)$$

Note that the inverse of the Reynolds number occurs throughout Eq. (7.2). The Reynolds number expressed in Eq. (7.3) is the conventional Reynolds number found in fluid mechanics. However, in fluid film lubrication because of the dominance of the viscous term  $\partial^2 \bar{u} / \partial Z^2$  the modified Reynolds number  $\mathfrak{R}_x$  is used. It is defined as

$$\mathfrak{R}_x = \frac{\text{inertia}}{\text{viscous}} = \frac{\rho_0 u_0 h_0^2}{\eta_0 \ell_0} \quad (7.4)$$

Note the occurrence of the modified Reynolds number in Eq. (7.2). The modified Reynolds numbers are also defined in the  $y$  and  $z$  directions as

$$\mathfrak{R}_y = \frac{\rho_0 v_0 h_0^2}{\eta_0 b_0} \quad (7.5)$$

$$\mathfrak{R}_z = \frac{\rho_0 w_0 h_0}{\eta_0} \quad (7.6)$$

The squeeze number is also defined as

$$\sigma_s = \frac{\rho_0 h_0^2}{\eta_0 t_0} \quad (7.7)$$

Recall that  $\mathfrak{R}_x$ ,  $\mathfrak{R}_y$ ,  $\mathfrak{R}_z$ , and  $\sigma_s$  are all dimensionless and of order  $h_0/\ell_0$ . Two examples illustrate that this is true.

---

## Example 7.1: Typical Journal Bearing

**Given** Typical values of parameters used in defining the modified Reynolds number for a journal bearing are

$$\begin{aligned}d &= 0.05 \text{ m} \\ \ell_0 &= \pi d = 0.157 \text{ m} \\ \eta_0 &= 0.5 \text{ N}\cdot\text{s}/\text{m}^2 \\ \rho_0 &= 850 \text{ kg}/\text{m}^3 \\ N_a &= 2000 \text{ r/min} \\ u_0 &= 2000 \text{ r/min } (\pi d/1r)(1 \text{ min}/60 \text{ s}) = 5.24 \text{ m/s} \\ h_0 &= c = d/1000 = 5 \times 10^{-5} \text{ m}\end{aligned}$$

**Find** The value of the Reynolds number for this bearing.

**Solution** From Eq. (7.4),

$$R_x = \frac{\rho_0 u_0 h_0^2}{\eta_0 \ell_0} = \frac{(850)(5.24)(5 \times 10^{-5})^2}{(0.5)(0.157)} = 0.142 \times 10^{-3}$$

---

## Example 7.2: Typical Thrust Bearing Pad

**Given**

$$\begin{aligned}\ell_0 &= 0.03 \text{ m} \\ h_0/\ell_0 &= 1 \times 10^{-3} \\ u_0 &= 20 \text{ m/s} \\ \eta_0 &= 0.5 \text{ N}\cdot\text{s}/\text{m}^2 \\ \rho_0 &= 850 \text{ kg}/\text{m}^3\end{aligned}$$

**Find** The value of the Reynolds number for this bearing.

**Solution** From Eq. (7.4)

$$R_x = \frac{\rho_0 u_0 h_0^2}{\eta_0 \ell_0} = \frac{(850)(20)(0.03)(10^{-6})}{(0.5)} = 1.02 \times 10^{-3}$$

---

In both sample problems the modified Reynolds number is considerably less than unity and of the order  $h_0/\ell_0$ . It is clear that in typical hydrodynamically lubricated bearings the viscous forces are much greater than the inertia forces.

Substituting Eqs. (7.4) to (7.7) into Eq. (7.2) gives the first Navier-Stokes

equation as

$$\begin{aligned} \sigma_s \frac{\partial \bar{u}}{\partial T} + \Re_x \bar{u} \frac{\partial \bar{u}}{\partial X} + \Re_y \bar{v} \frac{\partial \bar{u}}{\partial Y} + \Re_z \bar{w} \frac{\partial \bar{u}}{\partial Z} &= g \frac{\ell_0}{u_o^2} \Re_x - \frac{1}{\bar{\rho}} \frac{\partial P}{\partial X} + \frac{1}{\bar{\rho}} \frac{\partial}{\partial Z} \left( \bar{\eta} \frac{\partial \bar{u}}{\partial Z} \right) \\ &- \frac{2}{3} \left( \frac{h_0}{\ell_0} \right)^2 \frac{1}{\bar{\rho}} \frac{\partial}{\partial X} \left[ \bar{\eta} \left( \frac{\partial \bar{u}}{\partial X} + \frac{v_0}{u_0} \frac{\ell_0}{b_0} \frac{\partial \bar{v}}{\partial Y} + \frac{w_0}{u_0} \frac{\ell_0}{h_0} \frac{\partial \bar{w}}{\partial Z} \right) \right] \\ &+ \frac{1}{\bar{\rho}} \left( \frac{h_0}{b_0} \right)^2 \frac{\partial}{\partial Y} \left[ \bar{\eta} \left( \frac{\partial \bar{u}}{\partial Y} + \frac{v_0}{u_0} \frac{b_0}{\ell_0} \frac{\partial \bar{v}}{\partial X} \right) \right] \\ &+ \frac{2}{\bar{\rho}} \left( \frac{h_0}{\ell_0} \right)^2 \frac{\partial}{\partial X} \left( \bar{\eta} \frac{\partial \bar{u}}{\partial X} \right) + \frac{1}{\bar{\rho}} \frac{\partial}{\partial Z} \left( \bar{\eta} \frac{w_0}{u_0} \frac{h_0}{\ell_0} \frac{\partial \bar{w}}{\partial X} \right) \end{aligned} \quad (7.8)$$

In Eq. (7.8) the inertia terms and the gravity term are of order  $h_0/\ell_0$ . The term  $w_0/u_0$  is also of order  $h_0/\ell_0$ . The pressure gradient term and the first viscous term are of order 1. The remaining viscous terms are of order  $(h_0/\ell_0)^2$  or  $(h_0/b_0)^2$ . Therefore, neglecting terms of order  $(h_0/\ell_0)^2$  or  $(h_0/b_0)^2$  in Eq. (7.8) gives

$$\sigma_s \frac{\partial \bar{u}}{\partial T} + \Re_x \bar{u} \frac{\partial \bar{u}}{\partial X} + \Re_y \bar{v} \frac{\partial \bar{u}}{\partial Y} + \Re_z \bar{w} \frac{\partial \bar{u}}{\partial Z} = g \frac{\ell_0}{u_o^2} \Re_x - \frac{1}{\bar{\rho}} \frac{\partial P}{\partial X} + \frac{1}{\bar{\rho}} \frac{\partial}{\partial Z} \left( \bar{\eta} \frac{\partial \bar{u}}{\partial Z} \right) \quad (7.9)$$

Similarly, for the second and third Navier-Stokes equations, neglecting terms of order  $(h_0/\ell_0)^2$  or  $(h_0/b_0)^2$  gives

$$\sigma_s \frac{\partial \bar{v}}{\partial T} + \Re_x \bar{u} \frac{\partial \bar{v}}{\partial X} + \Re_y \bar{v} \frac{\partial \bar{v}}{\partial Y} + \Re_z \bar{w} \frac{\partial \bar{v}}{\partial Z} = g \frac{b_0}{v_o^2} \Re_y - \frac{1}{\bar{\rho}} \frac{\partial P}{\partial Y} + \frac{1}{\bar{\rho}} \frac{\partial}{\partial Z} \left( \bar{\eta} \frac{\partial \bar{v}}{\partial Z} \right) \quad (7.10)$$

$$\frac{\partial P}{\partial Z} = 0 \quad \rightarrow \quad P = f(X, Y, T) \quad (7.11)$$

Also, the continuity equation can be expressed as

$$\sigma_s \frac{\partial \bar{\rho}}{\partial T} + \Re_x \frac{\partial}{\partial X} (\bar{\rho} \bar{u}) + \Re_y \frac{\partial}{\partial Y} (\bar{\rho} \bar{v}) + \Re_z \frac{\partial}{\partial Z} (\bar{\rho} \bar{w}) = 0 \quad (7.12)$$

Therefore, Eqs. (7.9) to (7.12) are the Navier-Stokes and continuity equations to be used when higher order effects are considered.

### 7.2.2 Taylor Number

In journal bearings a regular toroidal vortex flow may occur before the laminar flow breaks down into turbulence (see Fig. 7.1). This phenomenon was studied by G. I. Taylor in relation to concentric cylinders, and in 1923 he reported that vortices formed at a Reynolds number of

$$\frac{\rho_0 u_0 c}{\eta_0} > 41.3 \left( \frac{r_o}{c} \right)^{1/2} \quad (7.13)$$

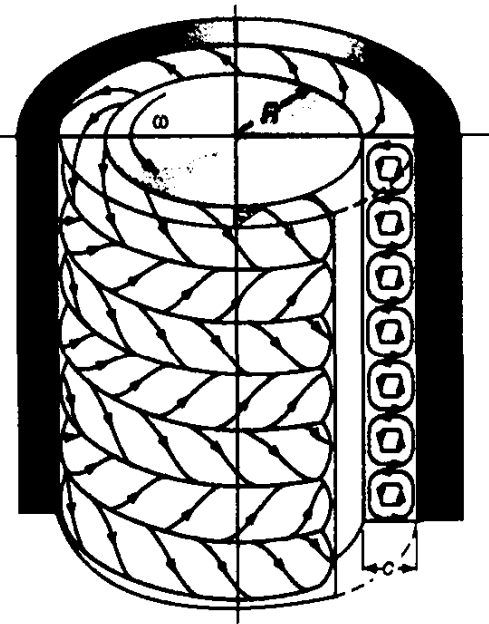


Figure 7.1: Toroidal vortex flow in a journal bearing.

Thus, the Taylor number  $T_a$  that describes when vortex flow first starts to occur can be expressed as

$$T_a = \frac{\rho_0^2 u_0^2 c^3}{r_o \eta_0^2} \geq 1700 \quad (7.14)$$

This describes when the vortices appear. Relating this to the modified Reynolds number defined in Eq. (7.4) requires that both sides of Eq. (7.13) be multiplied by  $h_0^2/c\ell_0$  which gives

$$\Re_x = \frac{\rho_0 u_0 \ell_0}{\eta_0} \left( \frac{h_0}{\ell_0} \right)^2 > 41.3 \left( \frac{r_o}{c} \right)^{1/2} \frac{h_0^2}{c \ell_0} \quad (7.15)$$

If  $h_0 = c$  and  $r_o/c = \ell_0/c = 1 \times 10^3$ ,

$$\Re_x = \frac{\rho_0 u_0 \ell_0}{\eta_0} \left( \frac{h_0}{\ell_0} \right)^2 > 1$$

This indicates that once the inertia terms approach the viscous terms, laminar flow conditions do not hold and vortices are formed.

### 7.2.3 Froude Number

The only body forces normally encountered in lubrication are gravity and magnetic forces. The Froude number shows the relation of inertia to gravity forces.

$$\text{Froude number} = \frac{\text{inertia}}{\text{gravity}} = \frac{u_0^2}{g \ell_0} \quad (7.16)$$

A direct ratio of gravity to viscous forces is found by dividing the Reynolds number by the Froude number.

$$\frac{\text{Reynolds number}}{\text{Froude number}} = \frac{\left(\frac{\text{inertia}}{\text{viscous}}\right)}{\left(\frac{\text{inertia}}{\text{gravity}}\right)} = \frac{\text{gravity}}{\text{viscous}} = \frac{\rho_0 h_0^2 g}{\eta_0 u_0} \quad (7.17)$$

For example, for a typical journal bearing, besides the information given earlier in Example 7.1,  $g = 9.8 \text{ m/s}^2$ .

$$\text{Froude number} = \frac{u_0^2}{g\ell_0} = \frac{(5.24)^2}{(9.8)(0.157)} = 17.8$$

This implies that the inertia forces are larger than the gravity forces. Also,

$$\frac{\text{Reynolds number}}{\text{Froude number}} = \frac{\rho_0 h_0^2 g}{\eta_0 u_0} = \frac{(850)(25 \times 10^{-10})(9.8)}{(0.5)(5.24)} = 0.8 \times 10^{-5}$$

Therefore, the gravity forces can be neglected in relation to the viscous forces.

#### 7.2.4 Euler Number

The importance of the pressure term relative to the inertia term can be judged from the value of the Euler number, which is defined as

$$\text{Euler number} = \frac{\text{pressure}}{\text{inertia}} = \frac{p_0}{\rho_0 u_0^2} \quad (7.18)$$

A direct ratio of the pressure to the viscous forces can be obtained by multiplying the Euler number by the Reynolds number, or

$$\begin{aligned} (\text{Euler number})(\text{Reynolds number}) &= \frac{\text{pressure}}{\text{inertia}} \frac{\text{inertia}}{\text{viscous}} = \frac{\text{pressure}}{\text{viscous}} \\ &= \frac{p_0}{\rho_0 u_0^2} \frac{\rho_0 u_0 \ell_0}{\eta_0} \left(\frac{h_0}{\ell_0}\right)^2 = \frac{p_0 \ell_0}{\eta_0 u_0} \left(\frac{h_0}{\ell_0}\right)^2 \end{aligned} \quad (7.19)$$

For example, for a typical journal bearing, besides the information given earlier in Example 7.1,  $p_0 = 5 \text{ MPa} = 5 \times 10^6 \text{ N/m}^2$ .

$$\text{Euler number} = \frac{p_0}{\rho_0 u_0^2} = \frac{5 \times 10^6}{(850)(5.24)^2} = 214.3$$

Therefore, the pressure term is much larger than the inertia term. Furthermore, from Eq. (7.19),

$$(\text{Euler number})(\text{Reynolds number}) = \frac{(5 \times 10^6)(0.157)}{(3142)^2(0.5)(5.24)} = 0.03$$

Therefore, the viscous term is larger than the pressure term, but both terms need to be considered. Furthermore, in elastohydrodynamic lubrication, where in Chapter 1 we discovered that the pressure is generally three orders of magnitude larger than in hydrodynamic lubrication, we might find the pressure term to be of more importance than the viscous term.

## 7.3 Reynolds Equation Derived

The differential equation governing the pressure distribution in fluid film lubrication is known as the “Reynolds equation.” This equation was first derived in a remarkable paper by Osborne Reynolds in 1886. Reynolds’ classical paper contained not only the basic differential equation of fluid film lubrication, but also a direct comparison between his theoretical predictions and the experimental results obtained by Tower (1883). Reynolds, however, restricted his analysis to an incompressible fluid. This is an unnecessary restriction, and Harrison (1913) included the effects of compressibility. In this section the Reynolds equation is derived in two different ways, from the Navier-Stokes and continuity equations and directly from the principle of mass conservation.

### 7.3.1 From Navier-Stokes and Continuity Equations

From the order-of-magnitude analysis in the preceding section it was discovered that the general Navier-Stokes equations given in Eqs. (6.25) to (6.27) reduce to Eqs. (7.9) to (7.11) when terms of order  $(h_0/\ell_0)^2$  and  $(h_0/b_0)^2$  and smaller are neglected. This then is the starting point of the derivation. Further neglecting terms of order  $h_0/\ell_0$  or  $h_0/b_0$  and only keeping terms of order 1 reduces Eqs. (6.25) to (6.27) to

$$\frac{\partial p}{\partial x} = \frac{\partial}{\partial z} \left( \eta \frac{\partial u}{\partial z} \right) \quad (7.20)$$

$$\frac{\partial p}{\partial y} = \frac{\partial}{\partial z} \left( \eta \frac{\partial v}{\partial z} \right) \quad (7.21)$$

From Eq. (7.11) for steady-state conditions the pressure has been shown to be a function of only  $x$  and  $y$ . Thus, Eqs. (7.20) and (7.21) can be integrated directly to give general expressions for the velocity gradients

$$\frac{\partial u}{\partial z} = \frac{z}{\eta} \frac{\partial p}{\partial x} + \frac{\tilde{A}}{\eta} \quad (7.22)$$

$$\frac{\partial v}{\partial z} = \frac{z}{\eta} \frac{\partial p}{\partial y} + \frac{\tilde{C}}{\eta} \quad (7.23)$$

where  $\tilde{A}$  and  $\tilde{C}$  are integration constants.

The viscosity of the lubricant may change considerably across the thin film ( $z$  direction) as a result of temperature variations that arise in some bearing

problems. In this case, progress toward a simple Reynolds equation is considerably complicated.

An approach that is satisfactory in most fluid film applications is to treat  $\eta$  as the average value of the viscosity across the film. Note that this does not restrict the variation of viscosity in the  $x$  and  $y$  directions. This approach is pursued here.

With  $\eta$  representing an average value of viscosity across the film, integrating Eqs. (7.22) and (7.23) gives the velocity components as

$$u = \frac{z^2}{2\eta} \frac{\partial p}{\partial x} + \tilde{A} \frac{z}{\eta} + \tilde{B} \quad (7.24)$$

$$v = \frac{z^2}{2\eta} \frac{\partial p}{\partial y} + \tilde{C} \frac{z}{\eta} + \tilde{D} \quad (7.25)$$

If zero slip at the fluid-solid interface is assumed, the boundary values for velocity are

$$1. z = 0, u = u_b, v = v_b$$

$$2. z = h, u = u_a, v = v_a$$

The subscripts  $a$  and  $b$  refer to conditions on the upper (curved) and lower (plane) surfaces, respectively. Therefore,  $u_a$ ,  $v_a$  and  $w_a$  refer to the velocity components of the upper surface in the  $x$ ,  $y$ , and  $z$  directions, respectively, and  $u_b$ ,  $v_b$ , and  $w_b$  refer to the velocity components of the lower surface in the same directions.

With the boundary conditions applied to Eqs. (7.24) and (7.25), the velocity gradients and velocity components are

$$\frac{\partial u}{\partial z} = \left( \frac{2z - h}{2\eta} \right) \frac{\partial p}{\partial x} - \frac{u_b - u_a}{h} \quad (7.26)$$

$$\frac{\partial v}{\partial z} = \left( \frac{2z - h}{2\eta} \right) \frac{\partial p}{\partial y} - \frac{v_b - v_a}{h} \quad (7.27)$$

$$u = -z \left( \frac{h - z}{2\eta} \right) \frac{\partial p}{\partial x} + u_b \frac{h - z}{h} + u_a \frac{z}{h} \quad (7.28)$$

$$v = -z \left( \frac{h - z}{2\eta} \right) \frac{\partial p}{\partial y} + v_b \frac{h - z}{h} + v_a \frac{z}{h} \quad (7.29)$$

Note that if  $u_b = 0$ , Eq. (7.26) is exactly Eq. (6.54) and Eq. (7.28) is exactly Eq. (6.53). With these expressions for the velocity gradients and the velocity components, expressions can be derived for the surface shear stresses and the volume flow rate.

The viscous shear stresses acting on the solids as defined in Eq. (6.7) can be expressed as

$$\tau_{zx} = \eta \left( \frac{\partial w}{\partial x} + \frac{\partial u}{\partial z} \right)$$

$$\tau_{zy} = \eta \left( \frac{\partial w}{\partial y} + \frac{\partial v}{\partial z} \right)$$

In the order-of-magnitude evaluation,  $\partial w/\partial x$  and  $\partial w/\partial y$  are much smaller than  $\partial u/\partial z$  and  $\partial v/\partial z$ . Therefore,

$$\tau_{zx} = \eta \frac{\partial u}{\partial z} \quad (7.30)$$

$$\tau_{zy} = \eta \frac{\partial v}{\partial z} \quad (7.31)$$

and the viscous shear stresses acting on the solid surfaces can be expressed, while making use of Eqs. (7.26) and (7.27), as

$$(\tau_{zx})_{z=0} = \left( \eta \frac{\partial u}{\partial z} \right)_{z=0} = -\frac{h}{2} \frac{\partial p}{\partial x} - \frac{\eta (u_b - u_a)}{h} \quad (7.32)$$

$$(-\tau_{zx})_{z=h} = -\left( \eta \frac{\partial u}{\partial z} \right)_{z=h} = -\frac{h}{2} \frac{\partial p}{\partial x} + \frac{\eta (u_b - u_a)}{h} \quad (7.33)$$

$$(\tau_{zy})_{z=0} = \left( \eta \frac{\partial v}{\partial z} \right)_{z=0} = -\frac{h}{2} \frac{\partial p}{\partial y} - \frac{\eta (v_b - v_a)}{h} \quad (7.34)$$

$$(-\tau_{zy})_{z=h} = -\left( \eta \frac{\partial v}{\partial z} \right)_{z=h} = -\frac{h}{2} \frac{\partial p}{\partial y} + \frac{\eta (v_b - v_a)}{h} \quad (7.35)$$

The negative signs on the viscous shear stresses indicate that they act opposite to the direction of motion.

The volume flow rates per unit width in the  $x$  and  $y$  directions are defined as

$$q'_x = \int_0^h u \, dz \quad (7.36)$$

$$q'_y = \int_0^h v \, dz \quad (7.37)$$

Substituting Eqs. (7.28) and (7.29) in these equations gives

$$q'_x = -\frac{h^3}{12\eta} \frac{\partial p}{\partial x} + \frac{u_a + u_b}{2} h \quad (7.38)$$

$$q'_y = -\frac{h^3}{12\eta} \frac{\partial p}{\partial y} + \frac{v_a + v_b}{2} h \quad (7.39)$$

Note that if  $u_b = 0$ , Eq. (7.38) is exactly Eq. (6.58), derived for the volume flow rate between parallel flat plates. The first term on the right side of Eqs. (7.38) and (7.39) represents the well-known Poiseuille (or pressure) flow, and the second term represents the Couette (or velocity) flow.

## Example 7.3

**Given** A piston pump without rings pumps an oil with a viscosity of 0.143 Pa·s at a pressure differential of 20 MPa. The piston moves concentrically in the cylinder so that the radial clearance is constant around the piston. The piston is 100 mm in diameter and 80 mm long and the radial clearance is 50  $\mu\text{m}$ . The piston moves with a speed of 0.2 m/s.

**Find** Determine the leakage past the piston when

- The piston pumps the oil (like a pump)
- The oil drives the piston (like a hydraulic cylinder)

**Solution** The pressure gradient is

$$\frac{\partial p}{\partial x} = \frac{\Delta p}{\Delta x} = \frac{(20)(10^6)}{0.080} = 2.5 \times 10^8 \text{ N/m}^3$$

- When the piston pumps the oil, the cylinder wall passes the piston from high pressure to low pressure. From Eq. (7.38) the pressure flow and the motion flow together are

$$\begin{aligned} q &= \pi d q'_x = \pi d \left[ \frac{h^3}{12\eta} \frac{\partial p}{\partial x} + \frac{h(u_a + u_b)}{2} \right] \\ &= \pi(0.100) \left( \frac{(50)^3 (10^{-18}) (2.5) (10^8)}{(12)(0.143)} + \frac{(50)(10^{-6})(0.2)}{2} \right) \\ &= 7.292 \times 10^{-6} \text{ m}^3/\text{s} \end{aligned}$$

- When the oil drives the piston, the pressure flow is opposite to the flow from the motion

$$\begin{aligned} q &= \pi d q'_x = \pi d \left[ \frac{h^3}{12\eta} \frac{\partial p}{\partial x} + \frac{h(u_a + u_b)}{2} \right] \\ &= \pi(0.100) \left( -\frac{(50)^3 (10^{-18}) (2.5) (10^8)}{(12)(0.143)} + \frac{(50)(10^{-6})(0.2)}{2} \right) \\ &= -4.150 \times 10^{-6} \text{ m}^3/\text{s} \end{aligned}$$

Thus, when the piston pumps the oil, the leakage is  $7.292 \text{ cm}^3/\text{s}$ ; and when the oil drives the piston, the leakage is  $-4.150 \text{ cm}^3/\text{s}$ . Therefore, the cylinder wall motion pulls oil into the high-pressure region.

---

Returning to Eqs. (7.28) and (7.29), the Reynolds equation is formed by introducing these expressions into the continuity equation derived in Eq. (6.47).

Before doing so, however, it is convenient to express the continuity equation in integral form.

$$\int_0^h \left( \frac{\partial \rho}{\partial t} + \frac{\partial}{\partial x} (\rho u) + \frac{\partial}{\partial y} (\rho v) + \frac{\partial}{\partial z} (\rho w) \right) dz = 0$$

Now a general rule of integration is that

$$\int_0^h \frac{\partial}{\partial x} [f(x, y, z)] dz = -f(x, y, h) \frac{\partial h}{\partial x} + \frac{\partial}{\partial x} \left( \int_0^h f(x, y, z) dz \right) \quad (7.40)$$

Hence, if  $\rho$  is assumed to be the mean density across the film (as was done earlier for the viscosity across the film), the  $u$  component term in the integrated continuity equation is

$$\int_0^h \frac{\partial}{\partial x} (\rho u) dz = -(\rho u)_{z=h} \frac{\partial h}{\partial x} + \frac{\partial}{\partial x} \left( \int_0^h \rho u dz \right) = -\rho u_a \frac{\partial h}{\partial x} + \frac{\partial}{\partial x} \left( \rho \int_0^h u dz \right)$$

Similarly, for the  $v$  component

$$\int_0^h \frac{\partial}{\partial y} (\rho v) dz = -\rho v_a \frac{\partial h}{\partial y} + \frac{\partial}{\partial y} \left( \rho \int_0^h v dz \right)$$

The  $w$  component term can be integrated directly to give

$$\int_0^h \frac{\partial}{\partial z} (\rho w) dz = \rho (w_a - w_b)$$

Therefore, the integrated continuity equation becomes

$$h \frac{\partial \rho}{\partial t} - \rho u_a \frac{\partial h}{\partial x} + \frac{\partial}{\partial x} \left( \rho \int_0^h u dz \right) - \rho v_a \frac{\partial h}{\partial y} + \frac{\partial}{\partial y} \left( \rho \int_0^h v dz \right) + \rho (w_a - w_b) = 0 \quad (7.41)$$

The integrals in this equation represent the volume flow rates per unit width ( $q'_x$  and  $q'_y$ ) described in Eqs. (7.38) and (7.39). Introducing these flow rate expressions into the integrated continuity equation yields the general Reynolds equation

$$\begin{aligned} 0 &= \frac{\partial}{\partial x} \left( -\frac{\rho h^3}{12\eta} \frac{\partial p}{\partial x} \right) + \frac{\partial}{\partial y} \left( -\frac{\rho h^3}{12\eta} \frac{\partial p}{\partial y} \right) + \frac{\partial}{\partial x} \left( \frac{\rho h (u_a + u_b)}{2} \right) \\ &+ \frac{\partial}{\partial y} \left( \frac{\rho h (v_a + v_b)}{2} \right) + \rho (w_a - w_b) - \rho u_a \frac{\partial h}{\partial x} - \rho v_a \frac{\partial h}{\partial y} + h \frac{\partial \rho}{\partial t} \end{aligned} \quad (7.42)$$

### 7.3.2 From Laws of Viscous Flow and Principle of Mass Conservation

The Reynolds equation can be derived directly by considering a control volume fixed in space and extended across the lubricating film. Consider the rate of

mass flow through a rectangular section of sides  $\Delta x$  and  $\Delta y$ , thus fixing the coordinate system and extending the lubricating film between the surfaces as shown in Fig. 7.2. Note that one surface is represented by the plane  $z = 0$  and the other by a curved surface so that the film thickness at any instant is a function of  $x$  and  $y$  only. This is exactly the coordinate system used in the previous derivation of the Reynolds equation.

The mass of lubricant in the control volume at any instant is  $\rho h \Delta x \Delta y$ . The rate of change within the control volume arises from the change in the difference between the rate of mass flowing into the control volume and the rate leaving the control volume, which is  $-(\partial \rho q'_x / \partial x) \Delta x \Delta y$  in the  $x$  direction and  $-(\partial \rho q'_y / \partial y) \Delta x \Delta y$  in the  $y$  direction.

The principle of mass conservation demands that the rate at which mass is accumulating in the control volume  $\partial((\rho h) / \partial t)$  must be equal to the difference between the rates at which mass enters and leaves. Therefore,

$$-\frac{\partial \rho q'_x}{\partial x} - \frac{\partial \rho q'_y}{\partial y} = \frac{\partial}{\partial t} (\rho h) \quad (7.43)$$

But

$$\frac{\partial}{\partial t} (\rho h) = \rho \frac{\partial h}{\partial t} + h \frac{\partial \rho}{\partial t}$$

and

$$\frac{\partial}{\partial t} (\rho h) = \rho \left( w_a - w_b - u_a \frac{\partial h}{\partial x} - v_a \frac{\partial h}{\partial y} \right) + h \frac{\partial \rho}{\partial t} \quad (7.44)$$

By making use of Eqs. (7.38), (7.39), and (7.44), Eq. (7.43) becomes

$$\begin{aligned} 0 &= \frac{\partial}{\partial x} \left( -\frac{\rho h^3}{12\eta} \frac{\partial p}{\partial x} \right) + \frac{\partial}{\partial y} \left( -\frac{\rho h^3}{12\eta} \frac{\partial p}{\partial y} \right) + \frac{\partial}{\partial x} \left( \frac{\rho h (u_a + u_b)}{2} \right) \\ &+ \frac{\partial}{\partial y} \left( \frac{\rho h (v_a + v_b)}{2} \right) + \rho (w_a - w_b) - \rho u_a \frac{\partial h}{\partial x} - \rho v_a \frac{\partial h}{\partial y} + h \frac{\partial \rho}{\partial t} \end{aligned} \quad (7.45)$$

This is exactly Eq. (7.42), the general Reynolds equation derived from the Navier-Stokes and continuity equations.

## 7.4 Physical Significance of Terms in Reynolds Equation

The first two terms of Eq. (7.45) are the Poiseuille terms and describe the net flow rates due to pressure gradients within the lubricated area; the third and fourth terms are the Couette terms and describe the net entraining flow rates due to surface velocities. The fifth to seventh terms describe the net flow rates due to a squeezing motion, and the last term describes the net flow rate due to local expansion. The flows or “actions” can be considered, without any loss of generality, by eliminating the side-leakage terms ( $\partial/\partial y$ ) in Eq. (7.45).

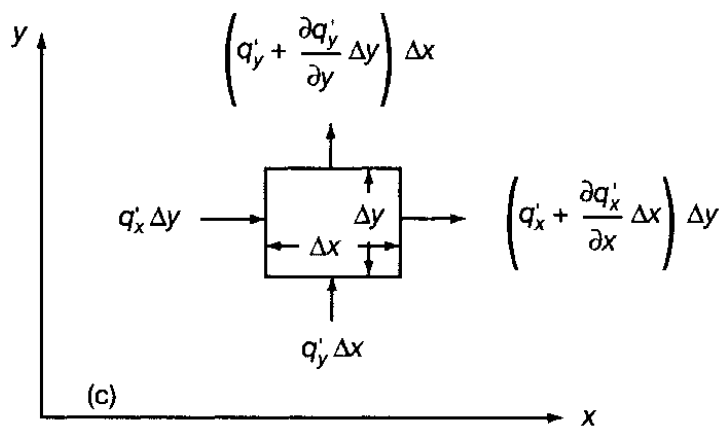
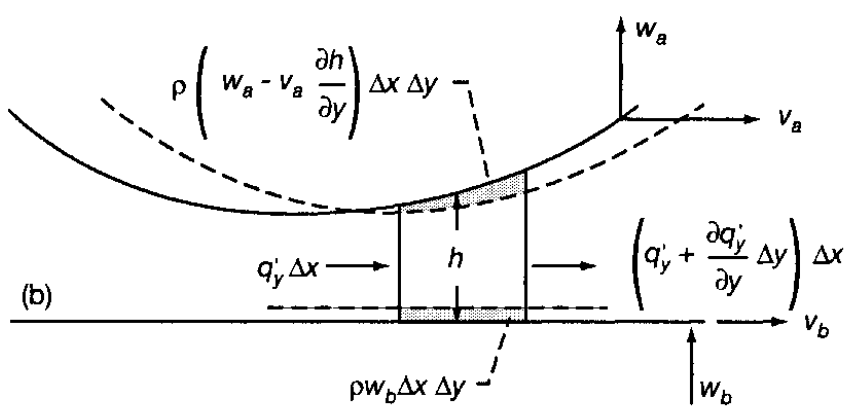
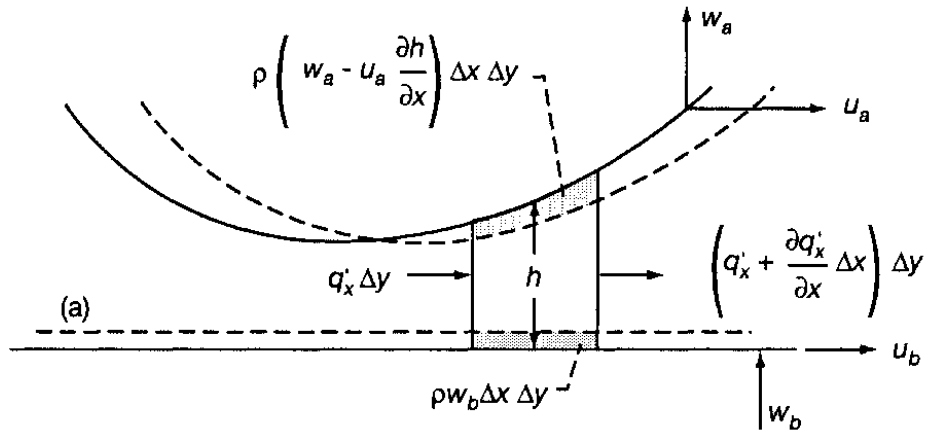


Figure 7.2: Mass flow through rectangular-section control volume. (a)  $x-y$  plane; (b)  $y-z$  plane; (c)  $x-y$  plane. [From Hamrock and Dowson (1981).]

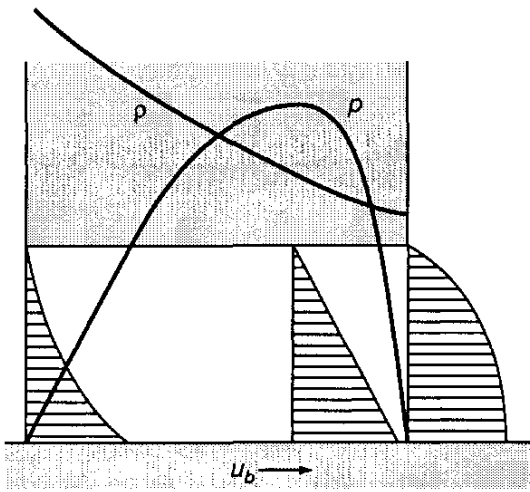


Figure 7.3: Density wedge.

$$\frac{\partial}{\partial x} \left( \frac{\rho h^3 \frac{\partial p}{\partial x}}{12\eta} \right) = \underbrace{\frac{\partial}{\partial x} \left[ \frac{\rho h (u_a + u_b)}{2} \right]}_{\text{Poiseuille}} + \underbrace{\rho \left( w_a - w_b - u_a \frac{\partial h}{\partial x} \right)}_{\text{Couette}} + \underbrace{h \frac{\partial \rho}{\partial t}}_{\text{Local expansion}} + \underbrace{\frac{h (u_a + u_b) \frac{\partial \rho}{\partial x}}{2}}_{\text{Density wedge}} + \underbrace{\frac{\rho h}{2} \frac{\partial}{\partial x} (u_a + u_b)}_{\text{Stretch}} + \underbrace{\frac{\rho (u_a + u_b) \frac{\partial h}{\partial x}}{2}}_{\text{Physical wedge}}$$
(7.46)

It can be seen that the Couette term leads to three distinct actions. The physical significance of each term within the Reynolds equation is now discussed in detail.

#### 7.4.1 Density Wedge Term $[(u_a + u_b) h/2] (\partial \rho / \partial x)$

The density wedge action is concerned with the rate at which lubricant density changes in the sliding direction as shown in Fig. 7.3. If the lubricant density decreases in the sliding direction, the Couette mass flows for each location of the three velocity profiles of Fig. 7.3 differ. For continuity of mass flow this discrepancy must be eliminated by generating a balancing Poiseuille flow.

Note from Fig. 7.3 that the density must decrease in the direction of sliding if positive pressures are to be generated. This effect could be introduced by raising the temperature of the lubricant as it passes through the bearing. The density wedge (sometimes called the “thermal wedge”) mechanism is not important in most bearings. It has been suggested that it may play a significant role in the performance of parallel-surface thrust bearings, where the major pressure-generating actions are absent.

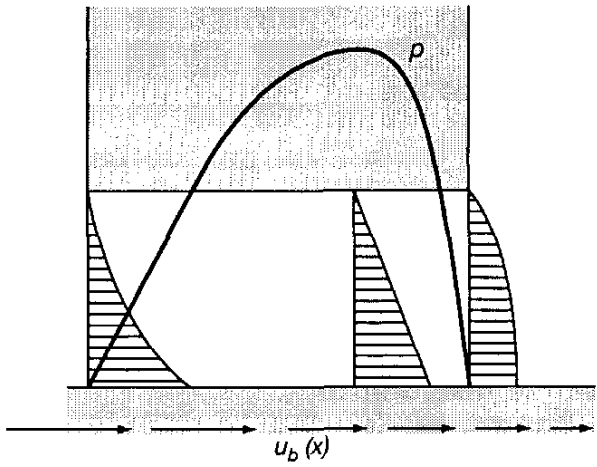


Figure 7.4: Stretch mechanism.

#### 7.4.2 Stretch Term $(\rho h/2) [\partial(u_a + u_b)/\partial x]$

The stretch action considers the rate at which surface velocity changes in the sliding direction. This effect is produced if the bounding solids are elastic and the extent to which the surfaces are stretched varies through the bearing. For positive pressures to be developed, the surface velocities have to decrease in the sliding direction, as shown in Fig. 7.4. This action is not encountered in conventional bearings.

#### 7.4.3 Physical Wedge Term $[\rho(u_a + u_b)/2] (\partial h/\partial x)$

The physical wedge action is extremely important and is the best known device for pressure generation. This action is illustrated for the case of a plane slider and a stationary bearing pad in Fig. 7.5. At each of the three sections considered, the Couette volume flow rate is proportional to the area of the triangle of height  $h$  and base  $u$ . Since  $h$  varies along the bearing, there is a different Couette flow rate at each section, and flow continuity can be achieved only if a balancing Poiseuille flow is superimposed. For a positive load-carrying capacity the thickness of the lubricant film must decrease in the sliding direction.

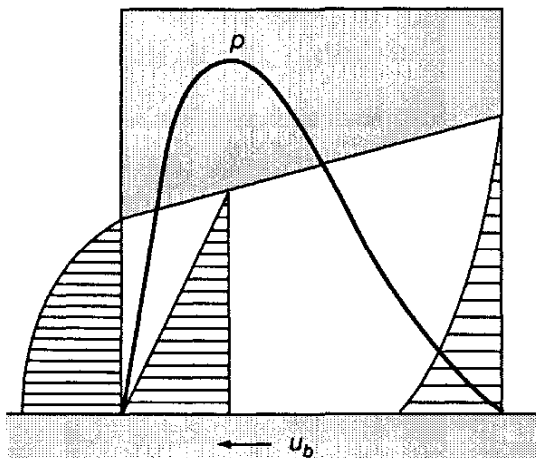


Figure 7.5: Physical wedge mechanism.

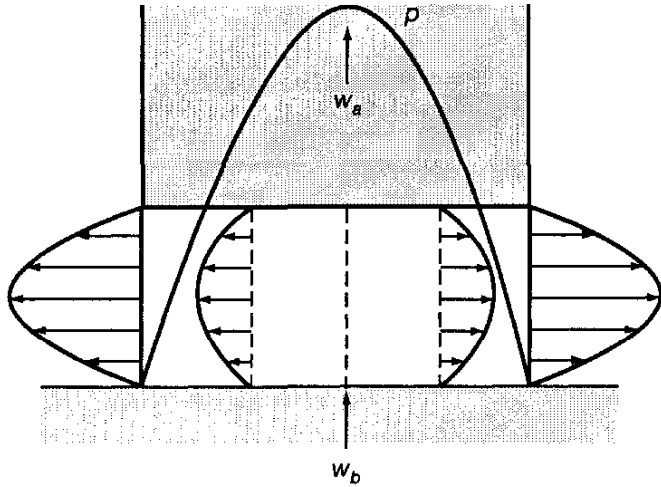


Figure 7.6: Normal squeeze mechanism.

#### 7.4.4 Normal Squeeze Term $\rho(w_a - w_b)$

Normal squeeze action provides a valuable cushioning effect when bearing surfaces tend to be pressed together. Positive pressures will be generated when the film thickness is diminishing. The physical wedge and normal squeeze actions are the two major pressure-generating devices in hydrodynamic or self-acting fluid film bearings. In the absence of sliding, the effect arises directly from the difference in normal velocities ( $w_a - w_b$ ), as illustrated in Fig. 7.6. Positive pressures will clearly be achieved if the film thickness is decreasing ( $w_b > w_a$ ).

#### 7.4.5 Translation Squeeze Term $-\rho u_a (\partial h / \partial x)$

The translation squeeze action results from the translation of inclined surfaces. The local film thickness may be squeezed by the sliding of the inclined bearing surface, as shown in Fig. 7.7. The rate at which the film thickness is decreasing is shown in the figure. Note that in this case the pressure profile is moving over the space covered by the fixed coordinate system, the pressure at any fixed point being a function of time.

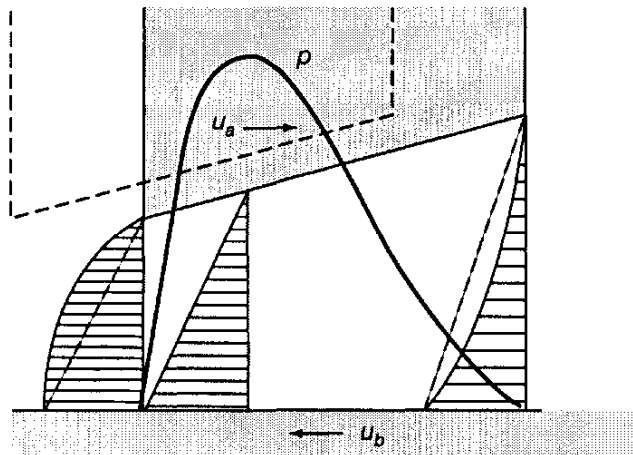


Figure 7.7: Translation squeeze mechanism.

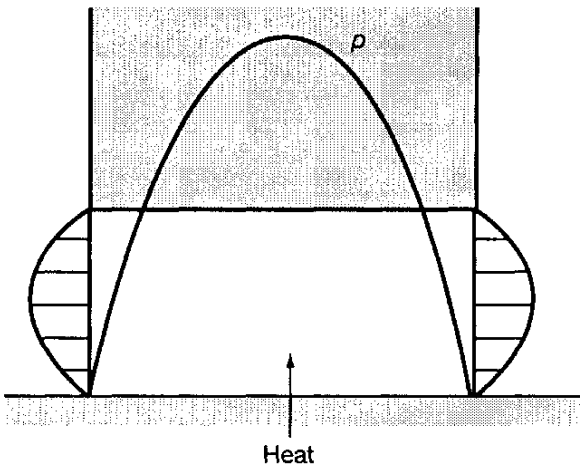


Figure 7.8: Local expansion mechanism.

#### 7.4.6 Local Expansion Term $h(\partial\rho/\partial t)$

The local time rate of density change governs the local expansion term. The pressure-generating mechanism can be visualized by considering the thermal expansion of the lubricant contained between stationary bearing surfaces, as shown in Fig. 7.8. If heat is supplied to the lubricant, it will expand and the excess volume will have to be expelled from the space between the bearing surfaces. In the absence of surface velocities the excess lubricant volume must be expelled by a pressure (Poiseuille) flow action. Pressures are thus generated in the lubricant, and for a positive load-carrying capacity,  $\partial\rho/\partial t$  must be negative (i.e., the volume of a given mass of lubricant must increase). Local expansion, which is a transient mechanism of pressure generation, is generally of no significance in bearing analysis.

### 7.5 Standard Reduced Forms of Reynolds Equation

For only tangential motion, where  $w_a = u_a \partial h / \partial x + v_a \partial h / \partial y$  and  $w_b = 0$ , the Reynolds equation given in Eq. (7.45) becomes

$$\frac{\partial}{\partial x} \left( \frac{\rho h^3}{\eta} \frac{\partial p}{\partial x} \right) + \frac{\partial}{\partial y} \left( \frac{\rho h^3}{\eta} \frac{\partial p}{\partial y} \right) = 12\tilde{u} \frac{\partial(\rho h)}{\partial x} + 12\tilde{v} \frac{\partial(\rho h)}{\partial y} \quad (7.47)$$

where

$$\tilde{u} = \frac{u_a + u_b}{2} = \text{constant} \quad \tilde{v} = \frac{v_a + v_b}{2} = \text{constant}$$

Equation (7.47) is applicable for elastohydrodynamic lubrication. For hydrodynamic lubrication the fluid properties do not vary significantly throughout the bearing and thus may be considered to be a constant. Also, for hydrodynamic lubrication the motion is pure sliding so that  $\tilde{v}$  is zero. Thus, the corresponding Reynolds equation is

$$\frac{\partial}{\partial x} \left( h^3 \frac{\partial p}{\partial x} \right) + \frac{\partial}{\partial y} \left( h^3 \frac{\partial p}{\partial y} \right) = 12\tilde{u}\eta_0 \frac{\partial h}{\partial x} \quad (7.48)$$

Equation (7.47) not only allows the fluid properties to vary in the  $x$  and  $y$  directions, but also permits the bearing surfaces to be of finite length in the  $y$  direction. Side leakage, or flow in the  $y$  direction, is associated with the second term in Eqs. (7.47) and (7.48). If the pressure in the lubricant film has to be considered as a function of  $x$  and  $y$ , the solution of Eq. (7.47) can rarely be achieved analytically.

In many conventional lubrication problems side leakage can be neglected, and this often leads to analytical solutions. If side leakage is neglected, Eq. (7.47) becomes

$$\frac{\partial}{\partial x} \left( \frac{\rho h^3}{\eta} \frac{\partial p}{\partial x} \right) = 12\tilde{u} \frac{\partial(\rho h)}{\partial x} \quad (7.49)$$

This equation can be integrated with respect to  $x$  to give

$$\frac{1}{\eta} \frac{dp}{dx} = \frac{12\tilde{u}}{h^2} + \frac{\tilde{A}}{\rho h^3} \quad (7.50)$$

Making use of the boundary condition that

$$\frac{dp}{dx} = 0 \quad \text{when } x = x_m \quad \rho = \rho_m \quad h = h_m$$

gives

$$\tilde{A} = -12\tilde{u}\rho_m h_m$$

Substituting this into Eq. (7.50) gives

$$\frac{dp}{dx} = 12\tilde{u}\eta \frac{\rho h - \rho_m h_m}{\rho h^3} \quad (7.51)$$

This is the *integrated form of the Reynolds equation*. Note that the subscript  $m$  refers to the condition at all points where  $dp/dx = 0$ , such as the point of maximum pressure. No assumptions were made about the density or viscosity of the fluid in Eq. (7.51). If the density does not vary much throughout the conjunction, it can be considered constant and Eq. (7.51) reduces to

$$\frac{dp}{dx} = 12\tilde{u}\eta \frac{h - h_m}{h^3} \quad (7.52)$$

The Reynolds equation that is valid for gas-lubricated bearings is discussed next. The equation of state for a perfect gas is

$$p = \rho \bar{R} t_m \quad (7.53)$$

where

$\bar{R}$  = gas constant (universal gas constant/molecular weight)  
 $t_m$  = absolute temperature

Therefore, from Eq. (7.53)

$$\rho = \frac{p}{\bar{R}t_m} \quad (7.54)$$

Substituting this equation into Eq. (7.47) yields the Reynolds equation normally used for gas-lubricated bearings for only tangential motion. Because the viscosity of a gas does not vary much, it can be considered to be constant.

$$\frac{\partial}{\partial x} \left( ph^3 \frac{\partial p}{\partial x} \right) + \frac{\partial}{\partial y} \left( ph^3 \frac{\partial p}{\partial y} \right) = 12\tilde{u}\eta_0 \frac{\partial ph}{\partial x} \quad (7.55)$$

The comparable equation to (7.47) as expressed in cylindrical polar coordinates is

$$\frac{\partial}{\partial r} \left( \frac{r\rho h^3}{\eta} \frac{\partial p}{\partial r} \right) + \frac{1}{r} \frac{\partial}{\partial \theta} \left( \frac{\rho h^3}{\eta} \frac{\partial p}{\partial \theta} \right) = 12 \left( \tilde{v}_r \frac{\partial}{\partial r} (\rho rh) + \tilde{v}_\theta \frac{\partial}{\partial \theta} (\rho h) \right) \quad (7.56)$$

where  $\tilde{v}_r = (v_{ra} + v_{rb})/2$  and  $\tilde{v}_\theta = (v_{\theta a} + v_{\theta b})/2$ . If the viscosity and the density are assumed to be constant, this equation reduces to

$$\frac{\partial}{\partial r} \left( rh^3 \frac{\partial p}{\partial r} \right) + \frac{1}{r} \frac{\partial}{\partial \theta} \left( h^3 \frac{\partial p}{\partial \theta} \right) = 12\eta_0 \left( \tilde{v}_r \frac{\partial}{\partial r} (rh) + \tilde{v}_\theta \frac{\partial}{\partial \theta} (h) \right) \quad (7.57)$$

It should be pointed out that Eqs. (7.56) and (7.57) express the Reynolds equation for cylindrical polar coordinates as applied to a thrust bearing where the film direction is in the  $z$  direction and the bearing dimensions are in the  $r, \theta$  directions. If one is interested in expressing the cylindrical polar coordinates as applied to a journal bearing, the Reynolds equation would be different in that  $\theta$  and  $z$  describe the dimensions of the bearing and  $r$  describes the film shape. The Reynolds equation that occurs for the general representation of Eq. (7.45) is

$$\begin{aligned} & \frac{\partial}{\partial x} \left( \frac{\rho h^3}{12\eta} \frac{\partial p}{\partial x} \right) + \frac{\partial}{\partial y} \left( \frac{\rho h^3}{12\eta} \frac{\partial p}{\partial y} \right) \\ &= \frac{\partial}{\partial x} \left( \frac{\rho h (u_a + u_b)}{2} \right) + \frac{\partial}{\partial y} \left( \frac{\rho h (v_a + v_b)}{2} \right) + \frac{\partial (\rho h)}{\partial t} \end{aligned} \quad (7.58)$$

This equation is exactly the same as (7.45) if

$$\rho (w_a - w_b) - \rho u_a \frac{\partial h}{\partial x} - \rho v_a \frac{\partial h}{\partial y} + h \frac{\partial \rho}{\partial t} = \frac{\partial (\rho h)}{\partial t}$$

This implies that

$$\frac{\partial h}{\partial t} = w_a - w_b - u_a \frac{\partial h}{\partial x} - v_a \frac{\partial h}{\partial y} \quad (7.59)$$

An attempt will be made to prove that Eq. (7.59) is true. First, observe that the film thickness  $h$  is a function of  $x, y$ , and  $t$ .

$$h = f(x, y, t)$$

From the definition of a total derivative,

$$Dh = \frac{\partial h}{\partial t} dt + \frac{\partial h}{\partial x} dx + \frac{\partial h}{\partial y} dy$$

or

$$\frac{Dh}{Dt} = \frac{\partial h}{\partial t} + \frac{\partial h}{\partial x} \frac{dx}{dt} + \frac{\partial h}{\partial y} \frac{dy}{dt}$$

But

$$u_a = \frac{dx}{dt} \quad v_a = \frac{dy}{dt} \quad \text{and} \quad \frac{Dh}{Dt} = w_a - w_b$$

$$w_a - w_b = \frac{\partial h}{\partial t} + u_a \frac{\partial h}{\partial x} + v_a \frac{\partial h}{\partial y}$$

or

$$\frac{\partial h}{\partial t} = w_a - w_b - u_a \frac{\partial h}{\partial x} - v_a \frac{\partial h}{\partial y} \quad (7.60)$$

thus proving that Eqs. (7.45) and (7.58) are the same.

Making use of Eqs. (6.51) and (6.44) to (6.46) while following the procedure given in Szeri (1980), the Reynolds equation for turbulent flow is

$$\frac{\partial}{\partial x} \left( \frac{h^3}{\eta k_x} \frac{\partial p^*}{\partial x} \right) + \frac{\partial}{\partial y} \left( \frac{h^3}{\eta k_y} \frac{\partial p^*}{\partial y} \right) = \frac{u^*}{2} \frac{\partial h}{\partial x} \quad (7.61)$$

Equation (7.61) is applicable for thrust or journal bearings. Constantinescu (1962) found that

$$k_x = 12 + 0.53 (k^2 R_{eh})^{0.725} \quad (7.62)$$

$$k_y = 12 + 0.296 (k^2 R_{eh})^{0.65} \quad (7.63)$$

where

$$R_{eh} = \frac{r \omega h \rho}{\eta} \quad (7.64)$$

$$k \approx 0.125 R_{eh}^{0.07} \quad (7.65)$$

## 7.6 Different Normal Squeeze and Sliding Motions

The last section described various Reynolds equations when only tangential motion exists. This section describes how the Reynolds equation is altered when considering various tangential and normal squeeze velocity components. The velocity components and the coordinates used are shown in Fig. 7.9. If the density is assumed to be constant and side leakage is neglected for simplicity, the Reynolds equation expressed in Eq. (7.45) can be rewritten as

$$\frac{\partial}{\partial x} \left( \frac{h^3}{12\eta} \frac{\partial p}{\partial x} \right) = \frac{u_a + u_b}{2} \frac{\partial h}{\partial x} + \frac{h}{2} \frac{\partial}{\partial x} (u_a + u_b) + w_a - w_b - u_a \frac{\partial h}{\partial x}$$

Table 7.1: Different tangential and normal squeeze motions that may occur in bearings.

	$u_a = w_a = 0$ $u_b = u_1, w_a = 0$	$I + II + III = \frac{u_1}{2} \frac{dh}{dx} + 0 + 0 = \frac{u_1}{2} \frac{dh}{dx}$
	$u_a = -u_1, w_a = 0$ $u_b = 0, w_b = 0$	$I+II+III=\frac{u_1}{2} \frac{dh}{dx} + 0 + 0 = \frac{u_1}{2} \frac{dh}{dx}$
	$u_a = -u_1, w_a = 0$ $u_b = u_1, w_b = 0$	$I+II+III=\frac{u_1 + u_1}{2} \frac{dh}{dx} + 0 + 0 = u_1 \frac{dh}{dx}$
	$u_a = u_1, w_a = 0$ $u_b = u_1, w_b = 0$	$I+II+III=\frac{u_1 - u_1}{2} \frac{dh}{dx} + 0 + 0 = 0$
	$u_a = u_1 \cos \alpha \approx u_1$ $w_a = -u_1 \sin \alpha = u_a \frac{dh}{dx}$ $u_b = 0, w_b = 0$	$I+II+III=-\frac{u_1}{2} \frac{dh}{dx} + 0 + u_1 \frac{dh}{dx} = \frac{u_1}{2} \frac{dh}{dx}$
	$u_a = 0, w_a = 0$ $u_b = u_1, w_b = 0$ Note that $x < 0 \quad \frac{dh}{dx} < 0$ $x > 0 \quad \frac{dh}{dx} > 0$	$I+II+III=\frac{u_1}{2} \frac{dh}{dx} + 0 + 0 = \frac{u_1}{2} \frac{dh}{dx}$
	$u_a = -u_1, w_a = 0$ $u_b = 0, w_b = 0$	$I+II+III=\frac{u_1}{2} \frac{dh}{dx} + 0 + 0 = \frac{u_1}{2} \frac{dh}{dx}$

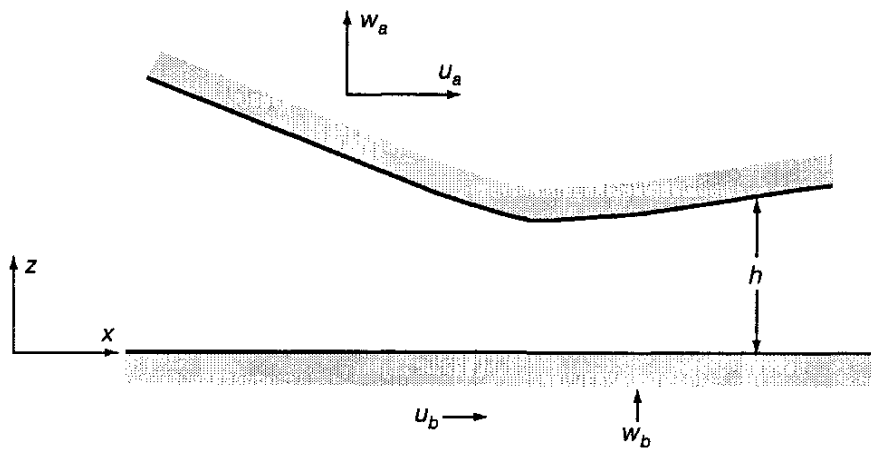
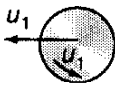
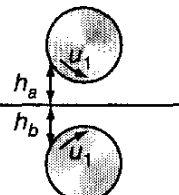


Figure 7.9: Normal squeeze and sliding velocities.

Table 7.1: Concluded

	$u_a = u_1, w_a = u_1 \frac{\partial h}{\partial x}$ $u_b = 0, w_b = 0$	$I+II+III = -\frac{u_1}{2} \frac{dh}{dx} + 0 + u_1 \frac{dh}{dx} = \frac{u_1}{2} \frac{dh}{dx}$
	$u_a = -u_1 + u_1 = 0$ $w_a = u_1 \frac{\partial h}{\partial x}$ $u_b = 0, w_b = 0$	$I+II+III = 0 + 0 + u_1 \frac{dh}{dx} = u_1 \frac{dh}{dx}$
	$u_a = u_1, w_a = u_1 \frac{\partial h}{\partial x}$ $u_b = u_1, w_b = 0$	$I+II+III = \frac{u_1 - u_1}{2} + 0 + u_1 \frac{\partial h}{\partial x} = u_1 \frac{\partial h}{\partial x}$
	$u_a = u_1, w_a = u_1 \frac{dh_a}{dx}$ $u_b = u_1, w_b = u_1 \frac{dh_b}{dx}$	$I+II+III = \frac{u_1 - u_1}{2} \frac{dh}{dx} + 0 + u_1 \frac{dh_a}{dx}$ $+ u_1 \frac{dh_b}{dx} = u_1 \frac{dh}{dx}$
	$u_a = u_1, w_a = u_1 \frac{dh_a}{dx}$ $u_b = -u_1, w_b = -u_1 \frac{dh_b}{dx}$	$I+I+III = -\frac{-u_1 - u_1}{2} \frac{dh}{dx} + 0 + u_1 \frac{dh_a}{dx}$ $+ u_1 \frac{dh_b}{dx} = 0$
	$u_a = u_1, w_a = u_1 \frac{dh}{dx}$ $u_b = 0, w_b = 0$	$I+II+III = \frac{-u_1}{2} \frac{dh}{dx} + 0 + u_1 \frac{dh}{dx} = \frac{u_1}{2} \frac{dh}{dx}$

Collecting terms gives

$$\frac{\partial}{\partial x} \left( \frac{h^3}{12\eta} \frac{\partial p}{\partial x} \right) = \underbrace{\frac{u_b - u_a}{2} \frac{\partial h}{\partial x}}_{I} + \underbrace{\frac{h}{2} \frac{\partial}{\partial x} (u_a + u_b)}_{II} + \underbrace{w_a - w_b}_{III} \quad (7.66)$$

A number of different tangential and normal squeeze motions may occur and are depicted in Table 7.1. The terms on the right side of Eq. (7.66) are designated as I, II, and III. As the table shows, care must be taken to make sure that the physical motion experienced in a particular application is represented by the appropriate Reynolds equation. Note that some quite different geometries and velocities produce the same equation. However, an understanding of why this is so is important in order to avoid improper interpretation.

## 7.7 Closure

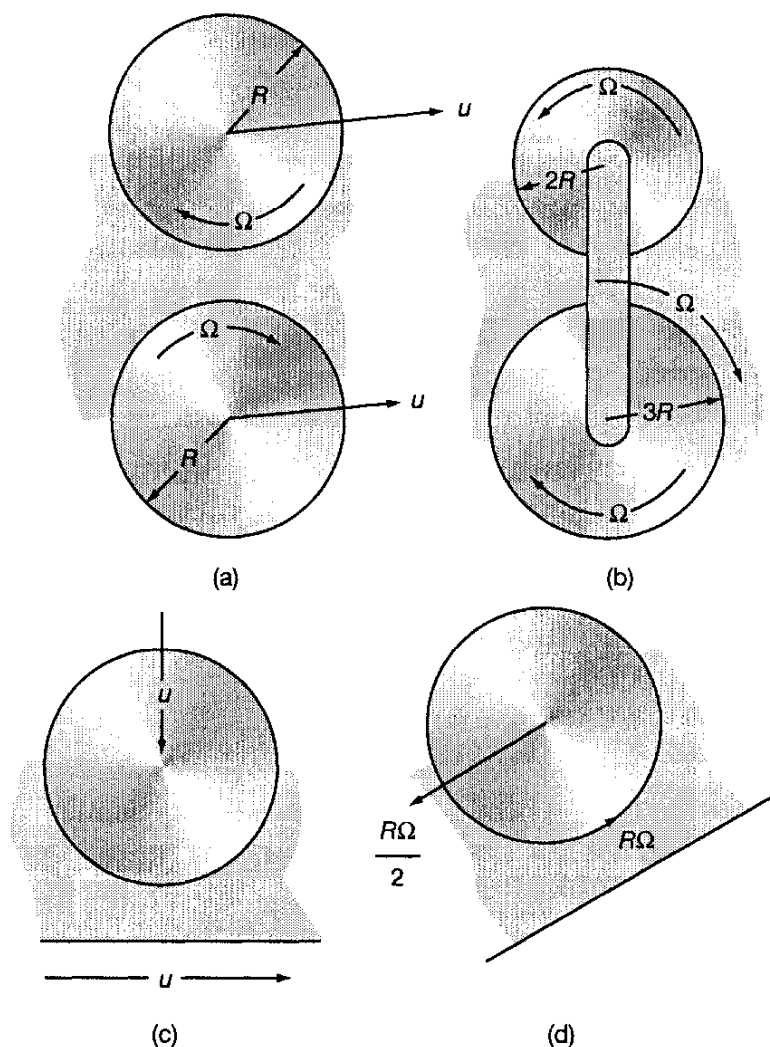
The chapter began with the exploration of various dimensionless numbers that describe the significance of the terms within the Reynolds equation. The Reynolds number compares the inertia and viscous terms; the Froude number compares the inertia and gravity terms. The ratio of the Reynolds number to the Froude number compares the gravity and viscous terms.

The Reynolds equation was derived by coupling the Navier-Stokes equations with the continuity equation and by using laws of viscous flow and the principle of mass conservation. The Reynolds equation contains Poiseuille, physical wedge, stretch, local compression, and normal and transverse squeeze terms. Each of these terms describes a specific type of physical motion, and the physical significance of each term was brought out. Standard forms of the Reynolds equations that are used throughout the text were also discussed. The chapter closed with a description of 13 different sliding and/or normal squeeze motions with the corresponding Reynolds equation.

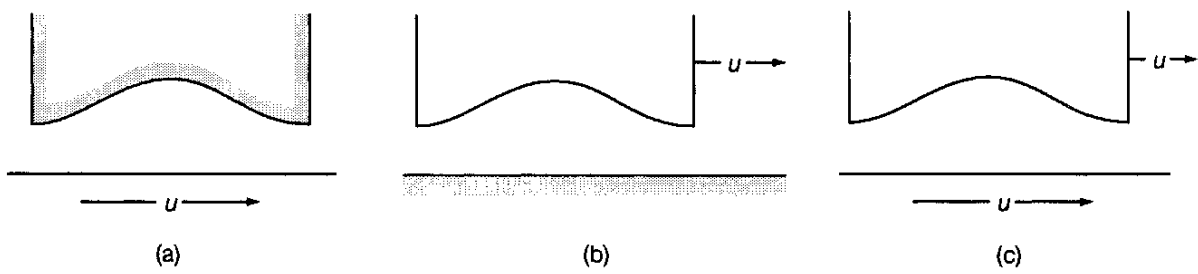
## 7.8 Problems

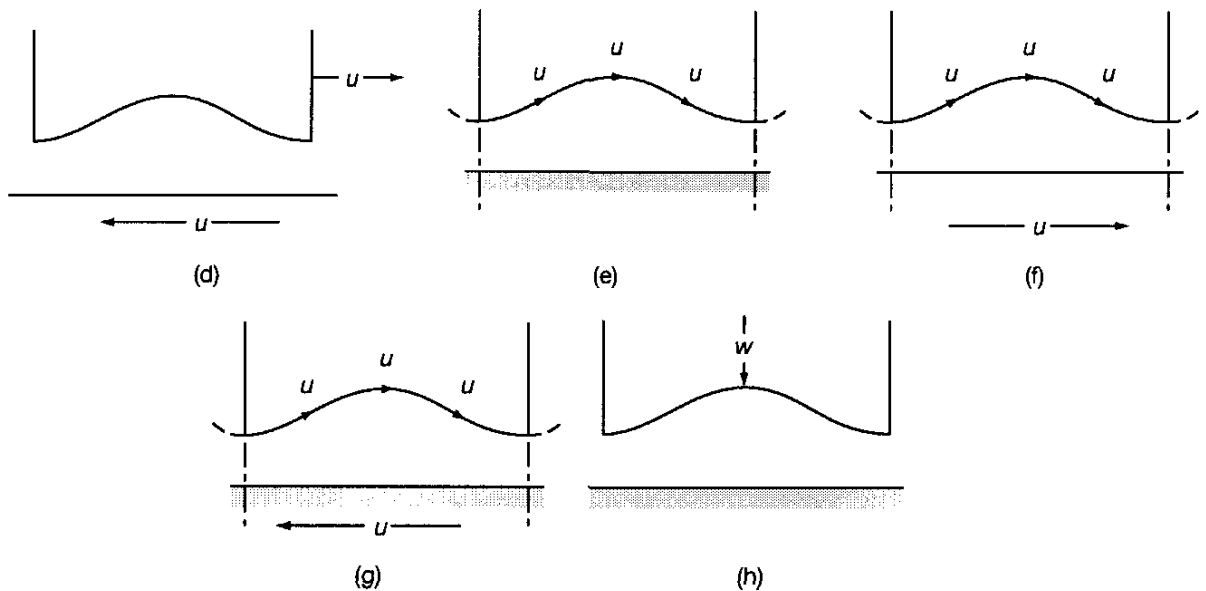
- 7.1 Starting from the Navier-Stokes equations expressed in cylindrical polar coordinates [Eqs. (6.31) to (6.33)] derive the Reynolds equation given in Eq. (7.56). Assume you are applying the cylindrical polar coordinates  $(r, \theta, z)$  to a thrust bearing where  $z$  is in the direction of the lubricating film ( $h$ ) and  $h \ll r$ .
- 7.2 From relationships between Cartesian and cylindrical polar coordinates prove that Eq. (7.47) when the viscosity and density are constant ( $\eta = \eta_0$  and  $\rho = \rho_0$ ) is equivalent to Eq. (7.57).
- 7.3 Compare the Reynolds equation for laminar flow conditions with that appropriate for turbulent flow conditions. Also list operating conditions and applications where turbulence in fluid film distribution is most likely to occur.
- 7.4 A water-lubricated journal bearing in a boiler feed pump has a shaft of radius 0.10 m which rotates at 10 rev/s. The kinematic viscosity in the full fluid film region may be taken as directly proportional to the film thickness and has a value of  $4 \times 10^{-7}$  m<sup>2</sup>/s at a film thickness equal to the radial clearance of 0.10 mm. Determine if the bearing is operating in the laminar or turbulent flow regime. If laminar flow is predicted, what change in these operating conditions would produce the onset of vortex flow.
- 7.5 Write the Reynolds equation for the situations shown below. The circles represent infinitely long cylinders, and all velocities are in relation to a

fixed coordinate system. The lubricant can be assumed to be Newtonian, incompressible, and isoviscous.



- 7.6 For the situation described in each diagram given below, express the appropriate Reynolds equation and sketch the expected pressure distributions. It can be assumed that the bearings are of infinite width and that the lubricant is Newtonian, isoviscous, and incompressible and does not experience cavitation. The shaded members shown in the diagrams are at rest.

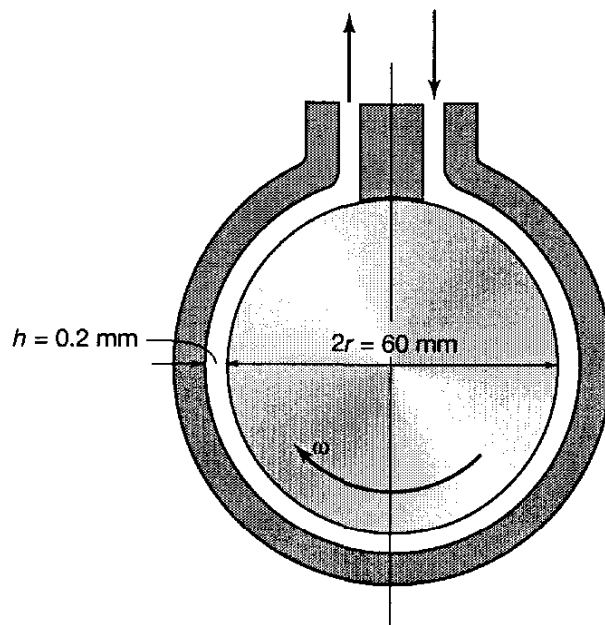




- 7.7 To decrease the leakage past a seal of the type discussed in Example 7.3, the sealing pump is tapered and the film shape is

$$h(x) = h_0 + x \frac{dh}{dx} = h_0 + kx$$

Because of the roughness of the surfaces the outlet (minimum) film thickness  $h_0$  has to be at least 10  $\mu\text{m}$ . Find the optimum film shape to minimize the total leakage past the 10-mm-wide seal during a full work cycle (back and forth) of the piston when the fluid viscosity is 0.075 Pa·s, the piston speed is 0.8 m/s in both directions, the stroke length is 85 mm, the sealing pressure is 1 MPa, and the piston diameter is 50 mm.



- 7.8 An oil pump is designed like a journal bearing with a constant oil film thickness according to the sketch above. The wrap angle is  $320^\circ$ . The

film thickness is 0.2 mm and the oil viscosity is  $0.022 \text{ N}\cdot\text{s}/\text{m}^2$ . The shaft diameter  $2r=60$  mm and the length of the pump in the axial direction is 50 mm. Find the volume pumped per unit time as a function of the resisting pressure at the rotational speed  $N_a=1500$  rpm.

## References

- Constantinescu, V. N. (1962): Analysis of Bearings Operating in Turbulent Regime. *Trans. ASME, Series D, J. Basic Engr.*, vol. 84, no. 1. pp. 139-151.
- Hamrock, B. J., and Dowson, D. (1981): *Ball Bearing Lubrication-The Elasto-hydrodynamics of Elliptical Contacts*. Wiley-Interscience, New York.
- Harrison, W. J. (1913): The Hydrodynamical Theory of Lubrication With Special Reference to Air as a Lubricant. *Trans. Cambridge Philos. Soc.*, xxii (1912-1925), pp. 6-54.
- Reynolds. O. (1886): On the Theory of Lubrication and Its Application to Mr. Beauchamp Tower's Experiments, Including an Experimental Determination of the Viscosity of Olive Oil. *Philos. Trans. R. Soc. London*, vol. 177, pp. 157-234.
- Szeri, A. Z. (ed.) (1980): *Tribology-Friction, Lubrication, and Wear*. Hemisphere Publishing Corp., Washington, D.C.
- Taylor, G. I. (1923): Stability of a Viscous Liquid Contained Between Two Rotating Cylinders. *Philos. Trans. R. Soc. London Ser. A*, vol. 223. pp. 289-343.
- Tower, B. (1883): First Report on Friction Experiments (Friction of Lubricated Bearings). *Proc. Inst. Mech. Eng. (London)*, pp. 632-659.

# Chapter 8

## Hydrodynamic Thrust Bearings - Analytical Solutions

### Symbols

$\tilde{A}, \tilde{B}$	integration constants	$P$	dimensionless pressure, $ps_h^2 / (\eta_0 u_b \ell)$
$b$	width of bearing, m	$P_i$	dimensionless inlet pressure, $p_i s_h^2 / (\eta_0 u_b \ell)$
$C_p$	specific heat of material at constant pressure, $J/(kg \cdot ^\circ C)$	$P_m$	dimensionless pressure where $dp/dx = 0$
$F$	dimensionless shear force	$P_o$	dimensionless outlet pressure, $p_o s_h^2 / (\eta_0 u_b \ell)$
$f'$	tangential (friction) force per unit width, N/m	$p$	pressure, Pa (or N/m <sup>2</sup> )
$g$	acceleration due to gravity (9.8 m/s <sup>2</sup> )	$p_a$	ambient pressure, Pa (or N/m <sup>2</sup> )
$H$	dimensionless film thickness, $h/s_h$	$p_i$	inlet pressure, Pa (or N/m <sup>2</sup> )
$H_m$	dimensionless film thickness where $dP/dX = 0$	$p_m$	pressure where $dp/dx = 0$ , Pa (or N/m <sup>2</sup> )
$H_p$	dimensionless total power loss, $h_p s_h / [\eta_0 u_b^2 \ell (r_o - r_i)]$	$p_o$	outlet pressure, Pa (or N/m <sup>2</sup> )
$h$	film thickness, m	$Q$	dimensionless volume flow rate, $2q'_x / u_b s_h$
$h_m$	film thickness where $dp/dx = 0$ , m	$q$	volumetric flow rate, m <sup>3</sup> /s
$h_o$	outlet film thickness, m	$q'$	volumetric flow rate per unit width, m <sup>2</sup> /s
$h_p$	rate of working against viscous stresses (power loss), N·m/s	$r_i$	inside radius, m
$\ell$	length in $x$ -direction, m	$r_o$	outside radius, m
$N_0$	Number of pads	$s_h$	shoulder height, m
$n_s$	location of parallel step from inlet	$\Delta t_m$	change in temperature, °C
		$u$	velocity in $x$ direction, m/s
		$\bar{u}$	mean surface velocity in $x$ -dir-

	ection, m/s	$y$	cartesian coordinate in side-leakage direction, m
$W_x$	dimensionless tangential load, $w'_x s_h / (\eta_0 u_b \ell)$	$Z$	dimensionless $z$ -coordinate
$W_z$	dimensionless normal load, $w'_z s_h^2 / (\eta_0 u_b \ell^2)$	$Z_{cr}$	critical dimensionless $z$ -coordinate, $z_{cr}/h_o$
$w$	velocity of fluid in $z$ -direction, m/s	$z$	Cartesian coordinate in direction of film, m
$w'$	load per unit width, N/m	$\eta$	absolute viscosity, Pa·s (or N·s/m <sup>2</sup> )
$w_t$	total thrust load, N	$\eta_0$	absolute viscosity at $p = 0$ and constant temperature, Pa·s (or N·s/m <sup>2</sup> )
$X$	dimensionless $x$ coordinate, $x/\ell$	$\mu$	coefficient of sliding friction
$X_{cp}$	dimensionless center of pressure, $x_{cp}/\ell$	$\rho$	density, kg/m <sup>3</sup>
$X_{cr}$	dimensionless critical $x$ coordinate, $x_{cr}/\ell$	$\tau$	shear stress, Pa (or N/m <sup>2</sup> )
$x$	Cartesian coordinate in direction of sliding, m	$\bar{\Phi}$	dimensionless stream function
$x_{cp}$	location of center of pressure in the $x$ direction, m	$\bar{\phi}$	dimensional stream function, m <sup>2</sup> /s
$x_{cr}$	location of critical location of $x$ coordinate, m	$\omega$	angular velocity, rad/s

## 8.1 Introduction

A hydrodynamically lubricated bearing is a bearing that develops load-carrying capacity by virtue of the relative motion of two surfaces separated by a fluid film. The processes occurring in a bearing with fluid film lubrication can be better understood by considering qualitatively the development of oil pressure in such a bearing.

## 8.2 Mechanism of Pressure Development

An understanding of the development of load-supporting pressures in hydrodynamic bearings can be gleaned by considering, from a purely physical point of view, the conditions of geometry and motion required to develop pressure. An understanding of the physical situation can make the mathematics of hydrodynamic lubrication much more meaningful. By considering only what must happen to maintain continuity of flow, much of what the mathematical equations tell us later in this chapter can be deduced.

Figure 8.1 shows velocity profiles for two plane surfaces separated by a constant lubricating film thickness. The plates are extremely wide so that side-leakage flow (into and out of the paper) can be neglected. The upper plate is moving with a velocity  $u_a$ , and the bottom plate is held stationary. No slip occurs at the surfaces. The velocity varies uniformly from zero at surface  $AB$  to  $u_a$  at surface  $A'B'$ , thus implying that the rate of shear  $du/dz$  throughout the oil film is constant. The volume of fluid flowing across section  $AA'$  in unit

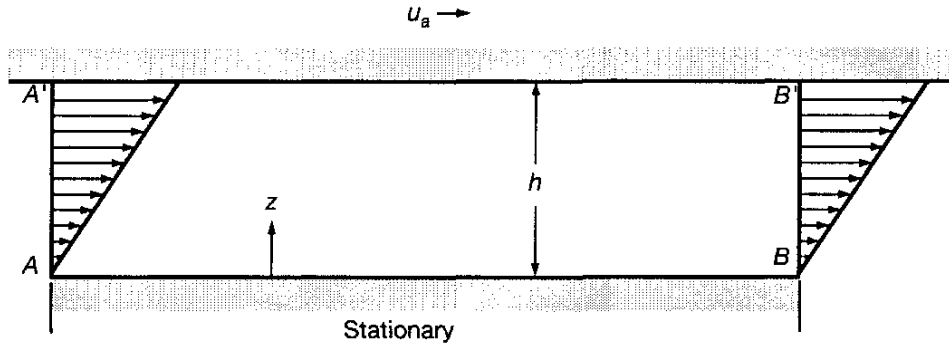


Figure 8.1: Velocity profiles in a parallel-surface slider bearing.

time is equal to that flowing across section  $BB'$ . The flow crossing the two boundaries results only from velocity gradients, and since they are equal, the flow continuity requirement is satisfied without any pressure buildup within the film. Because the ability of a lubricating film to support a load depends on the pressure buildup in the film, a slider bearing with parallel surfaces is not able to support a load by a fluid film. If any load is applied to the surface  $AB$ , the lubricant will be squeezed out and the bearing will operate under conditions of boundary lubrication.

Consider now the case of two nonparallel plates as shown in Fig. 8.2a. Again the width of the plates in the direction perpendicular to the motion is large so that lubricant flow in this direction is negligibly small. The volume of lubricant that the surface  $A'B'$  tends to carry into the space between the surfaces  $AB$  and  $A'B'$  through section  $AA'$  during unit time is  $AC'A'$ . The volume of lubricant that the surface tends to discharge from the space through section  $BB'$  during the same time is  $BD'B'$ . Because the distance  $AA'$  is greater than the distance  $BB'$ , the volume  $AC'A'$  is greater than the volume  $BD'B'$  by the volume  $AEC'$ . From flow continuity the actual volume of oil carried into the space must equal the volume discharged from this space.

It can be surmised that there will be a pressure buildup in the lubricating film until flow continuity is satisfied. The velocity profiles due to Poiseuille flow are shown in Fig. 8.2b. The flow is outward from both the leading and trailing edges of the bearing because flow is always from a region of higher pressure to a region of lower pressure. Note that the pressure flow at boundary  $AA'$  opposes the velocity flow but that the pressure flow at  $BB'$  is in the same direction as the velocity flow.

The results of superimposing Couette and Poiseuille flows are shown in Fig. 8.2c. The form of the velocity distribution curves obtained in this way must satisfy the condition that the flow rate through section  $AA'$  is equal to the flow rate through section  $BB'$ . Therefore, the area  $AHC'A'$  must be equal to the area  $BID'B'$ . The area between the straight, dashed line  $AC'$  and the curve  $AHC'$  in section  $AA'$  and the area between the dashed line  $BD'$  and the curve  $BID'$  represent the pressure-induced flow through these areas.

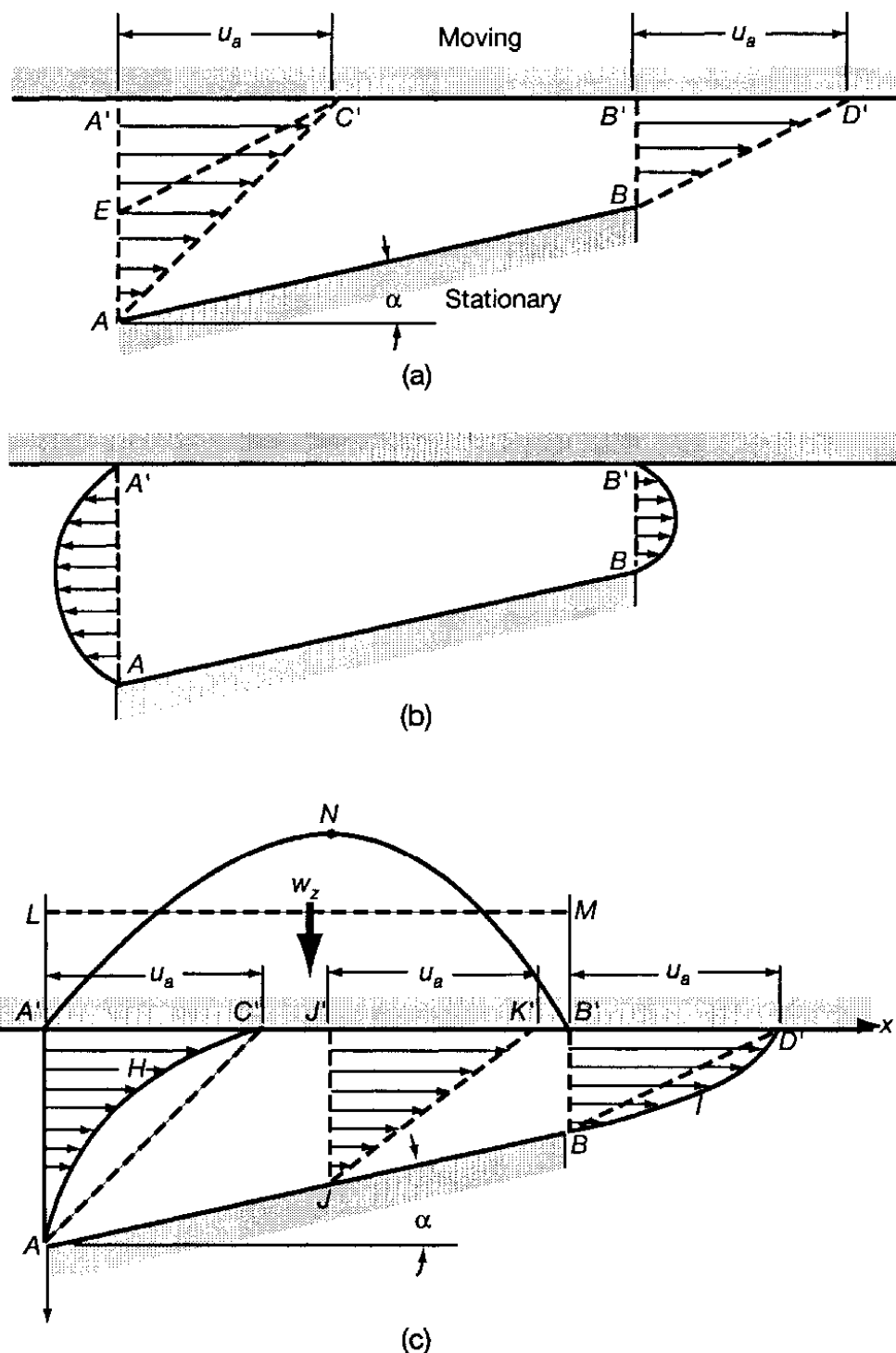


Figure 8.2: Flow within a fixed-incline slider bearing: (a) Couette flow; (b) Poiseuille flow; (c) resulting velocity profile.

The pressure is maximum in section  $JJ'$ , somewhere between sections  $AA'$  and  $BB'$ . There is no Poiseuille flow contribution in section  $JJ'$ , since the pressure gradient is zero at this location and all the flow is Couette. Note that continuity of flow is satisfied in that triangle  $JK'J'$  is equal to the areas  $AHC'A'$  and  $BID'B'$ .

## 8.3 General Thrust Bearing Theory

Solutions of the Reynolds equation for real bearing configurations are usually obtained in approximate numerical form. Analytical solutions are possible only for the simplest problems. By restricting the flow to two dimensions, say the  $x$ - $z$  plane, analytical solutions for many common bearing forms become available. The quantitative value of these solutions is limited, since flow in the third dimension  $y$ , which is known as "side leakage," plays an important part in fluid film bearing performance. The two-dimensional solutions have a definite value, since they provide a good deal of information about the general characteristics of bearings, information that leads to a clear physical picture of the performance of lubricating films.

Besides neglecting side leakage, another simplification is achieved by neglecting the pressure and temperature effects of the lubricant properties, namely, viscosity and density. The viscosity of common lubricants is particularly sensitive to temperature, and since the heat generated in hydrodynamic bearings is often considerable, the limitation imposed by this assumption is at once apparent.

Introducing variable viscosity and density into the analysis creates considerable complications, even in the case of two-dimensional flow. The temperature rise within the film can be calculated if it is assumed that all the heat produced by the viscous action is carried away by the lubricant (the adiabatic assumption).

From Chapter 7, Eq. (7.52), the two-dimensional Reynolds equation expressed in integrated form for constant density can be written as

$$\frac{dp}{dx} = 12\tilde{u}\eta \frac{h - h_m}{h^3} \quad (7.52)$$

This equation is used in this chapter as the starting point for analyzing various thrust bearing configurations. Before proceeding with the various film configurations in thrust bearings, more needs to be said about thrust bearings in general.

Many loads carried by rotary machinery have components that act in the direction of the shaft's axis of rotation. These thrust loads are frequently carried by self-acting or hydrodynamic bearings of the form shown in Fig. 8.3. A thrust plate attached to, or forming part of, the rotating shaft is separated from the sector-shaped bearing pads by a lubricant film. The load-carrying capacity of the bearing arises entirely from the pressures generated by the geometry of the thrust plate over the bearing pads. What was physically observed earlier

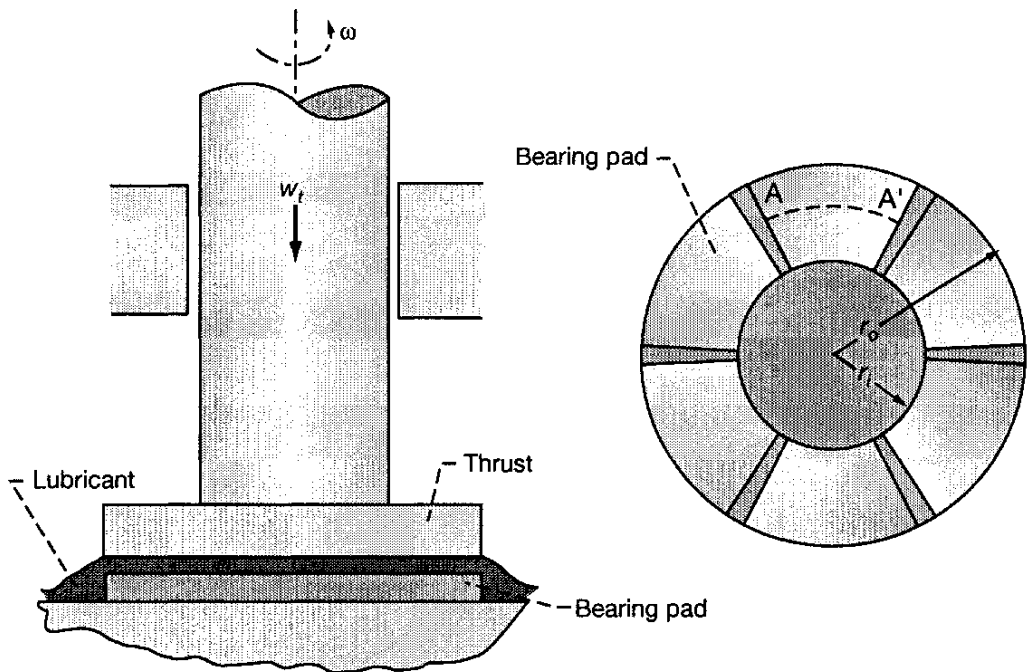


Figure 8.3: Thrust bearing geometry.

in this chapter will be demonstrated analytically, that this lubricating action is achieved only if the clearance space between the stationary and moving components is provided with certain geometrical forms.

It is clear that the lubricant flow between the thrust plate and the bearing pads represents a three-dimensional flow problem. However, for the present purpose, flow in the radial direction is neglected. In this chapter each pad is analyzed along a section formed by the mean arc  $AA'$ , as shown in Fig. 8.3. The effect of curvature on this section is neglected, the oil film geometry being represented by the  $x$ - $z$  plane. This simple representation allows the total load-carrying capacity of the thrust bearing to be written as

$$w_t = N_0 w'_z (r_o - r_i) \quad (8.1)$$

where

$N_0$  = number of pads in thrust bearing

$w'_z$  = normal load-carrying capacity per unit width of one pad, N/m

This expression will lead to an overestimate of the load-carrying capacity for a given oil film thickness, since lubricant flow in the radial direction (side-leakage direction) will tend to reduce the mean oil film pressure. Side-leakage effects are considered in Chapter 9.

Results from the analysis of various bearing configurations are expressed in dimensionless form for ease in comparing the important bearing characteristics. The following general definitions and relationships are employed. The definitions should be related to the bearing geometry shown in Fig. 8.4.

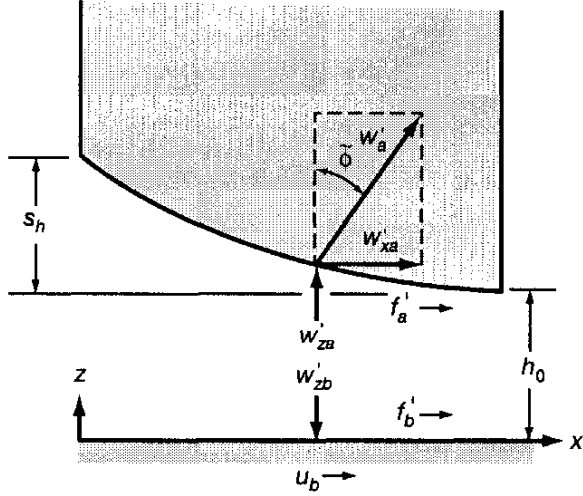


Figure 8.4: Force components and oil film geometry in a hydrodynamically lubricated thrust sector.

The forces acting on the solids can be considered in two groups. The loads, which act in the direction normal to the surface, yield normal loads that can be resolved into components  $w'_x$  and  $w'_z$ . The viscous surface stresses, which act in the direction tangent to the surface, yield shear forces on the solids that have components  $f'$  in the  $x$  direction. The component of the shear forces in the  $z$  direction is negligible.

Once the pressure is obtained for a particular film configuration from the Reynolds equation, the following force components act on the solids:

$$w'_{za} = w'_{zb} = \int_0^\ell p dx \quad (8.2)$$

$$w'_{xb} = 0 \quad (8.3)$$

$$w'_{za} = - \int_{h_0+s_h}^{h_0} p dh = - \int_0^\ell p \frac{dh}{dx} dx$$

$$\therefore w'_{za} = -(ph)_0^\ell + \int_0^\ell h \frac{dp}{dx} dx = \int_0^\ell h \frac{dp}{dx} dx \quad (8.4)$$

$$w'_b = \left( w'_{zb}^2 + w'_{xb}^2 \right)^{1/2} = w'_{zb} \quad (8.5)$$

$$w'_a = \left( w'_{za}^2 + w'_{xa}^2 \right)^{1/2} \quad (8.6)$$

$$\tilde{\phi} = \tan^{-1} \frac{w'_{xa}}{w'_{za}} \quad (8.7)$$

Shear forces per unit width acting on the solids are

$$f'_b = \int_0^\ell (\tau_{zx})_{z=0} dx$$

Substituting Eq. (7.32) into this equation gives

$$f'_b = \int_0^\ell \left( -\frac{h}{2} \frac{dp}{dx} - \frac{\eta u_b}{h} \right) dx$$

Making use of Eq. (8.4) gives

$$f'_b = -\frac{w'_{xa}}{2} - \int_0^\ell \frac{\eta u_b}{h} dx \quad (8.8)$$

Similarly, the shear force per unit width acting on solid *a* is

$$f'_a = - \int_0^\ell (\tau_{zx})_{z=h} dx = -\frac{w'_{xa}}{2} + \int_0^\ell \frac{\eta u_b}{h} dx \quad (8.9)$$

Note from Fig. 8.4 that

$$f'_b + f'_a + w'_{xa} = 0 \quad (8.10)$$

$$w'_{zb} - w'_{za} = 0 \quad (8.11)$$

These equations represent the condition of static equilibrium.

The viscous stresses generated by the shearing of the lubricant film give rise to a resisting force of magnitude  $-f_b$  on the moving surface. The rate of working against the viscous stresses, or power loss, for one pad is

$$h_p = -f_b u_b = -f'_b (r_o - r_i) u_b \quad (8.12)$$

The work done against the viscous stresses appears as heat within the lubricant. Some of this heat may be transferred to the surroundings by radiation or by conduction, or it may be convected from the clearance space by the lubricant flow.

The bulk temperature rise of the lubricant for the case in which all the heat is carried away by convection is known as the "adiabatic temperature rise." This bulk temperature increase can be calculated by equating the rate of heat generated within the lubricant to the rate of heat transferred by convection:

$$h_p = \rho q C_p (\Delta t_m)$$

Or the adiabatic temperature rise in degrees Celsius may be expressed as

$$\Delta t_m = \frac{h_p}{\rho q C_p} \quad (8.13)$$

where

$\rho$  = density of lubricant,  $\text{kg}/\text{m}^3$

$q$  = volume flow rate in direction of motion,  $\text{m}^3/\text{s}$

$C_p$  = specific heat of material at constant pressure,  $\text{J}/(\text{kg}\cdot^\circ\text{C})$

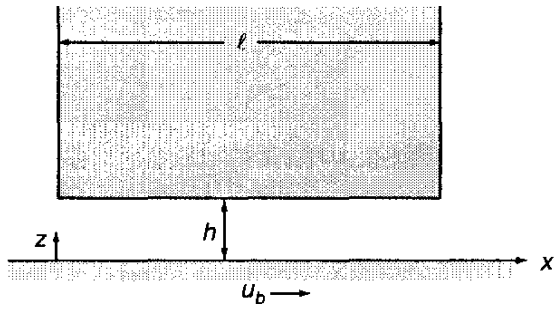


Figure 8.5: Parallel-surface slider bearing.

Some of the relevant equations used in thrust bearing analysis having been defined, attention will be focused on three simple slider bearings: (1) parallel surface, (2) fixed incline, and (3) parallel step. The same nondimensionalization is used to define the resulting performance parameters for all three types of bearing so that they can be directly compared. Throughout this chapter it is assumed that the pressure-generating mechanism is the physical wedge as discussed in Sec. 7.4.3.

## 8.4 Parallel-Surface Sliding Bearing

Figure 8.5 shows a parallel-surface slider bearing. The film thickness is constant for the entire bearing length. Using the Reynolds equation defined in Eq. (7.48) while neglecting the side-leakage term and assuming a constant film thickness gives the reduced Reynolds equation of

$$\frac{d^2 p}{dx^2} = 0 \quad (8.14)$$

Integrating twice gives

$$p = \tilde{A}x + \tilde{B}$$

The boundary conditions are:

1.  $p = 0$  at  $x = 0$ .

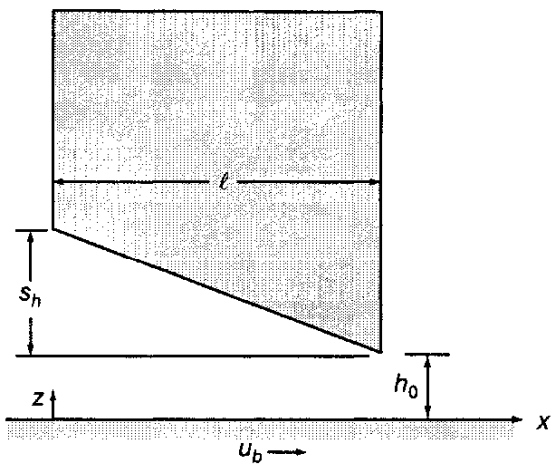


Figure 8.6: Fixed-incline slider bearing.

2.  $p = 0$  at  $x = \ell$ .

Making use of these boundary conditions gives  $p = 0$ . Hence, a parallel-surface slider bearing does not develop pressure due to the physical wedge mechanism. Having no pressure development implies that this type of bearing will not be able to support a load. This is the same conclusion arrived at earlier in the chapter (Sec. 8.2) from physical arguments.

## 8.5 Fixed-Incline Slider Bearing

Figure 8.6 shows a fixed-incline slider bearing. A fixed-incline slider consists of two nonparallel plane surfaces separated by an oil film. One surface is stationary while the other moves with a uniform velocity. The direction of motion and the inclination of planes are such that a converging oil film is formed between the surfaces and the physical wedge pressure-generating mechanism (described in Sec. 7.4.3) is developed in the oil film; it is this pressure-generating mechanism that makes the bearing able to support a load.

### 8.5.1 Pressure Distribution

The analysis of this type of bearing begins with the integrated form of the Reynolds equation as expressed in Eq. (7.52). The only change to this equation is that  $u_a = 0$  and a constant viscosity  $\eta_0$  is assumed.

$$\frac{dp}{dx} = 6\eta_0 u_b \frac{h - h_m}{h^3} \quad (8.15)$$

where  $h_m$  is the film thickness when  $dp/dx = 0$ .

The oil film thickness can be written as a function of  $x$ :

$$h = h_o + s_h \left(1 - \frac{x}{\ell}\right) \quad (8.16)$$

Choosing to write the film thickness and pressure in dimensionless terms, where

$$P = \frac{ps_h^2}{\eta_0 u_b \ell} \quad H = \frac{h}{s_h} \quad H_m = \frac{h_m}{s_h} \quad H_o = \frac{h_o}{s_h} \quad X = \frac{x}{\ell} \quad (8.17)$$

causes Eqs. (8.15) and (8.16) to become

$$\frac{dP}{dX} = 6 \left( \frac{H - H_m}{H^3} \right) \quad (8.18)$$

$$H = \frac{h}{s_h} = H_o + 1 - X \quad (8.19)$$

$$\frac{dH}{dX} = -1 \quad (8.20)$$

Integrating Eq. (8.18) gives

$$P = 6 \int \left( \frac{1}{H^2} - \frac{H_m}{H^3} \right) dX$$

Making use of Eq. (8.20) in the preceding equation gives

$$\begin{aligned} P &= -6 \int \left( \frac{1}{H^2} - \frac{H_m}{H^3} \right) dH \\ \therefore P &= 6 \left( \frac{1}{H} - \frac{H_m}{2H^2} \right) + \tilde{A} \end{aligned} \quad (8.21)$$

The boundary conditions are

1.  $P=0$  when  $X=0 \rightarrow H = H_o + 1$ .
2.  $P=0$  when  $X=1 \rightarrow H = H_o$ .

Making use of boundary conditions 1 and 2 gives

$$H_m = \frac{2H_o(1+H_o)}{1+2H_o} \quad (8.22)$$

and

$$\tilde{A} = -\frac{6}{1+2H_o} \quad (8.23)$$

Substituting Eqs. (8.22) and (8.23) into (8.21) gives

$$P = \frac{6X(1-X)}{(H_o + 1 - X)^2(1 + 2H_o)} \quad (8.24)$$

Note that the dimensionless pressure is a function of  $X$  and  $H_o$ . The variation of  $P$  with  $X$  for various values of  $H_o$  is shown in Fig. 8.7. It can be seen that the pressure distribution increases with decreasing  $H_o$ . Recall that  $H_o = h_o/s_h$ . Therefore, if the shoulder height  $s_h$  remains fixed, Fig. 8.7 indicates that as the outlet film thickness  $h_o$  becomes smaller, the pressure profile increases without any limits. This figure also shows that for large  $H_o$  there is little pressure buildup in a fixed-incline thrust bearing.

Evaluating the film thickness at the location where the pressure gradient is equal to zero gives

$$H_m = H_0 + 1 - X_m$$

Making use of Eq. (8.22) gives

$$X_m = \frac{1+H_o}{1+2H_o} \quad (8.25)$$

As  $H_o \rightarrow 0$ , the location of the maximum pressure  $X_m \rightarrow 1$ , but as  $H_o \rightarrow \infty$ ,  $X_m \rightarrow 1/2$ . Note that  $H_o \rightarrow 0$  implies that either  $h_o \rightarrow 0$  or  $s_h \rightarrow \infty$ , but

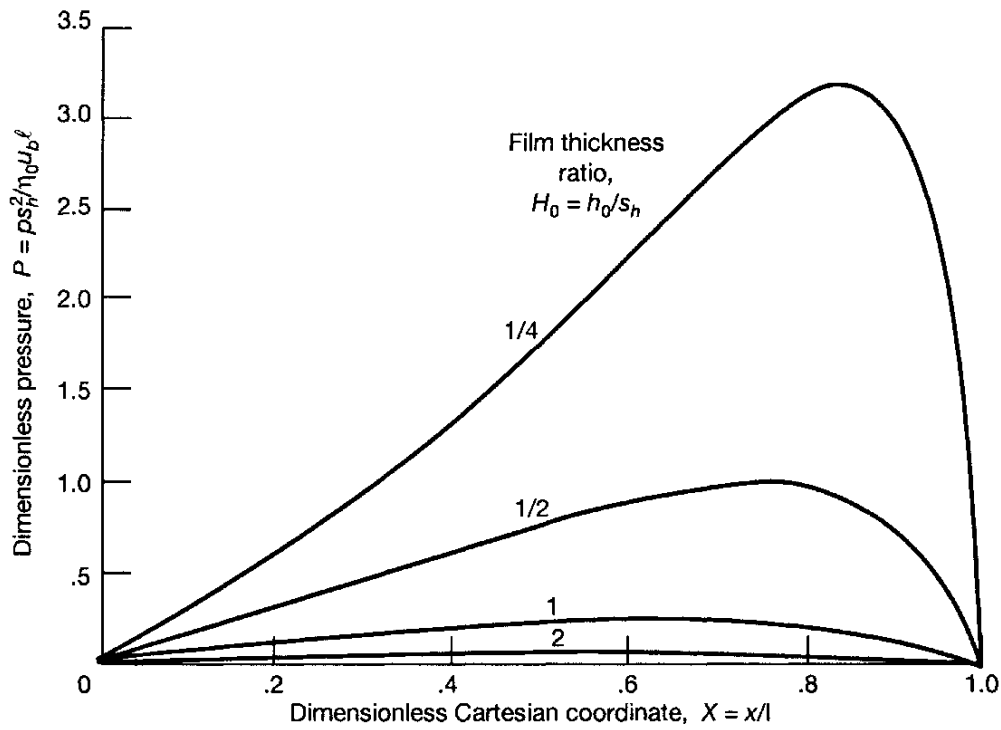


Figure 8.7: Pressure distributions of fixed-incline slider bearing.

$H_o \rightarrow \infty$  implies that either  $h_o \rightarrow \infty$  or  $s_h \rightarrow 0$ . The situation of  $s_h \rightarrow 0$  implies parallel surfaces, but as concluded in Sec. 8.4, parallel surfaces do not develop pressure.

With the location of the maximum pressure defined by Eq. (8.25), the maximum pressure can be found directly from Eq. (8.24), which when  $X = X_m$  gives

$$P_m = \frac{3}{2H_o(1+H_o)(1+2H_o)} \quad (8.26)$$

Note that as  $H_o \rightarrow 0$ ,  $P_m \rightarrow \infty$  and that as  $H_o \rightarrow \infty$ ,  $P_m \rightarrow 0$ . This corresponds to the conclusion made earlier while discussing Fig. 8.7. Equation (8.26) can be expressed in dimensional terms as

$$p_m = \frac{3\eta_0 u_b l s_h}{2h_o(s_h + h_o)(s_h + 2h_o)} \quad (8.27)$$

From Eq. (8.27) it is observed that  $s_h \rightarrow 0$ , which corresponds to a parallel film, and  $s_h \rightarrow \infty$  both produce  $p_m \rightarrow 0$ .

The shoulder height that produces a maximum pressure can be obtained from  $\partial p_m / \partial s_h = 0$ . Evaluating this gives

$$(s_h)_{\text{opt}} = \sqrt{2}h_o \quad (8.28)$$

Equation (8.28) will be helpful in practical designs, since if a description of the surface is known, one can (e.g., from Table 9.2) predict what the minimum

outlet film thickness should be. The shoulder height can then be established by using a safety factor and Eq. (8.28).

### 8.5.2 Normal Load Component

The normal load per unit width can be written as

$$w'_z = \int_o^\ell p dx$$

This equation can be written in dimensionless form by making use of Eq. (8.17).

$$W_z = \frac{w'_z s_h^2}{\eta_0 u_b \ell^2} = \int_0^1 P dX$$

Because  $dH/dX = -1$ , as shown in Eq. (8.20),

$$W_z = - \int_{H_o+1}^{H_o} P dH \quad (8.29)$$

Substituting Eqs. (8.21) to (8.23) into this equation gives

$$W_z = 6 \ln \left( \frac{H_o + 1}{H_o} \right) - \frac{12}{1 + 2H_o} \quad (8.30)$$

The variation of  $W_z$  with  $H_o$ , shown in Fig. 8.8, suggests that as  $H_o \rightarrow 0$ , this bearing has a tremendous potential to support a load. These results should be tempered by the knowledge of the assumptions imposed in getting this result, namely, that side leakage was neglected and smooth surfaces and isothermal conditions were assumed.

### 8.5.3 Tangential Force Components

The force per unit width in the direction of motion due to pressure being developed is

$$w'_{xb} = 0$$

$$w'_{xa} = - \int_{h_o+s_h}^{h_o} p dh$$

By making use of Eq. (8.17) the preceding equation may be expressed in dimensionless form as

$$W_{xa} = \frac{w'_{xa}}{\eta_0 u_b} \frac{s_h}{\ell} = - \int_{H_o+1}^{H_o} P dH = W_z \quad (8.31)$$

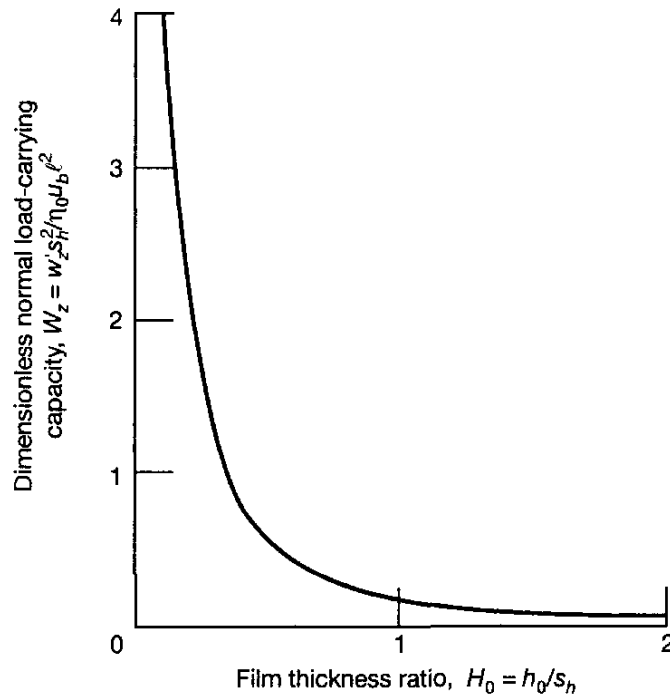


Figure 8.8: Effect of film thickness ratio on normal load-carrying capacity.

#### 8.5.4 Shear Force Components

The shear force components per unit width acting on the solids are

$$f'_b = \int_0^\ell (\tau_{zx})_{z=0} dx = \int_0^\ell \left( \eta_0 \frac{\partial u}{\partial z} \right)_{z=0} dx$$

$$f'_a = \int_0^\ell (-\tau_{zx})_{z=h} dx = - \int_0^\ell \left( \eta_0 \frac{\partial u}{\partial z} \right)_{z=h} dx$$

The viscous shear stresses were defined in Chapter 7 [Eqs. (7.32) and (7.33)]. Making use of these equations while letting  $u_a = 0$  and assuming a constant viscosity gives

$$f'_b = - \int_0^\ell \left( \frac{h}{2} \frac{dp}{dx} + \frac{u_b \eta_0}{h} \right) dx$$

$$f'_a = - \int_0^\ell \left( \frac{h}{2} \frac{dp}{dx} - \frac{u_b \eta_0}{h} \right) dx$$

Equation (8.17) can be used to put these equations in dimensionless form:

$$F_b = \frac{f'_b}{\eta_0 u_b} \frac{s_h}{\ell} = - \int_0^1 \left( \frac{H}{2} \frac{dP}{dX} + \frac{1}{H} \right) dX$$

$$F_a = \frac{f'_a}{\eta_0 u_b} \frac{s_h}{\ell} = - \int_0^1 \left( \frac{H}{2} \frac{dP}{dX} - \frac{1}{H} \right) dX$$

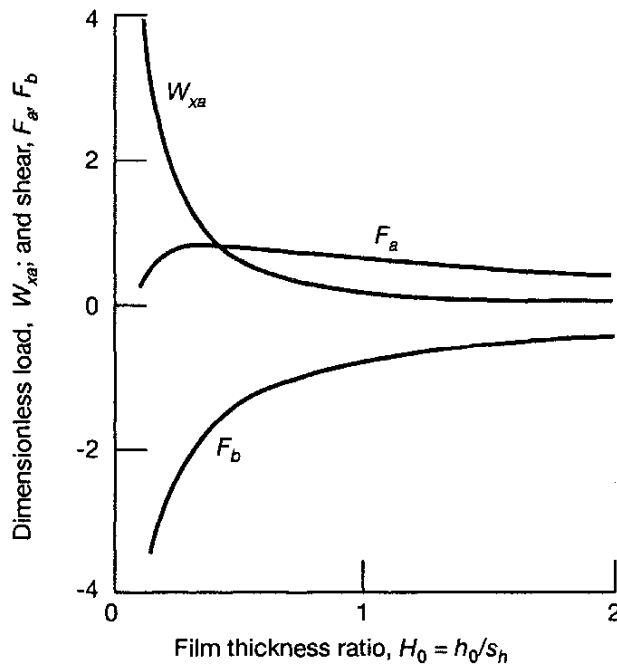


Figure 8.9: Effect of film thickness ratio on force components.

By making use of Eqs. (8.18) and (8.19) the preceding equations can be expressed as

$$F_b = 4 \ln \left( \frac{H_o}{H_o + 1} \right) + \frac{6}{1 + 2H_o} \quad (8.32)$$

$$F_a = 2 \ln \left( \frac{H_o}{H_o + 1} \right) + \frac{6}{1 + 2H_o} \quad (8.33)$$

The dimensionless force components  $W_{xa}$ ,  $F_b$ , and  $F_a$  are plotted as functions of  $H_0$  in Fig. 8.9. Note that the dimensionless force components  $W_{xa}$ ,  $F_b$ , and  $F_a$  have the term  $s_h/\ell$ , whereas  $W_z$  has the term  $(s_h/\ell)^2$ .

### 8.5.5 Friction Coefficient

The friction coefficient can be expressed as

$$\mu = -\frac{f'_b}{w'_{zb}} = \frac{f'_a + w'_{xa}}{w'_{za}}$$

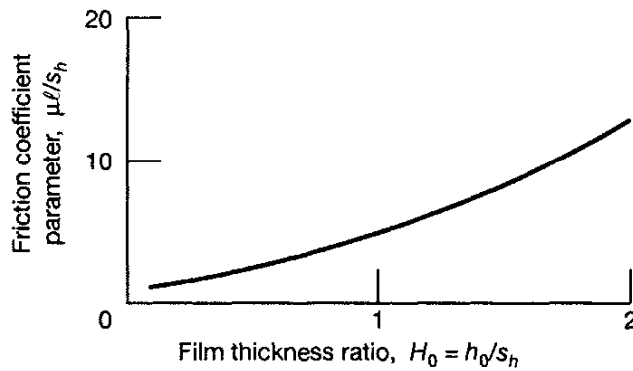


Figure 8.10: Effect of film thickness ratio on friction coefficient parameter.

Making use of Eqs. (8.30) and (8.32) gives

$$\mu = \frac{2s_h \ln\left(\frac{H_o}{H_o + 1}\right) + \frac{3s_h}{1 + 2H_o}}{3\ell \ln\left(\frac{H_o}{H_o + 1}\right) + \frac{6\ell}{1 + 2H_o}} \quad (8.34)$$

The variation of  $\mu\ell/s_h$  with  $H_0$  is shown in Fig. 8.10. Note that as  $H_0 \rightarrow 0$ , the friction coefficient approaches zero. This implies that the normal load component becomes much larger than the tangential load component as  $h_0$  decreases.

### 8.5.6 Volume Flow Rate

The volume flow rate per unit width can be expressed from Chapter 7 as

$$q'_x = -\frac{h^3}{12\eta} \frac{\partial p}{\partial x} + \frac{h(u_b + u_a)}{2} \quad (7.38)$$

Evaluating the flow rate where  $dp/dx = 0$  and setting  $u_a = 0$  gives the volume flow rate as

$$q'_x = \frac{u_b h_m}{2} \quad (8.35)$$

The dimensionless volume flow rate can be expressed as

$$Q = \frac{2q'_x}{u_b s_h} = H_m = \frac{2H_o(1 + H_o)}{1 + 2H_o} \quad (8.36)$$

The dimensionless volume flow rate  $Q$  is plotted as a function of  $H_0$  in Fig. 8.11. This figure shows that as  $H_0$  increases, the dimensionless volume flow rate increases.

### 8.5.7 Power Loss and Temperature Rise

The total rate of working against the viscous stresses, or the power loss, can be expressed from Eq. (8.12) as

$$h_p = -f_b u_b = -f'_b (r_o - r_i) u_b \quad (8.12)$$

Expressed in dimensionless form,

$$H_p = \frac{h_p s_h}{\eta_0 u_b^2 \ell (r_o - r_i)} = -\frac{f'_b s_h}{\eta_0 u_b \ell} = -F_b = -4 \ln\left(\frac{H_o}{H_o + 1}\right) - \frac{6}{1 + 2H_o} \quad (8.37)$$

All the heat produced by viscous shearing is assumed to be carried away by the lubricant (adiabatic condition). The bulk temperature increase can be

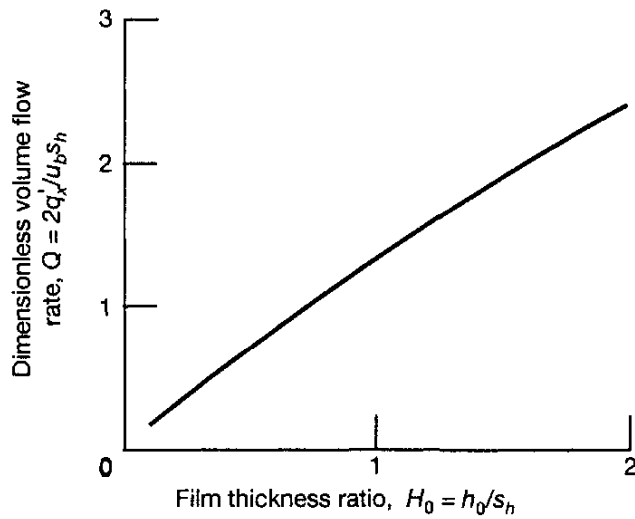


Figure 8.11: Effect of film thickness ratio on dimensionless volume flow rate.

calculated by equating the rate of heat generated within the lubricant to the rate of heat transferred by convection. Therefore, from Eq. (8.13) the lubricant's temperature rise is

$$\Delta t_m = \frac{h_p}{\rho_0 q'_x C_p} = \frac{2 u_b \ell \eta_0}{\rho_0 C_p s_h^2} \frac{H_p}{Q} \quad (8.13)$$

where

$\rho_0$  = constant lubricant density,  $\text{kg}/\text{m}^3$

$q'_x$  = volume flow rate per unit width in sliding direction,  $\text{m}^2/\text{s}$

$C_p$  = specific heat at constant pressure,  $\text{J}/(\text{kg}\cdot^\circ\text{C})$

The dimensionless temperature rise may be expressed as

$$\frac{\rho_0 C_p s_h^2}{2 u_b \ell \eta_0} \Delta t_m = \frac{H_p}{Q} = \frac{2(1 + 2H_o)}{H_o(1 + H_o)} \ln \left( \frac{H_o + 1}{H_o} \right) - \frac{3}{(1 + H_o) H_o} \quad (8.38)$$

Figure 8.12 shows the effect of film thickness ratio on dimensionless adiabatic temperature rise. As  $H_0 \rightarrow 0$ , the dimensionless adiabatic temperature rise approaches infinity.

### 8.5.8 Center of Pressure

The location of the center of pressure  $x_{cp}$  indicates the position at which the resulting force is acting. The expression for calculating the location is

$$w'_z x_{cp} = \int_0^\ell p x \, dx = \frac{\eta_0 u_b \ell^3}{s_h^2} \int_0^1 P X \, dX$$

Therefore, the dimensionless center of pressure can be written as

$$X_{cp} = \frac{x_{cp}}{\ell} = \frac{1}{W_z} \int_0^1 P X \, dX \quad (8.39)$$

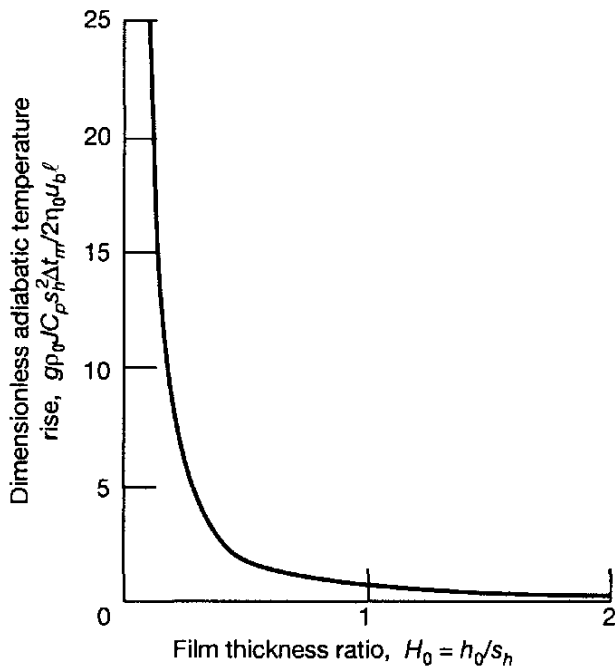


Figure 8.12: Effect of film thickness ratio on dimensionless adiabatic temperature rise.

Substituting Eqs. (8.19) to (8.21) into (8.39) gives

$$X_{cp} = -\frac{6}{W_z(1+2H_o)} \left[ (H_o + 1)(3H_o + 1) \ln \left( \frac{H_o}{H_o + 1} \right) + 3H_o + \frac{5}{2} \right] \quad (8.40)$$

Figure 8.13 shows the effect of film thickness ratio on center of pressure. The center of pressure is always more toward the outlet than toward the inlet ( $X_{cp} > 0.5$ ).

### 8.5.9 Velocity Profile and Stream Function

From Eq. (7.28) for a stationary top surface ( $u_a = 0$ ), the fluid velocity can be written as

$$u = -\frac{z(h-z)}{2\eta_0} \frac{dp}{dx} + \frac{u_b(h-z)}{h} \quad (8.41)$$

By using Eq. (8.17) this equation can be expressed in dimensionless form as

$$\frac{u}{u_b} = \left( 1 - \frac{Z}{H} \right) \left( 1 - \frac{ZH}{2} \frac{dP}{dX} \right) \quad (8.42)$$

where

$$Z = \frac{z}{s_h} \quad \text{and} \quad 0 \leq Z \leq H \quad (8.43)$$

From Eq. (8.42),  $u/u_b = 0$  when

1.  $Z_{cr} = H$

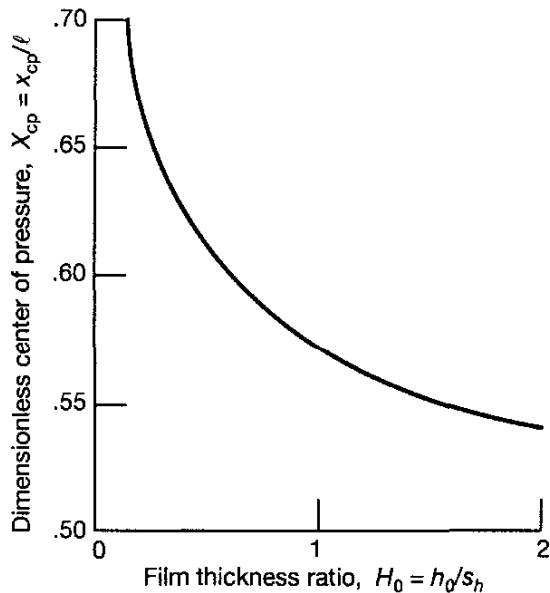


Figure 8.13: Effect of film thickness ratio on dimensionless center of pressure.

or at the top surface

2.

$$Z_{cr} = \frac{2}{H(dP/dX)} \quad (8.44)$$

Note that condition 2 can only exist when  $dP/dX > 0$  and thus when  $X < X_m$ .

Substituting Eq. (8.18) into Eq. (8.44) while making sure that the inequality in Eq. (8.43) is satisfied gives

$$0 \leq 2H - 3H_m \quad (8.45)$$

Making use of Eqs. (8.19) and (8.22) gives this inequality as

$$X \leq \frac{1 - H_o^2}{2H_o + 1} \quad (8.46)$$

This inequality is only satisfied if  $H_o \leq 1$ . This then implies that reverse flow exists when

$$H_o \leq 1 \quad \text{and} \quad X \leq \frac{1 - H_o^2}{2H_o + 1} \quad (8.47)$$

If these inequalities are satisfied, then  $dP/dX > 0$  and  $X < X_m$ .

Substituting Eq. (8.18) into Eq. (8.42) gives

$$\frac{u}{u_b} = \left(1 - \frac{Z}{H}\right) \left[1 - \frac{3Z}{H} \left(1 - \frac{H_m}{H}\right)\right] \quad (8.48)$$

where

$$\frac{Z}{H} = \frac{Z}{H_o + 1 - X} \quad (8.49)$$

$$\frac{H_m}{H} = \frac{2H_o(1+H_o)}{(1+2H_o)(H_o+1-X)} \quad (8.50)$$

Thus,  $u/u_b$  is just a function of  $X$ ,  $Z$ , and  $H_0$ .

A “streamline” is a type of curve that has been used to describe the flow of fluid. More specifically, a streamline is a curve everywhere parallel to the direction of the fluid flow. Surface boundaries are streamlines, since the fluid cannot cross the surface boundary. The definition of a streamline may be given mathematically, while neglecting the side-leakage term, as

$$\frac{dx}{u} = \frac{dz}{w} \quad (8.51)$$

The continuity equation given by Eq. (6.48) can be satisfied while neglecting the side-leakage term by introducing a new function defined by

$$u = \frac{\partial \bar{\phi}}{\partial z} \quad \text{and} \quad w = -\frac{\partial \bar{\phi}}{\partial x} \quad (8.52)$$

where  $\bar{\phi}$  is a function of  $x$  and  $z$  and is called the “stream function.” By using the chain rule of partial differentiation the total derivative of  $\phi$  can be expressed as

$$d\bar{\phi} = \frac{\partial \bar{\phi}}{\partial x} dx + \frac{\partial \bar{\phi}}{\partial z} dz \quad (8.53)$$

Making use of Eq. (8.52) gives

$$d\bar{\phi} = -wdx + udz \quad (8.54)$$

If  $d\bar{\phi}$  is set equal to zero, we obtain the definition of a streamline given in Eq. (8.51). That is, lines of constant  $\bar{\phi}$  represent streamlines.

Equation (8.52) can also be expressed in dimensionless terms of a stream function  $\bar{\Phi}$  as

$$\frac{u}{u_b} = \frac{1}{u_b} \frac{\partial \bar{\phi}}{\partial z} = \frac{\partial \bar{\Phi}}{\partial Z} \quad (8.55)$$

where  $\bar{\Phi} = \bar{\phi}/u_b s_h$ . Substituting Eq. (8.42) into this equation and integrating gives

$$\bar{\Phi}(X, Z) = \frac{Z^3}{6} \frac{dP}{dX} - \frac{Z^2}{2H} \left( 1 + \frac{H^2}{2} \frac{dP}{dX} \right) + Z = \text{constant} \quad (8.56)$$

This equation can be easily evaluated by using Eqs. (8.18), (8.19), and (8.22).

Also from the continuity equation, while neglecting the side-leakage term, the velocity in the  $z$  direction can be written as

$$\begin{aligned} w &= \int \left( -\frac{\partial u}{\partial x} \right) dz = \frac{s_h u_b}{\ell} \int \left( -\frac{\partial (u/u_b)}{\partial X} \right) dZ \\ \therefore \frac{w}{u_b s_h} &= - \int_0^Z \left[ \frac{\partial (u/u_b)}{\partial H} \right] \frac{\partial H}{\partial X} dZ = \int_0^Z \left( \frac{\partial (u/u_b)}{\partial H} \right) dZ \end{aligned}$$

Substituting Eq. (8.48) into this equation gives

$$\frac{w\ell}{u_b s_h} = \left( Z^2 - \frac{Z^3}{H} \right) \left( \frac{2}{H^2} - \frac{3H_m}{H^3} \right) = \frac{Z^2}{H^4} (Z - H)(3H_m - 2H) \quad (8.57)$$

Note from this equation that  $w/u_b (\ell/s_h) = 0$  when  $Z = 0$ , when  $Z = H$ , and at  $H = \frac{3}{2}H_m$ . Making use of Eqs. (8.19) and (8.22) gives the critical value of  $X$ , where  $H = \frac{3}{2}H_m$  as

$$X_{cr} = \frac{1 - H_o^2}{1 + 2H_o} \quad (8.58)$$

Note that  $0 \leq X_{cr} \leq 1$  when  $H_0 \leq 1$ .

By making use of Eq. (8.52) the stream function can be written as

$$\frac{w\ell}{u_b s_h} = -\frac{\partial \bar{\Phi}}{\partial X} = -\frac{\partial \bar{\Phi}}{\partial H} \frac{\partial H}{\partial X} = \frac{\partial \bar{\Phi}}{\partial H} \quad (8.59)$$

Figure 8.14 shows contours of streamlines within the lubrication film for four different film thickness ratios. In this figure the  $\Delta\bar{\Phi}$  value indicates the constant incrementation of  $\bar{\Phi}$  between the specified  $\bar{\Phi}$  values. No backflow is observed to occur in parts (a) and (b), which correspond to  $H_0 = 2.0$  and  $H_0 = 1.0$ , respectively. Backflow is, however, found in parts (c) and (d), which correspond to  $H_0 = 0.5$  and  $H_0 = 0.25$ , respectively. Also shown in this figure is the pressure distribution within the bearing as well as the locations where  $w = 0$  and  $u = 0$ . The straight line shown for  $w = 0$  is when  $H = 3/2H_m$  and when Eq. (8.58) is satisfied. The curved line shown when  $u = 0$  is when Eq. (8.44) is satisfied. The results of Fig. 8.14 indicate that as  $H_0$  becomes smaller, the more difficult it is for the fluid to pass through the bearing.

## 8.6 Parallel-Step Slider Bearing

Lord Rayleigh, as long ago as 1918, demonstrated that a parallel-step geometry produced the optimum load-carrying capacity when side leakage was neglected. This bearing has not, however, enjoyed the same development and applications as the pivoted-pad slider bearing. Past neglect of this mathematically preferable configuration has been due to doubts about the relative merits of this bearing when side leakage is considered. Figure 8.15 illustrates the geometric shape of the film in this bearing as well as a typical pressure profile resulting from the analysis.

The parallel-step slider bearing is analyzed here by considering two connected parallel-surface bearings. The subscripts  $i$  and  $o$  will be used to denote conditions in the inlet and outlet films, respectively.

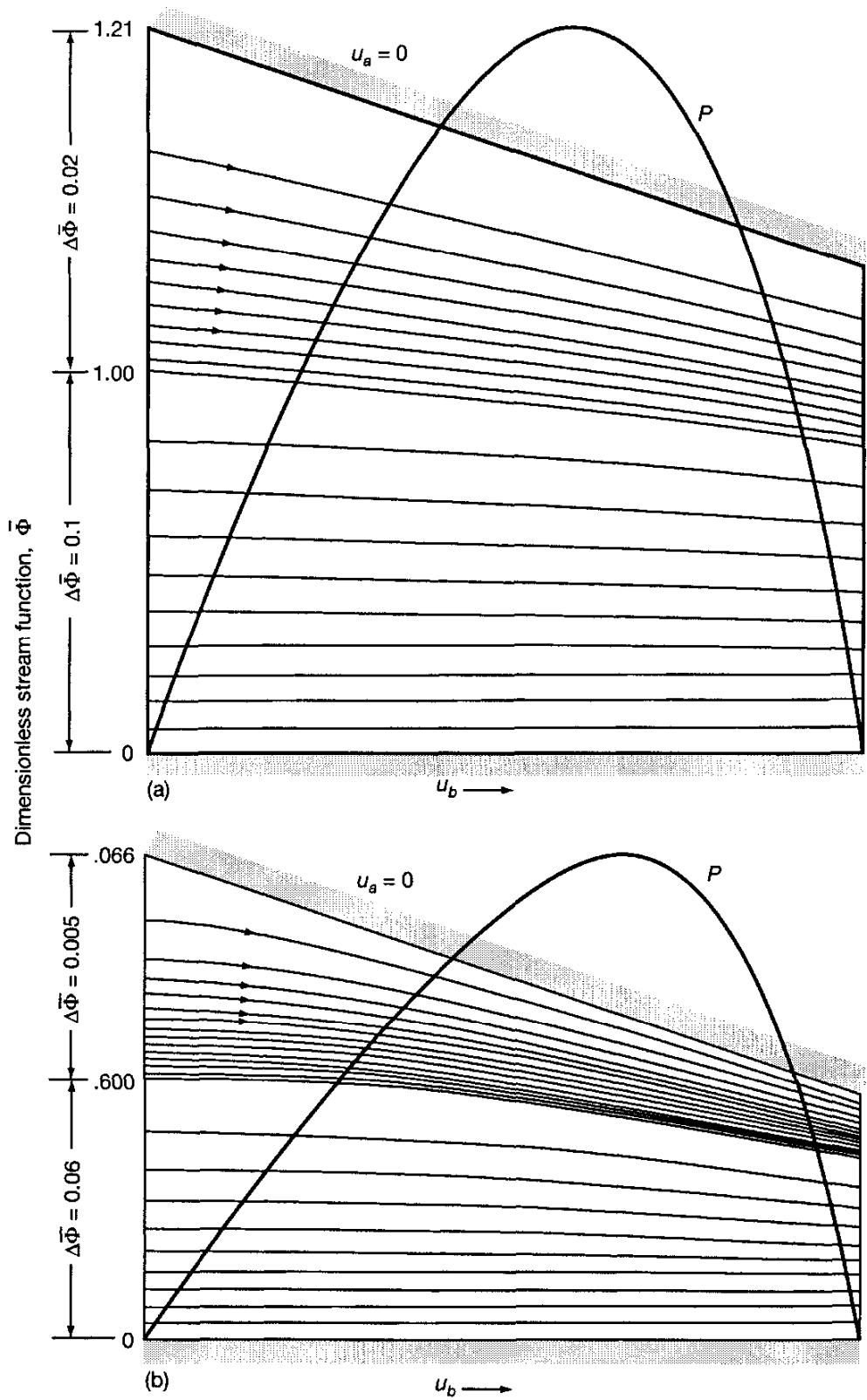


Figure 8.14: Streamlines in fixed-incline bearing at four film thickness ratios  $H_o$ . (a)  $H_o = 2$ ; (b)  $H_o = 1$  (critical value);

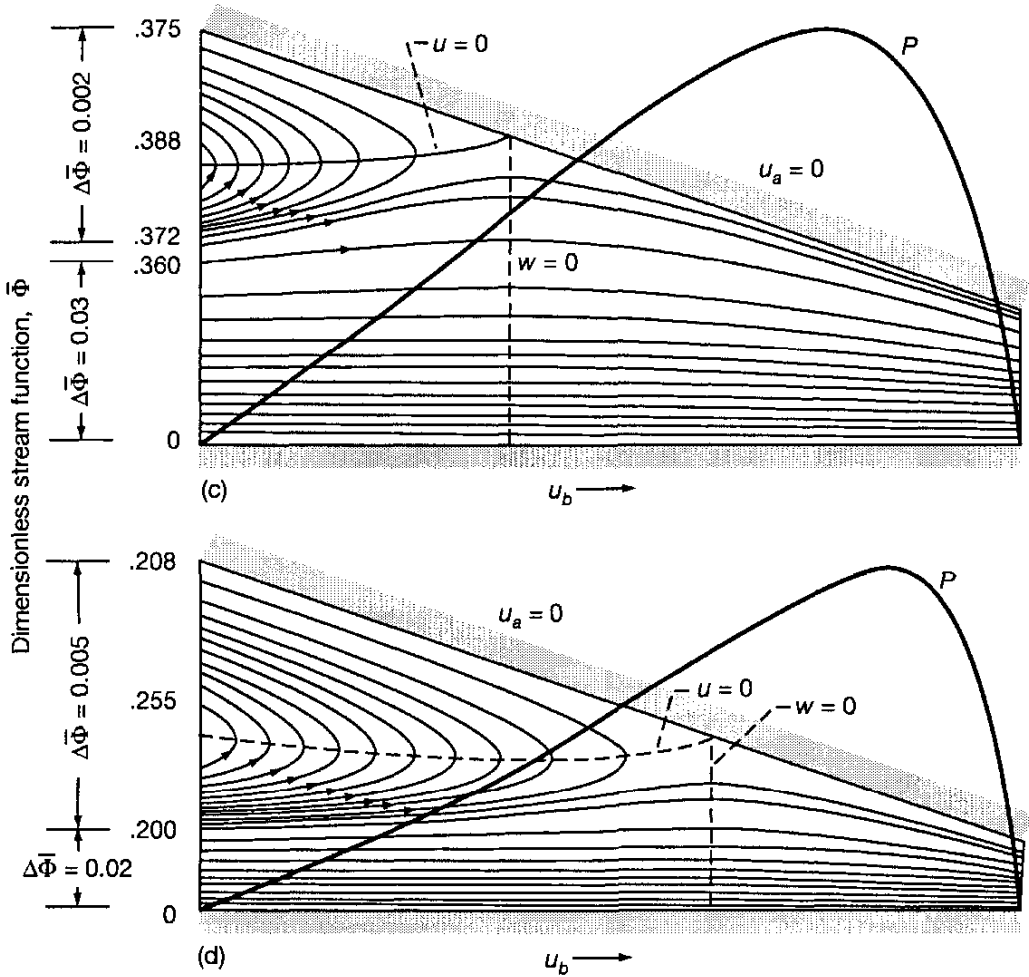


Figure 8.14: Concluded. (c)  $H_o = 0.5$ ; (d)  $H_o = 0.25$ .

### 8.6.1 Pressure Distribution

From Eq. (7.48), with side leakage neglected and a constant film thickness in the inlet and outlet regions, the appropriate Reynolds equation is

$$\frac{d^2 p}{dx^2} = 0$$

This equation can be integrated to give

$$\frac{dp}{dx} = \text{constant}$$

This result shows that the pressure gradients in the inlet and outlet regions are constant. Since the film thicknesses in the two regions are different, their pressure gradients are also different. Thus, since there will be no discontinuity in pressure at the step,

$$p_m = n_s \ell \left( \frac{dp}{dx} \right)_i = -(\ell - n_s \ell) \left( \frac{dp}{dx} \right)_o \quad (8.60)$$

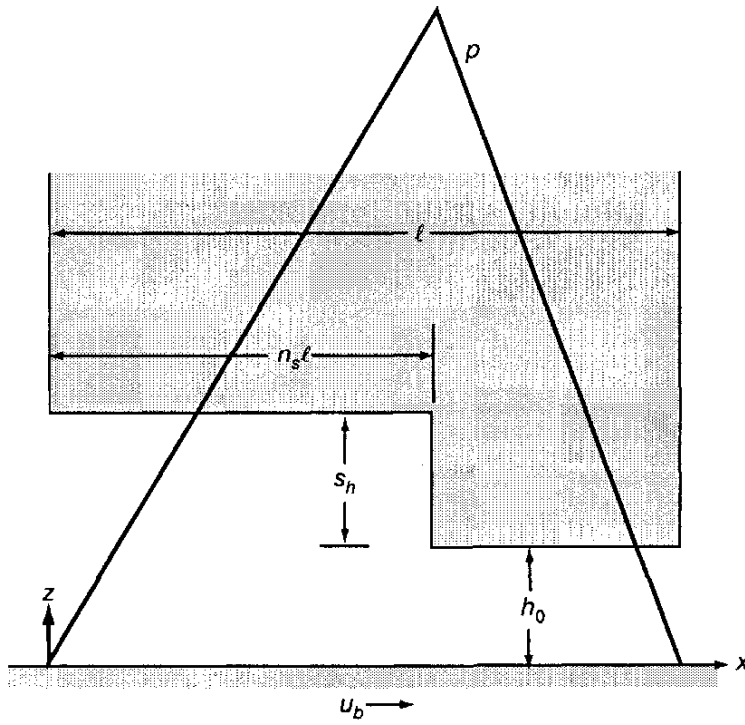


Figure 8.15: Parallel-step slider bearing.

Also the flow rate at the step must be the same, or  $q'_{x,o} = q'_{x,i}$ . Making use of Eq. (7.38) and equating the flow for the inlet and outlet regions while assuming constant viscosity gives

$$-\frac{(h_o + s_h)^3}{12\eta_0} \left( \frac{dp}{dx} \right)_i + \frac{u_b(h_o + s_h)}{2} = -\frac{h_o^3}{12\eta_0} \left( \frac{dp}{dx} \right)_o + \frac{u_b h_o}{2} \quad (8.61)$$

Equations (8.60) and (8.61) represent a pair of simultaneous equations with unknowns  $(dp/dx)_i$  and  $(dp/dx)_o$ . The solutions are

$$\left( \frac{dp}{dx} \right)_i = \frac{6\eta_0 u_b (1 - n_s) s_h}{(1 - n_s)(h_o + s_h)^3 + n_s h_o^3} \quad (8.62)$$

$$\left( \frac{dp}{dx} \right)_o = -\frac{6\eta_0 u_b n_s s_h}{(1 - n_s)(h_o + s_h)^3 + n_s h_o^3} \quad (8.63)$$

The maximum pressure (at the step) can be found directly by substituting Eqs. (8.62) and (8.63) into (8.60) to give

$$p_m = \frac{6\eta_0 u_b \ell n_s (1 - n_s) s_h}{(1 - n_s)(h_o + s_h)^3 + n_s h_o^3} \quad (8.64)$$

By making use of Eq. (8.17), Eq. (8.64) can be written in dimensionless form as

$$P_m = \frac{p_m s_h^2}{\eta_0 u_b \ell} = \frac{6n_s (1 - n_s)}{(1 - n_s)(H_o + 1)^3 + n_s H_o^3} \quad (8.65)$$

The bearing configuration that produces the largest  $p_m$  is achieved when

$$\frac{\partial p_m}{\partial n_s} = 0 \quad \text{and} \quad \frac{\partial p_m}{\partial s_h} = 0$$

Using these conditions in Eq. (8.64) gives

$$0 = (1 - n_s)^2 (h_o + s_h)^3 - n_s^2 h_o^3 \quad (8.66)$$

and

$$0 = (1 - n_s) (h_o + s_h)^2 (h_o - 2s_h) + n_s h_o^3 \quad (8.67)$$

Solving for  $n_s$  and  $s_h$  in these equations gives

$$H_o = \frac{h_o}{s_h} = 1.155 \quad (8.68)$$

$$n_s = 0.7182 \quad (8.69)$$

This is the optimum parallel-step bearing configuration that Lord Rayleigh (1918) described in his classic paper. Knowing the maximum pressure and that the pressure gradients are constants allows the dimensionless pressure in the inlet and outlet regions to be written as

$$P_i = \frac{XP_m}{n_s} = \frac{6X(1 - n_s)}{(1 - n_s)(H_o + 1)^3 + n_s H_o^3} \quad 0 \leq X \leq n_s \quad (8.70)$$

$$P_o = \frac{(1 - X)P_m}{1 - n_s} = \frac{6(1 - X)n_s}{(1 - n_s)(H_o + 1)^3 + n_s H_o^3} \quad n_s \leq X \leq 1 \quad (8.71)$$

The pressure distribution is shown diagrammatically in Fig. 8.15. Note that  $P = 0$  everywhere if  $H_0 \rightarrow \infty$  or if  $n_s = 0$  or 1. Also note that  $H_0 \rightarrow \infty$  implies that  $s_h \rightarrow 0$  (a parallel film) or that  $h_0 \rightarrow \infty$ .

### 8.6.2 Normal and Tangential Load Components

The normal load per unit width can easily be determined for this simple form of pressure distribution. That is,  $w'_z$  is directly proportional to the triangular area formed by the pressure distributions.

$$w'_z = \frac{p_m \ell}{2} = \frac{3\eta_0 u_b \ell^2 n_s (1 - n_s) s_h}{(1 - n_s)(h_o + s_h)^3 + n_s h_o^3} \quad (8.72)$$

The dimensionless normal load can be expressed as

$$W_z = \frac{w'_z}{\eta_0 u_b} \left( \frac{s_h}{\ell} \right)^2 = \frac{3n_s (1 - n_s)}{(1 - n_s)(H_o + 1)^3 + n_s H_o^3} = \frac{P_m}{2} \quad (8.73)$$

Note that  $W_z = 0$  if  $H_0 \rightarrow \infty$  or if  $n_s = 0$  or 1 and is thus a function of  $n_s$  and  $H_0$ .

The tangential load components per unit width acting on the bearing in the direction of motion are equal to the pressure at the step multiplied by the step height.

$$\begin{aligned} w'_{xb} &= W_{xb} = 0 \\ w'_{xa} &= - \int_{h_o+s_h}^{h_o} p dh = p_m s_h \end{aligned} \quad (8.74)$$

or

$$w'_{xa} = \frac{6\eta_0 u_b \ell n_s (1 - n_s) s_h^2}{(1 - n_s)(h_o + s_h)^3 + n_s h_o^3}$$

In dimensionless form this equation becomes

$$W_{xa} = \frac{w'_{xa}}{\eta_0 u_b} \frac{s_h}{\ell} = \frac{6n_s (1 - n_s)}{(1 - n_s)(H_o + 1)^3 + n_s H_o^3} = P_m \quad (8.75)$$

Note that  $W_{xa} = 0$  if  $H_o \rightarrow \infty$  or if  $n_s = 0$  or 1.

The general expression for the shear force per unit width at the moving surface can be written as

$$f'_b = \int_0^{n\ell} (\tau_{zx,i})_{z=0} dx + \int_{n\ell}^\ell (\tau_{zx,i})_{z=0} dx$$

Making use of Eq. (7.34) yields

$$f_b = \left[ -\frac{h_o + s_h}{2} \left( \frac{dp}{dx} \right)_i - \frac{\eta_0 u_b}{h_o + s_h} \right] n_s \ell + \left[ -\frac{h_o}{2} \left( \frac{dp}{dx} \right)_o - \frac{\eta_0 u_b}{h_o} \right] (1 - n_s) \ell$$

Making use of Eq. (8.60) gives

$$f'_b = -\frac{p_m s_h}{2} - \eta_0 u_b \ell \left( \frac{n_s}{h_o + s_h} - \frac{1 - n_s}{h_o} \right)$$

Making use of Eq. (8.74) gives

$$f'_b = -\frac{w'_{xa}}{2} - \frac{\eta_0 u_b \ell [n_s h_o + (1 - n_s)(h_o + s_h)]}{h_o(h_o + s_h)} \quad (8.76)$$

Similarly,

$$f'_a = -\frac{w'_{xa}}{2} + \frac{\eta_0 u_b \ell [n_s h_o + (1 - n_s)(h_o + s_h)]}{h_o(h_o + s_h)} \quad (8.77)$$

Equations (8.76) and (8.77) can be expressed in dimensionless form as

$$F_b = \frac{f'_b}{\eta_0 u_b} \frac{s_h}{\ell} = -\frac{P_m}{2} - \frac{H_o + 1 - n_s}{H_o(1 + H_o)} \quad (8.78)$$

$$F_a = \frac{f'_a}{\eta_0 u_b} \frac{s_h}{\ell} = -\frac{P_m}{2} + \frac{H_o + 1 - n_s}{H_o(1 + H_o)} \quad (8.79)$$

### 8.6.3 Friction Coefficient and Volume Flow Rate

The friction coefficient for a parallel-step slider bearing can be directly written from Eqs. (8.78) and (8.73) as

$$\mu = -\frac{f'_b}{w'_z} = -\frac{s_h}{\ell} \frac{F_b}{W_z} = \frac{s_h}{\ell} \left[ 1 + \frac{2(H_o + 1 - n_s)}{P_m H_o (1 + H_o)} \right] \quad (8.80)$$

The volume flow rate per unit width can be expressed by making use of Eqs. (7.38) and (8.60) as

$$q'_x = -\frac{(h_o + s_h)^3 p_m}{12\eta_0 n_s \ell} + \frac{u_b (h_o + s_h)}{2}$$

The volume flow rate expressed in dimensionless form is given by

$$Q = \frac{2q'_x}{u_b s_h} = -\frac{P_m (H_o + 1)^3}{6n_s} + H_o + 1 \quad (8.81)$$

This expression reduces to the simple parallel-step slider bearing result ( $Q=1$ ), corresponding to Couette flow between flat plates if  $H_0 = \infty$  or if  $n_s = 0$  or 1.

### 8.6.4 Power Loss, Temperature Rise, and Center of Pressure

The rate of work produced against viscous shearing, or the power loss, can be expressed from Eq. (8.12) in dimensionless form as

$$H_p = \frac{h_p s_h}{\eta_0 u_b^2 \ell (r_o - r_i)} = -\frac{f'_b s_h}{\eta_0 u_b \ell} = -F_b \quad (8.82)$$

The adiabatic temperature rise can be written from Eq. (8.13) as

$$\Delta t_m = \frac{h_p}{\rho_0 q'_x C_p} = \frac{2u_b \ell \eta_0}{\rho_0 C_p s_h^2} \frac{H_p}{Q} \quad (8.13)$$

Equations (8.82) and (8.81) were used in this equation. The center of pressure when both the inlet and outlet regions are considered can be expressed as

$$w'_z x_{cp} = \int_0^{n_s \ell} p_i x \, dx + \int_{n_s \ell}^\ell p_o x \, dx$$

This equation can be expressed in dimensionless form as

$$W_z X_{cp} = \int_0^{n_s} P_i X \, dX + \int_{n_s}^1 P_o X \, dX$$

Making use of Eqs. (8.70), (8.71), and (8.73) gives

$$X_{cp} = \frac{x_{cp}}{\ell} = \frac{2}{n_s} \int_0^{n_s} X^2 \, dX + \frac{2}{1 - n_s} \int_{n_s}^1 X(1 - X) \, dX$$

$$\therefore X_{cp} = \frac{1 + n_s}{3} \quad (8.83)$$

Therefore, the center of pressure coincides with the step location when  $n_s = \frac{1}{2}$ .

Also,  $X_{cp} \rightarrow \frac{1}{3}$  as  $n_s \rightarrow 0$  and  $X_{cp} \rightarrow \frac{2}{3}$  as  $n_s = 1$ . These results correspond to pressure profiles that approach the form of right triangles in pads having steps near their ends.

## 8.7 Closure

This chapter has considered film shapes in three different slider bearings: parallel surface, fixed incline, and parallel step. Only flow in the  $x$ - $z$  plane, or in the direction of motion, has been considered. The properties of the lubricant, namely, density and viscosity, were assumed to be constant. A positive pressure profile was obtained from the physical wedge effect in all the film shapes except a parallel film, where the pressure was zero throughout the bearing length. The appropriate Reynolds equation used to evaluate these film shapes was

$$\frac{d}{dx} \left( h^3 \frac{dp}{dx} \right) = 6\eta_0 u_b \frac{\partial h}{\partial x}$$

or

$$\frac{dp}{dx} = \frac{6\eta_0 u_b (h - h_m)}{h^3}$$

The pressure profile was determined from this equation and the particular film shape to be evaluated and then used to evaluate load components, shear force components, power loss, adiabatic temperature rise, friction coefficient, volume flow rate, stream functions, and center of pressure.

Of all these calculations the most important in most design considerations is the normal load-carrying capacity per unit width  $w'_z$ . For the fixed-incline slider bearing the dimensionless normal load-carrying capacity was found to be

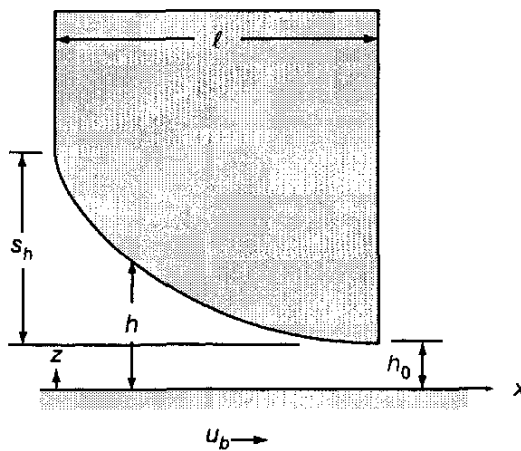
$$W_z = \frac{w'_z}{\eta_0 u_b} \left( \frac{s_h}{\ell} \right)^2 = f(H_o)$$

This implies that the normal applied load per unit width is directly proportional to the viscosity  $\eta_0$ , the velocity  $u_b$ , and the length  $\ell$  squared while also being inversely proportional to the shoulder height  $s_h$  squared. The film thickness ratio is defined as  $H_0 = h_0/s_h$ . The stream functions within the lubricated film in an infinitely long, fixed-incline slider bearing is presented. Locations of reverse flow within the conjunction are clearly visible.

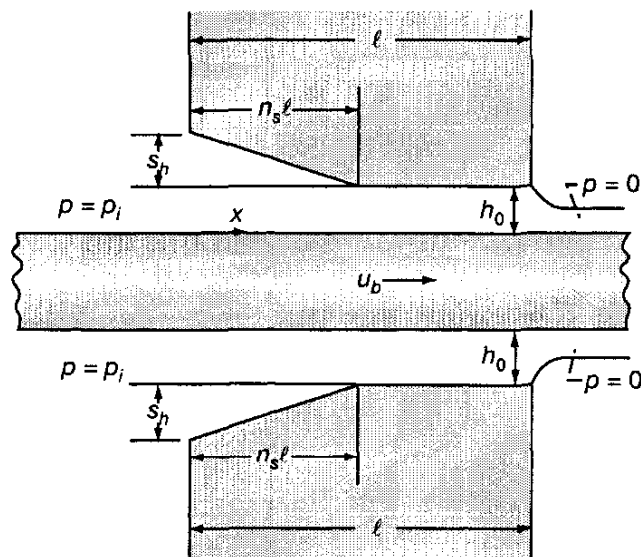
For a parallel-step slider bearing the dimensionless normal applied load is a function not only of the film thickness ratio, as was found for the fixed-incline slider bearing, but also of the location of the step. Recall that in this chapter side leakage was neglected.

## 8.8 Problems

- 8.1 A slider bearing has an exponential film shape, as shown in the sketch, and a film thickness defined as  $h = (h_0 + s_h) e^{-x/\ell}$ . An incompressible fluid is assumed, and no side flow is considered (only flow in the  $x$ - $z$  plane). Determine the pressure within the bearing as well as the normal load components, the shear force components, the friction coefficient, the volume flow rate, the power loss, and the adiabatic temperature rise within the bearing. Assume  $u_b = 10 \text{ m/s}$ ,  $h_0 = 60 \mu\text{m}$ ,  $\ell = 0.1 \text{ m}$ , and  $\eta_0 = 0.1 \text{ Pa}\cdot\text{s}$ .



- 8.2 A flat strip of metal emerges from a liquid bath of viscosity  $\eta_0$  and pressure  $p_i$  above ambient and has velocity  $u_b$  on passing through a slot of the form shown in the sketch. In the initial convergent part of the slot the film thickness decreases linearly from  $h_0 + s_h$  to  $h_0$  over a length  $n_s \ell$ , on each side of the strip. In the final section of the slot the film on each side of the strip has a constant thickness  $h_0$  over a length  $\ell(1 - n_s)$ .



State clearly the boundary conditions required to determine the pressure distribution along the slot length in the sliding direction on the assumption that the film thickness is zero at the trailing edge.

tion that the liquid is isoviscous and incompressible and the slot is infinitely wide.

Sketch the pressure distribution along the  $x$  axis and show that the volume flow rate per unit width  $q'_x$  on each side of the strip can be written in dimensionless form as

$$Q = \frac{2q'_x}{u_b s_h} = \frac{(H_o^3 P_i / 3) (H_o + 1)^2 + 2H_o (H_o + 1) (1 + H_o - n_s)}{n_s H_o (2H_o + 1) + 2(1 - n_s) (H_o + 1)^2}$$

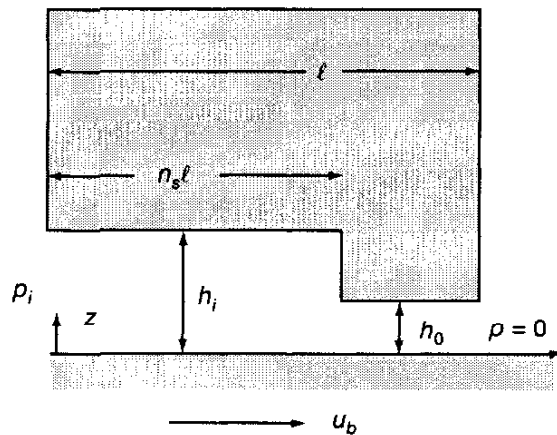
where

$$P_i = \frac{p_i s_h^2}{\eta_0 u_b \ell} \quad \text{and} \quad H_o = \frac{h_o}{s_h}$$

Demonstrate that for  $P_i$  equal to zero the expression for  $Q$  reduces to forms appropriate to the parallel-surface and fixed-incline-surface bearing situations as  $n_s$  approaches zero and unity, respectively.

Determine the minimum value of  $P_i$  required to ensure that the peak pressure in the slot is located at the inlet, where  $h = h_0 + s_h$  if  $n_s = \frac{1}{2}$  and  $H_o = 1$ .

- 8.3 In designing a fixed-incline self-acting thrust pad when the width of the pad is much larger than the length, it is of interest to know the magnitude and location of the maximum pressure. The viscosity of the lubricant is  $0.05 \text{ N}\cdot\text{s}/\text{m}^2$ , the sliding velocity is  $10 \text{ m/s}$ , the pad length is  $0.3 \text{ m}$ , the minimum film thickness is  $15 \mu\text{m}$ , and the inlet film thickness is twice the outlet film thickness.
- 8.4 A parallel-step thrust bearing is shown below. Side leakage is neglected. The inlet pressure is greater than zero but less than  $p_m$ , the pressure at the step. The outlet pressure is zero. Determine the velocity of the fluid across the film while in the inlet and outlet regions. That is,



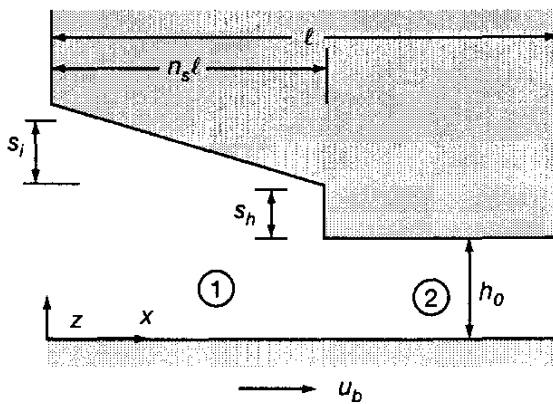
$$U_i = \frac{u_i}{u_b} = f(Z, P_i, P_m, H_i, n_s)$$

$$U_o = \frac{u_o}{u_b} = g(Z, P_i, P_m, H_i, n_s)$$

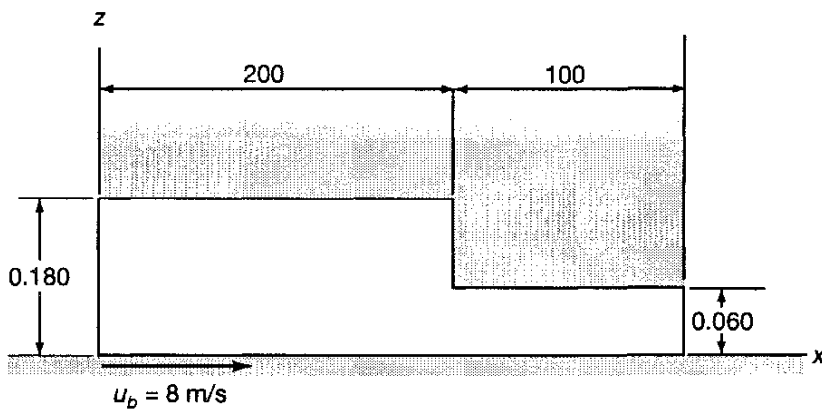
where

$$Z = \frac{z}{h_0} \quad P_i = \frac{p_i h_o^2}{\eta_0 u_b \ell} \quad P_m = \frac{p_m h_o^2}{\eta_0 u_b \ell} \quad H_i = \frac{h_i}{h_o}$$

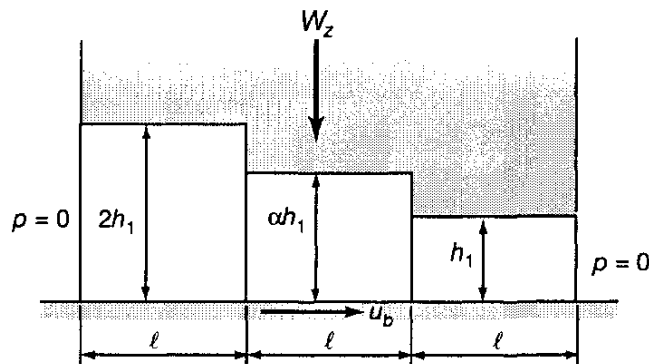
- 8.5 From the results of Problem 8.4 evaluate and plot the velocity profile in the inlet and outlet regions when  $n_s = 0.75$ ,  $H_i = 2.0$ ,  $P_m = 1.0$ , and  $P_i = 0.5$ .
- 8.6 A thrust bearing analysis is to be performed on the bearing shown below. The pressure at  $x = 0$  and at  $x = \ell$  is zero. The analysis should consist of considering the lubrication in the two separate regions (1)  $0 \leq x \leq n_s \ell$  and (2)  $n_s \ell \leq x \leq \ell$  and equated at the common boundary ( $x = n_s \ell$ ). Side leakage is to be neglected. Starting with the appropriate Reynolds equation, determine the pressure throughout the bearing. Also show that the pressure at the common boundary ( $x = n_s \ell$ ), when  $s_i = 0$ , is exactly Eq. (8.70) or (8.71) for a parallel-step bearing.



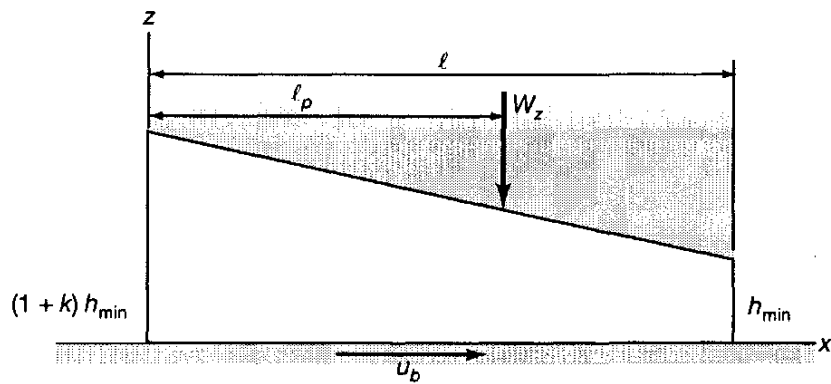
- 8.7 The very wide slider bearing shown is lubricated with an oil having a viscosity of  $0.03 \text{ N}\cdot\text{s}/\text{m}^2$  and consists of two parts, each with a constant film thickness. Find the pressure distribution in the oil and the load per unit width of the bearing. All dimensions are in millimeters.



- 8.8 An infinitely wide slider bearing, shown in the sketch, has three sections with film thicknesses  $2h_1$ ,  $\alpha h_1$ , and  $h_1$ , respectively. Find which value of  $\alpha$  gives the maximum load-carrying capacity for given values of  $h_1$ ,  $\ell$ ,  $u_b$ , and  $\eta$ . Use the Reynolds equation and the oil flow equation.



- 8.9 Given the infinitely wide slider bearing shown in the sketch, find the pressure distribution by using the Reynolds equation.



## Reference

Lord Rayleigh (1918): Notes on the Theory of Lubrication, *Philos. Mag.*, vol. 35, no. 1, pp. 1-12.

# Chapter 9

## Hydrodynamic Thrust Bearings - Numerical Solutions

### Symbols

$\tilde{A}_j, \dots$	integration constants	$q_s$	volumetric side flow rate, $\text{m}^3/\text{s}$
$b$	width of bearing, m	$r$	radius, m
$C_p$	specific heat of material at constant pressure, $\text{J}/(\text{kg}\cdot^\circ\text{C})$	$s_h$	shoulder height, m
$C_s$	volumetric specific heat, $\rho C_p$ , $\text{J}/(\text{m}^3\cdot^\circ\text{C})$	$t_i$	inlet temperature, $^\circ\text{C}$
$F^*$	Fourier coefficient	$t_m$	temperature, $^\circ\text{C}$
$H_o$	dimensionless outlet film thickness, $h_o/s_h$	$s_h$	shoulder height, m
$h$	film thickness, m	$u_b$	surface $b$ velocity, m/s
$h_o$	outlet film thickness, m	$W_z$	dimensionless normal load, $\left(\frac{w_z}{\eta_0 u_b b}\right) \left(\frac{s_h}{\ell}\right)^2$
$h_p$	rate of working against viscous stresses (power loss), $\text{N}\cdot\text{m}/\text{s}$	$w_t$	total thrust load of bearing, N
$L_p$	dimensionless pivot location, $\ell_p/\ell$	$w_z$	normal load, N
$\ell$	length in direction of sliding, m	$X, Y, Z$	dimensionless Cartesian coordinates
$\ell_p$	length from inlet to pivot position, m	$x, y, z$	Cartesian coordinates
$N_a$	rotational speed, r/min	$\Delta$	change
$N_0$	number of pads	$\eta$	absolute viscosity, $\text{Pa}\cdot\text{s}$ (or $\text{N}\cdot\text{s}/\text{m}^2$ )
$n_s$	location of parallel step	$\eta_0$	absolute viscosity at $p = 0$ and constant temperature, $\text{Pa}\cdot\text{s}$ (or $\text{N}\cdot\text{s}/\text{m}^2$ )
$P$	dimensionless pressure, $ps_h^2/(\eta_0 u_b \ell)$	$\lambda$	length-to-width ratio, $\ell/b$
$p$	pressure, $\text{N}/\text{m}^2$	$\mu$	coefficient of sliding friction
$q$	volumetric flow rate, $\text{m}^3/\text{s}$	$\rho$	density of lubricant, $\text{kg}/\text{m}^3$

### Subscripts

$i$	inner
$\min$	minimum
$o$	outer
$x, y, z$	coordinates

## 9.1 Introduction

The analysis of thrust slider bearings in Chapter 8 restricted the lubricant flow to two directions ( $x, z$ ). Flow of lubricant in the third direction ( $y$ ) is known as “side leakage.” The  $x$  coordinate is in the direction of sliding motion,  $y$  is transverse to the direction of sliding motion, and  $z$  is across the fluid film. This chapter is concerned with the side-leakage effect in slider bearings.

For bearings of finite width the pressure along the bearing side edges is ambient, and if hydrodynamic pressures are generated within the lubricant film due to the physical wedge mechanism, some flow will take place in the third ( $y$ ) direction. In this case the flow perpendicular to the direction of motion (side-leakage effect) has to be included, and the appropriate Reynolds equation is Eq. (7.48) with  $u_a = 0$ .

$$\frac{\partial}{\partial x} \left( h^3 \frac{\partial p}{\partial x} \right) + \frac{\partial}{\partial y} \left( h^3 \frac{\partial p}{\partial y} \right) = 6\eta_0 u_b \frac{\partial h}{\partial x} \quad (9.1)$$

Analytical solutions for slider bearings that consider side leakage are not normally available. Numerical solutions generally have to be resorted to when considering the side-leakage direction. One of the few analytical solutions that is available is for a parallel-step slider bearing.

For a thrust bearing, as considered in Chapter 8 and also in this chapter, a thrust plate attached to, or forming part of, the rotating shaft is separated from the sector-shaped bearing pads (see Fig. 8.3) by a lubricant film. The load-carrying capacity of the bearing arises entirely from the pressure generated by the motion of the thrust plate over the bearing pads. This action is achieved only if the clearance space between the stationary and moving components is convergent in the direction of motion (physical wedge pressure-generating mechanism).

The pad geometry parameters affecting the pressure generation and therefore the load-carrying capacity of the bearing are (1) pad length-to-width ratio  $\lambda = \ell/b$ , (2) film thickness ratio  $H_o = h_o/s_h$ , and (3) step or pivot location parameter  $n_s$ . This last parameter is not applicable to a fixed-incline thrust bearing. Recall that the pad length-to-width ratio did not appear in Chapter 8 because side leakage was neglected. Side leakage is considered in this chapter, and three different thrust bearings are investigated: two fixed-pad types (namely, a parallel-step and a fixed-incline) and a pivoted-pad bearing.

## 9.2 Finite-Width, Parallel-Step-Pad Slider Bearing

A sketch of the parallel-step-pad slider bearing is shown in Fig. 9.1. In the solution the inlet and outlet regions are first considered separately and then combined at the common boundary. Therefore, the film thickness is considered to be constant in the two regions.

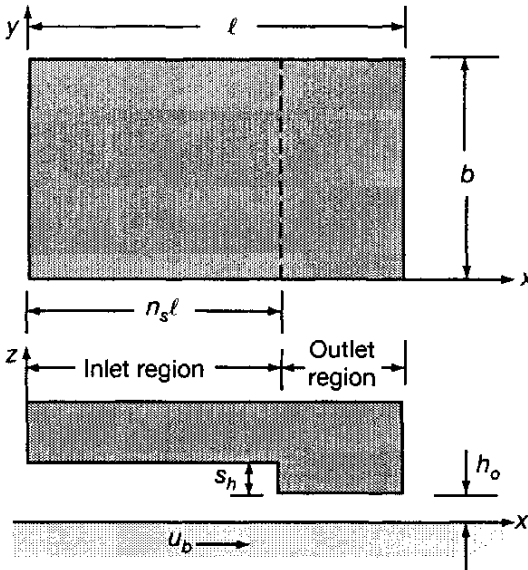


Figure 9.1: Finite parallel-step-pad slider bearing.

### 9.2.1 Pressure Distribution

The Reynolds equation given in Eq. (9.1) reduces to

$$\frac{\partial^2 p}{\partial x^2} + \frac{\partial^2 p}{\partial y^2} = 0 \quad (9.2)$$

when the film thickness is constant. Equation (9.2) is a Laplace partial differential equation. Letting

$$x = \ell X \quad y = bY \quad \lambda = \frac{\ell}{b} \quad p = \frac{\eta_0 u_b \ell}{s_h^2} P \quad (9.3)$$

causes Eq. (9.2) to become

$$\frac{\partial^2 P}{\partial X^2} + \lambda^2 \frac{\partial^2 P}{\partial Y^2} = 0 \quad (9.4)$$

The pressure on the exterior boundaries of the inlet and outlet regions is zero, but the pressure on the common boundary is not known. It is assumed that the pressure on the common boundary is given by the following Fourier sine series:

$$(P)_{X=n_s} = \sum_{j=1,3,\dots}^{\infty} F_j^* \sin(j\pi Y) \quad (9.5)$$

The summation is over the odd values because of symmetry, and  $F_j^*$  is the Fourier coefficient to be evaluated later.

The general solution for  $P$  can be put in the following form for the inlet region:

$$P_i = \sum_{j=1,3,\dots}^{\infty} \left[ \tilde{A}_j \cos(j\pi Y) + \tilde{B}_j \sin(j\pi Y) \right] \left[ \tilde{C}_j \cosh(j\pi\lambda X) + \tilde{D}_j \sinh(j\pi\lambda X) \right] \quad (9.6)$$

Note that Eq. (9.6) does satisfy Eq. (9.4).

The boundary conditions for the inlet region are:

1.  $P_i = 0$  when  $X = 0$  for all values of  $Y$ .
2.  $P_i = 0$  when  $Y = 0$  for all values of  $X$ .
3.  $P_i = 0$  when  $Y = 1$  for all values of  $X$ .
4.  $P_i = \sum_{j=1,3,\dots}^{\infty} F_j^* \sin(j\pi Y)$  when  $X = n_s$ .

From boundary conditions 1 and 2,  $\tilde{A}_j = \tilde{C}_j = 0$ . From boundary condition 4,

$$\begin{aligned} \sum_{j=1,3,\dots}^{\infty} F_j^* \sin(j\pi Y) &= \sum_{j=1,3,\dots}^{\infty} \tilde{B}_j \tilde{D}_j \sin(j\pi Y) \sinh(j\pi \lambda n_s) \\ \therefore \tilde{B}_j \tilde{D}_j &= \frac{F_j^*}{\sinh(j\pi \lambda n_s)} \end{aligned} \quad (9.7)$$

$$\therefore P_i = \sum_{j=1,3,\dots}^{\infty} \frac{F_j^* \sin(j\pi Y) \sinh(j\pi \lambda X)}{\sinh(j\pi \lambda n_s)} \quad (9.8)$$

Note that boundary condition 3 is automatically satisfied by Eq. (9.8).

For the outlet region the solution is taken to be of the same form as Eq. (9.6).

$$P_o = \sum_{j=1,3,\dots}^{\infty} \left[ \tilde{E}_j \cos(j\pi Y) + \tilde{G}_j \sin(j\pi Y) \right] \left[ \tilde{H}_j \cosh(j\pi \lambda X) + \tilde{I}_j \sinh(j\pi \lambda X) \right] \quad (9.9)$$

The boundary conditions for the outlet region are

1.  $P_o = 0$  when  $X = 1$  for all values of  $Y$ .
2.  $P_o = 0$  when  $Y = 0$  for all values of  $X$ .
3.  $P_o = 0$  when  $Y = 1$  for all values of  $X$ .
4.  $P_o = \sum_{j=1,3,\dots}^{\infty} F_j^* \sin(j\pi Y)$  when  $X = n_s$ .

From boundary condition 2,  $\tilde{E}_j = 0$ . From boundary condition 1,

$$\tilde{H}_j = -\tilde{I}_j \tanh(j\pi \lambda) \quad (9.10)$$

Therefore, Eq. (9.9) can be rewritten as

$$P_o = \sum_{j=1,3,\dots}^{\infty} \tilde{G}_j \tilde{I}_j \sin(j\pi Y) [\sinh(j\pi \lambda X) - \tanh(j\pi \lambda) \cosh(j\pi \lambda X)] \quad (9.11)$$

From boundary condition 4,

$$\begin{aligned} \sum_{j=1,3,\dots}^{\infty} F_j^* \sin(j\pi Y) &= \sum_{j=1,3,\dots}^{\infty} \tilde{G}_j \tilde{I}_j \sin(j\pi Y) \\ &\times [\sinh(j\pi\lambda n_s) - \tanh(j\pi\lambda) \cosh(j\pi\lambda n_s)] \\ \therefore \tilde{G}_j \tilde{I}_j &= \frac{F_j^*}{\sinh(j\pi\lambda n_s) - \tanh(j\pi\lambda) \cosh(j\pi\lambda n_s)} \end{aligned} \quad (9.12)$$

Substituting Eq. (9.12) into Eq. (9.11) gives

$$P_o = \sum_{j=1,3,\dots}^{\infty} \frac{F_j^* \sin(j\pi Y) \sinh[j\pi\lambda(1-X)]}{\sinh[j\pi\lambda(1-n_s)]} \quad n_s \leq X \leq 1 \quad (9.13)$$

Note that boundary condition 3 is satisfied by Eq. (9.13).

For the pressure to be calculated, the Fourier coefficient  $F_j^*$  must be evaluated. This is done by making use of the principle of flow continuity. It will be seen that at any point on the common boundary ( $X = n_s$ ) the volume rate of inlet flow is the same as the volume rate of outlet flow.

$$\therefore q_{xi}|_{X=n_s} = q_{xo}|_{X=n_s} \quad (9.14)$$

Making use of Eq. (7.38) while letting  $u_a = 0$  and assuming a constant viscosity yields

$$-\frac{(h_o + s_h)^3}{12\eta_0} \left( \frac{dp_i}{dx} \right)_{n_s \ell} + \frac{u_b (h_o + s_h)}{2} = -\frac{h_o^3}{12\eta_0} \left( \frac{dp_o}{dx} \right)_{n_s \ell} + \frac{u_b h_o}{2}$$

Then making use of Eq. (9.3) gives

$$-H_o^3 \left( \frac{dP_i}{dX} \right)_{X=n_s} + (1 + H_o)^3 \left( \frac{dP_i}{dX} \right)_{X=n_s} = 6 \quad (9.15)$$

where  $H_o = h_o/s_h$ . From Eqs. (9.8) and (9.13)

$$\left( \frac{\partial P_i}{\partial X} \right)_{X=n_s} = \sum_{j=1,3,\dots}^{\infty} \frac{j\pi\lambda F_j^* \sin(j\pi Y)}{\tanh(j\pi\lambda n_s)} \quad (9.16)$$

$$\left( \frac{\partial P_o}{\partial X} \right)_{X=n_s} = \sum_{j=1,3,\dots}^{\infty} -\frac{j\pi\lambda F_j^* \sin(j\pi Y)}{\tanh[j\pi\lambda(1-n_s)]} \quad (9.17)$$

Substituting Eqs. (9.16) and (9.17) into (9.15) gives

$$H_o^3 \sum_{j=1,3,\dots}^{\infty} \frac{j\pi\lambda F_j^* \sin(j\pi Y)}{\tanh[j\pi\lambda(1-n_s)]} + (1 + H_o)^3 \sum_{j=1,3,\dots}^{\infty} \frac{j\pi\lambda F_j^* \sin(j\pi Y)}{\tanh(j\pi\lambda n_s)} = 6 \quad (9.18)$$

But

$$6 = \sum_{j=1,3,\dots}^{\infty} 6 \frac{4}{j\pi} \sin(j\pi Y) \quad (9.19)$$

Then substituting Eq. (9.19) into Eq. (9.18) gives

$$\begin{aligned} & \sum_{j=1,3,\dots}^{\infty} j\pi\lambda F_j^* \sin(j\pi Y) \left\{ H_o^3 \coth [j\pi\lambda(1 - n_s)] + (1 + H_o)^3 \coth (j\pi\lambda n_s) \right\} \\ &= \sum_{j=1,3,\dots}^{\infty} \frac{24 \sin(j\pi Y)}{j\pi} \\ \therefore F_j^* &= \frac{24}{j^2\pi^2\lambda \left\{ H_o^3 \coth [j\pi\lambda(1 - n_s)] + (1 + H_o)^3 \coth (j\pi\lambda n_s) \right\}} \end{aligned} \quad (9.20)$$

Note that as  $H_o \rightarrow \infty$ , which is a parallel-surface bearing,  $F_j^* \rightarrow 0$  and  $P \rightarrow 0$ . Once an expression for the Fourier coefficient is known, the pressure in the inlet and outlet regions can be calculated by substituting Eq. (9.20) into Eqs. (9.8) and (9.13).

### 9.2.2 Normal Load Component

The normal applied load can be written as

$$w_z = \int_0^b \int_0^{n_s\ell} p_i \, dx \, dy + \int_0^b \int_{n_s\ell}^\ell p_0 \, dx \, dy$$

This equation can be written in dimensionless form as

$$W_z = \frac{w_z}{\eta_0 u_b b} \left( \frac{s_h}{\ell} \right)^2 = \int_0^1 \int_0^{n_s} P_i \, dX \, dY + \int_0^1 \int_{n_s}^1 P_o \, dX \, dY \quad (9.21)$$

Substituting Eqs. (9.8) and (9.13) into this equation gives

$$\begin{aligned} W_z &= \frac{w_z}{\eta_0 u_b b} \left( \frac{s_h}{\ell} \right)^2 = \sum_{j=1,3,\dots}^{\infty} \frac{2F_j^*}{j^2\pi^2\lambda} \\ &\times \left\{ \frac{\cosh(j\pi\lambda n_s) - 1}{\sinh(j\pi\lambda n_s)} + \frac{\cosh[j\pi\lambda(1 - n_s)] - 1}{\sinh[j\pi\lambda(1 - n_s)]} \right\} \end{aligned} \quad (9.22)$$

Equations (9.20) and (9.22) reveal that when side leakage is considered, the dimensionless normal applied load  $W_z$  is a function of  $\lambda$  as well as  $H_o$  and  $n_s$ .

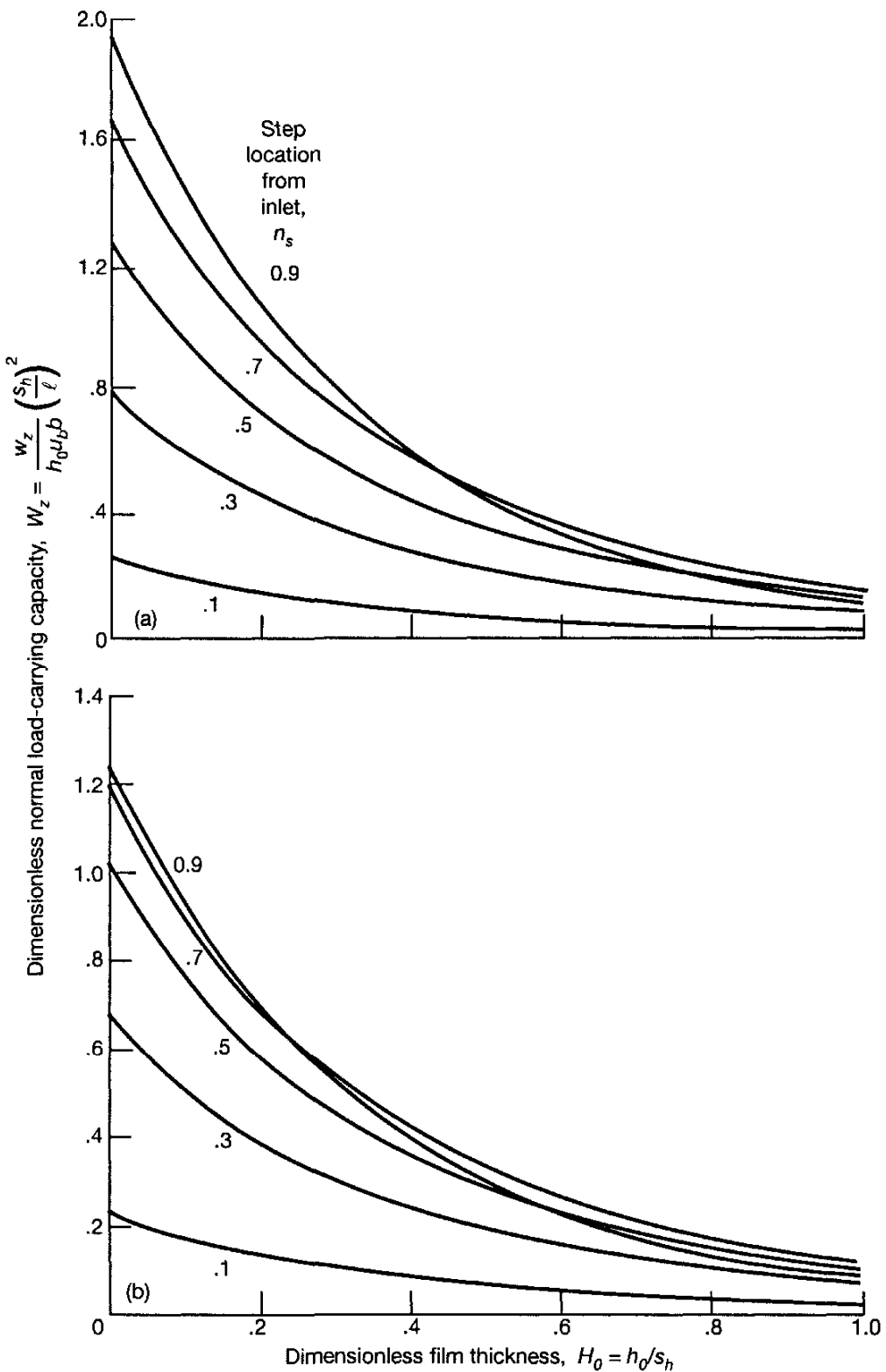


Figure 9.2: Effect of film thickness on dimensionless normal load-carrying capacity at five step locations  $n_s$  and four length-to-width ratios  $\lambda$ . (a)  $\lambda = \frac{1}{4}$ ; (b)  $\lambda = \frac{1}{2}$ .

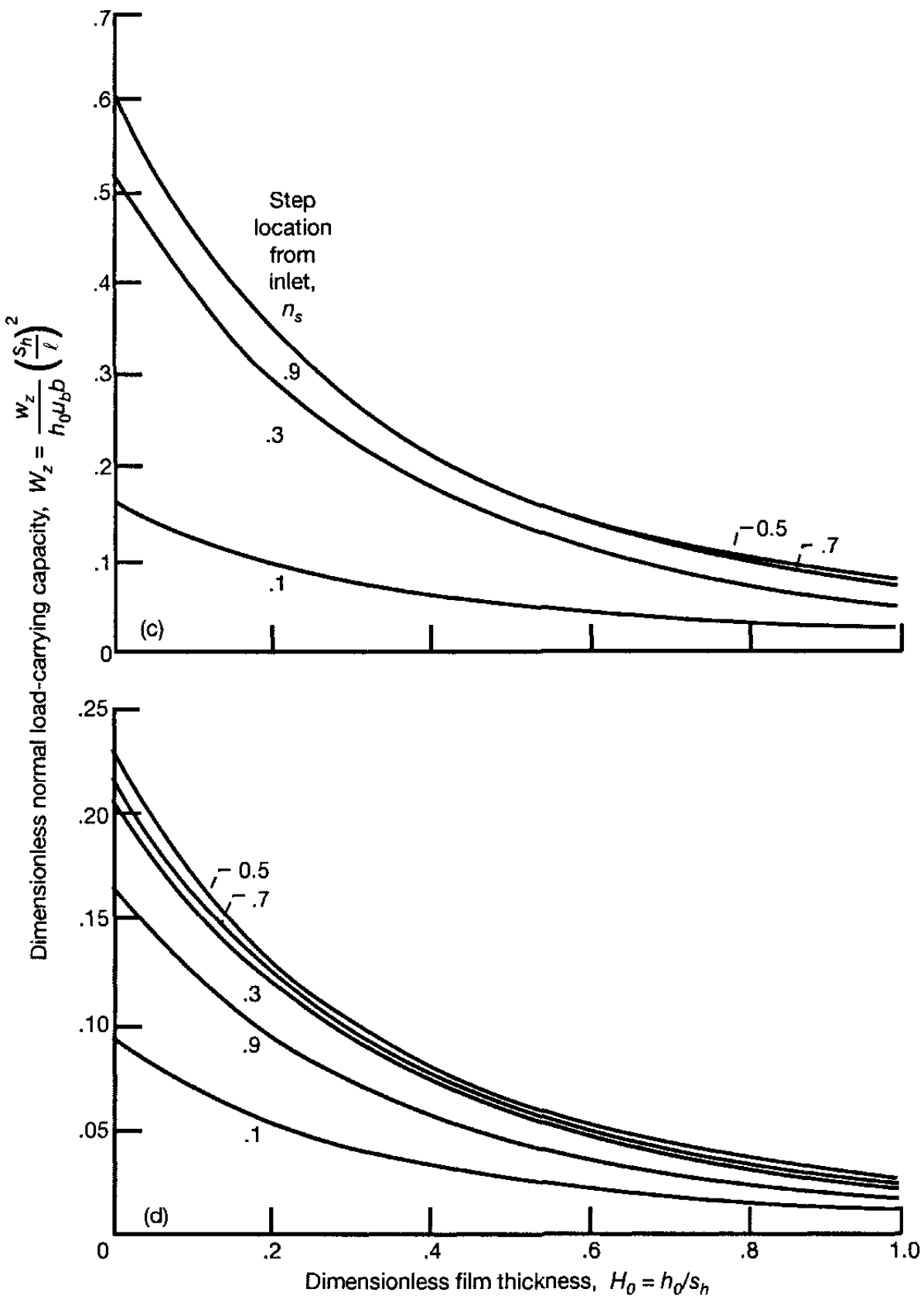


Figure 9.2: Concluded. (c)  $\lambda = 1$ ; (d)  $\lambda = 2$ .

Table 9.1: Maximum dimensionless normal load-carrying capacity [Dimensionless outlet film thickness  $H_o \rightarrow 0$ ]

Step location $n_s$	Length-to-width ratio, $\lambda$						
	1/100	1/4	1/2	3/4	1	3/2	2
	Maximum dimensionless normal load-carrying capacity, $W_z$						
0.1	0.298570	0.264269	0.228659	0.194657	0.164811	0.120508	0.092064
0.2	0.597193	0.529825	0.459748	0.391479	0.329074	0.230908	0.165224
0.3	0.895500	0.787513	0.675112	0.564927	0.463443	0.305444	0.205006
0.4	1.193245	1.031140	0.862610	0.700004	0.555898	0.346178	0.223081
0.5	1.490253	1.256341	1.014517	0.791103	0.607007	0.362142	0.228742
0.6	1.786400	1.460020	1.127112	0.839600	0.622694	0.359732	0.225744
0.7	2.081597	1.640043	1.200150	0.850630	0.609714	0.342147	0.214448
0.8	2.375785	1.795099	1.236016	0.830670	0.574190	0.311116	0.193714
0.9	2.668928	1.924660	1.238860	0.786357	0.521621	0.268646	0.162993

### 9.2.3 Results

The inclusion of side-leakage effects has introduced an additional parameter, the length-to-width ratio  $\lambda = \ell/b$ . Figure 9.2 shows the effect of the film thickness ratio  $H_o$  on the dimensionless load-carrying capacity  $W_z$  for five step locations  $n_s$  and four  $\lambda$  values ( $\frac{1}{4}$ ,  $\frac{1}{2}$ , 1, and 2). The following can be concluded from Fig. 9.2:

1. For any combination of  $H_o$  and  $\lambda$  the maximum load condition never occurs when the step location is less than 0.5. The location of the step should be closer to the outlet than to the inlet.
2. For small  $\lambda$ , where side leakage becomes less important, the step location that produces a maximum dimensionless load is larger than when side leakage is not considered.

Table 9.1 tabulates the results shown in Fig. 9.2 as  $H_o \rightarrow 0$  as well as results for three additional  $\lambda$ . From this table it is observed that as  $\lambda$  becomes smaller, the maximum load increases. This concurs with the results of Chapter 8 [Eq. (8.73)], which indicated that when side leakage is neglected and  $H_o \rightarrow \infty$ , the dimensionless normal load-carrying capacity approaches zero.

The parallel-step bearing shown in Fig. 9.1 has considerable side leakage, especially for large  $\lambda$ , which reduces its normal load-carrying capacity. Shrouds are sometimes introduced to restrict this side leakage and thereby increase the bearing's normal load-carrying capacity. Two types of shrouded-step bearings are shown in Fig. 9.3. The semicircular-step shrouded bearing (Fig. 9.3a) has a step radius of  $\ell/2$ , a film thickness ratio of 1.43, and a length-to-width ratio of 1. The resulting normal load-carrying capacity for this bearing is a 45% increase over that for an optimum unshrouded parallel-step thrust bearing. For a truncated triangular-step shrouded bearing (Fig. 9.3b) with  $H_o = 0.89$ , the resulting  $W_z$  is a 67% increase over that for an unshrouded bearing.

### 9.3 Fixed-Incline-Pad Slider Bearing

The simplest form of fixed-pad thrust bearing provides only straight-line motion and consists of a flat surface sliding over a fixed pad or land having a profile similar to that shown in Fig. 9.4. The fixed-pad bearing depends for its operation on the lubricant being drawn into a wedge-shaped space and thus producing pressure that counteracts the load and prevents contact between the sliding parts. Since the wedge action takes place only when the sliding surface moves in the direction in which the lubricant film converges, the fixed-incline bearing (Fig. 9.4) can carry load only in this direction. If reversibility is desired, a combination of two or more pads with their surfaces sloped in opposite directions is required. Fixed-incline pads are used in multiples as in the thrust bearing shown in Fig. 9.5.

The following procedure assists in designing a fixed-incline-pad thrust bearing:

1. Choose a pad length-to-width ratio. A square pad ( $\lambda = 1$ ) is generally felt to give good performance. If it is known whether maximum load or minimum power loss is more important in the particular application, a value of the minimum film thickness ratio can be determined from Fig. 9.6.
2. Determine lubricant temperature. Lubricant temperature can be expressed as

$$t_m = t_i + \frac{\Delta t_m}{2} \quad (9.23)$$

where

$t_i$  = inlet temperature

$\Delta t_m$  = change in temperature due to viscous shear heating

The inlet temperature is usually known beforehand, but the change in temperature due to viscous shear heating must be initially guessed. Once the temperature  $t$  is known, it can be used in Fig. 4.2 or 4.9 to determine the viscosity of SAE oils.

3. Determine outlet film thickness. Once the viscosity is known, the next least likely parameter to be preassigned is the outlet film thickness. That

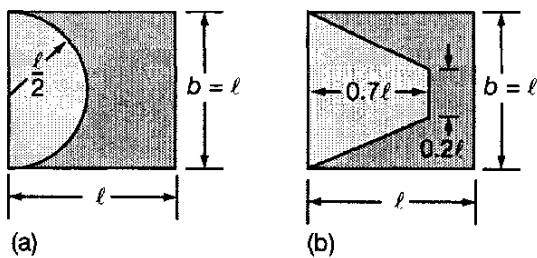


Figure 9.3: Shrouded-step slider bearings.  
(a) Semicircular step; (b) truncated triangular step.

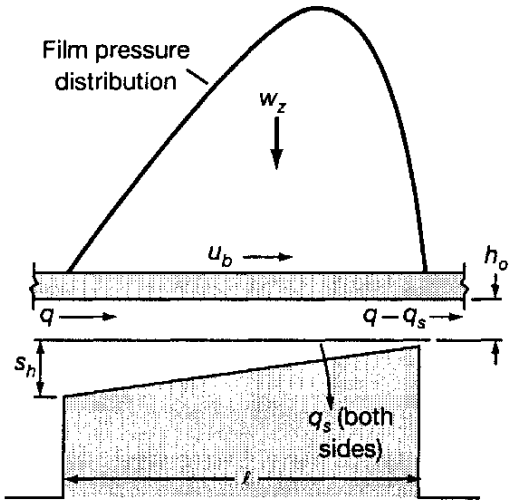


Figure 9.4: Side view of fixed-incline-pad bearing. [From Raimondi and Boyd (1955).]

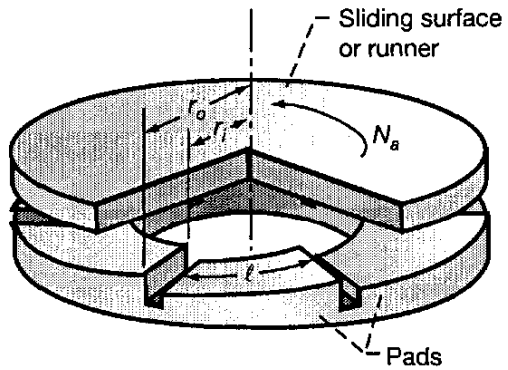


Figure 9.5: Configurations of multiple fixed-incline-pad thrust bearing. [From Raimondi and Boyd (1955).]

is, once a length-to-width ratio  $\lambda$  and a dimensionless minimum film thickness (from Fig. 9.7) are known, the dimensionless load can be determined. The outlet film thickness can be determined from

$$h_o = H_o \ell \left( \frac{W_z \eta_0 u_b b}{w_z} \right)^{1/2} \quad (9.24)$$

4. Check Table 9.2 to see if the minimum (outlet) film thickness is sufficient for the preassigned surface finish. If  $(h_o)_{\text{Eq. (9.24)}} \geq (h_o)_{\text{Table 9.2}}$ , go to step 5. If  $(h_o)_{\text{Eq. (9.24)}} < (h_o)_{\text{Table 9.2}}$ , consider one or more of the following steps:
  - (a) Increase the speed of the bearing.
  - (b) Decrease the load, the surface finish, or the inlet temperature.

Upon making this change, return to step 2.

5. From Fig. 9.8 determine the temperature rise due to shear heating for a given length-to-width ratio and bearing characteristic number. Recall from Sec. 4.8 that the volumetric specific heat  $C_s = \rho C_p$ , which is in the dimensionless temperature rise parameter, is relatively constant for mineral oils and is equivalent to  $1.36 \times 10^6 \text{ N}/(\text{m}^2 \cdot ^\circ\text{C})$ . If the temperature rise as obtained from Fig. 9.8 is within 5% of the previous value, go to step 6; otherwise return to step 2 with a new value of temperature rise.
6. Evaluate the performance parameters. Once an adequate minimum film thickness and proper lubricant temperature have been determined, the

Table 9.2: Allowable minimum outlet film thickness for a given surface finish. [From *Engineering Sciences Data Unit (1967)*]

Surface finish (centerline average, $R_a$ )		Description of surface	Examples of manufacturing methods	Approximate relative costs	Allowable minimum outlet film thickness <sup>a</sup> , $h_0$	
$\mu\text{m}$	$\mu\text{in.}$				$\mu\text{m}$	$\mu\text{in.}$
0.1-0.2	4-8	Mirror-like surface without toolmarks; close tolerances	Grind, lap, and superfinish	17-20	2.5	100
.2-.4	8-16	Smooth surface without scratches; close tolerances	Grind and lap	17-20	6.2	250
.4-.8	16-32	Smooth surface; close tolerances	Grind, file and lap	10	12.5	500
.8-1.6	32-63	Accurate bearing surface without toolmarks	Grind, precision mill, and file	7	25	1000
1.6-3.2	63-125	Smooth surface without objectionable toolmarks; moderate tolerances	Shape, mill, grind, and turn	5	50	2000

<sup>a</sup> The values of film thickness are given only for guidance. They indicate the film thickness required to avoid metal-to-metal contact under clean oil conditions with no misalignment. It may be necessary to take a larger film thickness than that indicated (e.g., to obtain an acceptable temperature rise). It has been assumed that the average surface finish of the pads is the same as that of the runner.

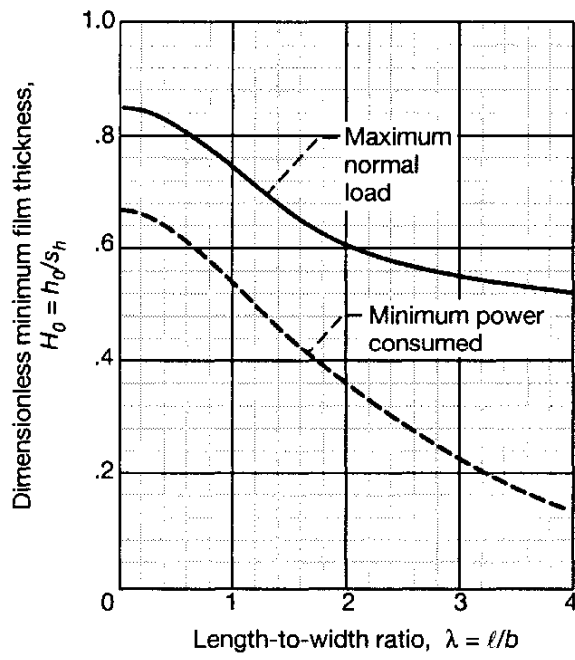


Figure 9.6: Chart for determining minimum film thickness corresponding to maximum load or minimum power loss for various pad proportions - fixed-incline-pad bearings. [From Raimondi and Boyd (1955).]

performance parameters can be evaluated. Specifically, from Fig. 9.9 the power loss, the friction coefficient, and the total and side flow can be determined.

## Example 9.1

**Given** A fixed-incline slider thrust bearing has the following operating parameters:  $w_z = 16 \text{ kN}$ ,  $u_b = 30 \text{ m/s}$ ,  $\ell = b = 75\text{mm}$ , SAE 10 oil, and  $t_i = 40^\circ\text{C}$ .

**Find** For the maximum load condition determine the following parameters:  $s_h$ ,  $h_0$ ,  $\Delta t_m$ ,  $\mu$ ,  $h_p$ ,  $q$ , and  $q_s$

**Solution:** From Fig. 9.6 for  $\lambda = \ell/b = 1$  and maximum normal load condition,  $H_o = 0.73$ . From Fig. 9.7 for  $H_o = 0.73$  and  $\lambda = 1$ ,  $1/W_z = 8.0$ . From Fig. 9.8 for  $1/W_z = 8.0$  and  $\lambda=1$ ,

$$\frac{0.9C_s b \ell \Delta t_m}{w_z} = 13$$

Inserting the input parameters and the fact that

$$C_s = \rho C_p = 1.36 \times 10^6 \text{ N}/(\text{m}^2 \cdot {}^\circ\text{C})$$

$$\Delta t_m = \frac{13w_z}{0.9C_s b \ell} = \frac{13(16)(10^3)}{(0.9)(1.36)(10^6)(0.075)(0.075)} = 30.21^\circ\text{C}$$

From Eq. (9.23)

$$t_m = t_i + \frac{\Delta t_m}{2} = 40 + \frac{30.2}{2} = 55.1^\circ\text{C}$$

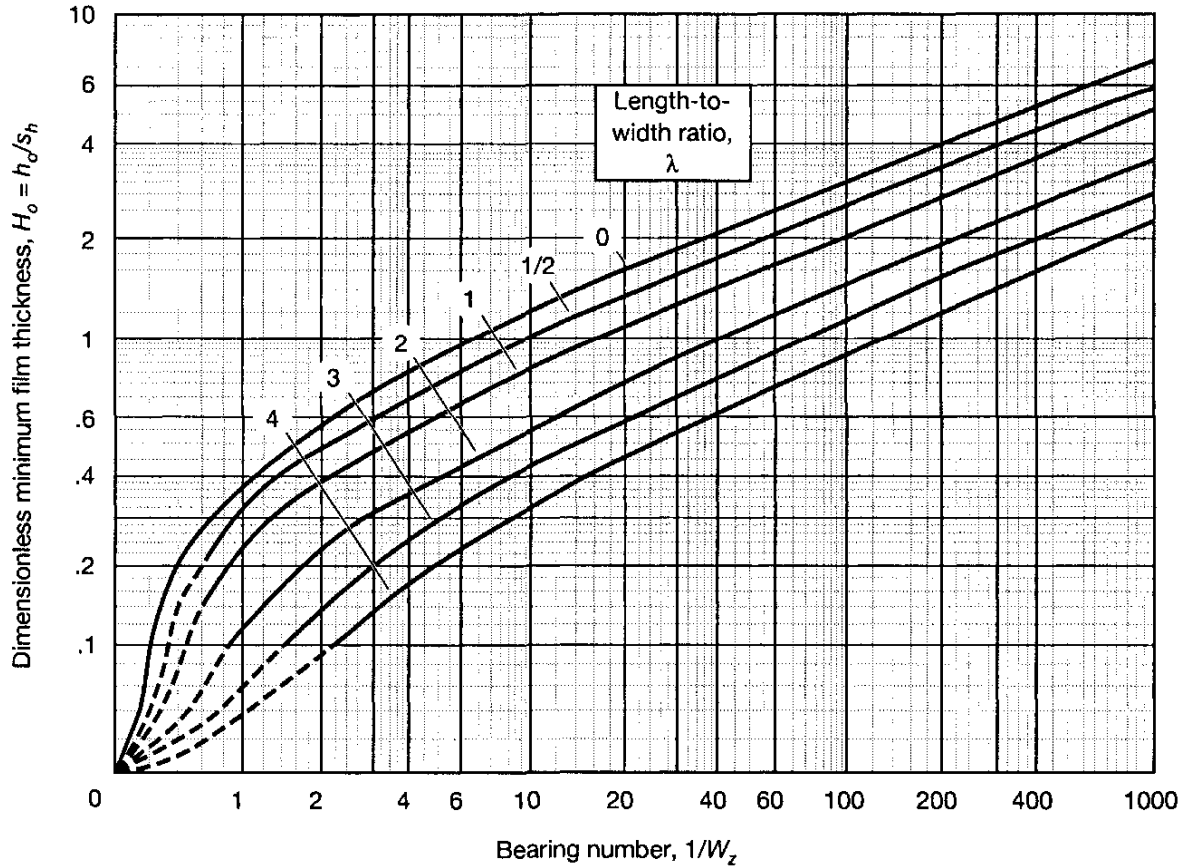


Figure 9.7: Chart for determining minimum film thickness for fixed-incline-pad thrust bearings. [From Raimondi and Boyd (1955)].

From Fig. 4.9 for SAE 10 oil at 55°C the absolute viscosity is 0.015 N·s/m<sup>2</sup>. Making use of Eq. (9.24) gives

$$h_o = H_o \ell \sqrt{\frac{\eta u_b b}{8w_z}} = (0.73)(0.075) \sqrt{\frac{(0.015)(30)(0.075)}{(8)(16,000)}} = 28 \text{ } \mu\text{m}$$

$$s_h = h_o / H_o = 28 / 0.73 = 38.3 \text{ } \mu\text{m}$$

All but the last row of surface finish will ensure that  $h_o > (h_o)_{all}$ . Thus, as long as the surface finish is less than 3.2  $\mu\text{m}$  the design is adequate.

For  $\lambda = 1$  and  $1/W_z = 8$  the performance parameters are

1. From Fig. 9.9a

$$\frac{\mu \ell}{s_h} = 8.5$$

$$\mu = \frac{(8.5)(38.3)(10^{-6})}{0.075} = 0.0043$$

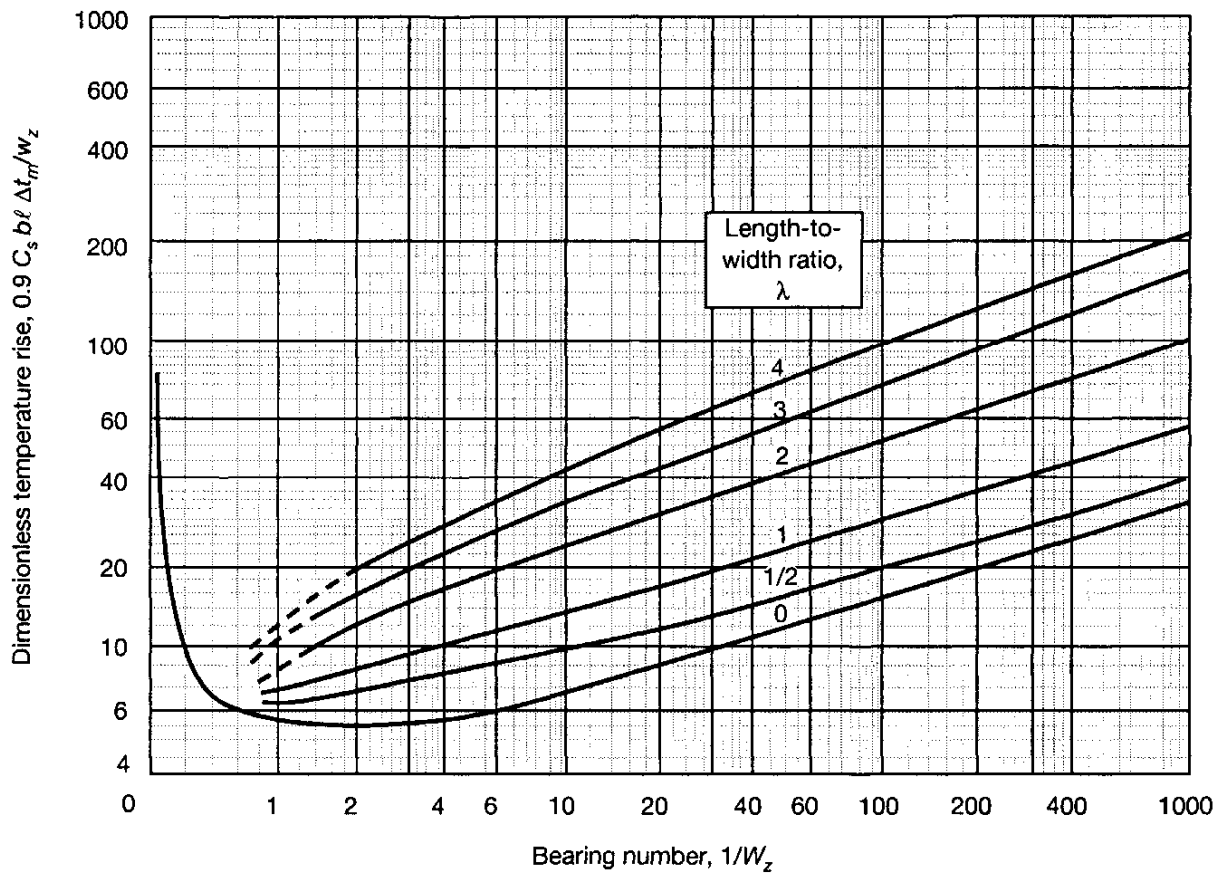


Figure 9.8: Chart for determining dimensionless temperature rise due to viscous shear heating of lubricant in fixed-incline-pad thrust bearings. [From Raimondi and Boyd (1955).]

2. From Fig. 9.9b

$$\frac{1.5h_p\ell}{w_z u_b s_h} = 11$$

$$h_p = \frac{11w_z u_b s_h}{1.5\ell} = \frac{(11)(16)(10^3)(30)(38.3)(10^{-6})}{(1.5)(0.075)}$$

$$h_p = 17.06 \times 10^3 \text{ W} = 17.06 \text{ kW}$$

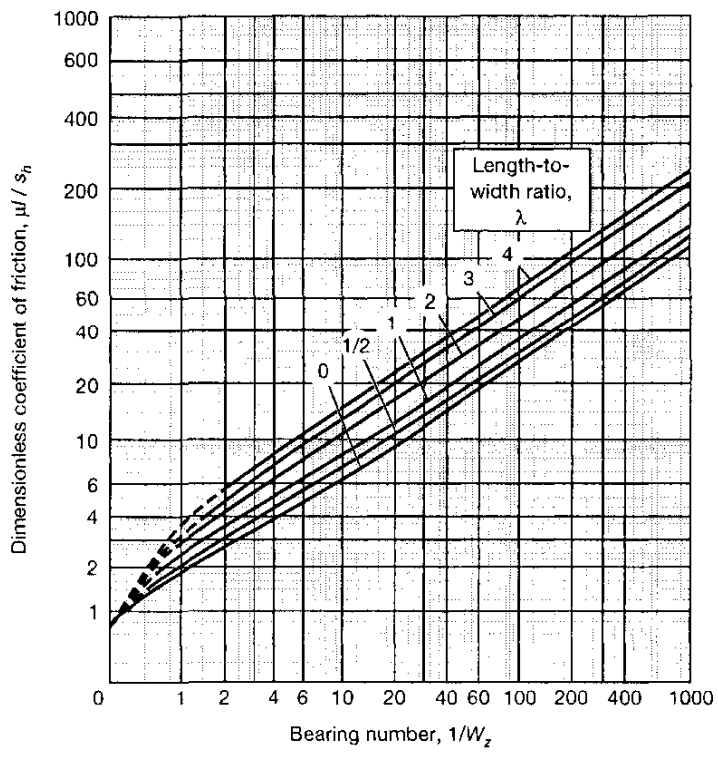
3. From Fig. 9.9c

$$\frac{q}{b u_b s_h} = 0.58$$

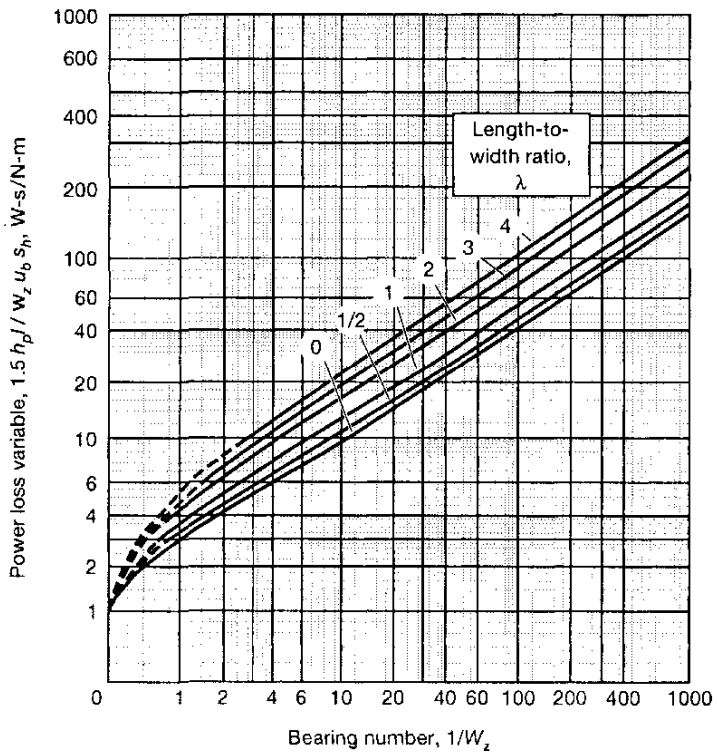
$$q = (0.58)b u_b s_h = (0.58)(0.075)(30)(38.3)(10^{-6}) = 5.00 \times 10^{-5} \text{ m}^3/\text{s}$$

4. From Fig. 9.9d

$$q_s = 0.3q = 1.50 \times 10^{-5} \text{ m}^3/\text{s}$$

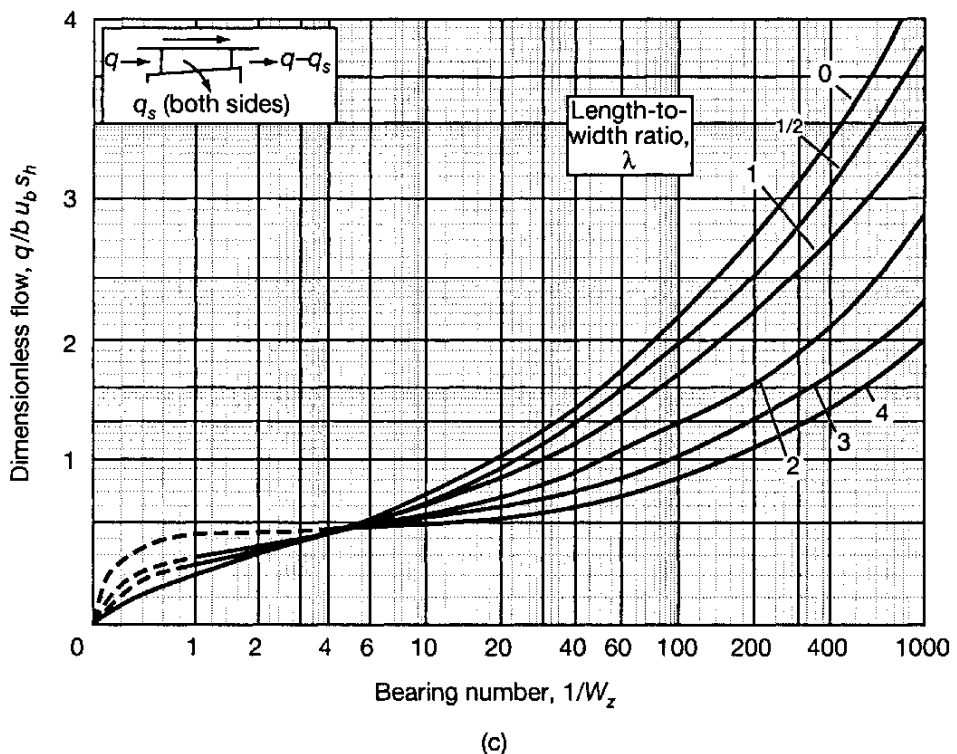


(a)

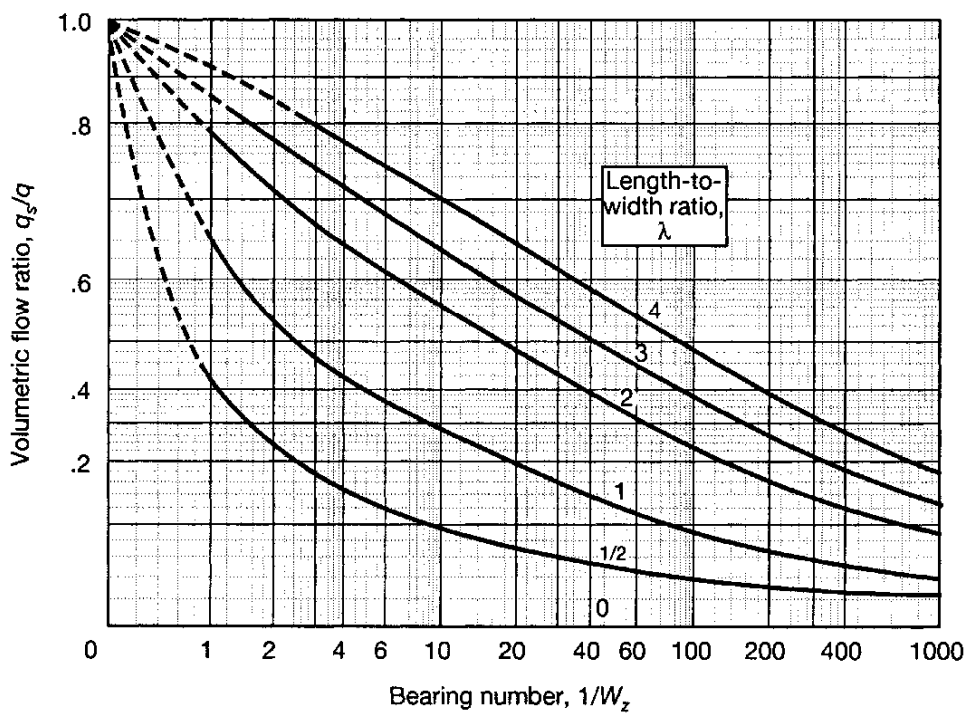


(b)

Figure 9.9: Chart for determining performance parameters of fixed-incline-pad thrust bearings. (a) Friction coefficient; (b) power loss; [From Raimondi and Boyd (1955)].



(c)



(d)

Figure 9.9: Concluded. (c) Lubricant flow; (d) lubricant side flow.

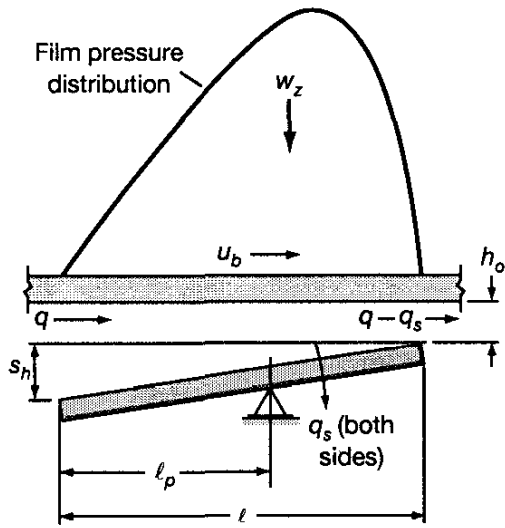


Figure 9.10: Side view of pivoted-pad thrust bearing. [From Raimondi and Boyd (1955).]

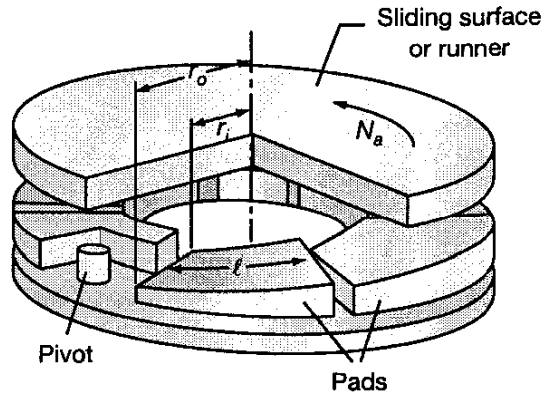


Figure 9.11: Configuration of multiple pivoted-pad thrust bearing. [From Raimondi and Boyd (1955).]

## 9.4 Pivoted-Pad Slider Bearing

The simplest form of pivoted-pad bearing provides only for straight-line motion and consists of a flat surface sliding over a pivoted pad as shown in Fig. 9.10. If the pad is assumed to be in equilibrium under a given set of operating conditions, any change in these conditions, such as a change in load, speed, or viscosity, will alter the pressure distribution and thus momentarily shift the center of pressure, creating a moment that causes the pad to change its inclination and shoulder height  $s_h$ . A pivoted-pad slider bearing is thus supported at a single point so that the angle of inclination becomes a variable and has much better stability than a fixed-incline slider under varying conditions of operation. The location of the shoe's pivot point can be found from the equilibrium of moments acting on the shoe about the point. For all practical purposes, only two significant forces may be considered in the moment equation: the resultant due to film pressure and the reaction force normal to the shoe surface. The force due to friction in the pivot is ignored.

Pivoted pads are sometimes used in multiples as pivoted-pad thrust bearings, shown in Fig. 9.11. Calculations are carried through for a single pad, and the properties for the complete bearing are found by combining these calculations in the proper manner, as discussed in Sec. 9.5.

Normally, a pivoted pad will only carry load if the pivot is placed somewhere between the center of the pad and the outlet edge ( $0.5 \leq n_s \leq 1.0$ ). For bidirectional operation the pivot is located at the center of the pad or at  $n_s = 0.5$ .

The following procedure helps in designing pivoted-pad thrust bearings:

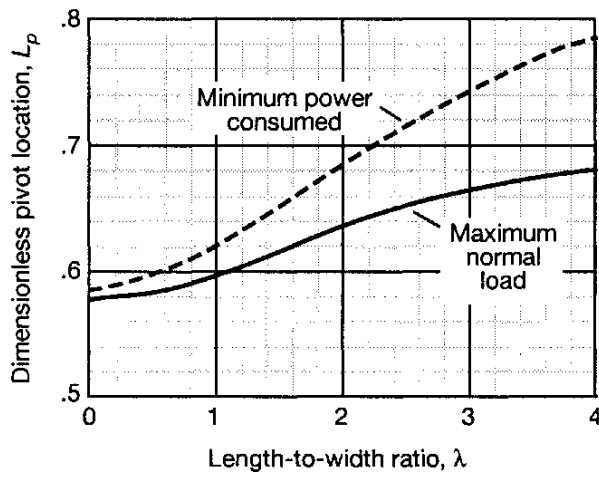


Figure 9.12: Chart for determining pivot location corresponding to maximum load or minimum power loss for various pad proportions - pivoted-pad bearings. [From Raimondi and Boyd (1955).]

1. Having established whether minimum power or maximum load is more critical in the particular application and having chosen a pad length-to-width ratio, establish the pivot location from Fig. 9.12.
2. Just as was done for a fixed-incline-pad thrust bearing, establish the lubricant temperature by using Eq. (9.23). Once the temperature is known, the viscosity can be obtained from Fig. 4.2 or 4.9.
3. Determine the dimensionless load from Fig. 9.13 and the outlet or minimum film thickness from Eq. (9.24).
4. Check Table 9.2 to see if the outlet film thickness is sufficient for the preassigned surface finish. If  $(h_o)_{\text{Eq. (9.24)}} \geq (h_o)_{\text{Table 9.2}}$ , go to step 5. If  $(h_o)_{\text{Eq. (9.24)}} < (h_o)_{\text{Table 9.2}}$ , consider
  - (a) Increasing the speed of the bearing
  - (b) Decreasing the inlet temperature of the bearing
  - (c) Decreasing the load on the bearing
  - (d) Decreasing the finish on the bearing lubricating surfaces, thereby making them smoother.

Upon making this change return to step 2.

5. From Fig. 9.14 determine the temperature rise due to shear heating for a given length-to-width ratio and bearing characteristic number. If it is within 5% of the guessed value, go to step 6; otherwise, let this value of the temperature rise become the new guess and return to step 2.
6. Evaluate the performance parameters once an adequate minimum film thickness and lubricant temperature have been determined. Specifically, from Fig. 9.15 the film thickness ratio  $H_o = h_o/s_h$ , friction coefficient  $\mu$ , total flow  $q$ , side flow  $q_s$ , and power loss  $h_p$ , can be determined.

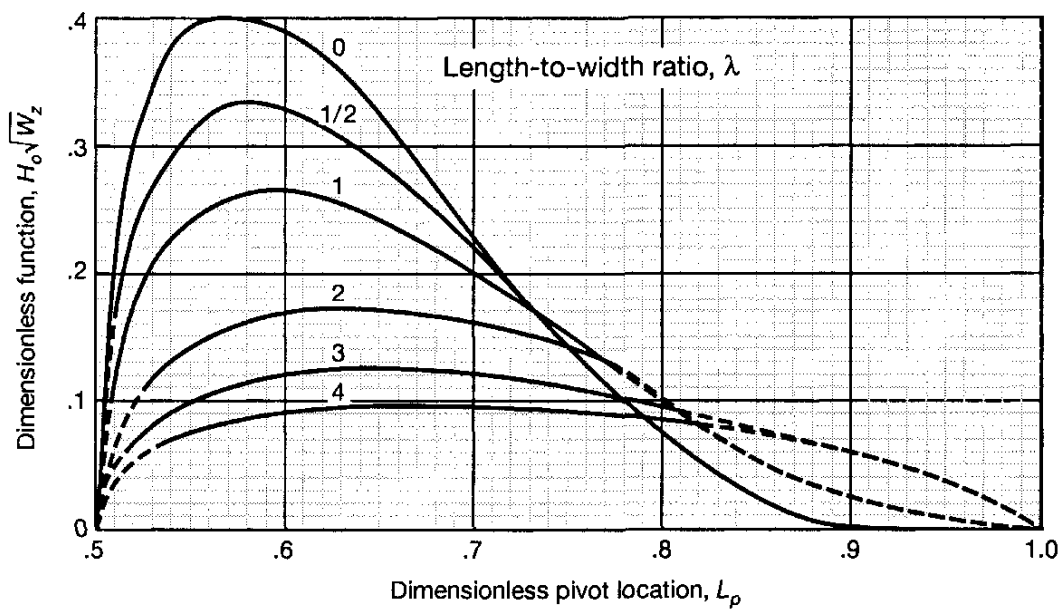


Figure 9.13: Chart for determining outlet film thickness for pivoted-pad thrust bearings. [From Raimondi and Boyd (1955).]

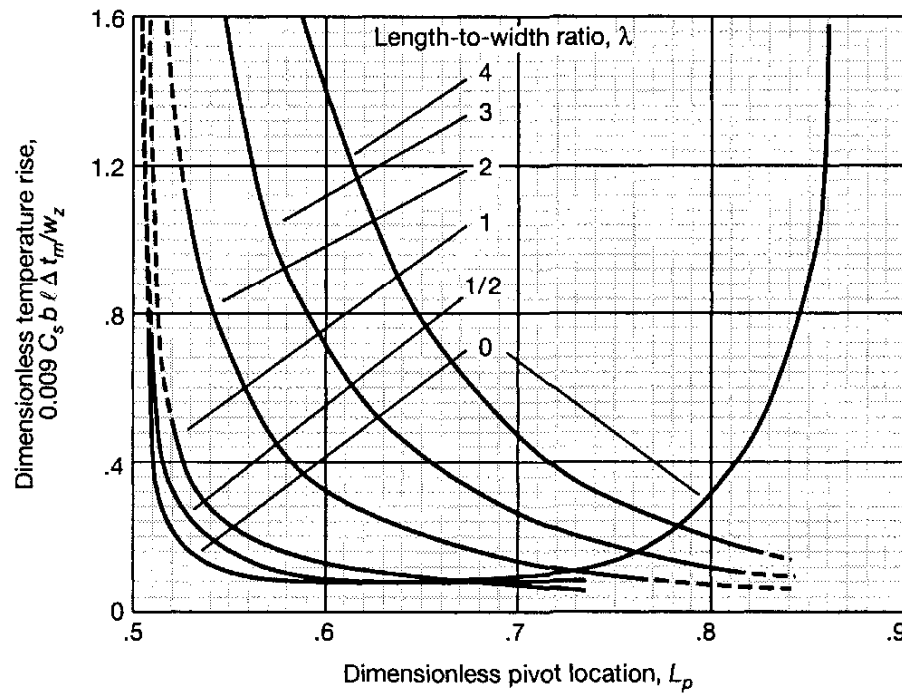


Figure 9.14: Chart for determining dimensionless temperature rise due to viscous shear heating of lubricant for pivoted-pad thrust bearing. [From Raimondi and Boyd (1955).]

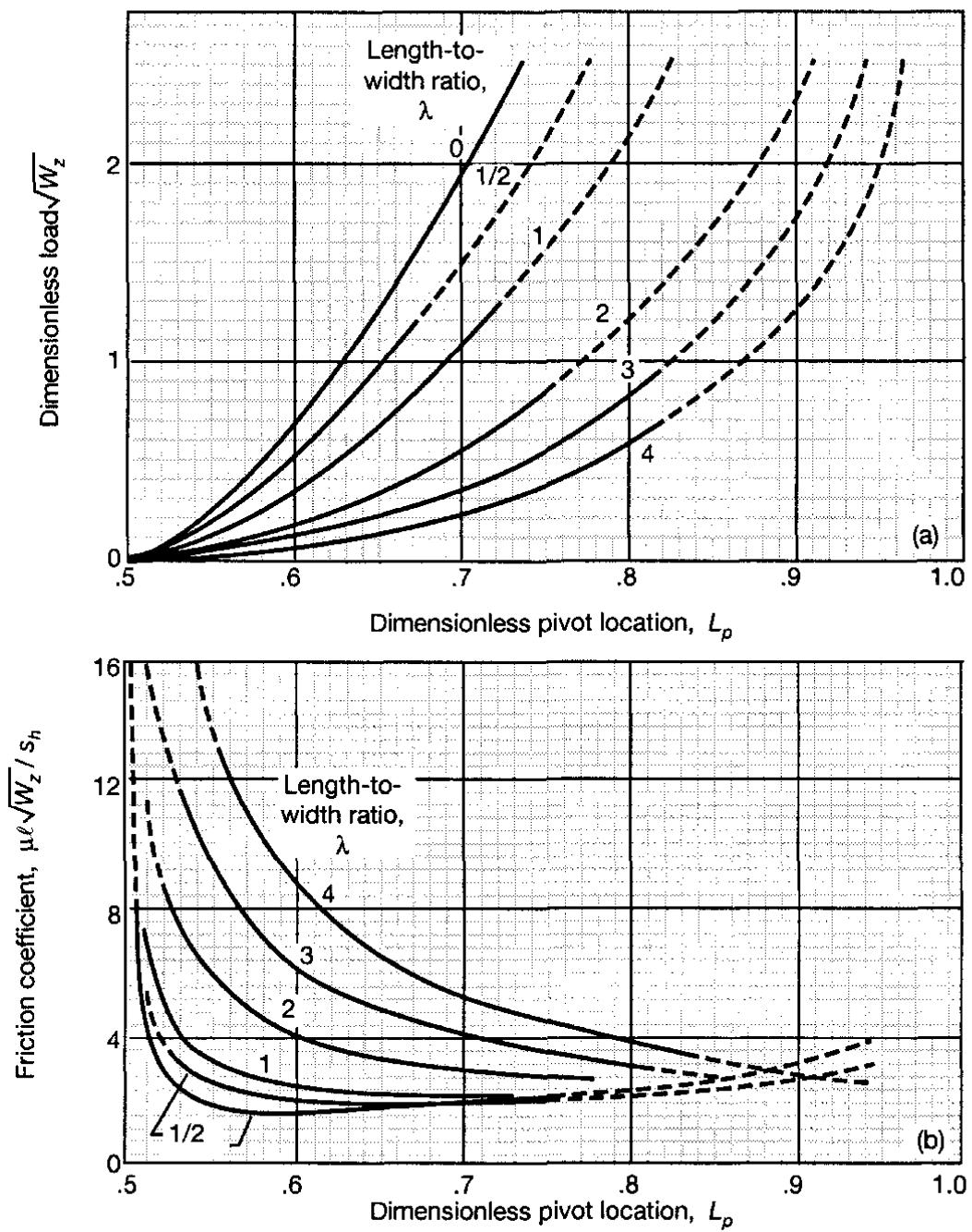


Figure 9.15: Chart for determining performance parameters for pivoted-pad thrust bearings. (a) Dimensionless load; (b) friction coefficient. [From Raimondi and Boyd (1955).]

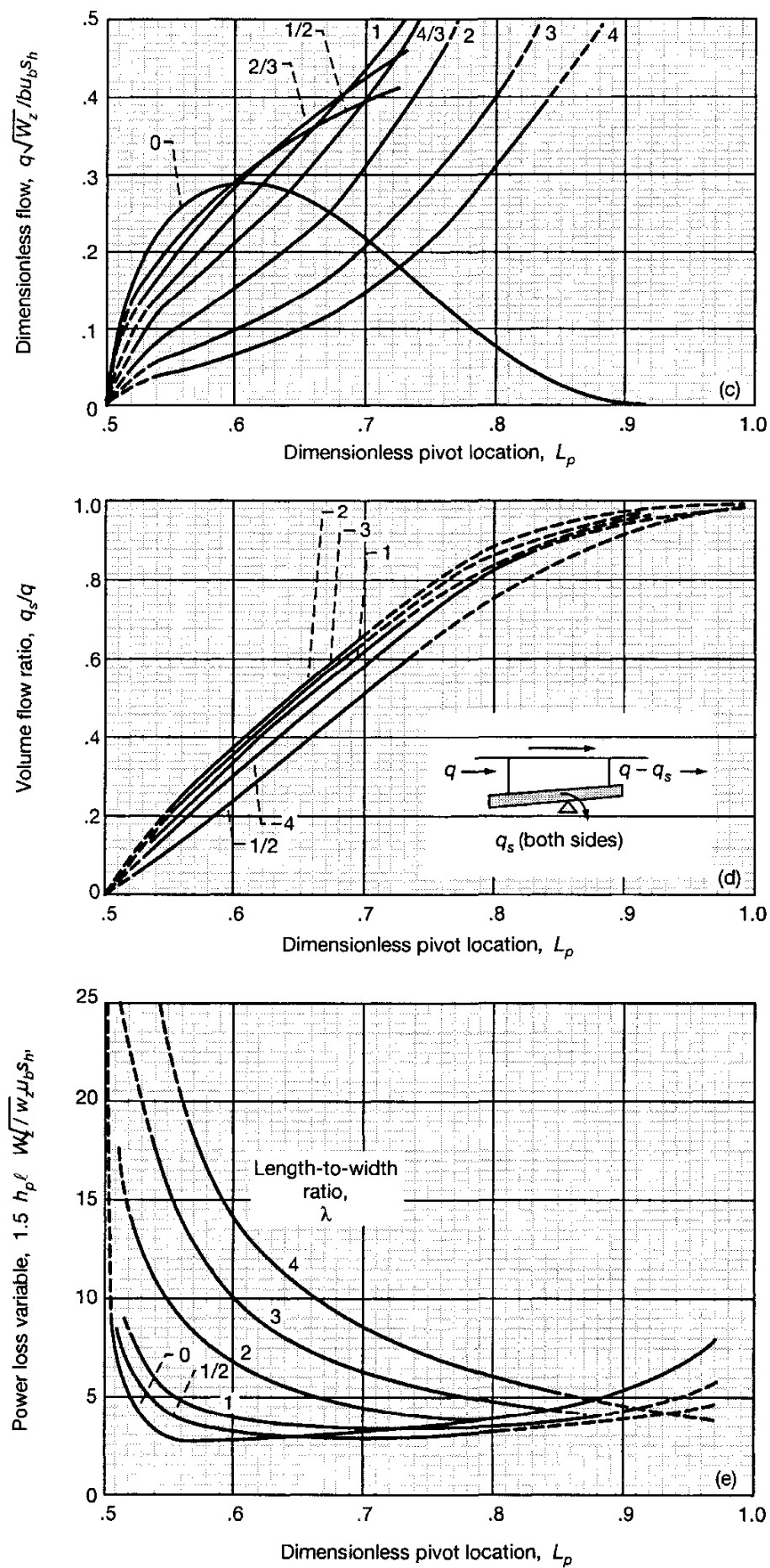


Figure 9.15: Concluded. (c) Lubricant flow; (d) lubricant side flow; (e) power loss.

---

## Example 9.2

**Given** A tilting thrust pad has a length and width of 25 mm. Determine the pivot location if the bearing operates with a minimum power consumption. Determine what the minimum film thickness is when supporting a normal applied load of 9000 N at a surface velocity of 7.5 m/s. The lubricant viscosity is assumed constant at  $0.035 \text{ N}\cdot\text{s}/\text{m}^2$ .

**Find** Is the minimum film thickness obtained from your calculations adequate if the surface finish is  $0.50 \mu\text{m}$ ? If not, could you give some suggestions to meet this requirement?

**Solution** From Fig. 9.12 for  $\lambda = 1$  and minimum power consumption,

$$L_p = 0.62$$

From Fig. 9.13 for  $L_p = 0.62$  and  $\lambda = 1$ ,

$$H_o \sqrt{W_z} = 0.26$$

or

$$h_o = 0.26 \ell \sqrt{\eta_0 u_b b / w_z}$$

It is given that

$$\eta_o = 0.035 \text{ N}\cdot\text{s}/\text{m}^2$$

$$w_z = 9000 \text{ N}$$

$$u_b = 7.5 \text{ m/s}$$

$$\ell = b = 0.025 \text{ m}$$

$$h_o = 0.26(0.025) \sqrt{(0.035)(7.5)(0.025)/9000} = 5.55 \mu\text{m}$$

From Fig. 9.15(a) for  $L_p = 0.62$  and  $\lambda = 1$ , we get

$$\sqrt{W_z} = 0.45$$

or

$$H_o = \frac{0.26}{0.45} = 0.578$$

But

$$H_o = \frac{h_o}{s_h}$$

$$s_h = h_o / H_o = (5.55)(10^{-6}) / 0.578 = 9.60 \times 10^{-6} \text{ m}$$

From Table 9.2 for a surface finish of  $0.50 \mu\text{m}$ , the allowable minimum film thickness is  $12.5 \mu\text{m}$ . Thus

$$(h_o)_{\min} = 12.5 \times 10^{-6} \text{ m}$$

Since the minimum film thickness that we calculated is less than the allowable minimum film thickness  $(h_o)_{\min}$  obtained from Table 9.2, the pad must be redesigned.

Some possible suggestions for the redesign are

1. Change the surface finish from 0.5 to 0.2  $\mu\text{m}$ .
2. Increase the fluid viscosity from 0.035 to 0.14  $\text{N}\cdot\text{s}/\text{m}^2$ .
3. Increase the speed from 7.5 to 30 m/s.
4. Decrease the load from 9000 to 1150 N.

Only one of these changes is necessary to meet the requirements, but combinations of these changes would make the overall redesign less demanding.

---

## 9.5 Thrust Bearing Geometry

This chapter, as well as Chapter 8, deals with the performance of an individual pad of a thrust bearing. Normally, a number of identical pads are assembled in a thrust bearing as shown, for example, in Figs. 9.5 and 9.11. The length, width, speed, and load of an individual pad can be related to the geometry of a thrust bearing by the following formulas:

$$b = r_o - r_i \quad (9.25)$$

$$\ell = \frac{r_o + r_i}{2} \left( \frac{2\pi}{N_0} - \frac{\pi}{36} \right) \quad (9.26)$$

$$u_b = \frac{(r_o + r_i)\omega}{2} \quad (9.27)$$

$$w_t = N_0 w_z \quad (9.28)$$

where  $N_0$  is the number of identical pads placed in the thrust bearing (usually  $N_0$  is between 3 and 20). The  $\pi/36$  portion of Eq. (9.26) accounts for feed grooves between the pads. These are deep grooves which ensure that ambient pressure is maintained between the pads. Also in Eq. (9.28)  $w_t$ , is the total thrust load on the bearing.

In the design of thrust bearings the total normal load-carrying capacity  $w_t$  and the angular velocity  $\omega$  are usually specified along with the overall bearing dimensions  $r_o$  and  $r_i$ . The lubricant is usually specified to suit the design requirements of the associated journal bearing of other components. It therefore remains only to determine the number of pads  $N_0$  and the pad geometry ( $H_o$ ,  $L_p$ , and  $\lambda$ ). The bearing performance characteristics may then be evaluated to check if the design meets the required specifications.

## 9.6 Closure

The appropriate form of the Reynolds equation for a hydrodynamically lubricated thrust bearing when side leakage is considered is

$$\frac{\partial}{\partial x} \left( h^3 \frac{\partial p}{\partial x} \right) + \frac{\partial}{\partial y} \left( h^3 \frac{\partial p}{\partial y} \right) = 6\eta u_b \frac{\partial h}{\partial x}$$

The only film shape that can be solved analytically when considering side leakage is that for a parallel-step slider bearing. Since the film shape is constant within the inlet and outlet regions, the preceding equation reduces to a Laplacian equation that can be readily solved for the pressure. Integrating the pressure over the bearing area enables the normal applied load to be obtained. Side leakage, which reduces the normal load-carrying capacity, is considerable for a parallel-step bearing, it therefore was suggested that shrouds be placed at the sides to restrict the side leakage and thereby increase the bearing's load-carrying capacity.

Results were presented for fixed-incline-pad and pivoted-pad thrust bearings from numerical evaluation of the Reynolds equation. A procedure was outlined to assist in designing these bearings. These procedures provide an optimum pad configuration as well as describe such performance parameters as normal applied load, friction coefficient, power loss, and lubricant flow through the bearing.

## 9.7 Problems

- 9.1 Compare the dimensionless normal applied load  $W_z$  for the following three types of thrust pad: (a) parallel step, (b) fixed incline, and (c) tilting pad for  $\lambda = \ell/b$  of  $\frac{1}{4}$ ,  $\frac{1}{2}$ , 1, and 2. Consider side-leakage effects. Use optimal geometry for each type of pad at each  $\lambda$ . Also compare these results with the  $W_z$  when side leakage is neglected.
- 9.2 Draw the pressure profile of an unshrouded parallel-step pad when  $\lambda = 1$ ,  $H_o = 1$ ,  $n_s = 0.5$ , and  $Y = 0.5$  for  $X = 0.1, 0.2, \dots, 0.9$ . Use Eqs. (9.8) and (9.13) in your evaluation. Give numerical values of pressure at the various values of  $X$ . Also for the film shape given, determine the dimensionless normal applied load  $W_z$ .
- 9.3 A thrust bearing carries a load of 50,000 N at a rotational speed of 2000 r/min. The bearing has an outside radius of 0.25 m and an inside radius of 0.15 m. A surface finish of 1  $\mu\text{m}$  CLA is recommended. The oil is SAE 10 and the operating inlet temperature is 50°C. Design a suitable tilting-pad bearing for maximum thrust load. The selected pad geometry, pivot location, number of pads, and minimum film thickness should be stated together with an estimate of  $\Delta t_m$ ,  $s_h$ ,  $h_p$ ,  $\mu$ ,  $q$ , and  $q_s$ .

- 9.4 For a fixed-incline-pad slider thrust bearing with  $w_z = 3600$  lbf,  $u_b = 1200$  in./s,  $\ell = 3$  in.,  $b = 3$  in., and SAE 10 oil with inlet temperature of  $40^\circ\text{C}$ , determine the following for a maximum normal load:  $s_h$ ,  $h_o$ ,  $\Delta t_m$ ,  $\mu$ ,  $h_p$ ,  $q$ , and  $q_s$ .
- 9.5 For a fixed-incline-pad thrust bearing with a total normal load of 12,000 lbf,  $r_o = 4$  in,  $r_i = 2$  in,  $\omega = 30$  r/s,  $\ell/b = 1$ , SAE 10 oil, and  $t_i = 100^\circ\text{F}$ , determine the following:  $N_0$ ,  $s_h$ ,  $h_o$ ,  $\Delta t_m$ ,  $\mu$ ,  $h_p$ ,  $q$ , and  $q_s$ .
- 9.6 For the input parameters given in Problem 9.5, determine the same output parameters given in Problem 9.5 but for a tilted-pad thrust bearing.
- 9.7 By starting with Eq. (9.22) show that as  $\lambda \rightarrow 0$  or as the situation is approached where side leakage can be neglected, the normal load is the same as discovered in Chapter 8, namely, Eq. (8.73).
- 9.8 A fixed-incline slider bearing and a pivoted-pad slider bearing are optimized to give minimum relative power loss. The pad length  $\ell$  equals the width  $b$ . The bearing carries the load  $w_z = 10$  kN. The viscosity has been chosen to avoid the surface contact through the lubricant film. The sliding speed  $u_b = 15$  m/s. Find the minimum film thickness for the bearing if  $\eta_0 = 0.08$  N·s/m<sup>2</sup>,  $\lambda = \ell/b = 1$  and  $\ell = 0.070$  m.
- 9.9 The flat slider bearing in Problem 9.8 is split into two equal halves, each with width  $b = 0.035$  m. Find the viscosity needed at the running temperature to get the same minimum film thickness as in Problem 9.8. The load is equally split between the two halves, with 5 kN per half. The bearing halves should both be optimized for minimum relative power loss.
- 9.10 The flat slider bearing in Problem 9.8 has load  $w_z = 10$  kN and sliding speed  $u_b = 15$  m/s. The oil viscosity  $\eta_0 = 0.08$  N·s/m<sup>2</sup>, the bearing width  $b = 0.070$  m, and the bearing length  $\ell = 0.070$ . Find the spring constant for the bearing if the force variation is small. The spring constant is defined as

$$c_s = \frac{\Delta w_z}{\Delta h_p}$$

where

$\Delta w_z$  = load variation

$\Delta h_p$  = oil film thickness variation at load application point

- 9.11 A pivoted-pad thrust bearing carrying the weight of a water turbine for a hydroelectric power plant is lubricated by water. The design should be optimized to give minimum power loss when the roughness of the bearing surface is  $R_a = 7 \mu\text{m}$ , indicating that the bearing minimum film thickness should be  $100 \mu\text{m}$ . The load on the bearing from the weight of the turbine and the water is 1 MN. The viscosity of water is 0.001 Pa·s and the bearing length-to-width ratio is 1, which gives minimum power loss for five pads

circumferentially around the bearing with a mean radius equal to the bearing pad width. Determine the bearing dimensions and calculate the coefficient of friction at a rotating speed of 100 rpm.

- 9.12 A propeller shaft thrust bearing for an oil tanker is a pivoted-pad slider bearing with 12 pads. Each pad is 300 mm wide and 300 mm long and has a mean radius of 800 mm. The shaft speed is 220 rpm. Find the bearing pivot position and the optimum lubricant viscosity to get minimum power loss. Calculate the coefficient of friction and the power loss. The lubricant inlet temperature is 63°C, the heat capacity of the oil is  $C_s = 1.72 \times 10^6$  J/(m<sup>3</sup>·°C), and the propeller thrust load is 1.3 MN.

## References

Engineering Sciences Data Unit (ESDU) (1967): *General Guide to the Choice of Thrust Bearing Type*. Item 67033. Institution of Mechanical Engineers, London.

Raimondi, A. A., and Boyd, J. (1955): Applying Bearing Theory to the Analysis and Design of Pad-Type Bearings. *ASME Trans.*, vol. 77, no. 3, pp. 287-309.

# Chapter 10

## Hydrodynamic Journal Bearings - Analytical Solutions

### Symbols

$\tilde{A}$	integration constant	$W_r$	dimensionless resultant load in a journal bearing
$b$	width of bearing, m	$w'_r$	resultant load per unit width in a journal bearing, N/m
$c$	radial clearance of journal bearing, m	$w'_x$	load per width perpendicular to line of centers, N/m
$e$	eccentricity of journal bearing, m	$w'_z$	load per width along line of centers, N/m
$h$	film thickness, m		normal applied load, N
$h_m$	film thickness where $dp/d\phi = 0$ , m		angle used in defining film thickness in journal bearing
$N_a$	angular velocity, rpm	$\alpha$	Sommerfeld variable
$P$	dimensionless pressure	$\gamma$	eccentricity ratio, $e/c$
$P_m$	dimensionless pressure where $dp/d\phi = 0$	$\epsilon$	absolute viscosity, Pa·s
$p$	pressure, N/m <sup>2</sup>	$\eta$	absolute viscosity at $p = 0$
$p_m$	pressure where $dp/d\phi = 0$	$\eta_0$	and constant temperature, Pa·s
$q$	volumetric flow rate, m <sup>3</sup> /s	$\Phi$	attitude angle
$q'_y$	volumetric flow rate per width in transverse direction, m <sup>2</sup> /s	$\phi$	angle in cylindrical coordinates
$q'_\phi$	volumetric flow rate per width in $\phi$ direction, m <sup>2</sup> /s	$\phi_m$	angle where $dp/d\phi=0$
$Q$	dimensionless flow rate	$\phi^*$	angle where $p = 0$ and $dp/d\phi = 0$
$r$	radius of journal, m	$\omega$	angular velocity, $2\pi N_a$ , rad/s
$r_a$	radius of shaft, m	$\omega_b$	angular velocity of surface $b$ , rad/s
$r_b$	radius of journal, m		

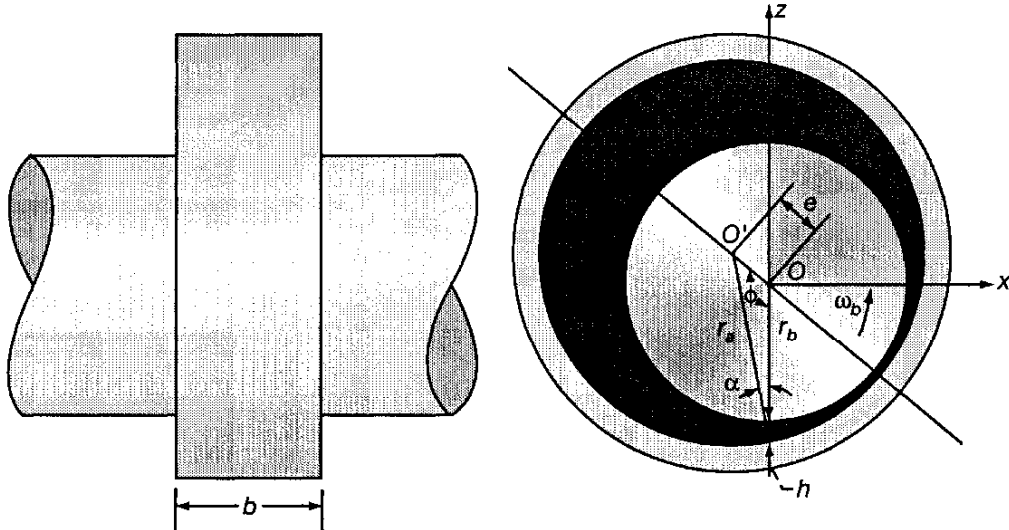


Figure 10.1: Hydrodynamic journal bearing geometry

## 10.1 Introduction

The past two chapters have dealt with slider bearing pads as used in thrust bearings. The surfaces of thrust bearings are perpendicular to the axis of rotation as shown in Fig. 8.3. This chapter and the next deal with journal bearings, where the bearing surfaces are parallel to the axis of rotation. Journal bearings are used to support shafts and to carry radial loads with minimum power loss and minimum wear. The journal bearing can be represented by a plain cylindrical sleeve (bushing) wrapped around the journal (shaft), but the bearings can adopt a variety of forms. The lubricant is supplied at some convenient point in the bearing through a hole or a groove. If the bearing extends around the full  $360^\circ$  of the journal, it is described as a “full journal bearing.” If the angle of wrap is less than  $360^\circ$ , the term “partial journal bearing” is used.

Journal bearings rely on shaft motion to generate the load-supporting pressures in the lubricant film. The geometry of the journal bearing is shown in Fig. 10.1. The shaft does not normally run concentric with the bearing. The displacement of the shaft center relative to the bearing center is known as the “eccentricity.” The shaft’s eccentric position within the bearing clearance is influenced by the load that it carries. The amount of eccentricity adjusts itself until the load is balanced by the pressure generated in the converging lubricating film. The line drawn through the shaft center and the bearing center is called the “line of centers.”

The pressure generated and therefore the load-carrying capacity of the bearing depend on the shaft eccentricity, the angular velocity, the effective viscosity of the lubricant, and the bearing dimensions and clearance.

$$w_z = f(e, \omega, \eta_0, r, b, c)$$

The load and the angular velocity are usually specified and the minimum shaft

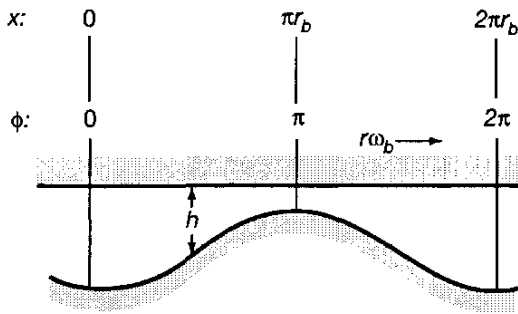


Figure 10.2: Unwrapped film shape in a journal bearing.

diameter is often predetermined. To complete the design, it will be necessary to calculate the bearing dimensions and clearance and to choose a suitable lubricant if this is not already specified.

The approach used in this chapter is to present two approximate journal bearing solutions: (1) an infinite-width solution (side leakage neglected) and (2) a short-width-journal-bearing theory. These two approximate solutions will illustrate the many important characteristics of journal bearings.

## 10.2 Infinitely-Wide-Journal-Bearing Solution

For an infinitely wide-journal-bearing solution the pressure in the axial direction is assumed to be constant. This approach is valid for diameter-to-width ratios ( $\lambda_k = 2r_b/b$ ) less than 0.5. The integrated form of the Reynolds equation can be written from Eq. (7.52), while assuming a constant viscosity, as

$$\frac{dp}{dx} = \frac{6\eta_0 r_b \omega_b (h - h_m)}{h^3} \quad (7.52)$$

where  $h_m$  denotes the film thickness when  $dp/dx = 0$ . Now

$$dx = r_b d\phi$$

$$\frac{dp}{d\phi} = \frac{6\eta_0 r_b^2 \omega_b (h - h_m)}{h^3} \quad (10.1)$$

The transition from Eq. (7.52) to (10.1) is acceptable, since the film thickness is small relative to the shaft radius and the curvature of the lubricant film can be neglected. This implies that the film shape can be unwrapped from around the shaft and viewed as a periodic stationary profile with wavelength  $2\pi r_b$  and that the plane surface of the shaft is moving with velocity  $r\omega$  as shown in Fig. 10.2. From Fig. 10.1,

$$\begin{aligned} \cos \alpha &= \frac{1}{r_a} [h + r_b + e \cos(\pi - \phi)] \\ \therefore h &= r_a \cos \alpha - r_b + e \cos \phi \end{aligned} \quad (10.2)$$

From the law of sines,

$$\frac{e}{\sin \alpha} = \frac{r_a}{\sin \phi}$$

$$\therefore \sin \alpha = \frac{e \sin \phi}{r_a}$$

and

$$\cos \alpha = (1 - \sin^2 \alpha)^{1/2} = \left[ 1 - \left( \frac{e}{r_a} \right)^2 \sin^2 \phi \right]^{1/2} \quad (10.3)$$

Substituting Eq. (10.3) into Eq. (10.2) gives

$$h = r_a \left[ 1 - \left( \frac{e}{r_a} \right)^2 \sin^2 \phi \right]^{1/2} - r_b + e \cos \phi$$

But

$$\left[ 1 - \left( \frac{e}{r_a} \right)^2 \sin^2 \phi \right]^{1/2} = 1 - \frac{1}{2} \left( \frac{e}{r_a} \right)^2 \sin^2 \phi - \frac{1}{8} \left( \frac{e}{r_a} \right)^4 \sin^4 \phi - \dots$$

$$\therefore h = r_a \left[ 1 - \frac{1}{2} \left( \frac{e}{r_a} \right)^2 \sin^2 \phi - \frac{1}{8} \left( \frac{e}{r_a} \right)^4 \sin^4 \phi - \dots \right] - r_b + e \cos \phi$$

or, since  $r_a - r_b = c$ ,

$$h = c + e \left[ \cos \phi - \frac{1}{2} \left( \frac{e}{r_a} \right) \sin^2 \phi - \frac{1}{8} \left( \frac{e}{r_a} \right)^3 \sin^4 \phi - \dots \right] \quad (10.4)$$

Since the ratio of  $e/r_a$  is of the order of magnitude  $10^{-3}$ , Eq. (10.4) can be safely reduced to

$$h = c(1 + \epsilon \cos \phi) \quad (10.5)$$

where

$$\epsilon = \frac{e}{c} \quad (10.6)$$

is the eccentricity ratio. Note that  $0 \leq \epsilon \leq 1$ .

Substituting the film thickness equation (10.5) into Eq. (10.1) gives

$$\frac{dp}{d\phi} = 6\eta_0 \omega_b \left( \frac{r_b}{c} \right)^2 \left( \frac{1}{(1 + \epsilon \cos \phi)^2} - \frac{h_m}{c(1 + \epsilon \cos \phi)^3} \right) \quad (10.7)$$

An expression for the pressure distribution can be obtained by direct integration of Eq. (10.7)

$$p = 6\eta_0 \omega_b \left( \frac{r_b}{c} \right)^2 \int \left( \frac{1}{(1 + \epsilon \cos \phi)^2} - \frac{h_m}{c(1 + \epsilon \cos \phi)^3} \right) d\phi + \tilde{A} \quad (10.8)$$

Table 10.1: Relationship between angle  $\phi$  and Sommerfeld variable  $\gamma$  (degrees) for various eccentricity ratios  $\epsilon$ .

Circumferential coordinate angle, $\phi$ , deg	Eccentricity ratio, $\epsilon$							
	0.2	0.4	0.5	0.6	0.7	0.8	0.9	0.95
Sommerfeld variable, $\gamma$ , deg								
0	0	0	0	0	0	0	0	0
10	8.17	6.55	5.78	5.01	4.21	3.34	2.30	1.60
20	16.38	13.16	11.62	10.07	8.47	6.72	4.63	3.23
30	24.68	19.89	17.58	15.26	12.84	10.20	7.03	4.91
40	33.10	26.80	23.73	20.62	17.36	13.83	9.54	6.67
50	41.68	33.95	30.13	26.24	22.16	17.67	12.21	8.54
60	50.47	41.41	36.87	32.20	27.26	21.78	15.09	10.56
70	59.51	49.25	44.02	38.59	32.78	26.27	18.25	12.79
80	68.83	57.56	51.69	45.52	38.83	31.25	21.79	15.30
90	78.46	66.42	60.00	53.13	45.57	36.87	28.84	18.19
100	88.43	75.92	69.06	61.57	53.18	43.33	30.58	21.60
110	98.76	86.14	79.01	71.05	61.92	50.91	36.28	25.76
120	109.47	97.18	90.00	81.78	72.08	60.00	43.34	31.00
130	120.53	109.07	102.14	93.99	84.03	71.11	52.39	37.90
140	131.94	121.85	115.54	107.89	98.18	84.96	64.44	47.49
150	143.66	135.48	130.20	123.62	114.93	102.41	81.14	61.72
160	155.62	149.85	146.03	141.14	134.46	124.24	104.90	84.48
170	167.76	164.77	162.76	160.15	156.47	150.58	138.25	122.66
180	180.00	180.00	180.00	180.00	180.00	180.00	180.00	180.00

Note: When  $\epsilon = 0$ ,  $\gamma = 0$ . When  $\epsilon = 1$ ,  $\gamma = 0$ . For  $180^\circ \leq \phi \leq 360^\circ$  the relationship is  $\gamma(-\phi) = \gamma(\phi)$ .

### 10.2.1 Full Sommerfeld Solution

The procedure for evaluating integrals of the type

$$\int \frac{d\phi}{(1 + \epsilon \cos \phi)^n}$$

is to introduce a new variable  $\gamma = \tan(\phi/2)$ . With this procedure the pressure can be evaluated, but the expression is not particularly useful, since it is difficult to obtain the load components from a further integration.

Sommerfeld in 1904 neatly overcame these difficulties by using the substitution

$$1 + \epsilon \cos \phi = \frac{1 - \epsilon^2}{1 - \epsilon \cos \gamma} \quad (10.9)$$

This relationship is known as the “Sommerfeld substitution,” and  $\gamma$  is known as the “Sommerfeld variable.” Table 10.1 shows the relationship between the circumferential coordinate angle  $\phi$  and  $\gamma$  for a number of eccentricity ratios. From Eq. (10.9) the following can be written:

$$\sin \phi = \frac{(1 - \epsilon^2)^{1/2} \sin \gamma}{1 - \epsilon \cos \gamma} \quad (10.10)$$

$$\cos \phi = \frac{\cos \gamma - \epsilon}{1 - \epsilon \cos \gamma} \quad (10.11)$$

$$\sin \gamma = \frac{(1 - \epsilon^2)^{1/2} \sin \phi}{1 + \epsilon \cos \phi} \quad (10.12)$$

$$\cos \gamma = \frac{\epsilon + \cos \phi}{1 + \epsilon \cos \phi} \quad (10.13)$$

$$d\phi = \frac{(1 - \epsilon^2)^{1/2} d\gamma}{1 - \epsilon \cos \gamma} \quad (10.14)$$

Making use of the Sommerfeld substitution and the periodic boundary condition yields

$$p - p_0 = \frac{6\eta_0 \omega_b (r_b/c)^2 \epsilon \sin \phi (2 + \epsilon \cos \phi)}{(2 + \epsilon^2) (1 + \epsilon \cos \phi)^2} \quad (10.15)$$

where  $p_o$  is the pressure at the point of maximum film thickness. This equation represents the Sommerfeld solution for pressure distribution in a full journal bearing. In dimensionless form this equation becomes

$$P = \frac{p - p_0}{\eta_0 \omega_b} \left( \frac{c}{r_b} \right)^2 = \frac{6\epsilon \sin \phi (2 + \epsilon \cos \phi)}{(2 + \epsilon^2) (1 + \epsilon \cos \phi)^2} \quad (10.16)$$

Booker (1965) has developed a useful tabulation of integrals normally encountered in journal bearing analysis.

The pressure distribution is shown in Fig. 10.3 for a full Sommerfeld solution. Note that positive pressures are generated in the convergent film ( $0 \leq \phi \leq \pi$ ) and negative pressures in the divergent film ( $\pi \leq \phi \leq 2\pi$ ). Figure 10.3 shows that the pressure distribution is skewed symmetrically, with the numerical values of the maximum and minimum pressures and their locations relative to the point of minimum film thickness being equal. In the derivation of Eq. (10.15), which is a problem at the end of this chapter,

$$h_m = \frac{2c(1 - \epsilon^2)}{2 + \epsilon^2} \quad (10.17)$$

Making use of Eqs. (10.17) and (10.5) gives the value of  $\phi$  where  $dp/dx = 0$  as

$$\phi_m = \cos^{-1} \frac{-3\epsilon}{2 + \epsilon^2} \quad (10.18)$$

Note that  $\phi_m \rightarrow \pm\pi/2$  as  $\epsilon \rightarrow 0$  and  $\phi_m \rightarrow \pm\pi$  as  $\epsilon \rightarrow 1$ . From Fig. 10.3 the maximum pressure occurs in the second quadrant, and the minimum pressure

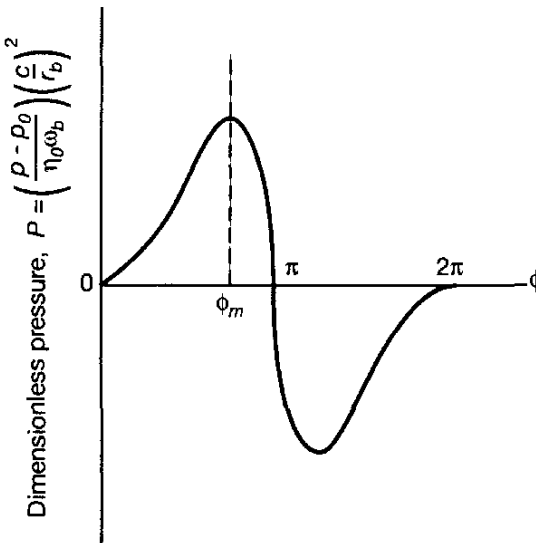


Figure 10.3: Pressure distribution for full Sommerfeld solution.

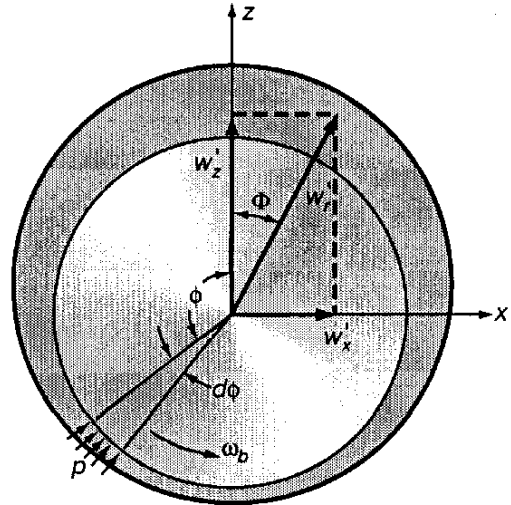


Figure 10.4: Coordinate system and force components in a journal bearing.

in the third quadrant. The maximum and minimum pressures are equidistant from the line of centers.

The maximum dimensionless pressure can be written from Eq. (10.16) as

$$P_m = \frac{p_m - p_0}{\eta_0 \omega_b} \left( \frac{c}{r_b} \right)^2 = \frac{6\epsilon \sin \phi_m (2 + \epsilon \cos \phi_m)}{(2 + \epsilon^2)(1 + \epsilon \cos \phi_m)^2}$$

Making use of Eq. (10.18) and

$$\sin \phi_m = (1 - \cos^2 \phi_m)^{1/2} = \frac{(4 - 5\epsilon^2 + \epsilon^4)^{1/2}}{2 + \epsilon^2}$$

gives

$$P_m = \frac{3\epsilon (4 - 5\epsilon^2 + \epsilon^4)^{1/2} (4 - \epsilon^2)}{2 (2 + \epsilon^2) (1 - \epsilon^2)^2} \quad (10.19)$$

Note that  $P_m \rightarrow 0$  as  $\epsilon \rightarrow 0$  and  $P_m \rightarrow \infty$  as  $\epsilon \rightarrow 1$ .

Once the pressure is known, the load components can be evaluated. It is convenient to determine the components of the resultant load along and perpendicular to the line of centers. The coordinate system and the load components are shown in Fig. 10.4, where

- $w'_x$  = load component per unit width perpendicular to line of centers, N/m
- $w'_z$  = load component per unit width along line of centers, N/m
- $w'_r$  = resultant load per unit width (equal but acting in opposite direction to applied load), N/m
- $\Phi$  = attitude angle (angle through which load vector has to be rotated in direction of journal rotation to bring it into line of centers)

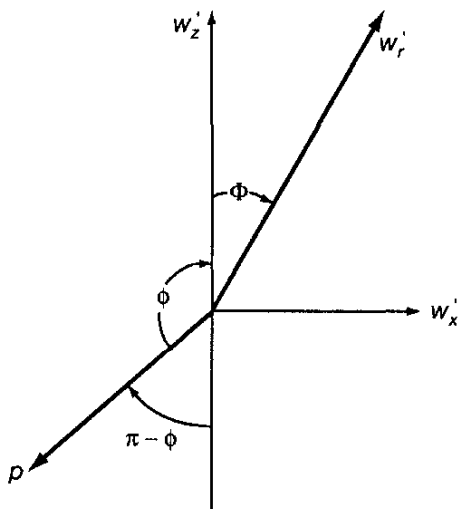


Figure 10.5: Vector forces acting on a journal.

From Fig. 10.5, which shows the vector forces acting on the journal,

$$w'_x = \int_0^{2\pi} pr_b \sin(\pi - \phi) d\phi$$

$$w'_z = \int_0^{2\pi} pr_b \cos(\pi - \phi) d\phi$$

These equations reduce to

$$w'_x = \int_0^{2\pi} pr_b \sin \phi d\phi \quad (10.20)$$

$$w'_z = - \int_0^{2\pi} pr_b \cos \phi d\phi \quad (10.21)$$

Equations (10.20) and (10.21) can be integrated by parts to give

$$w'_x = r_b \int_0^{2\pi} \cos \phi \frac{dp}{d\phi} d\phi \quad (10.22)$$

$$w'_z = r_b \int_0^{2\pi} \sin \phi \frac{dp}{d\phi} d\phi \quad (10.23)$$

Substituting Eq. (10.7) into these equations gives

$$w'_x = 6\eta_0 \omega_b r_b \left( \frac{r_b}{c} \right)^2 \int_0^{2\pi} \left( \frac{\cos \phi}{(1 + \epsilon \cos \phi)^2} - \frac{h_m \cos \phi}{c (1 + \epsilon \cos \phi)^3} \right) d\phi \quad (10.24)$$

$$w'_z = 6\eta_0 \omega_b r_b \left( \frac{r_b}{c} \right)^2 \int_0^{2\pi} \left( \frac{\sin \phi}{(1 + \epsilon \cos \phi)^2} - \frac{h_m \sin \phi}{c (1 + \epsilon \cos \phi)^3} \right) d\phi \quad (10.25)$$

Now

$$\int_0^{2\pi} \frac{\cos \phi}{(1 + \epsilon \cos \phi)^2} d\phi = \frac{1}{\epsilon} \left( \frac{\gamma}{(1 - \epsilon^2)^{1/2}} - \frac{\gamma - \epsilon \sin \gamma}{(1 - \epsilon^2)^{3/2}} \right) \Big|_{\gamma=0}^{\gamma=2\pi}$$

$$\int_0^{2\pi} \frac{\cos \phi d\phi}{(1 + \epsilon \cos \phi)^3} = \frac{1}{\epsilon} \left( \frac{\gamma - \epsilon \sin \gamma}{(1 - \epsilon^2)^{3/2}} + \frac{-2\gamma(2 + \epsilon^2) + 8\epsilon \sin \gamma - \epsilon^2 \sin 2\gamma}{4(1 - \epsilon^2)^{5/2}} \right)_{\gamma=0}^{\gamma=2\pi}$$

$$\int_0^{2\pi} \frac{\sin \phi d\phi}{(1 + \epsilon \cos \phi)^2} = \left( \frac{1}{\epsilon(1 + \epsilon \cos \phi)} \right)_{\phi=0}^{\phi=2\pi}$$

$$\int_0^{2\pi} \frac{\sin \phi d\phi}{(1 + \epsilon \cos \phi)^3} = \left( \frac{1}{2\epsilon(1 + \epsilon \cos \phi)^2} \right)_{\phi=0}^{\phi=2\pi}$$

Substituting these integrals into Eqs. (10.24) and (10.25) gives

$$w'_x = 6\eta_0 \omega_b r_b \left( \frac{r_b}{c} \right)^2 \left[ \frac{1}{\epsilon} \left( \frac{\gamma}{(1 - \epsilon^2)^{1/2}} - \frac{\gamma - \epsilon \sin \gamma}{(1 - \epsilon^2)^{3/2}} \right)_{\gamma=0}^{\gamma=2\pi} \right. \\ \left. - \frac{h_m}{c\epsilon} \left( \frac{\gamma + \epsilon \sin \gamma}{(1 - \epsilon^2)^{3/2}} + \frac{-2\gamma(2 + \epsilon^2) + 8\epsilon \sin \gamma - \epsilon^2 \sin 2\gamma}{4(1 - \epsilon^2)^{5/2}} \right)_{\gamma=0}^{\gamma=2\pi} \right]$$

$$w'_z = 6\eta_0 \omega_b r_b \left( \frac{r_b}{c} \right)^2 \left( -\frac{2\pi\epsilon}{(1 - \epsilon^2)^{3/2}} + \frac{3\pi\epsilon h_m}{c(1 - \epsilon^2)^{5/2}} \right)$$

Making use of Eq. (10.17) yields

$$w'_x = 12\pi\eta_0 \omega_b r_b \left( \frac{r_b}{c} \right)^2 \frac{\epsilon}{(2 + \epsilon^2)(1 - \epsilon^2)^{1/2}} \quad (10.26)$$

and

$$w'_z = 6\eta_0 \omega_b r_b \left( \frac{r_b}{c} \right)^2 \left( \frac{1}{\epsilon(1 + \epsilon \cos \phi)} - \frac{h_m}{2c\epsilon(1 + \epsilon \cos \phi)^2} \right)_{\phi=0}^{\phi=2\pi} = 0 \quad (10.27)$$

This result demonstrates that for a full Sommerfeld solution the resultant normal load acts at right angles to the line of centers; that is, the attitude angle is  $90^\circ$ . As load is applied to the bearing, the journal center moves away from the bearing center at right angles to the load vector.

$$\Phi = 90^\circ \quad (10.28)$$

$$w'_r = w'_x \quad (10.29)$$

Making use of Eq. (10.17) yields

$$W_r = \frac{w'_r}{r_b \omega_b \eta_0} \left( \frac{c}{r_b} \right)^2 = \frac{12\pi\epsilon}{(2 + \epsilon^2)(1 - \epsilon^2)^{1/2}} \quad (10.30)$$

where the dimensionless resultant load-carrying capacity is a function of the eccentricity ratio alone.

Attention is drawn to two important cases for full Sommerfeld solutions:

1.  $\epsilon \rightarrow 0$  as  $W_r \rightarrow 0$ .
2.  $\epsilon \rightarrow 1$  as  $W_r \rightarrow \infty$ .

The first case demonstrates that when the shaft is concentric relative to the bearing (constant clearance around the bearing), the bearing does not have any load-carrying capacity. The second case demonstrates the tremendous potential of a fluid film journal bearing for supporting radial loads. The result suggests that load increases can be accommodated by operating at higher eccentricity ratios, but this suggestion must be tempered by the knowledge that side leakage has been neglected, that bearing surfaces are not perfectly smooth, and that restrictively high temperatures will occur in the thin oil films that exist at high eccentricities. The operating eccentricity must be selected with several design points in mind, but as a design guide it is worth noting that most journal bearings operate with eccentricity ratios between 0.5 and 0.8.

### 10.2.2 Half Sommerfeld Solution

It has been noted that the Sommerfeld solution for a full  $360^\circ$  journal bearing leads to the skew-symmetrical pressure distribution shown in Fig. 10.3. The pressures in the divergent film are all lower than ambient pressure. Such pressures are rarely encountered in real bearings. Mineral oils contain between 8 and 12% dissolved air. This air will start to come out of solution whenever the pressure falls below the saturation pressure. In many situations the saturation pressure is similar to the ambient pressure surrounding the bearing, and in these cases gas liberation will maintain the pressure in the divergent clearance space at close to the ambient level.

This hindrance to predicting subambient pressures by the normal Sommerfeld analysis has led to the suggestion that the subambient pressures predicted by the analysis should be ignored. This approach, which limits the analysis to the convergent film, is known as the "half Sommerfeld solution." The approximation does, in fact, lead to more realistic predictions of some bearing characteristics, but the simple approach leads to a violation of the continuity of mass flow condition at the end of the pressure curve. The boundary condition to be applied at the outlet end of the pressure curve, where the full lubricant film gives way to a ruptured or cavitating film composed of a mixture of gas and liquid, is discussed later.

The pressure distribution assumed for the half Sommerfeld solution is exactly that shown in Fig. 10.3 for the region  $\phi = 0$  to  $\pi$ . However, from  $\phi = \pi$  to  $2\pi$ , instead of the negative pressures shown in the figure, the pressures are zero.

$$P = \frac{p - p_0}{\eta_0 \omega_b} \left( \frac{c}{r_b} \right)^2 = \frac{6\epsilon \sin \phi (2 + \epsilon \cos \phi)}{(2 + \epsilon^2) (1 + \epsilon \cos \phi)^2} \quad \text{for } 0 \leq \phi \leq \pi \quad (10.31)$$

and

$$P = 0 \quad \text{for} \quad \pi \leq \phi \leq 2\pi \quad (10.32)$$

The equations for the film thickness at the location of maximum pressure  $h_m$ , the angle of maximum pressure  $\phi_m$  and the maximum dimensionless pressure  $P_m$  are exactly the same as those developed for the full Sommerfeld solution. That is, Eqs. (10.17) to (10.19) provide values of  $h_m$ ,  $\phi_m$ , and  $P_m$  for the half Sommerfeld solution.

The load components per unit width  $w'_x$  and  $w'_z$  given in Eqs. (10.20) and (10.21) are exactly the same for the half Sommerfeld solution except that the integration limits must be written as 0 to  $\pi$ . When this is done, the load components turn out to be

$$w'_x = 6\eta_0\omega_b r_b \left(\frac{r_b}{c}\right)^2 \left( \frac{-\pi\epsilon}{(1-\epsilon^2)^{3/2}} + \frac{3\pi\epsilon h_m}{2c(1-\epsilon^2)^{5/2}} \right) \quad (10.33)$$

$$w'_z = 6\eta_0\omega_b r_b \left(\frac{r_b}{c}\right)^2 \left( \frac{2}{1-\epsilon^2} - \frac{2h_m}{c(1-\epsilon^2)^2} \right) \quad (10.34)$$

Introducing Eq. (10.17) for  $h_m$  into Eqs. (10.33) and (10.34),

$$w'_x = 6\eta_0\omega_b r_b \left(\frac{r_b}{c}\right)^2 \frac{\pi\epsilon}{(2+\epsilon^2)(1-\epsilon^2)^{1/2}} \quad (10.35)$$

$$w'_z = 12\eta_0\omega_b r_b \left(\frac{r_b}{c}\right)^2 \frac{\epsilon^2}{(2+\epsilon^2)(1-\epsilon^2)} \quad (10.36)$$

Note that  $w'_x$  in Eq. (10.35) is one-half the corresponding full Sommerfeld solution, since the resultant contribution of subambient pressures perpendicular to the line of centers is neglected in the present case. In addition, note that for the half Sommerfeld solution  $w'_z$  is not zero as it was for the full Sommerfeld solution, since the contributions from the convergent and divergent films do not now cancel.

In dimensionless form these components become

$$W_x = \frac{w'_x}{\eta_0\omega_b r_b} \left(\frac{c}{r_b}\right)^2 = \frac{6\pi\epsilon}{(2+\epsilon^2)(1-\epsilon^2)^{1/2}} \quad (10.37)$$

$$W_z = \frac{w'_z}{\eta_0\omega_b r_b} \left(\frac{c}{r_b}\right)^2 = \frac{12\epsilon^2}{(2+\epsilon^2)(1-\epsilon^2)} \quad (10.38)$$

The resultant load is

$$w'_r = \left(w'_x^2 + w'_z^2\right)^{1/2} = \eta_0\omega_b r_b \left(\frac{r_b}{c}\right)^2 \frac{6\epsilon [\pi^2 - \epsilon^2 (\pi^2 - 4)]^{1/2}}{(2+\epsilon^2)(1-\epsilon^2)} \quad (10.39)$$

In dimensionless form the resultant load is

$$W_r = \frac{w'_r}{\eta_0\omega_b r_b} \left(\frac{c}{r_b}\right)^2 = \frac{6\epsilon [\pi - \epsilon^2 (\pi^2 - 4)]^{1/2}}{(2+\epsilon^2)(1-\epsilon^2)} \quad (10.40)$$

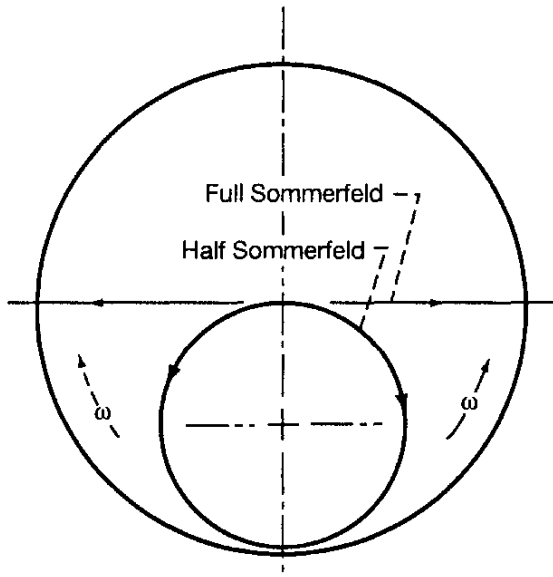


Figure 10.6: Location of shaft center for full and half Sommerfeld journal bearing solutions.

The attitude angle can be written as

$$\Phi = \tan^{-1} \frac{w'_x}{w'_z} = \tan^{-1} \left[ \frac{\pi}{2\epsilon} (1 - \epsilon^2)^{1/2} \right] \quad (10.41)$$

Note that  $\Phi = 90^\circ$  when  $\epsilon = 0$  and  $\Phi = 0^\circ$  when  $\epsilon = 1$ . The shaft starts to move at right angles to the applied load at extremely light loads, but ultimately the shaft meets the bearing along the load line. The locus of the shaft center for full and half Sommerfeld conditions is shown in Fig. 10.6.

### 10.2.3 Reynolds Boundary Conditions

As described earlier, the half Sommerfeld solution results in more realistic predictions of load components, but this simple approach leads to a violation of the continuity of mass flow at the outlet end of the pressure curve. That is, in Fig. 10.3 the pressure suddenly becomes zero at  $\Phi = \pi$  and then stays at zero from  $\pi$  to  $2\pi$ . The pressure distribution approaching  $\pi$  violates the continuity of mass flow condition. A better boundary condition is the Reynolds boundary condition, where

$$p = 0 \quad \text{and} \quad \frac{dp}{dx} = 0 \quad \text{at } \phi = \phi^* \quad (10.42)$$

Figure 10.7 shows a pressure profile for a bearing using the Reynolds boundary condition.

## 10.3 Short-Width-Journal-Bearing Theory

It is shown in Chapter 9 for thrust bearings that side leakage can account for a substantial reduction in the theoretical prediction of fluid film bearing load-carrying capacity. The complete solution of the Reynolds equation [Eq. (7.48)]

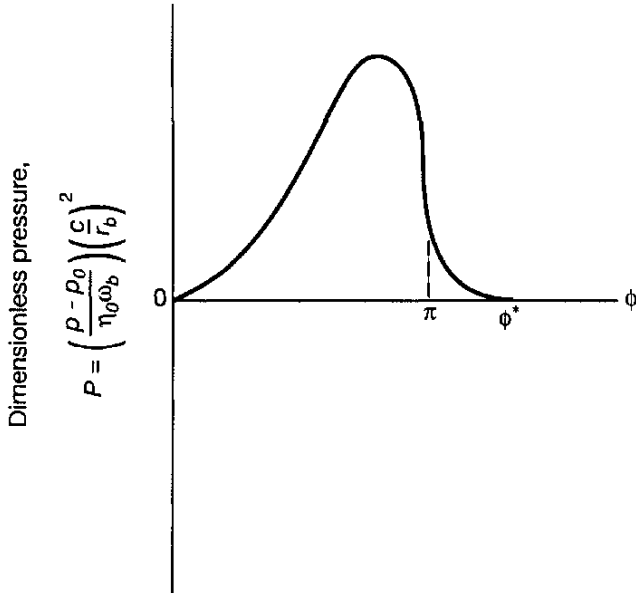


Figure 10.7: Pressure profile for a journal bearing using Reynolds boundary condition.

for three-dimensional flow generally requires considerable computational effort. A useful approximate analytical solution that takes account of side leakage was presented in 1953 by DuBois and Ocvirk.

When  $u_a = v_a = v_b = 0$ ,  $\partial x = r_b \partial \phi$ ,  $u_b = r_b \omega_b$ , and the viscosity is constant, Eqs. (7.38) and (7.39) become

$$q'_\phi = -\frac{h^3}{12\eta_0 r_b} \frac{\partial p}{\partial \phi} + \frac{hr_b \omega_b}{2} \quad (10.43)$$

$$q'_y = -\frac{h^3}{12\eta_0} \frac{\partial p}{\partial y} \quad (10.44)$$

DuBois and Ocvirk (1953) state that for short-width journal bearings the term  $(h^3/12\eta_0 r_b)(\partial p/\partial \phi)$  in Eq. (10.43) is small relative to  $hr_b \omega_b/2$ . That is, for short-width journal bearings the pressure-induced flow in the circumferential direction is small relative to the Couette flow term. Therefore, they assume that

$$q'_\phi = \frac{hr_b \omega_b}{2} \quad (10.45)$$

It should be emphasized that this assumption implies not that  $\partial p/\partial x = 0$ , but that  $(h^3/12\eta_0 r_b)(\partial p/\partial \phi)$  is small in terms of  $hr_b \omega_b/2$  for short-width journal bearings. This assumption further implies that the Poiseuille (pressure) flow is more significant in the  $y$  direction than in the circumferential ( $\phi$ ) direction. The result of this assumption is that the Reynolds equation given in Eq. (7.48) reduces to

$$\frac{\partial}{\partial y} \left( h^3 \frac{\partial p}{\partial y} \right) = 6\eta_0 \omega_b \frac{\partial h}{\partial \phi} \quad (10.46)$$

The short-width-journal-bearing theory is valid as long as the diameter-to-width ratio is greater than 2 ( $\lambda_k > 2$ ). Of course, the larger  $\lambda_k$  is, the better the agreement with the exact theory.

Assuming no misalignment, the film thickness is a function of  $\phi$  only, and hence the right side of Eq. (10.46) is independent of  $y$ . Integrating twice gives

$$p = \frac{6\eta_0\omega_b}{h^3} \frac{\partial h}{\partial \phi} \frac{y^2}{2} + \frac{\tilde{A}y}{h^3} + \tilde{B} \quad (10.47)$$

Now the  $y$  axis is chosen to be in the center of the bearing so that the boundary conditions, as they relate to the  $y$  coordinate, can be written as

$$p = 0 \quad \text{when } y = \pm \frac{b}{2}$$

Making use of these boundary conditions results in

$$\begin{aligned} \tilde{A} &= 0 \\ \tilde{B} &= -\frac{6\eta_0\omega_b}{h^3} \frac{\partial h}{\partial \phi} \frac{b^2}{8} \\ p &= \frac{3\eta_0\omega_b}{h^3} \frac{\partial h}{\partial \phi} \left( y^2 - \frac{b^2}{4} \right) \end{aligned} \quad (10.48)$$

The film thickness in a journal bearing was defined in Eq. (10.5). The film thickness gradient can be written as

$$\frac{dh}{d\phi} = -e \sin \phi \quad (10.49)$$

Substituting Eqs. (10.5) and (10.49) into (10.48) gives

$$p = \frac{3\eta_0\omega_b e}{c^2} \left( \frac{b^2}{4} - y^2 \right) \frac{\sin \phi}{(1 + e \cos \phi)^3} \quad \text{for } 0 \leq \phi \leq \pi \quad (10.50)$$

This equation shows that the parabolic function governs the axial variation of pressure, whereas the trigonometric function dictates the circumferential variation of pressure. Subambient pressures predicted by Eq. (10.50) are ignored, and it is assumed that the positive pressure region from  $\phi = 0$  to  $\phi = \pi$  carries the total load of the bearing (half Sommerfeld assumption).

The location of the maximum pressure is obtained when  $\partial p / \partial \phi = 0$ . From Eq. (10.48)

$$\frac{\partial p}{\partial \phi} = 3\eta_0\omega_b \left( y^2 - \frac{b^2}{4} \right) \frac{\partial}{\partial \phi} \left( \frac{1}{h^3} \frac{\partial h}{\partial \phi} \right) = 0$$

or

$$-3h^{-4} \left( \frac{\partial h}{\partial \phi} \right)^2 + h^{-3} \frac{\partial^2 h}{\partial \phi^2} = 0$$

Substituting Eqs. (10.5) and (10.49) into this equation gives

$$3\epsilon \sin^2 \phi_m + \cos \phi_m (1 + \epsilon \cos \phi_m) = 0$$

But  $\sin^2 \phi_m = 1 - \cos^2 \phi_m$

$$\phi_m = \cos^{-1} \left( \frac{1 - (1 + 24\epsilon^2)^{1/2}}{4\epsilon} \right) \quad (10.51)$$

Note that  $\phi_m \rightarrow \pm\pi/2$  as  $\epsilon \rightarrow 0$  and  $\phi_m \rightarrow \pm\pi$  as  $\epsilon \rightarrow 1$ . The maximum pressure occurs when  $\phi = \phi_m$ , and  $y = 0$ . Therefore, from Eq. (10.50) the equation for the maximum pressure is

$$p_m = \frac{3\eta_0 \omega_b \epsilon b^2 \sin \phi_m}{4c^2 (1 + \epsilon \cos \phi_m)^3} \quad (10.52)$$

The load components resulting from the pressure development parallel and perpendicular to the line of centers under the half Sommerfeld assumption are

$$w_x = 2 \int_0^\pi \int_0^{b/2} pr_b \sin \phi dy d\phi \quad (10.53)$$

$$w_z = -2 \int_0^\pi \int_0^{b/2} pr_b \cos \phi dy d\phi \quad (10.54)$$

Substituting Eq. (10.48) into these equations gives

$$w_x = \frac{\eta_0 \omega_b \epsilon r_b b^3}{2c^2} \int_0^\pi \frac{\sin^2 \phi d\phi}{(1 + \epsilon \cos \phi)^3}$$

$$w_z = -\frac{\eta_0 \omega_b \epsilon r_b b^3}{2c^2} \int_0^\pi \frac{\sin \phi \cos \phi}{(1 + \epsilon \cos \phi)^3} d\phi$$

When the Sommerfeld substitution given in Eq. (10.9) is used,

$$w_x = \frac{\eta_0 \omega_b \epsilon r_b b^3}{2c^2 (1 - \epsilon^2)^{3/2}} \int_0^\pi \sin^2 \gamma d\gamma$$

$$w_z = -\frac{\eta_0 \omega_b \epsilon r_b b^3}{2c^2 (1 - \epsilon^2)^2} \int_0^\pi (\sin \gamma \cos \gamma - \epsilon \sin \gamma) d\gamma$$

Evaluating these definite integrals yields

$$w_x = \frac{\eta_0 \omega_b r_b b^3}{4c^2} \frac{\pi \epsilon}{(1 - \epsilon^2)^{3/2}} \quad (10.55)$$

$$w_z = \frac{\eta_0 \omega_b r_b b^3}{c^2} \frac{\epsilon^2}{(1 - \epsilon^2)^2} \quad (10.56)$$

The resultant load vector is

$$w_r = (w_x^2 + w_z^2)^{1/2} = \frac{\eta_0 \omega_b r_b b^3}{4c^2} \frac{\epsilon}{(1 - \epsilon^2)^2} [16\epsilon^2 + \pi^2 (1 - \epsilon^2)]^{1/2} \quad (10.57)$$

The attitude angle is

$$\Phi = \tan^{-1} \frac{w_x}{w_z} = \tan^{-1} \frac{\pi (1 - \epsilon^2)^{1/2}}{4\epsilon} \quad (10.58)$$

Note that the attitude angle depends directly on the eccentricity ratio  $\epsilon$  so that a single polar curve of  $\epsilon$  against  $\Phi$  applies for all diameter-to-width ratios ( $\lambda_k = 2r_b/b$ ). Equations (10.55) to (10.57) can be written in dimensionless form as

$$W_x = \frac{w_x}{\eta_0 \omega_b r_b b} \left( \frac{c}{r_b} \right)^2 = \left( \frac{b}{r_b} \right)^2 \frac{\pi \epsilon}{4(1 - \epsilon^2)^{3/2}} \quad (10.59)$$

$$W_z = \frac{w_z}{\eta_0 \omega_b r_b b} \left( \frac{c}{r_b} \right)^2 = \left( \frac{b}{r_b} \right)^2 \frac{\epsilon^2}{(1 - \epsilon^2)^2} \quad (10.60)$$

$$W_r = \frac{w_r}{\eta_0 \omega_b r_b b} \left( \frac{c}{r_b} \right)^2 = \left( \frac{b}{r_b} \right)^2 \frac{\epsilon}{4(1 - \epsilon^2)^2} [16\epsilon^2 + \pi^2 (1 - \epsilon^2)]^{1/2} \quad (10.61)$$

The volume flow of lubricant supplied to the bearing through a central hole or groove must be equal to the net rate of outflow along the bearing axis ( $y$  direction). The total leakage from the sides of the bearing in the convergent film region (half Sommerfeld assumption) can be expressed as

$$q_y = -2r_b \int_0^\pi \left( \frac{h^3}{12\eta_0} \frac{\partial p}{\partial y} \right)_{y=b/2} d\phi$$

Introducing Eq. (10.48) gives

$$q_y = -\frac{\omega_b r_b b}{2} \int_0^\pi \frac{\partial h}{\partial \phi} d\phi$$

Making use of Eq. (10.49) gives

$$q_y = \frac{\omega_b r_b b e}{2} \int_0^\pi \sin \phi d\phi = -\frac{\omega_b r_b b e}{2} (\cos \phi)_{\phi=0}^{\phi=\pi} = \omega_b r_b b e \quad (10.62)$$

In dimensionless form this equation becomes

$$Q_y = \frac{2q_y \pi}{\omega_b r_b b c} = 2\epsilon\pi \quad (10.63)$$

It can be seen from this equation that  $q_y \rightarrow 0$  as  $\epsilon \rightarrow 0$  (no side leakage) and  $q_y \rightarrow \omega_b r_b b c$  as  $\epsilon \rightarrow 1$  (complete side leakage).

The load-carrying capacity as obtained from the long-width-bearing solution can be compared with the short-width bearing theory results by comparing Eqs. (10.40) and (10.61) to give

$$\frac{W_r \text{ (short-width bearing)}}{W_r \text{ (long-width bearing)}} = \left( \frac{b}{r_b} \right)^2 \frac{(2 + \epsilon^2) [16\epsilon^2 + \pi^2 (1 - \epsilon^2)]^{1/2}}{24 (1 - \epsilon^2) [\pi^2 - \epsilon^2 (\pi^2 - 4)]^{1/2}} \quad (10.64)$$

Note from this equation that the load ratios are functions of  $b/r_b$  and  $\epsilon$ . The long-width-bearing analysis overestimates the load-carrying capacity for all  $\epsilon$  and should be used for  $\lambda_k < 0.5$ . The short-width-bearing theory provides a much better estimate for finite bearings of diameter-to-width ratios greater than 2 ( $\lambda_k = 2r_b/b > 2$ ). The useful range of  $b/r_b$  for the short-width-bearing theory depends on the eccentricity ratio. Short-width-bearing theory leads to excessive load-carrying capacities (sometimes exceeding the long-width-bearing values) at small diameter-to-width ratios ( $\lambda_k = 2r_b/b$ ).

## 10.4 Closure

Just as was true in Chap. 8 for the thrust bearings, in this chapter the Reynolds equations for real journal bearings were obtained only in approximate form. Analytical solutions were possible only for the simplest problems. One of these solutions (infinitely wide solution) was obtained by restricting the flow to two dimensions, the circumferential and cross-film directions, neglecting the axial flow. The two-dimensional solutions have a definite value, since they provide a good deal of information about the general characteristics of journal bearings. Three types of boundary condition were imposed on the two-dimensional solutions. A full Sommerfeld solution produced a skew-symmetrical pressure distribution. The pressures in the divergent film were all lower than the ambient pressure, and such pressures are rarely encountered in real bearings. This led to the half Sommerfeld solution, which simply equates the negative pressures to zero. The half Sommerfeld solution is more realistic in predicting journal bearing characteristics than the full Sommerfeld solution, but this simple approach leads to a violation of the continuity of mass flow at the exit. This violation of continuity of mass flow leads to a third type of boundary condition used in analyzing journal bearings, namely, the Reynolds boundary conditions,  $p = 0$  and  $dp/dx = 0$  at the outlet end. This type of boundary condition gives excellent agreement with experimental results.

A useful approximate analytical approach also covered in this chapter was the short-width-journal-bearing theory. It is asserted that the circumferential Poiseuille flow term is less important for short-width journal bearings than either the axial Poiseuille flow term or the Couette flow term and therefore can be neglected. For diameter-to-width ratios greater than 2 ( $\lambda_k = 2r_b/b > 2$ ) the short-width journal bearings give a good estimate of load-carrying capacity for finite-width journal bearings. However, the useful range of short-width-journal-bearing theory depends not only on  $2r_b/b$ , but also on the eccentricity ratio  $\epsilon$ .

Short-width-bearing theory predicts excessive load-carrying capacities, sometimes exceeding the long-width-bearing solution at small  $2r_b/b$ . The half Sommerfeld boundary conditions used for the infinitely wide bearing overestimate the normal load-carrying capacity for all eccentricity ratios.

## 10.5 Problems

- 10.1 Starting with Eq. (10.7) show all the steps in arriving at Eq. (10.15) by using the Sommerfeld substitution.
- 10.2 Show how the resulting load-carrying capacity differs when using the full Sommerfeld solution from that when using the half Sommerfeld solution when considering an infinitely wide bearing. Show results in tabular and graphical form for the complete range of eccentricity ratios  $0 \leq \epsilon \leq 1$ .
- 10.3 Show how the resulting load-capacity differs when using infinite-width and short-width-bearing analysis while considering the complete range of eccentricity ratios  $0 \leq \epsilon \leq 1$ . Assume the half-Sommerfeld boundary condition for both analysis. Show results in tabular and graphical form for diameter-to-width ratios ( $\lambda_k$ ) of 1, 2, and 4.
- 10.4 A journal bearing has a diameter of 50 mm and a width of 100 mm and rotates at 1000 rpm. The bearing is lubricated by SAE 10 oil at a temperature of 110°C and supports 5 kN. Calculate the eccentricity for the Sommerfeld, the half Sommerfeld, and Reynolds approximations.

## References

- Booker, J. F. (1965): A Table of the Journal-Bearing Integrals. *J. Basic Eng.*.. Vol. 87, no. 2, pp. 533-535.
- DuBois, O. B., and Ocvirk, F. W. (1953): Analytical Derivation and Experimental Evaluation of Short-Bearing Approximation for Full Journal Bearings. *NASA Rep. 1157*.
- Sommerfeld. A. (1904): Zur Hydrodynamischen Theorie der Schmiermittelreibung. *Z. Angew. Math. Phys.*, vol. 50, pp. 97-155.

# Chapter 11

## Hydrodynamic Journal Bearings - Numerical Solutions

### Symbols

$B_j$	bearing number for journal bearings, $\left(\frac{\eta_0 \omega_b r_b b}{\pi w_r}\right) \left(\frac{r_b}{c}\right)^2$	$r_a$	radius of shaft, m
$b$	width (in side-leakage direction) of journal, m	$r_b$	radius of journal bearing, m
$c$	radial clearance of journal bearing, m	$\Delta t_m$	temperature change, °C
$c_b$	bearing clearance at pad minimum film thickness, m	$t_m$	absolute temperature, °C
$e$	eccentricity of journal, m	$t_{mi}$	inlet temperature, °C
$h$	film thickness, m	$\tilde{u}$	average velocity in sliding direction, m/s
$h_{\min}$	minimum film thickness, $c - e$ , m	$u_b$	velocity of journal, m/s
$m_p$	preload factor	$w_r$	radial load, N
$P_{\max}$	dimensionless maximum film pressure, $\frac{w_r}{2r_b b p_{\max}}$	$x, y, z$	Cartesian coordinates
$p$	pressure, N/m <sup>2</sup>	$\alpha_a$	offset factor
$p_{\max}$	maximum pressure, N/m <sup>2</sup>	$\epsilon$	eccentricity ratio, $e/c$
$p^*$	radial load per area, MPa	$\eta$	absolute viscosity, Pa·s
$Q$	dimensionless volumetric flow rate, $2\pi q/r_b c b \omega_b$	$\eta_0$	absolute viscosity at $p = 0$ and constant temperature, Pa·s
$q$	circumferential volumetric flow rate, m <sup>3</sup> /s	$\lambda_j$	diameter-to-width ratio, $2r_b/b$
$q_s$	side-leakage volumetric flow rate, m <sup>3</sup> /s	$\mu$	coefficient of sliding friction
		$\Phi$	attitude angle, deg
		$\phi$	cylindrical polar coordinate
		$\phi_{\max}$	location of maximum pressure, deg
		$\phi_o$	location of terminating pressure, deg
		$\omega_b$	angular velocity of journal, rad/s

## 11.1 Introduction

The preceding two chapters and this chapter focus on hydrodynamically lubricated journal bearings. Chapter 10 dealt with solutions that could be obtained analytically. These included an infinitely wide journal bearing [applicable for diameter-to-width ratios less than  $\frac{1}{2}$  ( $\lambda_k = 2r_b/b < \frac{1}{2}$ )] and short-width journal bearings [applicable for diameter-to-width ratios greater than 2 (*i.e.*,  $\lambda_k = 2r_b/b > 2$ )]. The present chapter utilizes numerical solutions in obtaining results for the complete range of diameter-to-width ratios. Steady loading conditions are considered throughout most of the chapter, and in the latter part of the chapter dynamic loading effects are considered.

## 11.2 Operating and Performance Parameters

From Eq. (7.48) the Reynolds equation appropriate when considering the finite journal bearing can be expressed as

$$\frac{\partial}{\partial x} \left( h^3 \frac{\partial p}{\partial x} \right) + \frac{\partial}{\partial y} \left( h^3 \frac{\partial p}{\partial y} \right) = 12\tilde{u}\eta_0 \frac{\partial h}{\partial x} \quad (7.48)$$

Now for a journal bearing  $x = r_b\phi$  and  $\tilde{u} = u_b/2 = r_b\omega_b/2$ .

$$\frac{\partial}{\partial \phi} \left( h^3 \frac{\partial p}{\partial \phi} \right) + r_b^2 \frac{\partial}{\partial y} \left( h^3 \frac{\partial p}{\partial y} \right) = 6\eta_0\omega_b r_b^2 \frac{\partial h}{\partial \phi} \quad (11.1)$$

In Chapter 10 the film thickness around the journal is expressed as

$$h = c(1 + \epsilon \cos \phi) \quad (10.5)$$

Therefore, Eq. (11.1) can be expressed as

$$\frac{\partial}{\partial \phi} \left( h^3 \frac{\partial p}{\partial \phi} \right) + r_b^2 h^3 \frac{\partial^2 p}{\partial y^2} = -6\eta_0\omega_b r_b^2 e \sin \phi \quad (11.2)$$

Analytical solutions to Eq. (11.2) are not normally available, and numerical methods are needed. Equation (11.2) is often solved by using a relaxation method. In the relaxation process the first step is to replace the derivatives in Eq. (11.2) by finite difference approximations. The lubrication area is covered by a mesh, and the numerical method relies on the fact that a function can be represented with sufficient accuracy over a small range by a quadratic expression. The Reynolds boundary condition covered in Sec. 10.2.3 is used. Only the results from using this numerical method are presented in this chapter.

The three dimensionless groupings normally used to define the operating parameters in journal bearings are

1. Bearing number (also called Sommerfeld number) for journal bearings,

$$B_j = \left( \frac{\eta_0\omega_b r_b b}{\pi w_r} \right) \left( \frac{r_b}{c} \right)^2 \quad (11.3)$$

2. The angular extent of the journal (full or partial)
3. The diameter-to-width ratio  $\lambda_j = 2r_b/b$

Recall from Chapter 10 that when the side-leakage term was neglected in Eq. (11.2),  $\lambda_k$  did not exist in the formulation, whereas for the short-width-journal-bearing theory all three parameters occurred although the region of applicability was somewhat limited. The results presented in this chapter are valid for the complete range of operating parameters.

This chapter focuses on the following performance parameters:

1. Eccentricity  $e$
2. Location of minimum film thickness, sometimes referred to as “attitude angle,”  $\Phi$
3. Friction coefficient  $\mu$
4. Total and side flow  $q$  and  $q_s$
5. Angle of maximum pressure  $\phi_m$
6. Location of terminating pressure  $\phi_0$
7. Temperature rise due to lubricant shearing  $\Delta t_m$

The parameters  $\Phi$ ,  $\phi_m$ , and  $\phi_0$  are described in Fig. 11.1, which gives the pressure distribution around a journal bearing. Note from this figure that if the bearing is concentric ( $e = 0$ ), the film shape around the journal is constant and equal to  $c$  and no fluid film pressure is developed. At the other extreme, at heavy loads the journal is forced downward and the limiting position is reached when  $h_{\min} = 0$  and  $e = c$ ; that is, the journal is touching the bearing.

Temperature rise due to lubricant shearing will be considered in this chapter as was done in Chapter 8 for thrust bearings. In Eq. (11.2) the viscosity of the lubricant corresponds to the viscosity when  $p = 0$  but can vary as a function of temperature. Since work is done on the lubricant as the fluid is being sheared, the temperature of the lubricant is higher when it leaves the conjunction than on entry. In Chapter 4 (Figs. 4.5 and 4.6) it was shown that the viscosity of oils drops off significantly with rising temperature. This is compensated for by using a mean of the inlet and outlet temperatures:

$$t_m = t_i + \frac{\Delta t_m}{2} \quad (11.4)$$

where

$t_i$  = inlet temperature

$\Delta t_m$  = temperature rise of lubricant from inlet to outlet

The viscosity used in the bearing number  $B_j$  and other performance parameters is at the mean temperature  $t_m$ . The temperature rise of the lubricant from inlet to outlet  $\Delta t_m$  can be determined from the performance charts provided in this chapter.

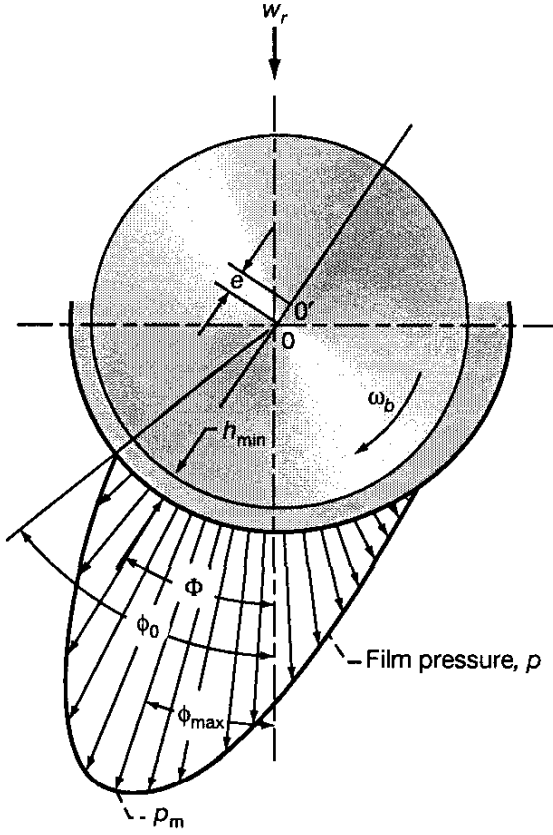


Figure 11.1: Pressure distribution around a journal bearing.

### 11.3 Design Procedure

Now that the operating and performance parameters have been defined, the design procedure for a hydrodynamic journal bearing can be presented. The results are for a full journal bearing. Results for a partial journal bearing can be obtained from Raimondi and Boyd (1958).

Figure 11.2 shows the effect of the bearing number  $B_j$  on the minimum film thickness for four diameter-to-width ratios. The following relationship should be observed:

$$h_{\min} = c - e \quad (11.5)$$

In dimensionless form,

$$H_{\min} = \frac{h_{\min}}{c} = 1 - \epsilon \quad (11.6)$$

where

$$\epsilon = e/c = \text{eccentricity ratio} \quad (11.7)$$

The bearing number for journal bearings is expressed in Eq. (11.3). In a given design the bearing number is affected by

1. Absolute lubricant viscosity  $\eta_0$
2. Angular shaft speed  $\omega_b$
3. Radial load  $w_r$

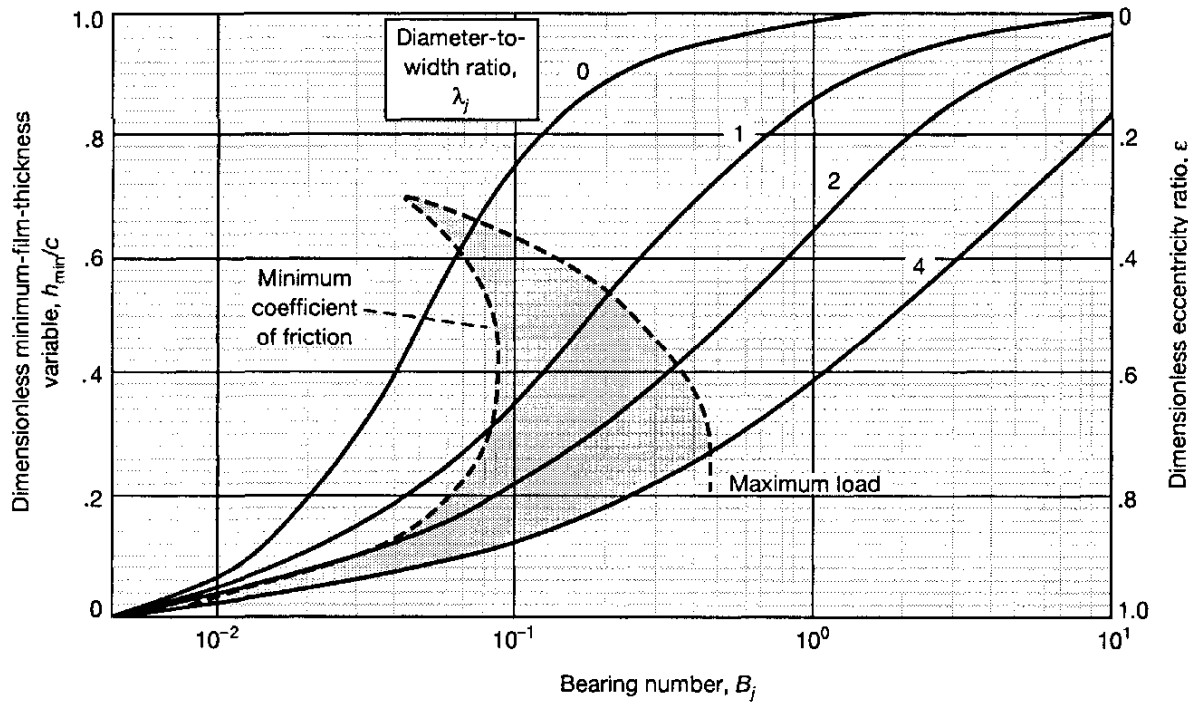


Figure 11.2: Effect of bearing number on minimum film thickness for four diameter-to-width ratios. [From Raimondi and Boyd (1958).]

#### 4. Radial clearance $c$

#### 5. Journal dimensions $r_b$ and $b$

All these parameters affect the bearing number and thus the design of the journal bearing.

In Fig. 11.2 a recommended operating eccentricity ratio, or minimum film thickness, is indicated as well as a preferred operating area. The left boundary of the shaded zone defines the optimum eccentricity ratio for a minimum coefficient of friction, and the right boundary the optimum eccentricity ratio for maximum load. The recommended operating eccentricity for general application is midway between these two boundaries.

Figure 11.3 shows the effect of the bearing number in the attitude angle  $\Phi$  [angle between the load direction and a line drawn through the centers of the bearing and journal (see Fig. 11.1)] for four values of  $\lambda_j$ . This angle establishes where the minimum and maximum film thicknesses are located within the bearing. Figure 11.4 shows the effect of the bearing number on the coefficient of friction for four values of  $\lambda_j$ . The effect is small for a complete range of dimensionless load parameters. Figure 11.5 shows the effect of bearing number on the dimensionless volumetric flow rate  $Q = 2\pi q/r_b c b \omega_b$  for four values of  $\lambda_j$ . The dimensionless volumetric flow rate  $Q$  that is pumped into the converging space by rotating the journal can be obtained from this figure. Of the volume of oil  $q$  pumped by the rotating journal, an amount  $q_s$  flows out the ends and

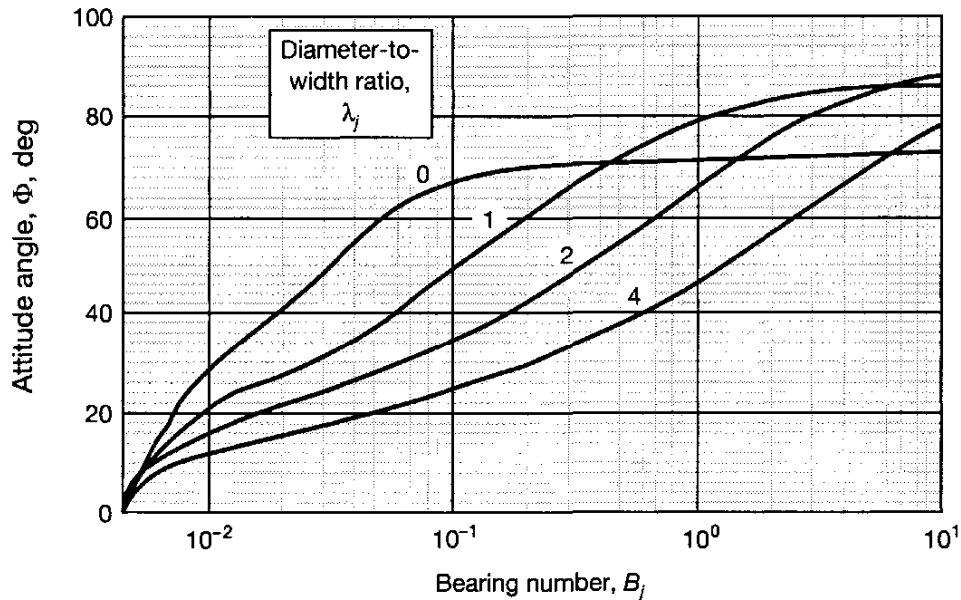


Figure 11.3: Effect of bearing number on attitude angle for four diameter-to-width ratios. [From Raimondi and Boyd (1958).]

hence is called *side-leakage volumetric flow*. This side leakage can be computed from the volumetric flow ratio  $q_s/q$  of Fig. 11.6.

Figure 11.7 illustrates the maximum pressure developed in a journal bearing. In this figure the maximum film pressure is made dimensionless with the load per unit area. The maximum pressure as well as its location are shown in Fig. 11.1. Figure 11.8 shows the effect of bearing number on the location of the terminating and maximum pressures for four values of  $\lambda_j$ .

The temperature rise in degrees Celsius of the lubricant from the inlet to the outlet can be obtained from Shigley and Mischke (1983) as

$$\Delta t_m = \frac{8.3p^*(r_b/c)\mu}{Q(1 - 0.5q_s/q)} \quad (11.8)$$

where  $p^* = w_r/2r_b b$  and is in megapascals. Therefore, the temperature rise can be directly obtained by substituting the values of  $r_b\mu/c$  obtained from Fig. 11.4,  $Q$  from Fig. 11.5, and  $q_s/q$  from Fig. 11.6 into Eq. (11.8). The temperature rise in degrees Fahrenheit is given by

$$\Delta t_m = \frac{0.103p^*(r_b/c)\mu}{Q(1 - 0.5q_s/q)} \quad (11.9)$$

where

$$p^* = \frac{w_r}{2r_b b} \quad (11.10)$$

and  $p^*$  here in Eq. (11.9) is in pounds per square inch.

Once the viscosity is known, the bearing number can be calculated and then the performance parameters can be obtained from Figs. 11.2 to 11.8 and Eqs. (11.9) and (11.10).

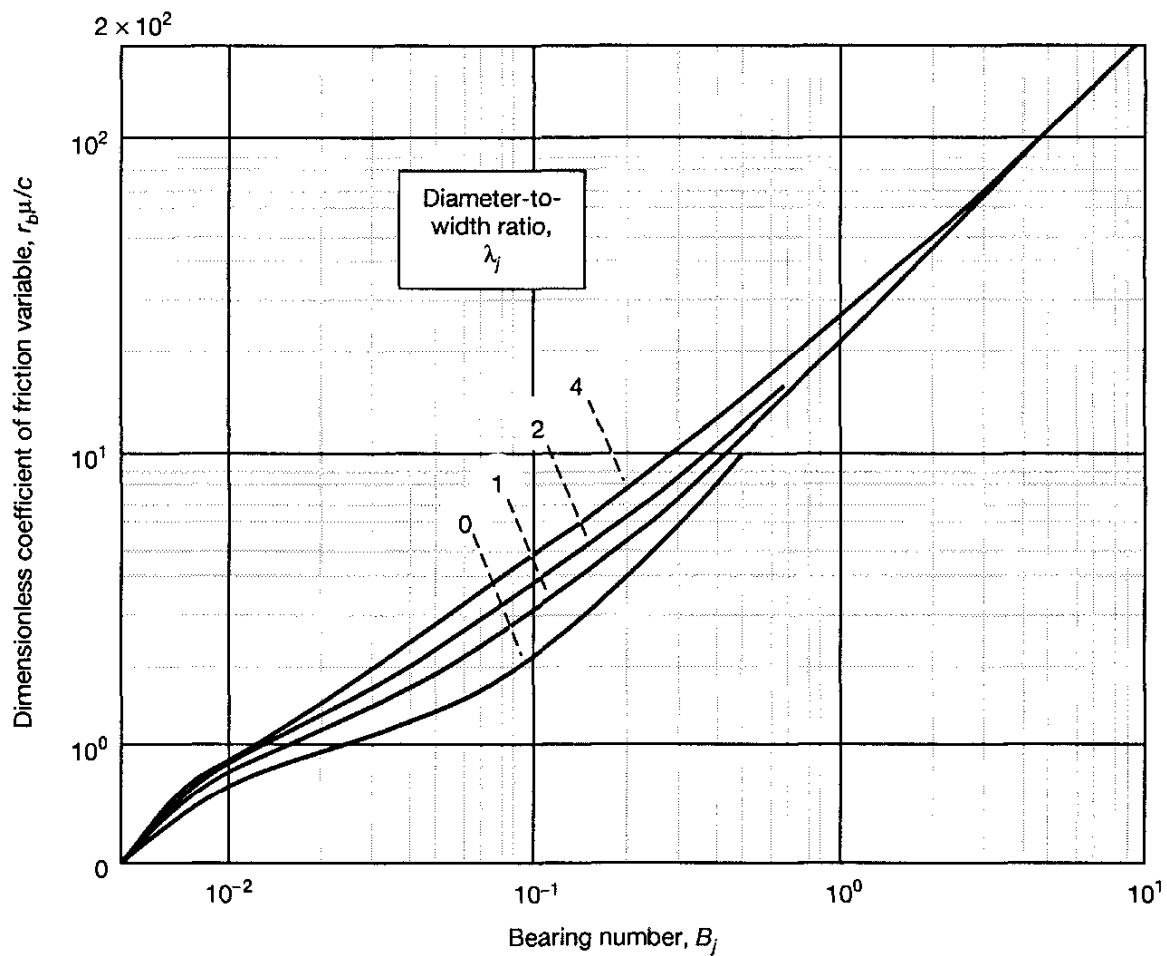


Figure 11.4: Effect of bearing number on friction coefficient for four diameter-to-width ratios. [From Raimondi and Boyd (1958).]

The results presented thus far have been for  $\lambda_j$  of 0, 1, 2, and 4. If  $\lambda_j$  is some other value, use the following formula for establishing the performance parameters:

$$\begin{aligned}
 y = & \frac{1}{(b/2r_b)^3} \left[ -\frac{1}{8} \left( 1 - \frac{b}{2r_b} \right) \left( 1 - \frac{b}{r_b} \right) \left( 1 - 2\frac{b}{r_b} \right) y_0 \right. \\
 & + \frac{1}{3} \left( 1 - \frac{b}{r_b} \right) \left( 1 - \frac{2b}{r_b} \right) y_1 - \frac{1}{4} \left( 1 - \frac{b}{2r_b} \right) \left( 1 - \frac{2b}{r_b} \right) y_2 \\
 & \left. + \frac{1}{24} \left( 1 - \frac{b}{2r_b} \right) \left( 1 - \frac{b}{r_b} \right) y_4 \right] \quad (11.11)
 \end{aligned}$$

where  $y$  is any one of the performance parameters ( $H_{\min}$ ,  $\Phi$ ,  $r_b \mu/c$ ,  $Q$ ,  $q_s/q$ ,  $p_{\max}$ ,  $\phi_0$ , or  $\phi_{\max}$ ) and where the subscript on  $y$  is the  $\lambda_j$  value; for example,  $y_1$  is equivalent to  $y$  evaluated at  $\lambda_j = 1$ . All the results presented are valid for a full journal bearing.

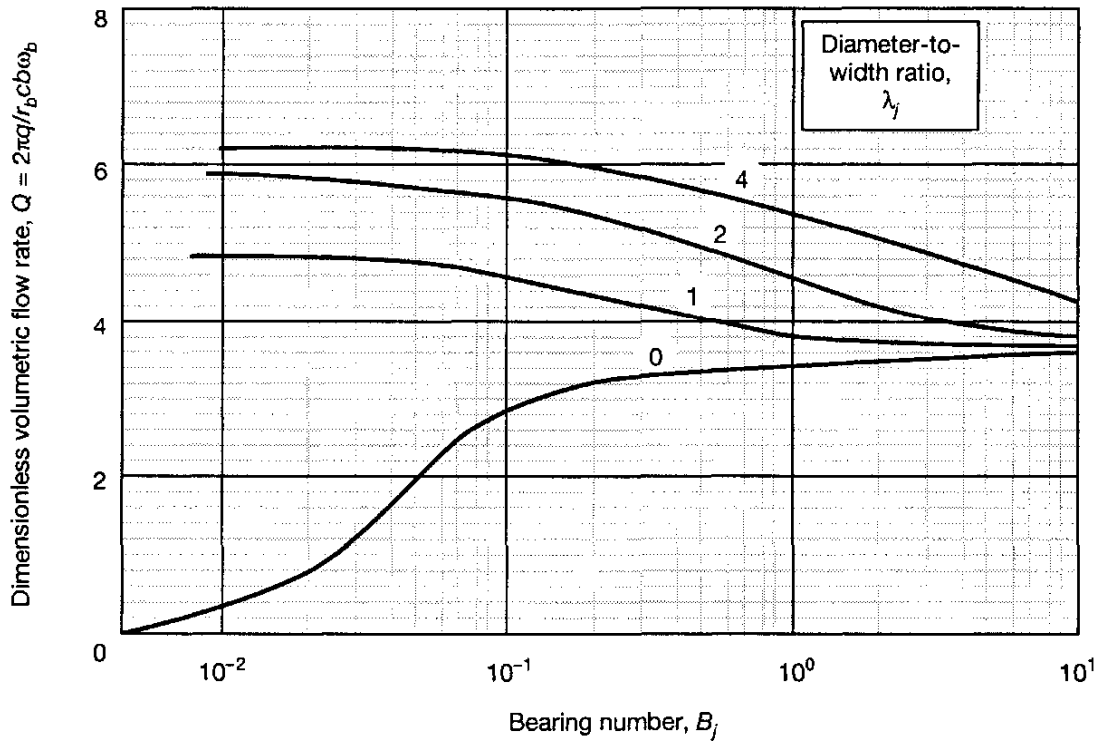


Figure 11.5: Effect of bearing number on dimensionless flow rate for four diameter-to-width ratios. [From Raimondi and Boyd (1958).]

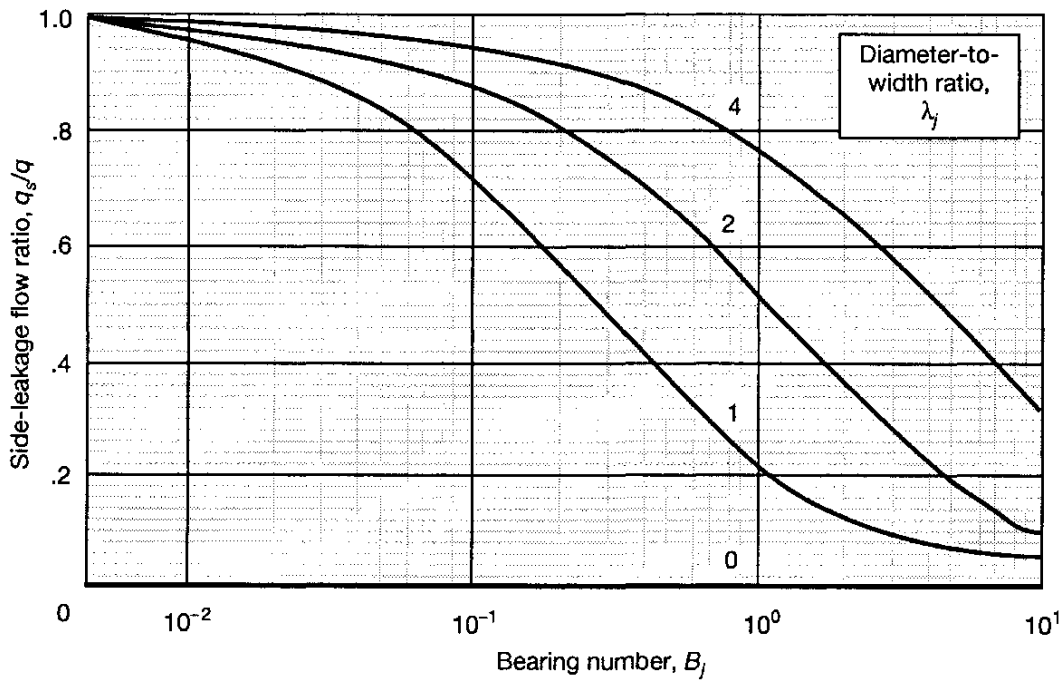


Figure 11.6: Effect of bearing number on volume side flow ratio for four diameter-to-width ratios. [From Raimondi and Boyd (1958).]

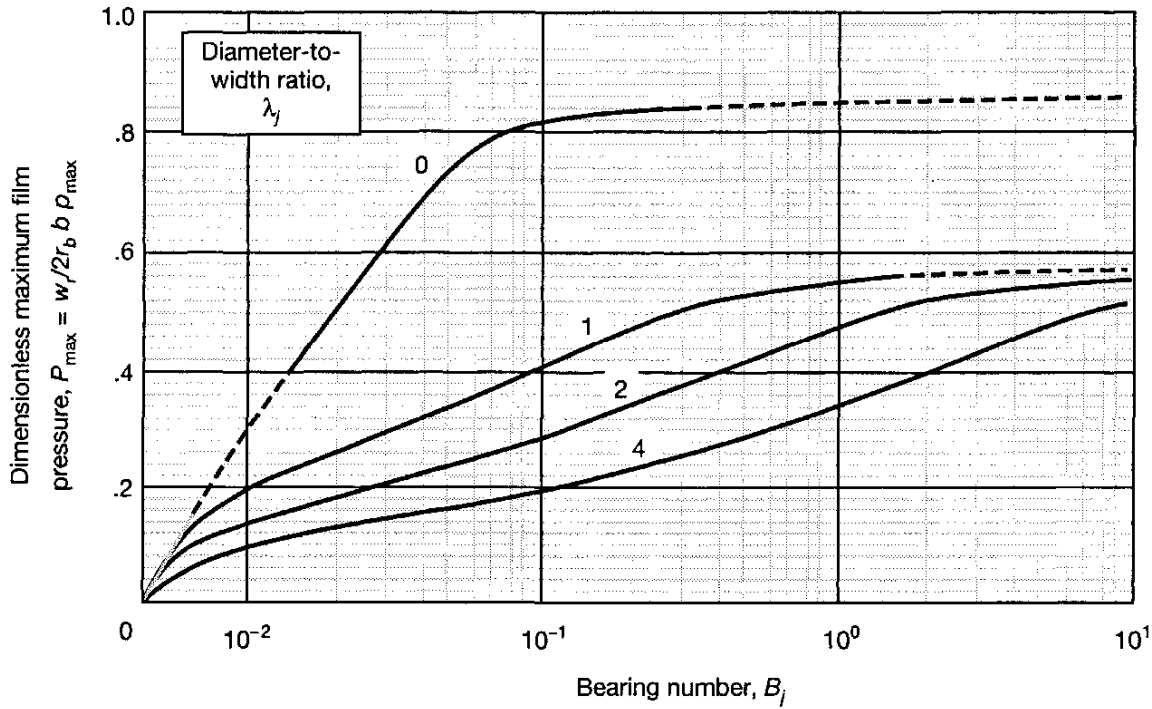


Figure 11.7: Effect of bearing number on dimensionless maximum film pressure for four diameter-to-width ratios. [From Raimondi and Boyd (1958).]

## Example 11.1

**Given** A full journal bearing has the specifications of SAE 60 oil with an inlet temperature of  $40^\circ\text{C}$ ,  $N_a = 30$  rps,  $w_r = 2200$  N,  $r_b = 2$  cm, and  $b = 4$  cm.

**Find** From the figures given in this section establish the operating and performance parameters for this bearing while designing for maximum load.

**Solution** The angular speed can be expressed as

$$\omega_b = 2\pi N_a = 2\pi(30) = 60\pi \text{ rad/s}$$

The diameter-to-width ratio is

$$\lambda_j = \frac{2r_b}{b} = \frac{2(2)}{4} = 1$$

From Fig. 11.2 for  $\lambda_j = 1$  and designing for maximum load

$$B_j = 0.2 \quad \frac{h_{\min}}{c} = 0.53 \quad \text{and} \quad \epsilon = 0.47 \quad (a)$$

For  $B_j = 0.2$  and  $\lambda_j = 1$  from Figs. 11.4 to 11.6

$$\frac{r_b \mu}{c} = 4.9 \quad Q = 4.3 \quad \text{and} \quad \frac{q_s}{q} = 0.6 \quad (b)$$

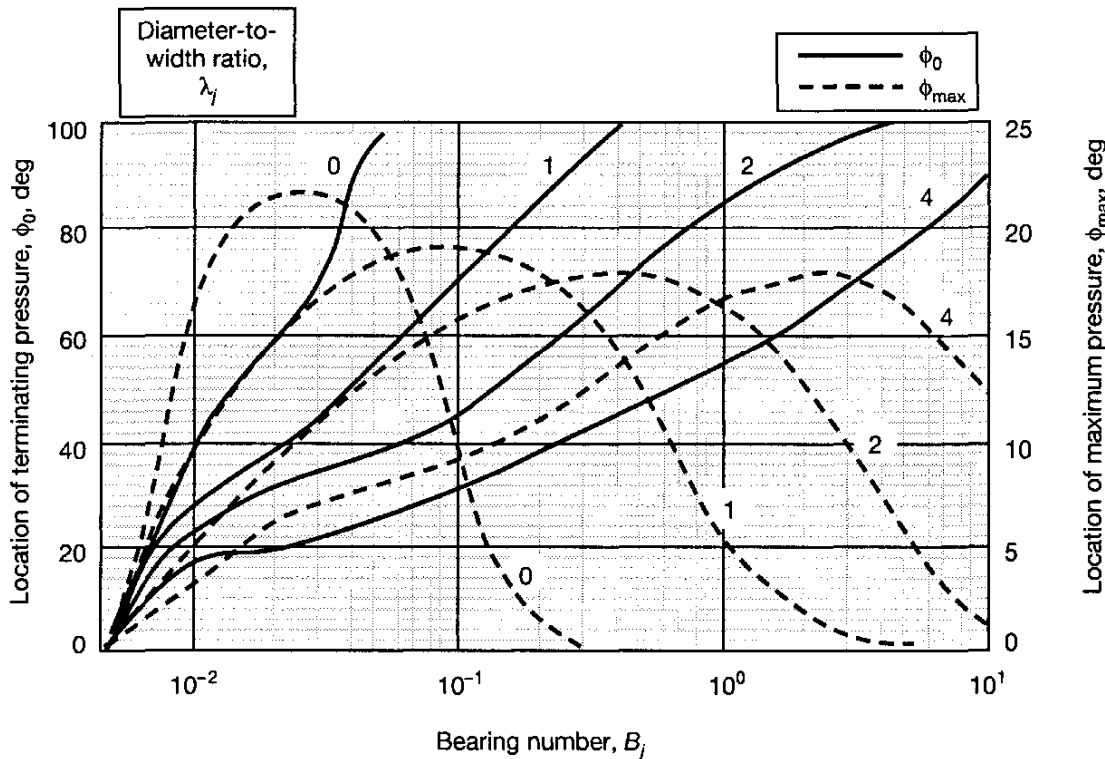


Figure 11.8: Effect of bearing number on location of terminating and maximum pressures for four diameter-to-width ratios. [From Raimondi and Boyd (1958).]

From Eq. (11.10) the radial load per area is

$$p^* = \frac{w_r}{2r_b b} = \frac{2200}{2(2)(4)(10^{-4})} \text{ Pa} = 1.375 \text{ MPa} \quad (c)$$

The lubricant temperature rise in degrees Celsius obtained by using Eq. (11.8) and the results from Eqs. (b) and (c) is

$$\Delta t_m = \frac{8.3p^*(r_b/c)\mu}{Q(1 - 0.5q_s/q)} = \frac{8.3(1.375)(4.9)}{4.3[1 - (0.5)(0.6)]} = 18.58^\circ\text{C}$$

From Eq. (11.4) the mean temperature in the lubricant conjunction is

$$\bar{t}_m = t_{mi} + \frac{\Delta t_m}{2} = 40 + \frac{18.58}{2} = 49.29^\circ\text{C}$$

From Fig. 4.6 for SAE 60 oil at 49.3°C the absolute viscosity is

$$2.5 \times 10^{-5} \text{ reyn} = 1.70 \times 10^2 \text{ centipoise} = 0.170 \text{ N}\cdot\text{s}/\text{m}^2$$

From Eq. (11.3) the radial clearance can be expressed as

$$c = r_b \sqrt{\frac{\eta_0 \omega_b r_b b}{\pi w_r B_j}} = (2)(10^{-2}) \sqrt{\frac{(0.170)60\pi(2)(10^{-2})(4)(10^{-2})}{\pi(2.2)(10^3)(0.2)}} = 0.0861 \times 10^{-3} \text{ m}$$

The coefficient of friction from Eq. (b) is

$$\mu = \frac{4.9c}{r_b} = \frac{(4.9)(0.0861)(10^{-3})}{(2)(10^{-2})} = 0.021$$

The circumferential volumetric flow rate is

$$q = \frac{Qr_bcb\omega_b}{2\pi} = \frac{(4.3)(2)(10^{-2})(0.0861)(10^{-3})(4)(10^{-2})60\pi}{2\pi} = 8.89 \times 10^{-6} \text{ m}^3/\text{s}$$

From Fig. 11.3 for  $B_j = 0.2$  and  $\lambda_j = 1$  the attitude angle is  $61^\circ$ . From Fig. 11.7 for  $B_j = 0.2$  and  $\lambda_j = 1$  the dimensionless maximum pressure is  $P_{\max} = 0.46$ . The maximum pressure is

$$p_{\max} = \frac{w_r}{2r_bbP_{\max}} = \frac{2200}{2(2)(10^{-2})(4)(10^{-2})(0.46)} \text{ Pa} = 2.989 \text{ MPa}$$

From Fig. 11.8 for  $B_j = 0.2$  and  $\lambda_j = 1$  the location of the maximum pressure from the applied load is  $18^\circ$  and the location of the terminating pressure from the applied load is  $86^\circ$ .

---

## 11.4 Optimization Techniques

The most difficult of the parameters in the operating conditions to control is the radial clearance  $c$ . The radial clearance is difficult to control accurately during manufacturing, and it may increase because of wear. Figure 11.9 shows the performance of a particular bearing calculated for a range of radial clearances and plotted with radial clearance as the independent variable. If the clearance is too tight, the temperature will be too high and the minimum film thickness too low. High temperature may cause the bearing to fail by fatigue. If the oil film is too thin, dirt particles may not pass without scoring or may embed themselves in the bearing. In either event there will be excessive wear and friction, resulting in high temperatures and possible seizing. A large clearance will permit dirt particles to pass through and also permit a large flow of oil. This lowers the temperature and lengthens bearing life. However, if the clearance becomes too large, the bearing becomes noisy and the minimum film thickness begins to decrease again.

Figure 11.9 shows the best compromise, when both the production tolerance and the future wear on the bearing are considered, to be a clearance range slightly to the left of the top of the minimum-film-thickness curve. In this way, future wear will move the operating point to the right, increasing the film thickness and decreasing the operating temperature.

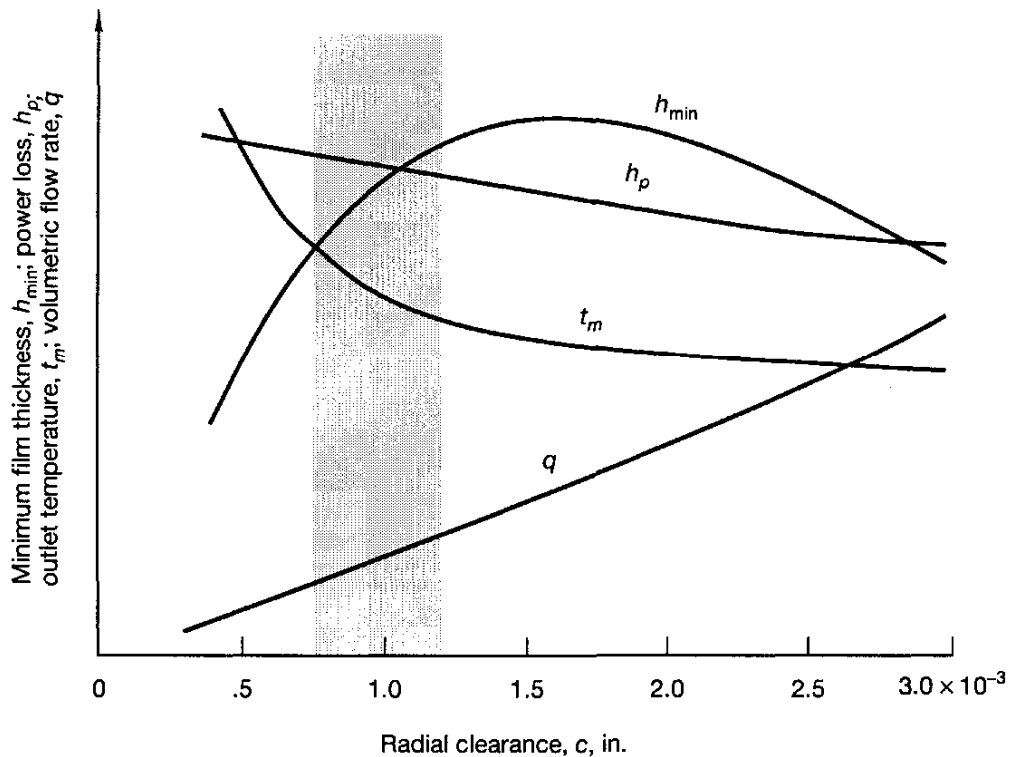


Figure 11.9: Effect of radial clearance on some performance parameters for a particular case.

## 11.5 Dynamic Effects

The design procedures for steadily loaded journal bearings given in Chapter 10 and thus far in Chapter 11 enable the designer to estimate the performance parameters in terms of the operating parameters. For example, the attitude angle and the eccentricity ratio can be calculated for any steady-state operating condition. From these values the minimum film thickness, a most important quantity affecting the performance of the bearing, can be calculated.

In many important bearing operating situations the load varies in both magnitude and direction, often cyclically. Examples include reciprocating machinery such as diesel and gasoline engines, reciprocating gas compressors, and out-of-balance rotating machinery such as turbine rotors. Bearings are generally dynamically loaded. Furthermore, it must be stressed that journal bearings are not inherently stable. For certain combinations of steady-state operating parameters, self-excited whirl of the journal can be sustained. If this occurs in a case with varying load, the whirl orbit will increase rapidly until the journal and the sleeve come into contact. Journal bearing stability is an important consideration in high-speed rotating machinery, and unstable operation should always be avoided.

Half-frequency whirl occurs if the journal center rotates about the sleeve center at one-half the shaft rotational speed while the eccentricity remains con-

stant and the sleeve is stationary. When half-frequency whirl occurs, a constant (zero) pressure exists throughout the bearing. If the shaft precesses about the bearing center at a rotational speed equal to one-half the shaft speed, the theoretical load-carrying capacity is zero and thus the phenomenon is known as "half-speed whirl."

With dynamically loaded journal bearings the eccentricity and the attitude angle will vary throughout the loading cycle, and care must be taken to ensure that the combination of load and speed does not yield a dangerously small minimum film thickness. It is not easy to state a unique value of minimum film thickness that can be assumed to be safe, since a great deal depends on the manufacturing process, the alignment of the machine elements associated with the bearings, and the general operating conditions, including the environment of the machine.

It is also important to recognize the difference between dynamic effects in hydrodynamically lubricated bearings and in rolling-element bearings, which are dealt with in Chapter 22. Although the supporting structure formed by the rolling elements is discontinuous and moving, the bearing as a whole may still be treated as though it were a solid, elastic, springlike element. Spring constants for rolling-element bearings usually fall in the range  $1 \times 10^8$  to  $4 \times 10^8$  N/m in the direction of the load application. The rolling elements act in series with the shaft and support stiffnesses and combine according to the reciprocal summation equation. Thus, the dynamic effects as they relate to the fluid film effects in rolling-element bearings are not important and are generally not considered.

Hydrodynamic fluid film bearings are quite another matter, and thus the need for the present chapter. Unfortunately, they cannot be treated as a simple, direct spring. Although the hydrodynamic fluid film bearing does exhibit a springlike resistance that is dependent on journal displacement relative to the sleeve, this force is not linearly related to the displacement nor is it collinear with it. A hydrodynamic fluid film bearing exhibits damping effects that play a very important role in the stability of this type of bearing.

## 11.6 Nonplain Configurations

Thus far this chapter has focused on plain full journal bearings. As applications have demanded higher speeds, vibration problems due to critical speeds, imbalance, and instability have created a need for journal bearing geometries other than plain journal bearings. These geometries have various patterns of variable clearance so as to create pad film thicknesses that have more strongly converging and diverging regions. Figure 11.10 shows elliptical, offset half, three-lobe, and four-lobe bearings—bearings different from the plain journal bearing. An excellent discussion of the performance of these bearings is provided in Allaire and Flack (1980), and some of their conclusions are presented here. In Fig. 11.10 each pad is moved toward the bearing center some fraction of the pad

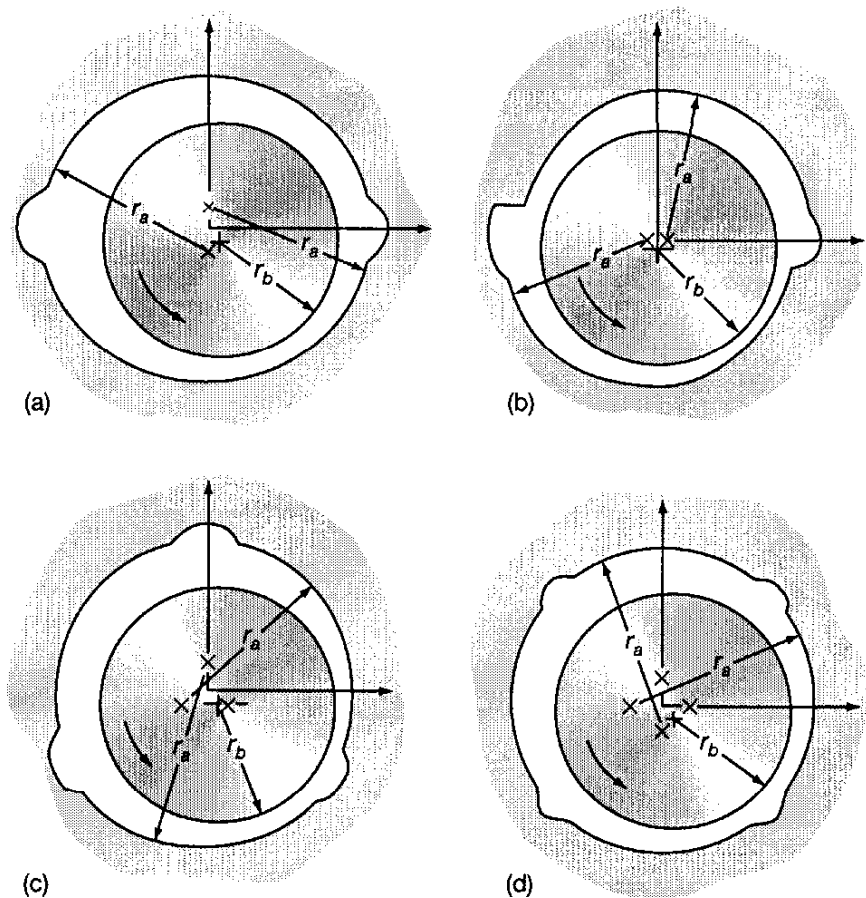


Figure 11.10: Types of fixed-incline-pad preloaded journal bearing and their offset factors  $\alpha_a$ . Preload factor  $m_p$ , 0.4. (a) Elliptical bore bearing ( $\alpha_a = 0.5$ ); (b) offset-half bearing ( $\alpha_a = 1.125$ ); (c) three-lobe bearing ( $\alpha_a = 0.5$ ); (d) four-lobe bearing ( $\alpha_a = 0.5$ ) [From Allaire and Flack (1980).]

clearance in order to make the fluid film thickness more converging and diverging than that occurring in a plain journal bearing. The pad center of curvature is indicated by a cross. Generally, these bearings suppress instabilities in the system well but can be subject to subsynchronous vibration at high speeds. They are not always manufactured accurately.

A key parameter used in describing these bearings is the fraction of length in which the film thickness is converging to the full pad length, called the “offset factor,” and defined as

$$\alpha_a = \frac{\text{length of pad with converging film thickness}}{\text{full pad length}}$$

In an elliptical bearing (Fig. 11.10a) the two pad centers of curvature are moved along the vertical axis. This creates a pad with half the film shape converging and the other half diverging (if the shaft were centered), corresponding to an offset factor  $\alpha_a$  of 0.5. The offset-half bearing (Fig. 11.10b) is a two-axial-groove bearing that is split by moving the top half horizontally. This results

in low vertical stiffness. Generally, the vibration characteristics of this bearing are such as to avoid oil whirl, which can drive a machine unstable. The offset-half bearing has a purely converging film thickness with a converged pad arc length of  $160^\circ$  and the point opposite the center of curvature at  $180^\circ$ . Both the three-lobe and four-lobe bearings (Figs. 11.10c and d) have an  $\alpha_a$  of 0.5.

The fractional reduction of the film clearance when the pads are brought in is called the “preload factor”  $m_p$ . Let the bearing clearance at the pad minimum film thickness (with the shaft center) be denoted by  $c_b$ . Figure 11.11a shows that the largest shaft that can be placed in the bearing has a radius  $r_b + c_b$ , thereby establishing the definition of  $c_b$ . The preload factor  $m_p$  is given by

$$m_p = \frac{c - c_b}{c}$$

A preload factor of zero corresponds to all the pad centers of curvature coinciding at the bearing center; a preload factor of 1.0 corresponds to all the pads touching the shaft. Figures 11.11b and c illustrate these extreme situations. For the various types of fixed journal bearing shown in Fig. 11.10 the preload factor is 0.4.

## 11.7 Closure

The side-leakage term in the Reynolds equation was considered in this chapter for a journal bearing. Analytical solutions to this form of the Reynolds equation are not normally available, and numerical methods are used. When side leakage is considered, an additional operating parameter exists, the diameter-to-width ratio  $\lambda_k$ . Results from numerical solution of the Reynolds equation were presented. These results focused on a full journal bearing, four values of  $\lambda_k$ , and a complete range of eccentricity ratios or minimum film thicknesses. The performance parameters presented for these ranges of operating parameters were

1. Bearing number
2. Attitude angle
3. Friction coefficient
4. Total and side flow
5. Maximum pressure and its location
6. Location of terminating pressure
7. Temperature rise due to lubricant shearing

These performance parameters were presented in the form of figures that can easily be used for designing plain journal bearings. An interpolation formulation

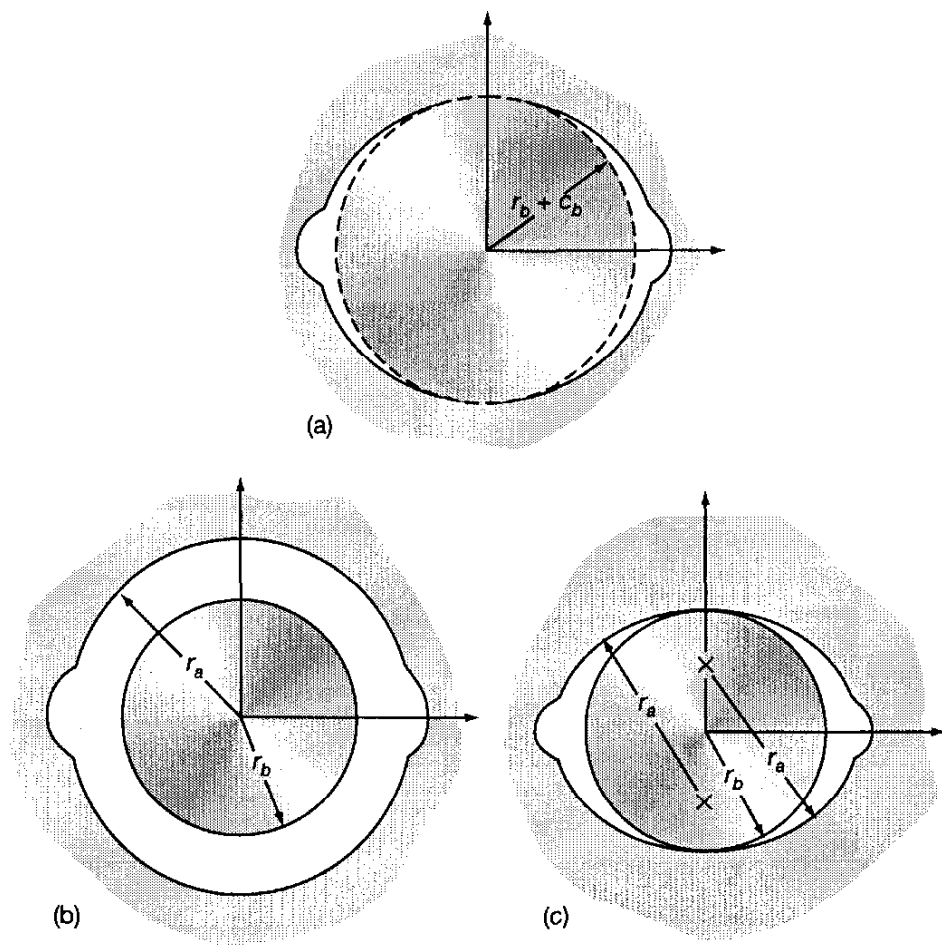


Figure 11.11: Effect of preload factor  $m_p$  on two-lobe bearings. (a) Largest shaft that fits in bearing. (b)  $m_p = 0$ ; largest shaft,  $r_a$ ; bearing clearance  $c_b = c$ . (c)  $m_p = 1.0$ ; largest shaft,  $r_b$ ; bearing clearance  $c_b = 0$ . [From Allaire and Flack (1980).]

was provided so that if  $\lambda_k$  is something other than the four specified values, the complete range of  $\lambda_k$  can be considered. Nonplain journal configurations were also considered. It was found that bearing designs with more converging and less diverging film thickness suppressed instabilities of the system. Steady-state and dynamic parameters are given for a plain journal bearing and three nonplain journal bearings.

## 11.8 Problems

- 11.1 For the same bearing considered in Example 11.1 determine what the operating and performance parameters are when (a) the half Sommerfeld infinitely-long-journal-bearing theory of Chapter 10 is used and (b) the short-width-journal-bearing theory of Chapter 10 is used. Compare the results.

- 11.2 Describe the process of transition to turbulence in the flow between concentric cylinders when the outer cylinder is at rest and the inner cylinder rotates. How is the process influenced by (a) eccentricity and (b) a superimposed axial flow?
- 11.3 A plain journal bearing has a diameter of 2 in. and a length of 1 in. The full journal bearing is to operate at a speed of 2000 r/min and carries a load of 750 lbf. If SAE 10 oil at an inlet temperature of 110°F is to be used, what should the radial clearance be for optimum load-carrying capacity? Describe the surface finish that would be sufficient and yet less costly. Also indicate what the temperature rise, coefficient of friction, flow rate, side flow rate, and attitude angle are.
- 11.4 Discuss the stability of flow between eccentric, rotating cylinders with reference to Rayleigh's criterion. Describe the steps involved in the process of transition to turbulence via the Taylor vortex regime in the flow, and compare the experimentally determined critical Taylor numbers with the results of the Rayleigh criterion analysis.

## References

- Allaire, P. E., and Flack, R. D. (1980): *Journal Bearing Design for High Speed Turbomachinery in Bearing Design-Historical Aspects, Present Technology and Future Problems*. W. J. Anderson (ed.). American Society of Mechanical Engineers, New York, pp. 111-160.
- Lund, J. W. (1979): "Rotor-Bearing Dynamics," Lecture notes. Technical University of Denmark, ISBN 83-04-00267-1.
- Raimondi, A. A., and Boyd, J. (1958): A Solution for the Finite Journal Bearing and Its Application to Analysis and Design-I, -II, and -III. *ASLE Trans.*, vol. 1, no. I, I- pp. 159-174; II- pp. 175-193; III- pp. 194-209.
- Shigley, J. E., and Mitchell, L. D. (1983): *Mechanical Engineering Design*, 4th ed. McGraw-Hill, New York.